Influence of sand characteristics on the piping process

Research to the influence of the grain size and other sand characteristics on the critical head of piping

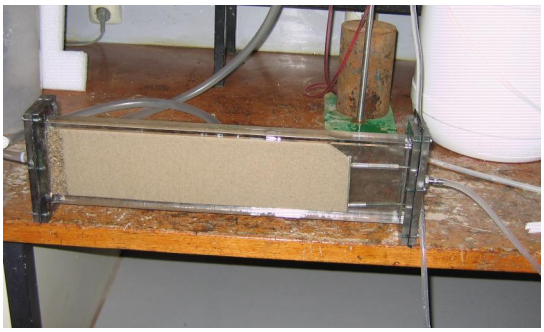

R.A. van der Zee
Delft, March 2011

Technische Universiteit Delft

Deltares
Enabling Delta Life

Influence of sand characteristics on the piping process

Research to the influence of the grain size and other sand characteristics on the critical head of piping

Author:

R.A. van der Zee
Coppelstockstraat 24
3231 VD Brielle
The Netherlands
Telephone 0639633120
E-mail r.a.vanderzee@student.tudelft.nl
Roeland.vanderZee@deltares.nl
Student number 1143824

Graduation committee:

Prof. drs. ir. J.K. Vrijling	Delft University of Technology, section of Hydraulic Engineering – chairman of the graduation committee
Prof. dr. M.A. Hicks	Delft University of Technology, section of Geo-Engineering
Prof. (em) dr. ir. F.B.J. Barends	Deltares
Dr. ir. J.B. Sellmeijer	Deltares
Ir. V.M. van Beek	Deltares
Ir. W. Kanning	Delft University of Technology, section of Hydraulic Engineering

Pictures on front page
- *One-dimensional test facility*
- *Ceci n'est pas une pipe (René Magritte)*
- *Sand boil (Weijers, 2010)*

Preface

This report is the result of the research as part of the Master thesis at the faculty of Civil Engineering and Geosciences of Delft University of Technology.
The research is titled: 'Research to the influence of the grain size and other sand characteristics on the critical head of piping'. This research has been conducted at Deltares.

I would like to thank my graduation committee, Prof. drs. ir. J.K. Vrijling, Prof. dr. M.A. Hicks, Prof. (em) dr. ir. F.B.J. Barends, dr. ir. J.B. Sellmeijer, ir. W. Kanning and ir. V.M. van Beek for their supervision and support. Additionally, I would like to thank ing. F.M. Schenkeveld for his endless support and help in the laboratory.

Delft, March 2011

Roel van der Zee

Summary

One of the failure mechanisms of a dike is piping. A water level difference between the two sides of a dike causes a groundwater flow in the sand layer under the (clay)dike. This flow can transport sand from under the dike to the exit point of the groundwater flow. This is called piping. A pipe develops at the interface of a granular layer and a cohesive layer as a result of backward erosion. Piping can eventually lead to the collapse of the dike. Piping has a high probability of occurrence in the Netherlands, as was found by ter Horst (2005) and ENW (2010). In the Netherlands, the method of Bligh and Lane (both empirical) and Sellmeijer are used as a model to calculate piping. The Sellmeijer model is used in this thesis because it is the most sophisticated model. The formula of Sellmeijer is derived mathematically from the equation of continuity, Poiseuille flow in the slit and equilibrium of grains on the bed of the channel, modeled with the equation of White. The influence of D_{70} on the critical gradient is linear in the Sellmeijer formula. However, coarse-grained sands are generally more permeable than fine-grained sands, which generally results in a net influence of the grain size on the critical gradient to be less than linear, but still positive. De Wit did experimental research and found that coarse grained sands have a higher critical gradient than fine grained sands. In the framework of Strength and Solicitation Flood Defences (SBW), small-scale, medium-scale and full-scale experiments with piping were performed at Deltares. It was found the influence of D_{70} on the critical gradient is less than is predicted with the Sellmeijer model.

1. Problem definition and objective of the research

The objective of this thesis is to research the influence of the grain size and other sand characteristics on the critical head of piping, and to find an explanation for the difference found between SBW results and the Sellmeijer formula. Besides the mean objective of this thesis, a theoretical research to the velocity in the channel according to the current Sellmeijer model has been done.

2. Approach and results of the study of variables

A study is performed to variables which are considered to have influence on the critical gradient. A multi variate analysis (MVA) has been performed successfully on SBW. The results of the MVA confirm the results found by (López de la Cruz, 2009). The influence of the D_{70} is less than is predicted with the Sellmeijer formula. For fine sands, the Sellmeijer formula agreed quite well with the experiments, for coarse sands, it gives an unsafe prediction. Based on the MVA on SBW, an adapted Sellmeijer formula was formulated by Sellmeijer (Sellmeijer 2010a). The MVA was also tried on the dataset of de Wit, but was not successful. The data of de Wit was inserted in the adapted Sellmeijer formula. The outcome did not agree, this may be because the data of de Wit was possibly not corrected

for the filter resistance, or because the range of variables in the de Wit dataset is different than the range of variables in the dataset of SBW.

3. Approach and results of research to the erosion mechanism

In the Sellmeijer model, the equilibrium of grains is according to the model of White, which assumes individual grain erosion. It is researched if this is correct. A test facility was built to research the erosion process experimentally. It was found the grains are dislodged from the granular matrix as mass erosion, with a layer thickness of roughly 7 grains. The transport of sand in the test facility occurs in the pipe in mass transport, in waves, called slurry flow. It is not sure that the observed erosion of the grains from the sand matrix is normative for determining the critical gradient, as the observed erosion may be the erosion type that is present when the critical gradient has already been exceeded. This is still under discussion.

It is probable that the observed dislodging of grains is also present in case of a real dike. The implication of the found dislodging mechanism is that the Sellmeijer formula may possibly describe the dislodging of grains and the piping process in an improper way, however more research is needed to validate if the observed erosion process is normative for determining the critical gradient.

4. Possible explanations of differences between SBW and Sellmeijer

It is concluded that the assumed formula of equilibrium of grains according to the erosion model of White may possibly not be applicable in a piping model. This conclusion is based on experimental observations in the test facility, however, more research is needed to validate if the observed erosion process is normative for determining the critical gradient. This is a possible reason for the difference between the influence of D_{70} on the critical gradient according to the Sellmeijer formula and the outcome of SBW. Several other explanations have been found which contribute little or moderate to the difference between the Sellmeijer formula and the SBW results. These are (more explanations are possible):

- a correction on the critical gradient is needed because of the vertical pressure gradient, if the outcome of the small-scale experiments is compared or extrapolated to real dike dimensions
- the filter influences the experiment so that the outcome is not reliable
- the amount of coarse grained experiments performed with small-scale SBW is insufficient, as is the amount of medium-scale and full-scale experiments
- the Sellmeijer model is a 2D model, while reality is 3D

5. Research to the relation between variables in the channel

A relation between channel height and discharge (or velocity) based on the current Sellmeijer model was found with a mathematical derivation.

Samenvatting

Een van de faalmechanismen van een dijk is piping. Een waterstandsverschil tussen de twee zijden van een dijk zorgt ervoor dat er een grondwaterstroming optreedt in de zandlaag onder de (klei)dijk. Deze grondwaterstroming kan zand transporteren van onder de dijk vandaan naar het uittreepunt van het grondwater. Dit wordt piping genoemd. Een kanaal vormt zich op de interface van het zand en de cohesieve toplaag. Piping kan leiden tot bezwijken van een dijk. Piping heeft een hoge kans van optreden in Nederland, zoals gevonden is door ter Horst (2005) en ENW (2010). In Nederland worden de modellen van Bligh en Lane (beide empirisch) en Sellmeijer gebruikt om piping mee te toetsen. Het Sellmeijer model is gebruikt in deze thesis omdat deze het meest geavanceerde is. De formule van Sellmeijer is wiskundig afgeleid op basis van de continuïteitsvergelijking, Poiseuille stroming en het evenwicht van korrels volgens White. De invloed van D_{70} op het kritieke gradiënt is lineair in de Sellmeijer formule. Omdat grof zand in het algemeen meer doorlatend is dan fijn zand, is de netto invloed van korrelgrootte op het kritiek verval in het algemeen minder dan lineair, maar nog wel positief. De Wit heeft experimenteel onderzoek gedaan en heeft gevonden dat grof zand een hogere kritieke gradiënt heeft dan fijn zand. In het kader van Sterkte en Belastingen Waterkeringen (SBW), zijn kleine schaal, medium schaal en ware grootte proeven uitgevoerd bij Deltares. De invloed van D_{70} op de kritieke gradiënt is minder dan is voorspeld op basis van het Sellmeijer model.

1. Probleem definitie en doelstelling van het onderzoek

Het doel van deze thesis is de invloed van de korrelgrootte en andere zand eigenschappen op het kritiek verval te onderzoeken, en een verklaring te vinden voor het verschil dat gevonden is tussen de SBW resultaten en de Sellmeijer formule. Behalve de hoofddoelstelling van deze thesis, is theoretisch onderzoek gedaan naar de snelheid in het erosiekanaal volgens het Sellmeijer model.

2. Aanpak en resultaten van de studie van de variabelen

Een studie naar de invloed van variabelen op het kritiek verval is uitgevoerd. Een multi variate analyse (MVA) is succesvol uitgevoerd op SBW. De resultaten van de MVA bevestigen de resultaten gevonden door (López de la Cruz, 2009). De invloed van D_{70} op het kritieke verval is minder dan is voorspeld op basis van het Sellmeijer model. Voor fijne zanden komt de Sellmeijer formule redelijk goed overeen met de experimenten, voor grof zand geeft de Sellmeijer formule een onveilige predictie. Gebaseerd op de MVA op SBW is een aangepaste Sellmeijer formule geformuleerd door Sellmeijer (Sellmeijer 2010a). De MVA was ook geprobeerd op de data van de Wit, maar was niet succesvol. De data van de Wit is ingevoerd in de aangepaste Sellmeijer formule, en de uitkomst kwam niet overeen, mogelijk omdat de data van de Wit mogelijk niet gecorrigeerd is voor de

filterweerstand van de proefopstelling, of omdat de range van variabelen in de dataset van de Wit niet hetzelfde is als in de dataset van SBW.

3. Aanpak en resultaten van het onderzochte erosie mechanisme

In het Sellmeijer model wordt het evenwicht van de korrels beschreven volgens het model van White, die individuele korrel erosie aanneemt. Het is onderzocht of dit correct is. Een proefopstelling is gebouwd om het erosie proces experimenteel te onderzoeken. De korrels worden losgemaakt uit de korrelmatrix met enkele honderden tegelijk, met een laag dikte van ongeveer 7 korrels. Het transport van zand vond plaats in massatransport, in golven, slurry flow genaamd. Het is niet zeker of het waargenomen erosie proces van de korrels uit de zandmatrix maatgevend is voor het bepalen van de kritieke gradiënt. Het moet verder onderzocht worden of het waargenomen erosie mechanisme maatgevend is voor bepalen van de kritieke gradiënt.

Het is waarschijnlijk dat het waargenomen loskomen van korrels ook aanwezig is in geval van een echte dijk. De implicatie van de gevonden resultaten is dat het Sellmeijer model mogelijk het loskomen van de korrels en het piping proces niet correct beschrijft. Meer onderzoek is nodig om te valideren dat het waargenomen erosie proces maatgevend is voor het bepalen van de kritieke gradiënt.

4. Mogelijke verklaringen van verschillen tussen SBW en Sellmeijer

Het is geconcludeerd dat de aangenomen formule van het evenwicht van korrels volgens White mogelijk niet toepasbaar is in een piping model. Deze conclusie is gebaseerd op experimenteel onderzoek in de proefopstelling, echter meer onderzoek is nodig om te valideren dat het waargenomen erosie proces maatgevend is om het kritiek verval te bepalen. Dit is een mogelijke reden voor het verschil de invloed van D_{70} op het kritieke gradiënt volgens de Sellmeijer formule en de uitkomst van SBW. Enkele andere verklaringen zijn gevonden die weinig tot middelmatig bijdragen aan het verschil tussen de Sellmeijer formule en de resultaten van SBW. Deze zijn (meer verklaringen zijn mogelijk):

- vanwege de verticale druk gradiënt is een correctie nodig als de uitkomsten van de kleine schaal proeven vergeleken of geëxtrapoleerd worden naar ware dijk dimensies
- het filter beïnvloedt de experimenten zodat de uitkomsten onbetrouwbaar zijn
- er zijn te weinig experimenten met de kleine schaal proefopstelling op grof zand uitgevoerd net als het aantal medium schaal en ware schaal proeven
- het Sellmeijer model is een 2D model, terwijl de werkelijkheid 3D is

5. Onderzoek naar de relatie tussen variabelen in het kanaal

Een relatie tussen de kanaalhoogte en debiet gebaseerd op de huidige Sellmeijer formule was gevonden met een wiskundige afleiding.

Table of Contents Final Report

Preface iv

Summary vi

Samenvatting viii

List of illustrations xvi

List of symbols xxiii

1. Introduction 1

1.1 The failure mechanism piping 1
1.2 Research that has been done in the past 3
1.3 Current design formula's for piping 6
1.3.1 The design formula of Bligh 6
1.3.2 The design formula of Lane 8
1.3.3 The design formula of Sellmeijer 8
1.4 The Sellmeijer model 12
1.5 Available experimental data 15
1.6 Problem description 18
1.7 Problem definition 18
1.8 Objective of the research 18
1.9 Approach of the research 18
1.10 Outline report 20

2. Study of variables 21

2.1 The adapted Sellmeijer formula 22
2.2 Statistical definitions used in this chapter 28
2.3 Description of the variables 29
2.4 Multi variate analysis 34
2.5 Multi variate analysis on SBW data 39

2.5.1 Analysis of small-scale SBW data 40
2.5.2 Analysis of medium-scale SBW data 49
2.5.3 Analysis of full-scale SBW and Deltagoot data 50
2.5.4 Concluding remarks of analysis on SBW data 51
2.6 Multi variate analysis on de Wit data 53
2.6.1 Analysis of small-scale de Wit data 53
2.6.2 Analysis of medium-scale de Wit data 62
2.6.3 Concluding remarks of analysis on de Wit data 65
2.7 Conclusions and a summary about multi variate analysis on SBW and de Wit data 66

3. Research to the transport and erosion mechanism 68

3.1 The equilibrium of grains on a bed according to White 69
3.2 Use of the equation of White in the Sellmeijer model 73
3.3 Theoretical arguments against the use of White in a piping model 74
3.4 Set-up of the experiments with the one-dimensional test facility 76
3.5 Results of the experiments with the one-dimensional test facility 78
3.5.1 Results of the experiments with a RD of 40-50% 79
3.5.2 Results of the experiments with a RD of 60% 87
3.5.3 Results of the experiments with a relative density of 80% 89
3.5.4 Results of the experiments with a RD of 25% 89
3.5.5 Additional remarks about the experiments 90
3.6 Explanations and conclusions about the experimentally observed erosion mechanism 91
3.7 Agreement of experiments with reality 93
3.8 Implications of the found results on the Sellmeijer model 96
3.9 Conclusions and a summary about the erosion mechanism and flow in the channel 100

4. Possible explanations of differences between SBW experiments and the Sellmeijer model 103

4.1 The results of SBW 103
4.2 The possible incorrect modeling of piping in the small-scale and medium-scale test facility 105
4.3 The interpretation of the experiments 109
4.4 The possible not applicableness of White in the Sellmeijer model 115
4.5 Evaluation of the found possible explanations 115
4.6 Conclusions and a summary about the found possible explanations 117

5. Theoretical research of the relation between variables in the channel 118
5.1 The normalized model of Sellmeijer 118
5.2 Theoretical research of the velocity in the slit 120
5.3 Conclusions and a summary about the theoretical research of the relation between variables in the channel 121

6. Conclusions 122

7. Recommendations 125

References 127

A) Appendix A – The test facility used by de Wit 133

B) Appendix B – The test data from de Wit's experiments 134

C) Appendix C – The small-scale test facility used for SBW by Deltares 140

D) Appendix D – The medium-scale test facility used for SBW by Deltares 143

E) Appendix E – The full-scale test facility (IJkdijk) used for SBW by Deltares 146

F) Appendix F – The test data from SBW's experiments 150

G) Appendix G – De Deltagoot test facility 156

H) Appendix H – The test data from de Deltagoot 157

I) Appendix I – The test data from the one-dimensional test facility 158

J) Appendix J – Comparison between measured and calculated SBW experiments..... 160

K) Appendix K – Plots of the dataset of SBW 163

L) Appendix L – Comparison between measured and calculated de Wit experiments..... 166

M) Appendix M –Plots of the dataset of de Wit 170

N) Appendix N – Figures of Bligh data 180

O) Appendix O – Additional figures of slurry flow 183

P) Appendix P – The factual reports of the one-dimensional test facility 189

List of illustrations

List of figures

Figure 1-1 two sand boils as result of the piping process (Weijers, 2010)....1
Figure 1-2 the outflow of seepage water, but no piping (TAW, 1999)....1
Figure 1-3 the formation of a pipe and the failure of the dike (Boon, 2007)....2
Figure 1-4 two aquifer layers separated by an impermeable layer (TAW, 1999)....2
Figure 1-5 the idealized geometry (TAW, 1999)....3
Figure 1-6 the failure probability of dike ring 43 for four different failure mechanism as a function of the return period of the high water (ter Horst, 2005)....4
Figure 1-7 sand bags around a sand boil ("opkisten") (Weijers, 2010)....5
Figure 1-8 the critical gradient according to Bligh as a function of the grain size on a logarithmic scale....7
Figure 1-9 the critical gradient as a function of D_{70} according to the current Sellmeijer formula....10
Figure 1-10 the critical gradient as a function of D_{70} and C_u according to the Sellmeijer model....11
Figure 1-11 the vertical seepage length trough the torn (semi) impermeable layer (Weijers, 2009)....12
Figure 1-12 the slit under a dike (van Beek, 2009d)....12
Figure 1-13 a picture of the geometrical plane with the boundary conditions which was studied by Sellmeijer in his PhD thesis (left) and the transformed geometrical plane (right) (Sellmeijer, 1988)....13
Figure 1-14 the maximum gradient as a function of the pipe length (Sellmeijer, 1988)....15
Figure 1-15 part of the test facility used by de Wit (de Wit, 1982)....15
Figure 1-16 de Wit found a positive trend between D_{70} and critical gradient for small-scale experiments....16
Figure 1-17 the critical gradient against the D_{70} for small-scale tests found by SBW....17
Figure 1-18 an overview of the test facility used for the small-scale SBW experiments....17
Figure 1-19 the outline of the report....20
Figure 2-1 a top view and an oversight view of the test facility filled with sand (van Beek, 2009c)....22
Figure 2-2 the critical gradient as a function of D_{70} and C_u according to the adapted Sellmeijer 2-forces formula, for a constant RD and KAS....24
Figure 2-3 the current and the adapted Sellmeijer 2-forces formulas, for a constant RD, KAS and C_u....24
Figure 2-4 the critical gradient as a function of D_{70} and C_u according to the current and adapted Sellmeijer 2-forces formula, for a constant RD and KAS....25
Figure 2-5 the flow chart for a deriving a new piping formula with a multi variate analysis....27
Figure 2-6 two fictitious datasets. The one has correlated variables, the other has not....29
Figure 2-7 the sieve diagram of Baskarp sand....30
Figure 2-8 a very loose packing (left) and a very tight packing (right) (Verruijt, 2001)....31
Figure 2-9 the definition of KAS value (van Beek, 2009a)....31
Figure 2-10 fine grained sand with a low permeability (left) and coarse grained sand with a high permeability (right) (Verruijt, 2001)....32
Figure 2-11 small and big sized grains in one sample (Schiereck, 2004)....32
Figure 2-12 the permeability as a function of D_{10} and RD (Hunt, 2005)....33
Figure 2-13 part of the model of the piping process under a dike (Sellmeijer, 1988, the colours are added in this thesis)....33
Figure 2-14 the flow chart for a multi variate analysis....35

Figure 2-15 the test facility is not a dike, it is a model of a dike, and the outcome of the model may not be considered to be true for a real dike (picture of pipe and apple: René Magritte).....36
Figure 2-16 a graph of $y = (\frac{x}{x_{mean}})^{\alpha}$ *for different values of* α 37
Figure 2-17 variable 1 and 3 show behaviour as is shown in Figure 2-16. A linear MVA can be done on these datasets. Variable 2 does not show behaviour as shown in Figure 2-16 at al. A linear MVA can not be done on the dataset of variable 2.....38
Figure 2-18 the plot of the critical gradient against RD for small-scale SBW measurements.....41
Figure 2-19 the plot of the critical gradient against k_{Darcy} *for small-scale SBW measurements* 41
Figure 2-20 the plot of the critical gradient against D_{70} *for small-scale SBW measurements*.....42
Figure 2-21 the plot of the critical gradient against C_u *for small-scale SBW measurements*.....42
Figure 2-22 the plot of the critical gradient against KAS for small-scale SBW measurements.....43
Figure 2-23 a histogram of the D_{70} *of the sand samples used for the small-scale SBW experiments* 46
Figure 2-24 an overview of de Wit's test facility (de Wit, 1984).....53
Figure 2-25 part of the test facility used by de Wit, where the location of the filter is pointed out with a blue arrow (de Wit, 1982, the blue arrow is added in this thesis).....53
Figure 2-26 the plot of the critical gradient against RD for small-scale de Wit experiments.....55
Figure 2-27 the plot of the critical gradient against k_{Darcy} *for small-scale de Wit experiments* 55
Figure 2-28 the plot of the critical gradient against D_{70} *for small-scale de Wit experiments*.....56
Figure 2-29 the plot of the critical gradient against C_u *for small-scale de Wit experiments*.....56
Figure 2-30 the plot of the critical gradient against KAS for small-scale de Wit experiments.....57
Figure 2-31 a histogram of the D_{70} *of the sand samples used for the small-scale de Wit experiments* 59
Figure 2-32 C_u *plotted against the* D_{70} *for the small-scale de Wit experiments*.....60
Figure 2-33 the measured critical head (small-scale de Wit experiments) and the critical head according to the prediction with the 2-forces and adapted Sellmeijer formula 61
Figure 2-34 the measured critical head (medium-scale de Wit experiments) and the critical head according to the prediction with the 2-forces and adapted Sellmeijer formula 65
Figure 3-1 a picture of the geometrical plane of the Sellmeijer model (Sellmeijer, 1988).....68
Figure 3-2 the equilibrium of an individual sand grain according to White when the tangential forces are of major importance (White, 1939).....70
Figure 3-3 the equilibrium of an individual sand grain according to White when the fluid acts normally to the surface and tangential stresses are negligible (White, 1939).....71
Figure 3-4 stresses on grains with a tight packing (left) and a loose packing (right) according to White.....72
Figure 3-5 the test facility.....77
Figure 3-6 the filter gravel at the inflow side (left) the filter at the outflow side (middle) and the exit point of the grains (right).....77
Figure 3-7 the set-up for the video camera.....78
Figure 3-8 a top view of the sinusoidal channel, with a length of 4cm.....80
Figure 3-9 a top view of the part what is blocked after a sinusoidal channel is formed.....80
Figure 3-10 a picture from the top, the grains between the yellow lines move as a cloud to the right 81
Figure 3-11 the slow movement of a layer what is called a "cloud" in this chapter 81
Figure 3-12 the blocking of a channel.....81
Figure 3-13 the movement of a wave of grains in experiment Q17 03:00.....82
Figure 3-14 six screen shots of the wave in experiment Q17 at 3:10.....83
Figure 3-15 the movement of a wave of grains in experiment Q17 03:32.....84

Figure 3-16 the displacement of the top layer (red box) and the layer beneath that layer (blue box) in a wave in video Q17 03:10 85
Figure 3-17 the erosion process which occurs when the channel is almost cleared Q17 03:45 86
Figure 3-18 a sketch of the situation after the channel is completely cleared 86
Figure 3-19 the bottom of the channel after the channel is completely cleared Q17 04:04 87
Figure 3-20 the movement of a layer of two grains thick of experiment Q06 7:05 87
Figure 3-21 the movement of a wave of grains in experiment Q06 07:18 88
Figure 3-22 the erosion process which occurs when the channel is almost cleared Q06 07:28 89
Figure 3-23 the sheet flow in Q12 14:29 90
Figure 3-24 the filter at the outflow side. The red dye is only present in the lower part 90
Figure 3-25 the presence of a slit because of the transport of grains in clouds (left) and some grains are transported (right) 91
Figure 3-26 the transported grains get jammed and a pressure builds up behind it 91
Figure 3-27 the meandering of the channels (van Beek, 2009a) 93
Figure 3-28 the one-dimensional test facility is not a dike, it is a model of a dike 93
Figure 3-29 the location where the erosion process is filmed 94
Figure 3-30 pressure gradients in the sand according to the Sellmeijer 4-forces model for l/L=0.4 (Sellmeijer, 1988 96
Figure 3-31 the behaviour of a Bingham plastic (Wikipedia, 2010) 98
Figure 4-1 the critical gradient as function of D_{70} according to the small-scale SBW experiments and the current Sellmeijer formula 104
Figure 4-2 the critical gradient as function of D_{70} according to the medium- and full-scale SBW experiments 104
Figure 4-3 a cross-section of the small-scale test facility (left) (Knoeff, 2008) and part of the geometrical plane on which the Sellmeijer model is derived on (right) (Sellmeijer, 1988) 105
Figure 4-4 the downstream filter at the outflow side. The red dye is only present in the lower part 106
Figure 4-5 contraction of flow lines in the one-dimensional test facility 106
Figure 4-6 contraction of flow lines under a real dike (van Beek, 2009d, the flow lines are added) 107
Figure 4-7 the resistance of the filter (and the rest of the test facility) as a function of D_{70} of the small-scale experiments of SBW 108
Figure 4-8 the critical gradient as function of D_{70} according to the small-scale SBW experiments without the filter correction applied 108
Figure 4-9 the critical gradient versus the D_{70} of the small-scale SBW experiments 110
Figure 4-10 a histogram of the sand samples used for the small-scale SBW experiments 111
Figure 4-11 the negative trend between D_{70} and critical gradient for medium-scale and full-scale (IJkdijk) tests in SBW 111
Figure 4-12 the estimated gradient of failures and non-failures as a function of grain size (coarse and fine sand and gravel) according to Bligh data (Kanning, 2010, adapted) 112
Figure 4-13 the data of the small-scale and medium-scale experiments of de Wit 114
Figure 4-14 the test facility of SBW (left) and the test facility of de Wit (right) 115
Figure A-1 the test facility that was used by de Wit (de Wit, 1984) 133
Figure C-1 a 3D illustration of the small-scale box (Knoeff, 2008) 140
Figure C-2 a cross-section of the small-scale box (Knoeff, 2008) 141
Figure C-3 an overview of the small-scale test facility, which includes the box, the bucket, the camera and the pump (Knoeff, 2008) 141
Figure C-4 a top view of the box filled with sand (Knoeff, 2008) 142
Figure D-1 a top view of the medium-scale test facility (Rietdijk, 2009) 144
Figure D-2 a side view of the medium-scale test facility, where the box is turned 90° (Rietdijk, 2009) 144

Figure D-3 a cross-section of the medium-scale box (van Beek, 2009b) 144
Figure D-4 a schematic overview of the medium-scale test facility (van Beek, 2009b) 145
Figure E-1 a cross-section of de IJkdijk (van Beek, 2010a) 146
Figure E-2 a top view of the location of de IJkdijk (Koelewijn, 2010) 147
Figure E-3 the construction of the sand layer in de IJkdijk (de Bruijn, 2009) 148
Figure E-4 the construction of the clay dike in de IJkdijk (de Bruijn, 2009) 148
Figure E-5 a sand boil at de IJkdijk (de Bruijn, 2009) 149
Figure E-6 failure of de IJkdijk because of piping (de Bruijn, 2009) 149
Figure F-1 the sieve curves of the sands that were used for SBW 155
Figure G-1 an overview of the test facility in de Deltagoot 156
Figure G-2 a photo of de Deltagoot 156
Figure K-1 a histogram of the RD of the sand samples used for the small-scale SBW experiments 163
Figure K-2 a histogram of the C_u of the sand samples used for the small-scale SBW experiments 164
Figure K-3 a histogram of the KAS of the sand samples used for the small-scale SBW experiments 164
Figure K-4 a histogram of k_{Darcy} of the sand samples used for the small-scale SBW experiments . 165
Figure M-1 a histogram of the RD of the sand samples used for the small-scale de Wit experiments 170
Figure M-2 a histogram of the C_u of the sand samples used for the small-scale de Wit experiments 171
Figure M-3 a histogram of the KAS of the sand samples used for the small-scale de Wit experiments 171
Figure M-4 a histogram of K_{Darcy} of the sand samples used for the small-scale de Wit experiments 172
Figure M-5 KAS plotted against the D_{70} for the small-scale de Wit experiments 172
Figure M-6 RD plotted against the D_{70} for the small-scale de Wit experiments 173
Figure M-7 the plot of the critical gradient against RD for medium-scale de Wit measurements .. 173
Figure M-8 the plot of the critical gradient against k_{Darcy} for medium-scale de Wit measurements 174
Figure M-9 the plot of the critical gradient against D_{70} for medium-scale de Wit measurements .. 174
Figure M-10 the plot of the critical gradient against C_u for medium-scale de Wit measurements .. 175
Figure M-11 the plot of the critical gradient against KAS for medium-scale de Wit measurements 175
Figure M-12 a histogram of the D_{70} of the sand samples used for the medium-scale de Wit experiments 176
Figure M-13 a histogram of the RD of the sand samples used for the medium-scale de Wit experiments 176
Figure M-14 a histogram of the C_u of the sand samples used for the medium-scale de Wit experiments 177
Figure M-15 a histogram of K_{Darcy} of the sand samples used for the medium-scale de Wit experiments 177
Figure M-16 a histogram of the KAS of the sand samples used for the medium-scale de Wit experiments 178
Figure M-17 RD plotted against the D_{70} for the medium-scale de Wit experiments 178
Figure M-18 C_u plotted against the D_{70} for the medium-scale de Wit experiments 179
Figure M-19 KAS plotted against the D_{70} for the medium-scale de Wit experiments 179
Figure N-1 the head as a function of the creep distance, for failures and non failures for fine sand, when the Bligh formula is applied on Bligh data (Kanning, 2010) 180
Figure N-2 the head as a function of the creep distance, for failures and non failures for coarse sand when the Bligh formula is applied on Bligh data (Kanning, 2010) 181
Figure N-3 the estimated critical gradient of failures as a function of grain size according to Bligh data (Kanning, 2010, adapted) 181

Figure N-4 the estimated gradient of failures and non failures as a function of grain size (only coarse and fine sand) according to Bligh data (Kanning, 2010, adapted).....182
*Figure N-5 the estimated gradient of failures and non-failures as a function of grain size (coarse*182
Figure O-1 the movement of a wave of grains in experiment Q14 5:08.....183
Figure O-2 the movement of a wave of grains in experiment Q14 05:10.....184
Figure O-3 the movement of a wave of grains in experiment Q14 5:10.....185
Figure O-4 the movement of a wave of grains in experiment Q06 07:19.....186
Figure O-5 the movement of a wave of grains in experiment Q15 8:22.....187
Figure O-6 the movement of a wave of grains in experiment Q18 1:41.....188
Figure P-1 k_{Darcy} as a function of the head for experiment Q01.....192
Figure P-2 k_{Darcy} as a function of the head for experiment Q02.....195
Figure P-3 k_{Darcy} as a function of the head for experiment Q03.....198
Figure P-4 k_{Darcy} as a function of the head for experiment Q04.....202
Figure P-5 k_{Darcy} as a function of the head for experiment Q05.....205
Figure P-6 k_{Darcy} as a function of the head for experiment Q06.....208
Figure P-7 k_{Darcy} as a function of the head for experiment Q07.....211
Figure P-8 k_{Darcy} as a function of the head for experiment Q08.....214
Figure P-9 k_{Darcy} as a function of the head for experiment Q09.....217
Figure P-10 k_{Darcy} as a function of the head for experiment Q10.....220
Figure P-11 k_{Darcy} as a function of the head for experiment Q11.....223
Figure P-12 k_{Darcy} as a function of the head for experiment Q12.....226
Figure P-13 k_{Darcy} as a function of the head for experiment Q13.....229
Figure P-14 k_{Darcy} as a function of the head for experiment Q14.....232
Figure P-15 k_{Darcy} as a function of the head for experiment Q15.....235
Figure P-16 k_{Darcy} as a function of the head for experiment Q16.....238
Figure P-17 k_{Darcy} as a function of the head for experiment Q17.....241
Figure P-18 k_{Darcy} as a function of the head for experiment Q18.....244

List of tables

Table 1-1 seepage line factors for the rules of Bligh and Lane (TAW, 1999).....7
Table 2-1 the interpretation of the correlation coefficient.....28
Table 2-2 the correlation coefficients of the normalized variables of the SBW small-scale samples 44
Table 2-3 the correlation coefficients of the natural logarithms of the normalized variables of the SBW small-scale samples.....45
Table 2-4 the regression coefficients are the outcome of the MVA 47
Table 2-5 the regression coefficients are the outcome of the redone MVA.....49
Table 2-6 overview of de Deltagoot experiments.....51
Table 2-7 overview of de IJkdijk experiments 51
Table 2-8 the regression coefficients and standard deviations for three different MVA formulas 52
Table 2-9 the correlation coefficients of the normalized variables of de Wit small-scale samples....58
Table 2-10 the correlation coefficients of the natural logarithms of the normalized variables of the de Wit small-scale samples 58
Table 2-11 an overview of the types of sand used for the small-scale de Wit experiments 59
Table 2-12 the correlation coefficients of the normalized variables of de Wit medium-scale samples 63
Table 2-13 the correlation coefficients of the natural logarithms of the normalized variables of the de Wit medium-scale samples.....63
Table 2-14 an overview of the types of sand used for the medium-scale de Wit experiments.....64
Table 2-15 the regression coefficients are the outcome of the MVA.....67

Table 3-1 results of $\alpha\eta$ according to experiments of White for steady viscous motion (White, 1939) 72
Table B-1 the results and sand characteristics of de Wit's experiments for L = 80cm part 1 135
Table B-2 the results and sand characteristics of de Wit's experiments for L = 80cm part 2 136
Table B-3 the results and sand characteristics of de Wit's experiments for L = 240cm part 1 137
Table B-4 the results and sand characteristics of de Wit's experiments for L = 240cm part 2 138
Table B-5 the results and sand characteristics of de Wit's experiments for L = 450cm part 1 138
Table B-6 the results and sand characteristics of de Wit's experiments for L = 450cm part 2 138
Table B-7 the results and sand characteristics of de Wit's experiments which are not used part 1 139
Table B-8 the results and sand characteristics of de Wit's experiments which are not used part 2 139
Table E-1 a summary of the three used full-scale experiments (van Beek, 2010a) 147
Table F-1 the results and sand characteristics of SBW's small-scale experiments part 1 151
Table F-2 the results and sand characteristics of SBW's small-scale experiments part 2 152
Table F-3 the results and sand characteristics of SBW's medium-scale experiments part 1 153
Table F-4 the results and sand characteristics of SBW's medium-scale experiments part 2 153
Table F-5 the results and sand characteristics of SBW's full-scale experiments part 1 153
Table F-6 the results and sand characteristics of SBW's full-scale experiments part 2 153
Table F-7 the results and sand characteristics of SBW's experiments which are not used part 1 .. 154
Table F-8 the results and sand characteristics of SBW's experiments which are not used part 2 .. 154
Table H-1 the results and sand characteristics of de Deltagoot experiments part 1 157
Table H-2 the results and sand characteristics of de Deltagoot experiments part 2 157
Table H-3 the result and sand characteristics of de Deltagoot's experiments which are not used part 1 157
Table H-4 the result and sand characteristics of de Deltagoot's experiments which are not used part 2 157
Table I-1 the results and sand characteristics of the experiments with the one-dimensional test facility part 1 158
Table I-2 the results and sand characteristics of the experiments with the one-dimensional test facility part 2 159
Table J-1 the measured and calculated critical gradients and the difference for the small-scale SBW experiments 161
Table J-2 the error and standard deviation of the formula's for the small-scale SBW experiments 162
Table J-3 comparison of H_c /L for the medium-scale experiments with the MVA derived from small-scale experiments and the Sellmeijer models and the measured values 162
Table J-4 the error and standard deviation of the formula's 162
Table L-1 the measured and calculated critical gradients and the difference for the small-scale de Wit experiments 167
Table L-2 the error and standard deviation of the formula's for the small-scale de Wit experiments 168
Table L-3 the measured and calculated critical gradients and the difference for the medium-scale (L=240cm) de Wit experiments 168
Table L-4 the error and standard deviation of the formula's for the medium-scale (L=240cm) de Wit experiments 168
Table L-5 the measured and calculated critical gradients and the difference for the medium-scale (L= 450cm) de Wit experiments 169
Table L-6 the error and standard deviation of the formula's for the medium-scale (L=450cm) de Wit experiments 169
Table P-1 the properties of the sand and the test facility for experiment Q01 190
Table P-2 the head, discharge and permeability as a function of time for experiment Q01 191
Table P-3 the properties of the sand and the test facility for experiment Q02 193

Table P-4 the head, discharge and permeability as a function of time for experiment Q02 194
Table P-5 the properties of the sand and the test facility for experiment Q03..... 196
Table P-6 the head, discharge and permeability as a function of time for experiment Q03 197
Table P-7 the properties of the sand and the test facility for experiment Q04..... 199
Table P-8 the head, discharge and permeability as a function of time for experiment Q04 200
Table P-9 the properties of the sand and the test facility for experiment Q05..... 203
Table P-10 the head, discharge and permeability as a function of time for experiment Q05 204
Table P-11 the properties of the sand and the test facility for experiment Q06..... 206
Table P-12 the head, discharge and permeability as a function of time for experiment Q06 207
Table P-13 the properties of the sand and the test facility for experiment Q07..... 209
Table P-14 the head, discharge and permeability as a function of time for experiment Q07 210
Table P-15 the properties of the sand and the test facility for experiment Q08..... 212
Table P-16 the head, discharge and permeability as a function of time for experiment Q08 213
Table P-17 the properties of the sand and the test facility for experiment Q09..... 215
Table P-18 the head, discharge and permeability as a function of time for experiment Q09 216
Table P-19 the properties of the sand and the test facility for experiment Q10..... 218
Table P-20 the head, discharge and permeability as a function of time for experiment Q10 219
Table P-21 the properties of the sand and the test facility for experiment Q11..... 221
Table P-22 the head, discharge and permeability as a function of time for experiment Q11 222
Table P-23 the properties of the sand and the test facility for experiment Q12..... 224
Table P-24 the head, discharge and permeability as a function of time for experiment Q12 225
Table P-25 the properties of the sand and the test facility for experiment Q13..... 227
Table P-26 the head, discharge and permeability as a function of time for experiment Q13 228
Table P-27 the properties of the sand and the test facility for experiment Q14..... 230
Table P-28 the head, discharge and permeability as a function of time for experiment Q14 231
Table P-29 the properties of the sand and the test facility for experiment Q15..... 233
Table P-30 the head, discharge and permeability as a function of time for experiment Q15 234
Table P-31 the properties of the sand and the test facility for experiment Q16..... 236
Table P-32 the head, discharge and permeability as a function of time for experiment Q16 237
Table P-33 the properties of the sand and the test facility for experiment Q17..... 239
Table P-34 the head, discharge and permeability as a function of time for experiment Q17 240
Table P-35 the properties of the sand and the test facility for experiment Q18..... 242
Table P-36 the head, discharge and permeability as a function of time for experiment Q18 243

List of symbols

Symbol	Description	Unit
a	Vertical seepage length through the torn impermeable layer	m
a	Height of the slit	m
$\hat{a}$	Normalized height of the slit	-
C	Coefficient of Martin	-
C_{creep}	Seepage line factor	-
cov	Covariance operator	
C_u	The coefficient of uniformity, D_{60}/D_{10}	-
$C_{u,mean}$	The mean of the coefficient of uniformity of a certain data set	-
$C_{w,creep}$	Weighted seepage line factor	-
D	The thickness of the sand layer	m
D	The grain diameter, the percentile is not specified yet	µm or m
D_{10}	The 10^{th} percentile of the grain diameter	µm or m
D_{60}	The 60^{th} percentile of the grain diameter	µm or m
D_{70}	The 70^{th} percentile of the grain diameter	µm or m
$D_{70,mean}$	The mean of the 70^{th} percentile of the grain diameter of a certain data set	µm or m
d	The grain diameter, the percentile is not specified yet	µm or m
E	Expectation operator	
F_g	Geometry factor	-
F_r	Resistance factor	-
F_s	Scale factor	-
g	Gravitational acceleration	m/s^2
i	Complex number	-
i	Gradient	-
k	Permeability	m/s
k_{mean}	The mean of the permeability of a certain data set	m/s
KAS	The roundness of the grain particles	-
KAS_{mean}	The mean of the roundness of the grain particles of a certain data set	-
k_{Beyer}	Permeability based on Beyer's law	m/s
$k_{Beyer,mean}$	The mean of the Permeability based on Beyer's law of a certain data set	m/s
k_{Darcy}	Permeability based on Darcy's law	m/s
$k_{Darcy,mean}$	The mean of the permeability of a certain data set based on Darcy's law	m/s
L	Seepage length	m
l	Pipe length	m
L_c	Required piping length	m
L_h	Horizontal seepage length	m
L_v	Vertical seepage length	m
RD	Relative density	%
RD_{mean}	The mean of the relative density of a certain data set	%
T	Temperature	°C
p	The horizontal pressure gradient	-
$\hat{p}$	Normalized gradient of head	-
Q	Discharge at exit point slit[*1]	m^3/s or m^2/s

Symbol	Description	Unit
$\hat{Q}$	Normalized discharge	-
q	Discharge along the bottom of the slit[*1]	m^3/s or m^2/s
q	The vertical pressure gradient	-
$\hat{q}$	Normalized discharge along the bottom of the slit	-
V	Volume of sand transported out of slit[*1]	m^3 or m^2
$\hat{V}$	Normalized volume of sand transported out of slit	-
X	Normalized horizontal coordinate	-
x	Horizontal coordinate	m
Y	Normalized vertical coordinate	
y	Vertical coordinate	m
α	Regression factor	-
α	Factor depending on the aquifer dimensions	-
β	Regression factor	-
β	Slope of pipe	°
γ	Regression factor	-
γ_p'	The (apparent) volume weight of sand grains under water	kN/m^3
γ_w	The volume weight of water	kN/m^3
δ	Regression factor	-
δ	Normalization parameter	-
ΔH_c	Critical head difference	m
ε	Regression factor	-
η	The drag force factor (coefficient of White)	-
η	Porosity	%
η_{max}	Maximum porosity	%
η_{min}	Minimum porosity	%
θ	The rolling resistance angle of the sand grains (bedding angle)	°
θ	Regression factor	-
κ	Intrinsic permeability	m^2
κ_{Beyer}	Intrinsic permeability based on Beyer's law	m^2
κ_{Darcy}	Intrinsic permeability based on Darcy's law	m^2
$\kappa_{Darcy,mean}$	Mean intrinsic permeability based on Darcy's law	m^2
κ_{mean}	Mean intrinsic permeability	m^2
λ	Normalization parameter	-
ν	Kinematic viscosity	m^2/s
ρ	Correlation coefficient	-
σ	Standard deviation	
τ τ_b τ_s	Shear stress	Pa
Φ	Normalized head	-
φ	Head	m
ψ	Complex potential	m
ω	Stream function	m

[*1] The unit depends if the process is described per running meter or not per running meter

1. Introduction

This chapter gives an introduction of the failure mechanism piping. Section 1.1 describes the piping process in general. In section 1.2 some research that has been done in the past is discussed. Section 1.3 describes the formula's of Bligh, Lane and Sellmeijer. In section 1.4 the Sellmeijer model is treated. In section 1.5 available experimental data is discussed, and in section 1.6, the problem description is treated. In section 1.7, 1.8 and 1.9 respectively, the problem definition, the objective of the research and the approach of the research is treated. Finally, in section 1.10 the outline of the report is shown.

1.1 The failure mechanism piping

A dike has several failure mechanisms. One of those failure mechanisms is piping. Piping is the failure mechanism when a water level difference between the two sides of a dike causes a groundwater flow under the dike. This groundwater flow transports sand from under the dike to the exit point of the groundwater flow. A sand boil is then created behind the dike as is shown in Figure 1-1. A pipe develops at the interface of a granular layer and a cohesive layer as a result of backward erosion. In Figure 1-2 the outflow of seepage water is shown. Since only water flows out and no sand is transported, this is not the piping process.

Figure 1-1 two sand boils as result of the piping process (Weijers, 2010)

Figure 1-2 the outflow of seepage water, but no piping (TAW, 1999)

If the hydraulic gradient reaches a certain level, the seepage water will transport sand with it. The outflow of water which transports sand out of the substrate is formerly called a sand boil. Piping is the creation of hollow spaces ("pipes") under a dike or hydraulic structure, as a consequence of a concentrated seepage flow carrying ground particles. In the factual definition, piping is the forming of an open channel from entry point to exit point (TAW, 1999). Piping can eventually lead to collapsing of the dike. In Figure 1-3, two stages in the piping process are shown: the formation of a pipe and the failure of the dike. Critical gradient is defined as critical head divided by the seepage length, where the critical head is the head when a continuous pipe under the dike has developed.

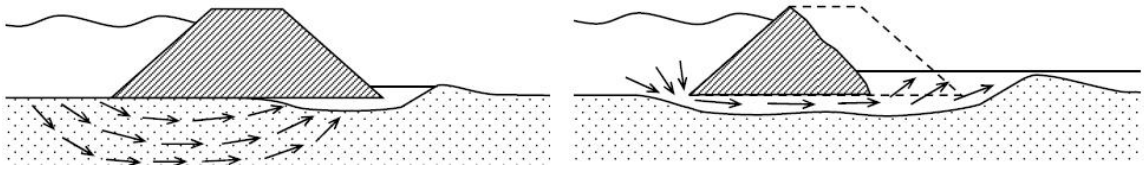

Figure 1-3 the formation of a pipe and the failure of the dike (Boon, 2007)

Several configurations of soil layers can lead to the piping process, e.g. sand layers, gravel layers, layers of gravel with sand. Also, several layers of different aquifer layers op top of each other are possible (coarse sand on top of fine sand or vice versa or a sand layer on top of a gravel layer or two aquifer layers separated by an impervious layer, see Figure 1-4).

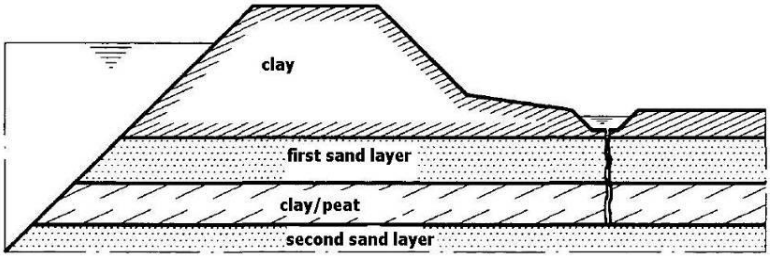

Figure 1-4 two aquifer layers separated by an impermeable layer (TAW, 1999)

The presence of several layers of aquifers can lead to a more complicated piping process and these types are often encountered in practice. In this report, unless otherwise mentioned, the so called idealized geometry is used. This idealized geometry consists of a clay dike with a ditch on top of a homogeneous sand layer with constant and finite thickness and is shown in Figure 1-5.

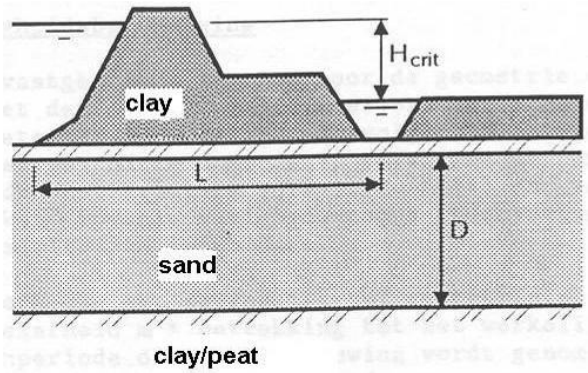

Figure 1-5 the idealized geometry (TAW, 1999)

1.2 Research that has been done in the past

In this paragraph research that has been done in the past is treated. Some of the results of this research is used in this thesis, as other research show why it is important more research to piping is needed. It is also important to know how researchers came to certain conclusions, if different formula's and datasets are compared with each other.

Clibborn and Beresford found that the ratio between critical head and seepage length is a constant that depends on soil properties (Clibborn, 1902). Bligh extended this research and investigated the failure and non-failure of masonry dams in India (Bligh, 1910) and derived a formula for piping. The formula of Bligh and its background are described in paragraph 1.3.1. Griffith developed this rule further (Griffith, 1913). Lane extended the research done by Bligh by including the effect of a vertical sheet pile (Lane, 1935). The formula of Lane and its background are described in paragraph 1.3.2. The formula of Bligh and Lane are both empirical of nature. Harza proposes the electric analogy method, where groundwater flow is simulated with electric currents (Harza, 1935). Terzaghi proposed a formula for heave near sheet piles, which takes into account the vertical gradient of the water flow (Terzaghi, 1948). Müller-Kirchenbauer did experiments with test facilities to research the influence of multiple layers of sand on the piping process, however the grain size was not varied in these experiments (Müller-Kirchenbauer, 1978). De Wit did extensive model tests on piping, this is elaborated on in paragraph 1.5 and appendix A and B (de Wit, 1984). Since then, many scientists have been involved in piping research. In the 80's, the Dutchman Sellmeijer devoted his PhD thesis on piping and found a sophisticated piping formula (Sellmeijer, 1988). The simplified design formula itself is presented in paragraph 1.3.3. and the model is explained in paragraph 1.4. Kohno researched the influence of multiple sand layers on the critical head with a test facility (Kohno, 1987).

Researchers who also performed small-scale test include amongst others Schmertmann (Schmertmann, 2000). Schmertmann found that the results of the

piping experiments were independent of the applied effective stresses. Ojha researched the influence of the porosity on piping, and found that the outcome of the study supports the formula of Bligh (Ojha, 2001). Zeping studied the difference between the Dutch and the Chinese method of calculating piping, and concluded that in the Netherlands, a critical gradient is determined, while in China a critical exit gradient is normative (Zeping, 2001).

Schmertmann provides, based on the failure (and damage) probability of dams due to piping, an excellent economical substantiated argument to invest heavily in piping experiments (Schmertmann, 2002). Several years ago Sellmeijer published about neural network for piping (Sellmeijer, 2003). In this neural network, other geometries that the idealized geometry can be used, and a fast and accurate computation can be performed.

Ter Horst did research to the conditional failure probability of several failure mechanisms of dikes in the Netherlands, and concluded that piping is the most dangerous failure mechanism in the Netherlands because of the high uncertainty in the resistance of a dike (ter Horst, 2005). In a case study, four different failure mechanisms as a function of the return period of dike ring 43 were researched. This dike ring is situated between the rivers Lek and Waal, and according to the safety standard, the dike ring should withstand high water with a probability of exceedance of 1/1250 years. The failure mechanisms that were considered were piping, instability, erosion and overtopping. In Figure 1-6 the failure probability of dike ring 43 for these four different failure mechanism as a function of the return period of the high water is shown. As can be seen, the piping mechanism has a quite high probability of occurrence, even when the water level is lower than the normative water level.

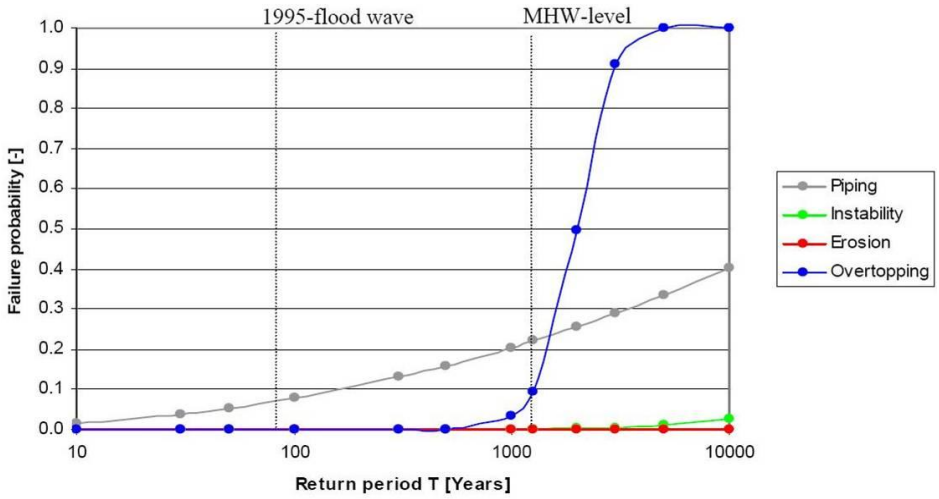

Figure 1-6 the failure probability of dike ring 43 for four different failure mechanism as a function of the return period of the high water (ter Horst, 2005)

Achmus has defined a critical exit gradient for piping (Achmus, 2006). The method of a critical exit gradient method is used in several countries. Ammerlaan made a comparison between dike evaluation methods which are used in the Netherlands and the USA (Ammerlaan, 2007). Ammerlaan concluded that in the USA sand boils may not occur, in the Netherlands, the creation of sand boils is allowed, as long as the critical gradient is not exceeded. In the USA values of C_{Bligh} of 43 or 44 are used.

Hoffmans suggests that piping can be described with the Shields (equilibrium) equation and that the solution gives a better fit with the experiments than the Sellmeijer formula (Hoffmans, 2009).

ENW concluded in the report "Piping, Reality or Calculation error" (Dutch: *"Piping, Realiteit of Rekenfout")* that piping is a more serious threat than was assumed (ENW, 2010). In the project VNK1 (safety assessment of the Dutch dikes), piping was considered one of the most dominant failure mechanisms. This did not agree with the judgment of the managers of the dikes. After research had been done, it appeared the failure probability decreased only slightly if the schematization was improved. Still the failure probability is higher than was expected. The following was concluded. The risk of piping in the Netherlands is higher than was assumed in the past. No mistakes were found in the VNK models. It is calculated the net present value of the risk of flooding because of piping in the Netherlands is €5.7 billion. The three options that were considered were:

- Maintain current rules and perform more research
- Design and prepare repressive measures
- Design and execute preventive measures

The first option was not advised because the net present value of the risk reduction is €2.2 billion. The third option, designing and executing preventive measures, costs €1.4 billion. Also loss of human life, indirect consequences and damage to the image of the Netherlands plays an important role in the decision whether to take the risk or use preventive measures. The second option, designing and preparing repressive measures such as placing sand bags around a sand boil if one occurs (*Dutch: "opkisten"*), shown in Figure 1-7, is not advised because the strength of the sand bags and the failure probability due to human errors is not known in this case.

Figure 1-7 sand bags around a sand boil ("opkisten") (Weijers, 2010)

The third option, designing and executing preventive measures, is advised. In rural areas, berms should be constructed, which has also a positive effect on other failure mechanisms, as macro-stability. In urban areas, sheet pile walls are advised.

31% of the primary flood defences in the Netherlands (1100km) need to be improved to withstand the piping mechanism. Because piping is a failure mechanism with a lot of uncertainty in the strength, the length effect of the dike rings is heavily present in the failure probability. (The failure probability of failure mechanisms where the main uncertainty in the load, like overtopping, depend very little on the length effect of the dike ring). The length effect should be included in the design rules and the design rules should be composed in such a way, that a probability analysis gives the same judgment as the design rule. The current rules used for safety assessment of piping in the Netherlands are not very conservative. The current rules in use in the Netherlands check if a continuous pipe does develop, the creation of a sand boil is not considered failure and is accepted. In other countries, the creation of sand boils is considered unacceptable. The value of the constant in the Bligh formula for fine sands, C_{Creep} = 18, is not always safe enough and a more conservative value should be used, or the use of the Bligh formula should be abandoned. Also from history, there are some indications that piping is more relevant than was assumed in the past. There is a non-negligible probability that the occurring of piping is underestimated and unsafe procedures with respect to the schematizations of the piping models are implemented. The reliability of the calculation models is doubtful.

1.3 Current design formula's for piping

Several design formulas for the safety assessment with respect to piping can be used. The formulas of Bligh, Lane and Sellmeijer are used in the Dutch practice and these formulas are discussed in section 1.3.1, 1.3.2 and 1.3.3. All of these three formulas predict an increasing critical gradient as the grain diameter increases.

1.3.1 The design formula of Bligh

A number of cases of collapses due to piping and a high number of non collapses of small flood control dams in India have been catalogued and analyzed in the early 20th century by an English engineer called Bligh, who had a lot of experience with the construction of dams and irrigation channels. Bligh's criterion determines the required piping length (Lc) for a certain water level (critical head ΔHc). $L \geq \Delta H_c * C_{creep}$ ***(eq 1-1)***. C_{creep} is defined by Bligh according to the values specified in Table 1-1 (TAW, 1999). This rule is a pure empirical rule. This method is known as the line of creep method. In Figure 1-8 the critical gradient according to Bligh (eq 1-1) is shown as a function of the grain size on a logarithmic scale.

Table 1-1 seepage line factors for the rules of Bligh and Lane (TAW, 1999)

Type of soil	Lower limit grain size	Upper limit grain size	C_{creep}	$C_{w,creep}$
Extremely fine sand or silt	63µm	105µm		8.5
Very fine sand	105µm	150µm	18	
Very fine sand (mica)	105µm	150µm	18	7
Moderately fine sand (quartz)	150µm	210µm	15	7
Moderately coarse sand	210µm	300µm		6
Very/extremely coarse sand	300µm	2mm	12	5
Fine shingle	2mm	5.6mm	9	4
Moderately coarse shingle	5.6mm	16mm		3.5
Very coarse shingle	16mm	63mm	4	3

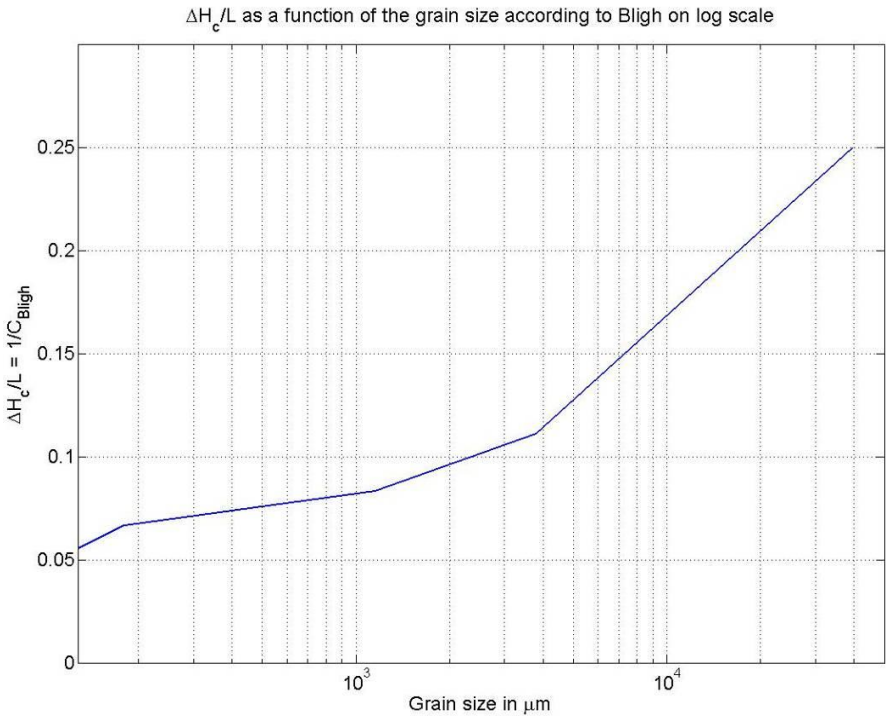

Figure 1-8 the critical gradient according to Bligh as a function of the grain size on a logarithmic scale

The advantage of the method of Bligh, compared with the Sellmeijer formula, is that the formula of Bligh is simple. Besides the seepage length and the head difference, only the size of the sand grains is needed. This way, a safety assessment for piping can be made with little effort. If the method of Bligh gives a positive result in the safety assessment, the dike is considered safe against piping, although there are some exceptions, for example when the C_{creep} is not conservative enough (ENW, 2010) or when the dimensions of the dike exceeds the dimensions of the dams that were investigated by Bligh, as for example is encountered in the Yangtze River in China. Another advantage of the method of Bligh, compared with the Sellmeijer rule, is that the rule is derived from data from real case dams. Length-scale effects, that

are present in small-scale and medium-scale (laboratory) tests, are not present in the rule and the measurement data of Bligh is not influenced by a laboratory set-up.

One of the disadvantages of Bligh, compared with the Sellmeijer rule, is that the layer thickness of the sand layer is not taken into account. In addition, certain variables as the permeability, the relative density and the uniformity of the sand are not taken into account. Also, certain characteristics of the sand layer(s) that are present in nature, such as a coarse grained sand layer on top of a fine sand layer or vice versa, heterogenic groundwater flow and an unknown thickness of the aquifers, is present in the data acquired by Bligh. This is one of the reasons why cases cannot easily be compared with each other. We cannot derive anymore on what conditions the values of the outcomes of Bligh's observations are based. Figures of data of the failure and non-failure of dams researched by Bligh are shown in appendix N.

1.3.2 The design formula of Lane

When the pipe also follows a vertical path, for example when a vertical seepage screen is used, the formula of Lane can be used to asses the critical head. In this formula, the vertical seepage length contributes three times as much as the horizontal seepage length.

$$\Delta H \le \Delta H_c = \frac{\frac{1}{3}L_h + L_v}{C_{w,creep}}$$ (TAW, 1999) *(eq 1-2)*.

L_h is the horizontal seepage length and L_v is the vertical seepage length. Paths with an angle lower than 45° are considered horizontal and paths with an angle higher than 45° are considered vertical. $C_{w,creep}$ is defined in Table 1-1. This method is known as the weighted line of creep method. As the method of Bligh, the formula of Lane is an empirical rule and has, besides taking into account the vertical seepage length, the same advantages and disadvantages as the formula of Bligh, compared with the Sellmeijer formula, as mentioned in 2.2.1. If the vertical length is 0, the formula of Lane does not result in the same outcome as the formula of Bligh.

1.3.3 The design formula of Sellmeijer

Sellmeijer derived a formula for the safety assessment against piping based on the mathematical and physical equilibrium of the sand grains, groundwater flow and Poiseuille flow in the pipe. The outcome of the analysis made by Sellmeijer are several equations which describe the piping process but can not be solved analytically. These equations describe the piping process itself. These equations are called in this thesis the piping model of Sellmeijer. In paragraph 1.4 these equations are treated. In MSEEP, these equations can be used for a high amount of simulations for different sets of variables. When the results of the outcomes of the MSEEP analysis is fitted, a simplified and easy to use formula can be determined which can be used in

engineering practice. In this way a so-called 2-forces and a 4-forces formula was developed. These formula's are called in this thesis the Sellmeijer formula's. In paragraph 1.4 the model and the research done by Sellmeijer is explained in more detail. In this paragraph the formula's are explained. For the single particle force balance for a grain at the bottom of the erosion channel, four distinct forces are considered. The horizontal ones are the drag force due to the channel flow and the horizontal pressure gradient. The vertical ones are the weight of a particle and the vertical pressure gradient. The 4-forces formula of Sellmeijer is defined as follows (Sellmeijer, 1988).

$$\frac{H_c}{L} = F_R \, F_S \, F_G \, C$$

$$F_R = \frac{\gamma'_p}{\gamma_w} \eta \tan(\theta)$$

$$F_S = \frac{D_{70}}{\sqrt[3]{\kappa L}} \qquad \textit{(eq 1-3).}$$

$$F_G = \left(\frac{D}{L} \right)^{\frac{0.28}{\left(\frac{D}{L}\right)^{2.8} - 1}}$$

$$C = 0.68 - 0.10 \ln\left(\eta F_S\right) = 0.82 - 0.10 \ln\left(F_S\right)$$

TAW suggests a value of $\eta = 0.25$, $\gamma_w = 10 \; kN/m^3$, $\gamma'_p = 17 \; kN/m^3$ and $\theta = 41°$ (TAW, 1999). Since the particle density of (quartz) sand is 2650 kg/m^3, a value of $\gamma'_p = 16.5 \; kN/m^3$ seems more appropriate. Also, Sellmeijer suggests (in deviation with TAW) that $\theta = 39°$ results in a better fit with experiments. The role of the horizontal and vertical pressure gradient is questioned. It is put forward that the particle at limit equilibrium sticks out, so that the pressure gradient does not affect it. Consequently, a 2-forces approach is selected where the drag force and weight of the particle are applied. The 2-forces formula of Sellmeijer is defined as follows (van Beek, 2009b).

$$\frac{H_c}{L} = F_R \, F_S \, F_G$$

$$F_R = \frac{\gamma'_p}{\gamma_w} \eta \tan(\theta)$$

$$F_S = \frac{D_{70}}{\sqrt[3]{\kappa L}} \qquad \textit{(eq 1-4).}$$

$$F_G \overset{\text{standarddike}}{=} 0.91 \left(\frac{D}{L} \right)^{\frac{0.28}{\left(\frac{D}{L}\right)^{2.8} - 1} + 0.04}$$

Sellmeijer suggests the following parameters.
$\eta = 0.25$, $\gamma_w = 10\ kN/m^3$, $\gamma_p' = 16.5\ kN/m^3$ and $\theta = 37°$.

The grain size appears to be linearly present in $F_S = \frac{D_{70}}{\sqrt[3]{\kappa L}}$, however $\kappa \approx C * D_{70}^2$ (actually $\kappa \approx C * D_{10}^2$, and D_{10} and D_{70} are correlated via the coefficient of uniformity C_u, (Hunt, 2005)). This means that theoretically according the 2-forces Sellmeijer formula the critical head increases with the cubic root of the grain size. In Figure 1-9 the critical gradient as formulated in (eq 1-4) as a function of the D_{70} is shown.

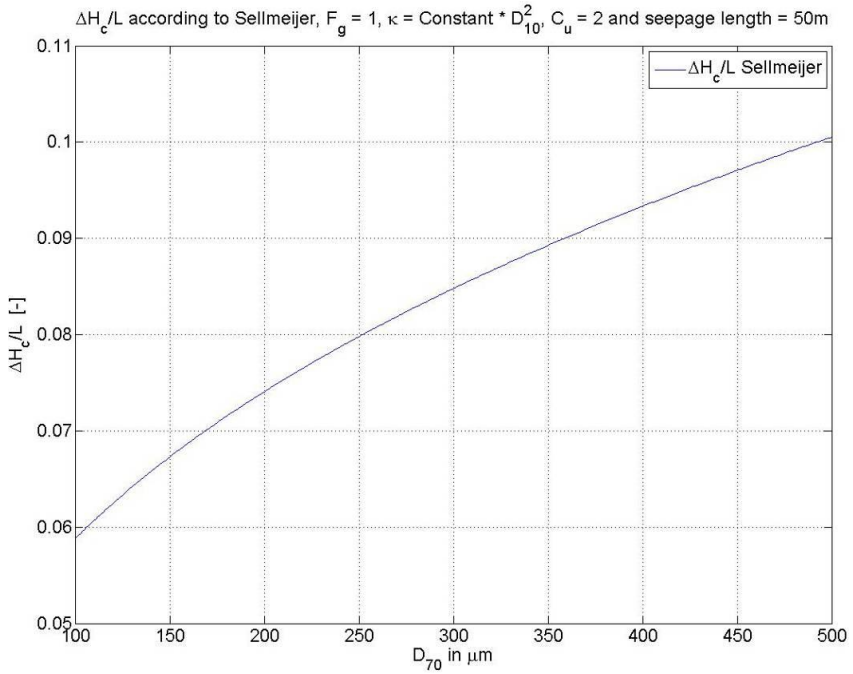

Figure 1-9 the critical gradient as a function of D_{70} according to the current Sellmeijer formula

In this graph a constant coefficient of uniformity is used and a seepage length of 50m. In this thesis, when is referred to the current Sellmeijer formula, (eq 1-4) is meant.
In Figure 1-10 the critical gradient according to the Sellmeijer formula (eq 1-4) is shown as both a function of D_{70} and the coefficient of uniformity ($C_u = \frac{D_{60}}{D_{10}}$). The coefficient of uniformity is not a variable itself in the Sellmeijer formula, but the intrinsic permeability (κ) is, and $\kappa =$ constant * D_{10}^2 (it is plotted this way because it is easier to interpreted D_{70} in combination of C_u than D_{70} in combination with κ). Figure 1-9 is actually a cross-section of Figure 1-10 in the plane C_u=2.

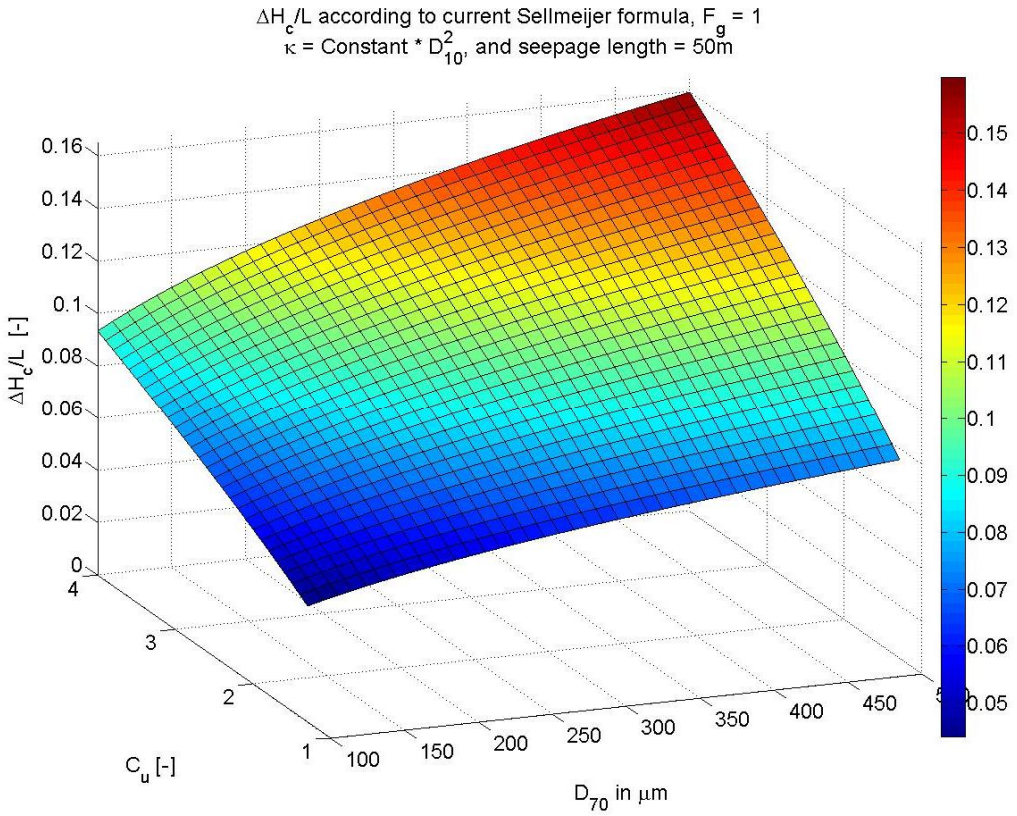

Figure 1-10 the critical gradient as a function of D_{70} and C_u according to the Sellmeijer model

Sellmeijer defined later an adapted 2-forces formula. This formula is explained in chapter 2.

The advantage of the Sellmeijer formula, compared with Bligh, is that more relevant variables and the layer thickness effect of the aquifer are included in the formula. This leads to a more sophisticated design and dike sections which fail to pass the safety check of Bligh, may be tested sufficient with the Sellmeijer formula. (In exceptional cases the method of Bligh can give a positive outcome while Sellmeijer's method does not, as is described in (ENW, 2010)). The disadvantage compared with the Bligh formula is that more knowledge about the sand characteristics is needed.

In Figure 1-11 the vertical seepage length through the torn open (semi) impermeable layer is shown. This vertical seepage length increases the critical head with 0.3*a, where a is the vertical seepage length through the torn impermeable layer.

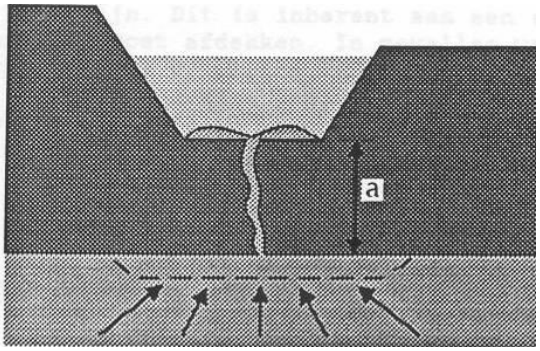

Figure 1-11 the vertical seepage length trough the torn (semi) impermeable layer (Weijers, 2009)

1.4 The Sellmeijer model

In this paragraph, the Sellmeijer model is explained. All information in this paragraph was found in (Sellmeijer, 1988) unless stated otherwise. In Figure 1-13 (left), the geometrical plane of the model which was analyzed by Sellmeijer in his PhD thesis is shown. The model is a 2-D model. Sellmeijer describes with some assumptions and simplifications the equilibrium of the piping process mathematically. These equations are based on groundwater flow (Darcy and continuity), flow in the erosion channel (Poiseuille) and state of the limit equilibrium of the grains on the bottom of the channel (White). Sellmeijer assumes a slit under the dike is present that exits in a ditch, see Figure 1-12. This slit is assumed because of the convergence of streamlines at the exit point of the groundwater flow. The Sellmeijer model is a 2-dimensional model, and the slit is assumed to be infinitely wide, and the outcome of the model is per running meter. Due to groundwater flow, the length of the slit can increase in the direction of the river and sand boils occur in the ditch. If the slit reaches the river, a full passage under the dike is present.

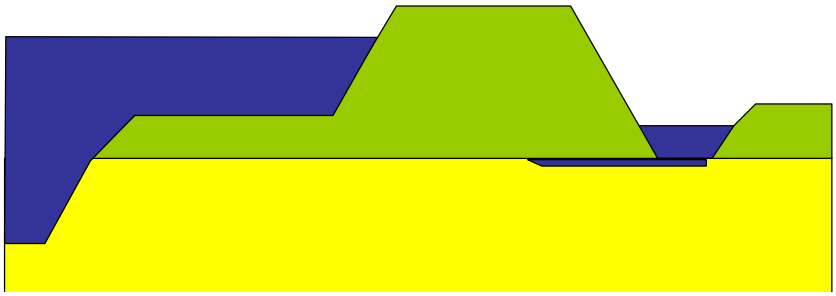

Figure 1-12 the slit under a dike (van Beek, 2009d)

Because the way the boundary conditions are imposed, it is very difficult (or impossible) to solve the equations with real numbers. That is why the problem is solved in terms of $\omega = \phi + i\psi$, where ω is the complex potential, ϕ is the head and ψ is the stream function. ω is a holomorphic function, because per definition, $\frac{d\phi}{dx} = \frac{d\psi}{dy}$

and $\frac{d\psi}{dx} = -\frac{d\phi}{dy}$, which are the Cauchy-Riemann relations (Barends, 2003). This equation is very helpful, as now complex variable theories can be used to solve the equations. A solution is obtained with use of the Cauchy integral formula (Polubarinova-Kochina, 1962). Another method is the use of conformal mapping. A Schwarz-Christoffel transformation can be applied, and the geometrical plane shown in Figure 1-13 (right) is the transformation of the geometrical plane shown in Figure 1-13 (left).

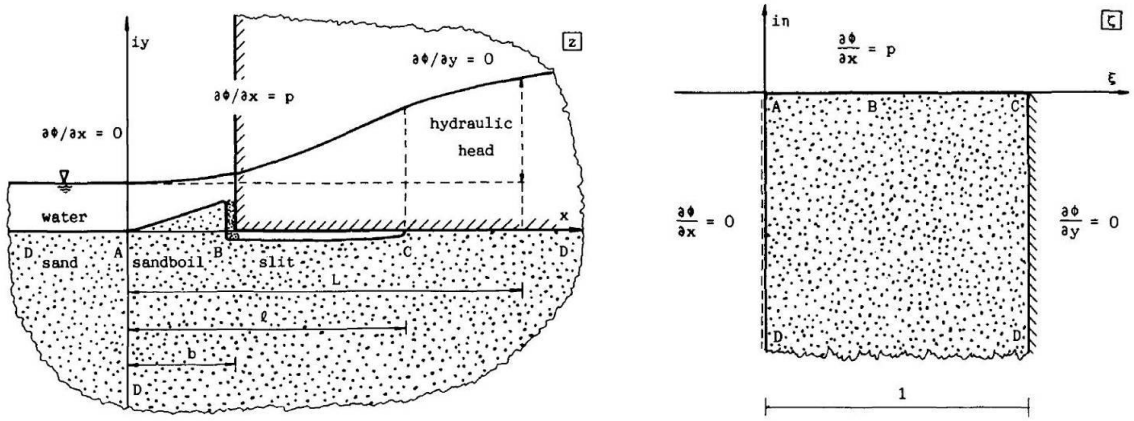

Figure 1-13 a picture of the geometrical plane with the boundary conditions which was studied by Sellmeijer in his PhD thesis (left) and the transformed geometrical plane (right) (Sellmeijer, 1988)

If the influence of the sand boil shown in Figure 1-13 is not taken into account, a singularity appears in the solution. This singularity is solved by taking into account the presence of the sand boil. The presence of the sand boil itself contributes very little to the calculated critical gradient. In the slit, Poiseuille flow is assumed. The equilibrium of grains on the bed is considered to be according to the model of White (White, 1939). In the model of White the grains are assumed to roll over each other in the model, resulting in a rolling resistance angle as a resistance parameter introduced by Sellmeijer. White considers the equilibrium of one single grain in a flow, unlike Shields who considers a surface where grain and flow properties are averaged out. The equilibrium of grains according to White is treated in more detail in chapter 3.

The equations of groundwater flow (LaPlace), flow in the slit (Poiseuille) and the equilibrium of grains on the bed of the slit (White) are considered the piping model suggested by Sellmeijer. First the so-called 4-forces model was considered, later this model was adapted to the 2-forces model. The formula for continuity of flow in the sand layer (LaPlace) is $\nabla^2\phi = 0$ (eq 1-5).

The formula for continuity of flow in the pipe (Poiseuille) is $a^3 \frac{\partial\phi}{\partial x} = 12\kappa \int \frac{\partial\phi}{\partial y} dx$ (eq 1-6).

The formula of equilibrium of the grains on the bed according to the 2-forces model (White) is $\frac{a}{d}\frac{\partial\phi}{\partial x} = \frac{\pi}{3}\eta\frac{\gamma'_p}{\gamma_w}\frac{\sin(\theta+\beta)}{\cos\theta}$ (eq 1-7).

With:
- a height of the slit
- d grain size
- x, y the horizontal and vertical coordinate
- ϕ the hydraulic head
- κ the intrinsic permeability
- η the coefficient of White
- γ'_p the (effective) particle density of the sand
- γ_w the density of water
- θ the rolling resistance angle
- β the slope of the pipe

The factor $\frac{\sin(\theta+\beta)}{\cos\theta}$ in (eq 1-7) reduces to $\tan(\theta)$ if the slope of the pipe is equal to 0°, which is the case in the idealized geometry, which is shown in Figure 1-5. It is not specified yet which mass percentile of the grain diameter d is normative. Sellmeijer concludes later, based on the erosion model of White, that D_{70} is the normative diameter. Unfortunately, it is not possible to solve the outcome of the relations between groundwater flow, flow in the slit and the equilibrium of grains on the bed of the slit analytically. In the program MSEEP these equations are implemented and a safety check on a dike can be done with MSEEP numerically. That's why Sellmeijer researched the relation between critical gradient and several dimensionless clusters of parameters with MSEEP. Based on this analysis, the design formula (which is explained in paragraph 1.3.3.) for the critical gradient is proposed by Sellmeijer.

As can be seen in Figure 1-14 the model shows a quasi-static equilibrium. For a certain gradient, a pipe will start to grow until a certain pipe length has been reached and an equilibrium situation has been reached. If the gradient is increased more, the pipe length will increase again, until a pipe length of roughly half the seepage length is reached. As can be seen in Figure 1-14, at this pipe length there is no equilibrium present. The gradient corresponding to this pipe length is called the critical gradient. Because there is no equilibrium, the pipe will grow until an open channel from entry point to exit point is present.

Later a geometry factor for the influence of the aquifer thickness was added (Sellmeijer, 1989). Then the formula is fitted on de Deltagoot tests to determine the rolling resistance angle.

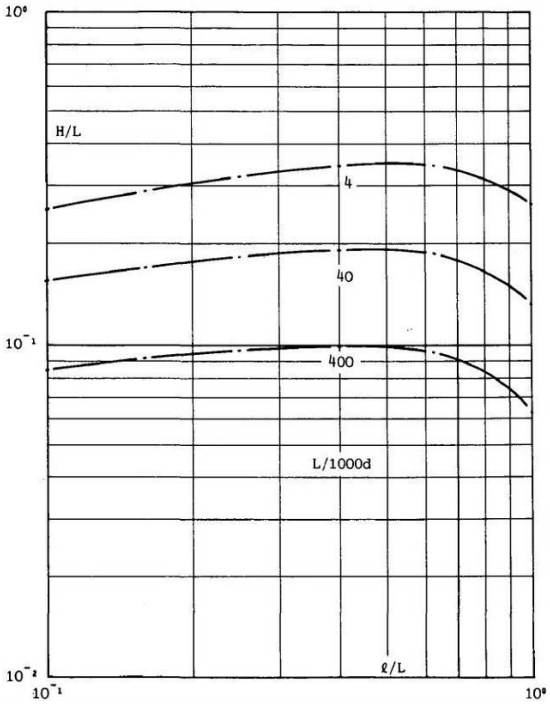

Figure 1-14 the maximum gradient as a function of the pipe length (Sellmeijer, 1988)

1.5 Available experimental data

Bligh and Lane did a lot of research, and figures of the data from Bligh is shown in appendix N, for the Bligh formula for fine and coarse sand.

De Wit has done experiments on piping from 1974 to 1982. Part of the test facility used by de Wit is shown in Figure 1-15.

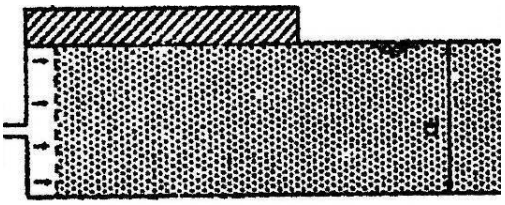

Figure 1-15 part of the test facility used by de Wit (de Wit, 1982)

The grain size used by de Wit varied from 220 to 1390µm. The values of the critical gradient against grain size for small-scale experiments are shown in Figure 1-16. The medium-scale experiments of de Wit show the same trend. Larger grain size results in a higher critical gradient, which is in agreement with the Sellmeijer formula and the formula of Bligh. When the piping started in the experiments, no quasi-static equilibrium was reached. More detailed information about the experiments of de Wit can be found in appendices A and B.

In the 90's, four full-scale test were done in de Deltagoot. These experiments were used to calibrate the rolling resistance angle of the sand grains. Only one sand type was tested. Information about de Deltagoot experiments can be found in appendices G and H.

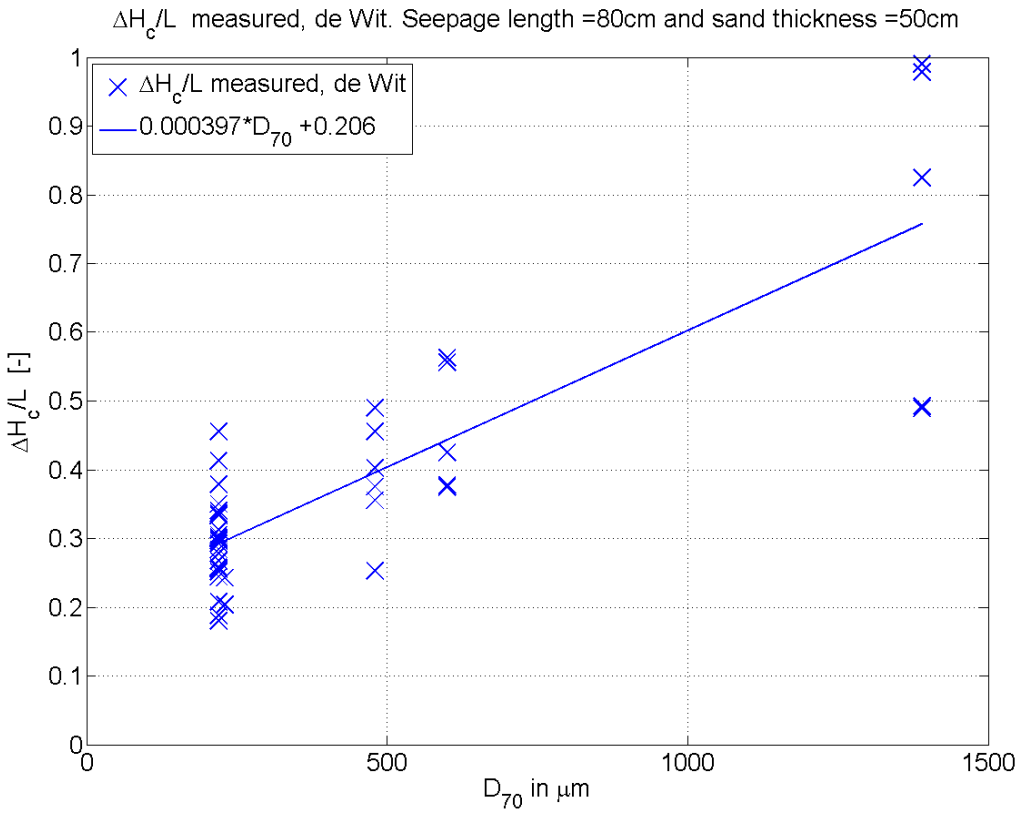

Figure 1-16 de Wit found a positive trend between D_{70} and critical gradient for small-scale experiments

From 2008 until 2010, in the context of the program SBW (Strength and Solicitation flood defences, Dutch: *Sterkte en Belastingen Waterkeringen*) Deltares performed a lot of research to failure mechanisms of flood defences. One of the failure mechanisms that was researched is the failure mechanism piping. In the laboratory of Deltares small-scale and medium-scale experiments were performed. At a test site in Booneschans, the Netherlands several full-scale experiments on piping were done. A new formula was derived from the outcome of the experiments. One of the (surprising) outcomes of the small-scale experiments was that coarse sand has a lower critical gradient than fine sand (see Figure 1-17). The outcome of the experiments do not agree with the formulas of Bligh, Lane and Sellmeijer. Until now, no conclusive explanation has been found for the observed negative trend. In this thesis, when SBW is mentioned, the piping part of SBW is meant. Detailed information about the experiments of SBW can be found in appendices C, D, E and F. The grain size (D_{70}) used by SBW varied from 154 to 431μm. Other surprising outcomes of SBW

include the process of forward erosion in the test facility when the sand has a low relative density, which appeared to be because of the absence of effective stresses in the test facility (van Beek, 2010b), and the high influence of the relative density on the critical head difference. When the piping started in the experiments, no quasi-static equilibrium was reached. In Figure 1-18 an overview of the small-scale test facility used for SBW is shown.

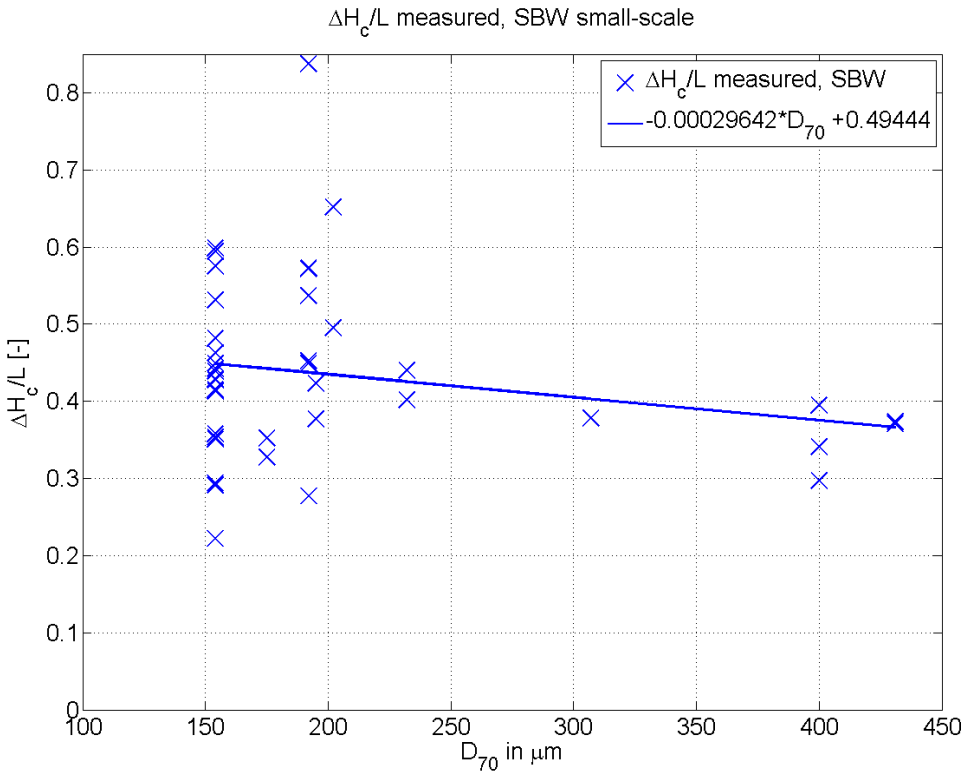

Figure 1-17 the critical gradient against the D_{70} for small-scale tests found by SBW

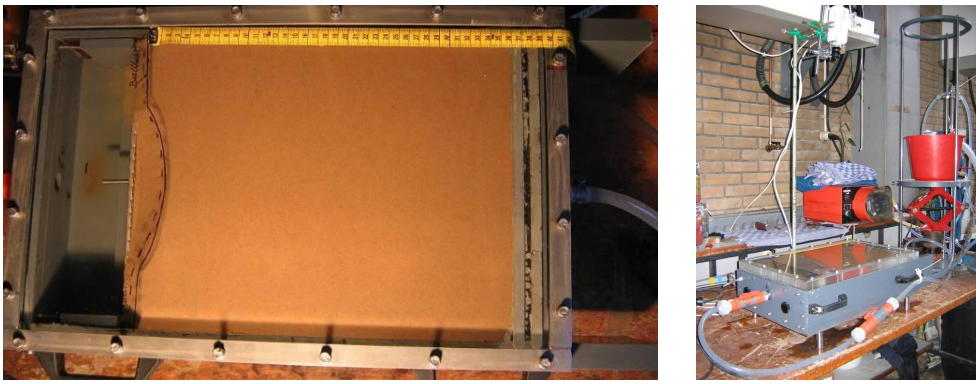

Figure 1-18 an overview of the test facility used for the small-scale SBW experiments

1.6 Problem description

To reduce uncertainties within the current piping rules used in the Netherlands, the project “SBW: Hervalidatie Piping” (Strength and Solicitation Flood Defences: Revalidation piping) was started (van Beek, 2009a). During tests on piping that have been done in the SBW framework, a negative trend between D_{70} and the critical head appeared. For the experiments on coarse sands, the current 2-forces Sellmeijer formula gave an unsafe prediction. The outcome of SBW is in contradiction with the current Sellmeijer formula and the formulas of Bligh (Bligh, 1910) and Lane (Lane, 1935) and it also goes against the current ideas of piping. Also, the outcome of the experiments showed the strong influence of the relative density (RD) on the piping process. At very low RD, an erosion mechanism other that the classic (backward) piping process occurred, the so-called forward erosion, which was attributed later to the absence of effective stresses in the test facility (van Beek, 2010b). The RD is not taken into account in the formulas of Bligh and Sellmeijer, although the RD influences the permeability, which is included in the Sellmeijer formula.

A multi-variate analysis (MVA) has been performed by (López de la Cruz, 2009) on the data from the SBW experiments to find the influence of variables on the critical gradient. It was found the influence of D_{70} is less that is predicted with the Sellmeijer model. The influence of permeability agrees with the Sellmeijer model.

1.7 Problem definition

At this moment, there is no proper explanation for the difference between the influence of D_{70} on the critical head that was found in the SBW experiments and the critical head according to the Sellmeijer formula. The influence of D_{70} on the critical gradient that has been found in SBW arouses suspicion and lessens the robustness about the current formulas that are used or about the SBW experiments that have been performed.

1.8 Objective of the research

As stated in the problem description, an explanation is needed for the difference between the SBW results and the Sellmeijer formula, regarding the influence of D_{70} on the critical gradient. The relation between D_{70} and the critical head and the influence of several other variables on the critical gradient must be investigated. The objective of this masters thesis is to research the influence of the grain size and other sand characteristics on the critical gradient of piping, and to find an explanation for the difference found between SBW results and the Sellmeijer formula.

1.9 Approach of the research

1) Literature study

In paragraph 1.3 references are made to several researchers. Data from several researchers was found and is used for the variable study. From the literature, it was found how researchers came to their conclusions about the influence of variables on the critical gradient.

2) Variable study and validation negative trend.
The influence of variables is investigated. Amongst others, a multi variate analysis (MVA) is performed. With a MVA, the influence of a deviation of a variable with respect to the variable's mean on the critical head can be investigated. A MVA has already been done on the data of SBW by (López de la Cruz, 2009). A MVA is done on de Wit's experimental outcomes, so a comparison between the two datasets can be made. Correlations between variables must be taken into account, where distinction must be made between statistical correlations and causality.

3) Hypothesis of possible causes of the reduced influence of D_{70} on the critical gradient. Several hypothesis can be named. In this thesis the following hypothesis is researched.

Transport and erosion mechanism
In the model of Sellmeijer, a mathematical description of the equilibrium of the individual sand grains is made. In Sellmeijer's model, the grains are assumed to roll over each other, according to the erosion model of White. In this model the equilibrium of the grains is checked based on rolling grains. The resistance against rolling is modeled with the resistance parameter θ, the rolling resistance angle of the grains. It is unclear if the piping process shows indeed the described behaviour. The erosion mechanism may be different than was assumed. The grains may flow like a thick fluid, where a lot of grains are transported at the same time. This process was also observed by Schmertmann (Schmertmann, 2000). The grains at the beginning of the pipe may slide down and erode in another manner than the equilibrium described by White. This should be investigated with experiments. A test facility can be made to investigate and observe the piping process from the side. The piping process can be observed from the side, to gain insight in the transport and erosion mechanism. A test facility has to be designed and built for this experiment. This one-dimensional test facility is described in paragraph 3.4.

Besides the mean objective of this thesis, a theoretical research of the relation between variables in the channel has been done. With use of the equations of continuity, Poiseuille and White described in paragraph 1.4, research is done at the relation between variables in the channel. This is not the mean objective of this thesis, but some very interesting aspects of piping are researched.

1.10 Outline report

The outline of the report can be schematized according to Figure 1-19.

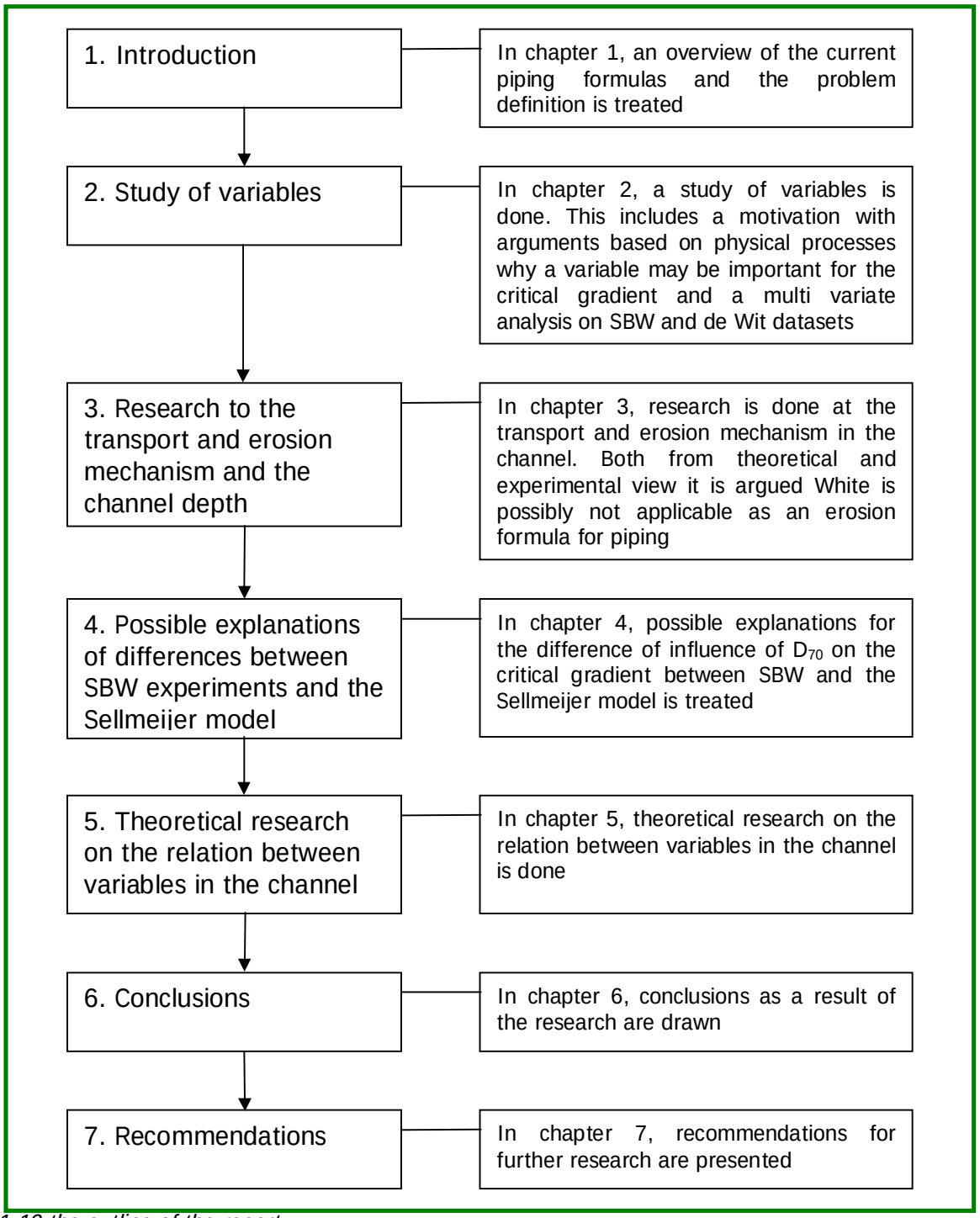

Figure 1-19 the outline of the report

2. Study of variables

In this chapter a study is done to find the influence of the grain size and other sand characteristics on the hydraulic gradient of piping based on experimental outcomes. This study is done on the outcomes of SBW's and de Wit's experiments. The study on SBW's experiments is amongst others to verify the influence of variables on the critical gradient that was found, and the study on de Wit's experiments is done to make a comparison possible between SBW's and de Wit's experimental outcomes.

One of the tools to find the influence of these variables is to perform a multi variate analysis (MVA). With the MVA the exponential influence of a deviation of a variable with respect to the variable's mean on the critical gradient can be determined. It answers the question, if a certain input variable is X% higher than the mean of that input variable, what happens with the output variable?

If the outcome of the MVA on both datasets support each other, this will increase the reliance of the experiments. If the outcome of the MVA on both datasets contradict each other, a cause must be found for the different influences of the variables.

The measured values of medium-scale and full-scale experiments are compared with the predictions with the adapted Sellmeijer formula (which is explained later), so that validation or disapprovement of the outcome of the MVA on small-scale experiments can be done, as trends in the test facility need not to be present in case of a real dike.

A MVA has been performed by López de la Cruz on the small-scale dataset of SBW to find the influence of the variables on the critical head, so that an adapted Sellmeijer formula could be developed (López de la Cruz, 2009, Sellmeijer, 2010a). This adapted Sellmeijer formula is explained in paragraph 2.1. Sellmeijer derived this new formula to account for the influences of certain variables, which have a different influence in the SBW test facility than is present in the current 2-forces Sellmeijer formula. Deriving a new formula is not the objective of this thesis, but to find the influence of several variables in the datasets of de Wit and SBW, some of the same steps which were done by López de la Cruz and Sellmeijer to derive the new formula have to be taken.

In paragraph 2.2 some statistical definitions used in this chapter are explained. The variables which are considered to have an influence on the piping process are described in paragraph 2.3. The MVA is explained in detail in paragraph 2.4.

In paragraph 2.5 and 2.6, the MVA is performed on the dataset of SBW and de Wit, respectively. Conclusions and a summary about the study of variables is given in paragraph 2.7.

2.1 The adapted Sellmeijer formula

According to Sellmeijer the current 2-forces Sellmeijer formula (eq 1-4) as discussed in paragraph 1.3.3 agrees quite well for fine sands (Sellmeijer 2010a). Sellmeijer based this on the outcome of several full-scale tests, as de Deltagoot experiments, which are explained in detail in appendix G and H, and de IJkdijk experiments, which are explained in detail in appendix E and F. For coarser sand, the current 2-forces formula does not perform well and gives an unsafe prediction. To create a new formula, the current 2-forces formula was taken and multiplied with certain factors. The influence of these factors are determined with a multi variate analysis on the SBW dataset, done by López de la Cruz (López de la Cruz, 2009). For the variables that are considered the most important for the critical head difference, a multi variate analysis (MVA) on the SBW small-scale experiment results has been done. The small-scale test facility is shown in Figure 2-1. Appendix C gives a more detailed description of the test facility.

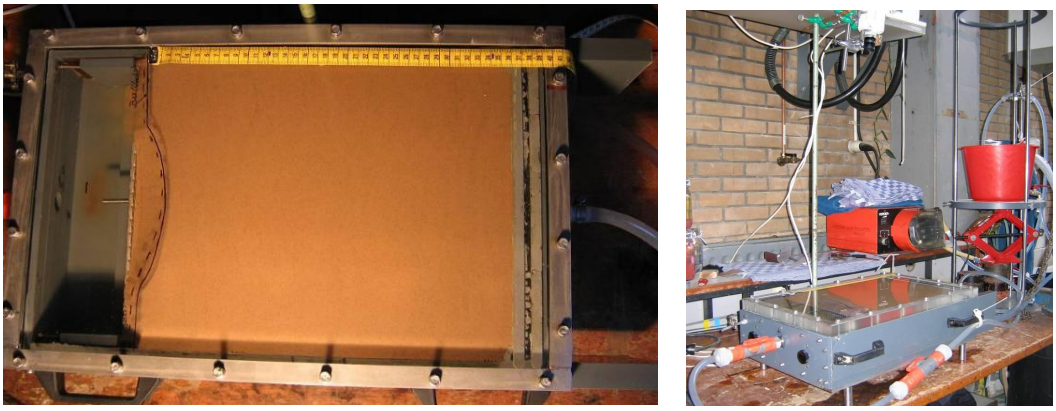

Figure 2-1 a top view and an oversight view of the test facility filled with sand (van Beek, 2009c)

The current Sellmeijer 2-forces formula is defined as follows (treated in paragraph 1.3.3, (eq 1-4)).

$$\frac{H_c}{L} = F_R F_S F_G \qquad F_R = \frac{\gamma'_p}{\gamma_w}\eta \tan(\theta) \qquad F_S = \frac{D_{70}}{\sqrt[3]{\kappa L}} \qquad F_G^{\text{standard dike}} = 0.91\left(\frac{D}{L}\right)^{\frac{0.28}{\left(\frac{D}{L}\right)^{2.8}-1}+0.04}$$

With the following parameters
$\eta = 0.25$, $\gamma_w = 10\ kN/m^3$, $\gamma'_p = 16.5\ kN/m^3$ and $\theta = 37°$.

The proposed adapted formula by Sellmeijer is as follows.

The current 2-forces formula, $\frac{H_c}{L} = F_R\, F_S\, F_G$, is multiplied with several normalized factors of variables which are not included in the current formula, such as $(\frac{RD}{RD_{mean}})^{\beta}$, $(\frac{C_u}{C_{u,mean}})^{\varepsilon}$ and $(\frac{KAS}{KAS_{mean}})^{\theta}$. The variables D_{70} and κ which are already included in the current model, are replaced by $D_{70,mean}$ and κ_{mean}, and the model is multiplied with the factors $(\frac{k_{Darcy}}{k_{Darcy,mean}})^{\gamma}$ and $(\frac{D_{70}}{D_{70,mean}})^{\delta}$. F_R, F_S and F_G are defined according to the current 2-forces model, and all the mean values mentioned are the mean values of the SBW small-scale dataset. The regression coefficients $\beta, \gamma, \delta, \varepsilon$ and θ were determined with a MVA on the SBW small-scale data. Since the regression coefficient of κ found by López de la Cruz was -0.35, and this agrees with the $\frac{1}{\sqrt[3]{\kappa}}$ which is present in the current 2-forces Sellmeijer formula, and the influence of the permeability is the variable the least concern was about, the intrinsic permeability is not changed in the adapted formula. The best fit for the small-scale dataset of SBW found by López de la Cruz is:

$$\frac{H_c}{L} = \left[\frac{H_c}{L}\right]_{mean} \left[\frac{RD}{RD_{mean}}\right]^{0.35} \left[\frac{C_u}{C_{u,mean}}\right]^{0.13} \left[\frac{KAS}{KAS_{mean}}\right]^{-0.02} \left[\frac{\kappa}{\kappa_{mean}}\right]^{-0.35} \left[\frac{D_{70}}{D_{70,mean}}\right]^{0.39} \quad \textit{(eq 2-1).}$$

It is mentioned, (eq 2-1) is not a piping formula, it is a best fit for the small-scale SBW dataset found by López de la Cruz.

The proposed formula by Sellmeijer is formulated below (Sellmeijer, 2010a).

$$\frac{H}{L} = F_R\, F_S\, F_G$$

$$F_R = \eta \frac{\gamma'_p}{\gamma_w} \tan\theta \left(\frac{RD}{RD_{mean}}\right)^{0.35} \left(\frac{U}{U_{mean}}\right)^{0.13} \left(\frac{KAS}{KAS_{mean}}\right)^{-0.02} \quad \textit{(eq 2-2)}$$

$$F_S = \frac{d_{70,mean}}{\sqrt[3]{\kappa L}} \left(\frac{d_{70}}{d_{70,mean}}\right)^{0.39} = \frac{d_{70}}{\sqrt[3]{\kappa L}} \left(\frac{d_{70,mean}}{d_{70}}\right)^{0.61}$$

$$F_G = 0.91 \left(\frac{D}{L}\right)^{\frac{0.28}{\left(\frac{D}{L}\right)^{2.8}-1}+0.04}$$

In Figure 2-2 the adapted Sellmeijer formula (eq 2-2) is shown. In Figure 2-3 a comparison of the current (eq 1-4) and the adapted Sellmeijer formula (eq 2-2) is shown, for a constant RD, C_u and KAS. As can be seen, the trend as a function of grain diameter is opposite for the two formula's. In Figure 2-4 the current (eq 1-4) and the adapted Sellmeijer formula (eq 2-2) are also compared with each other for a constant RD and KAS. The critical gradient is plotted against the D_{70} and C_u. The

curve with a positive trend is the current Sellmeijer formula, the curve with a negative trend is the adapted Sellmeijer formula. Figure 2-3 is a cross-section of Figure 2-4 in the plane C_u=2.

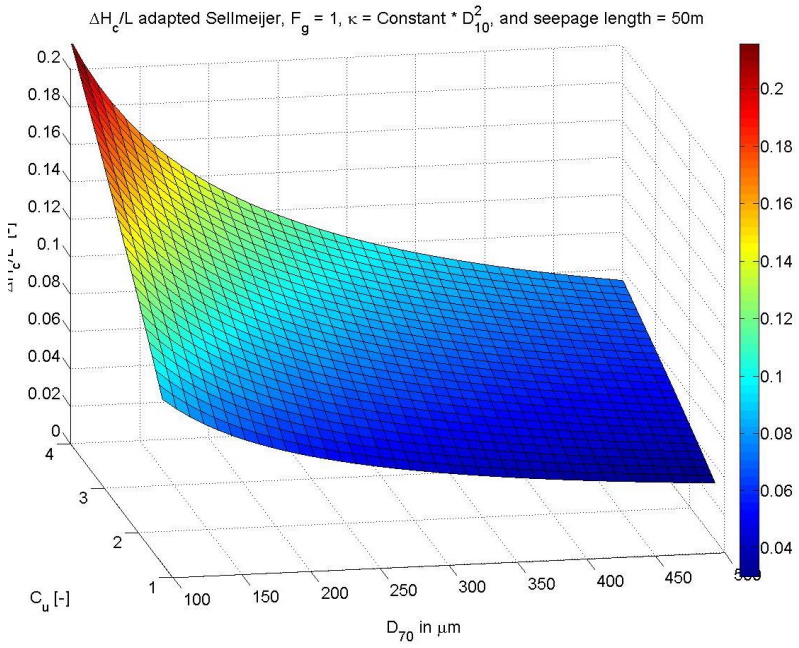

Figure 2-2 the critical gradient as a function of D_{70} and C_u according to the adapted Sellmeijer 2-forces formula, for a constant RD and KAS

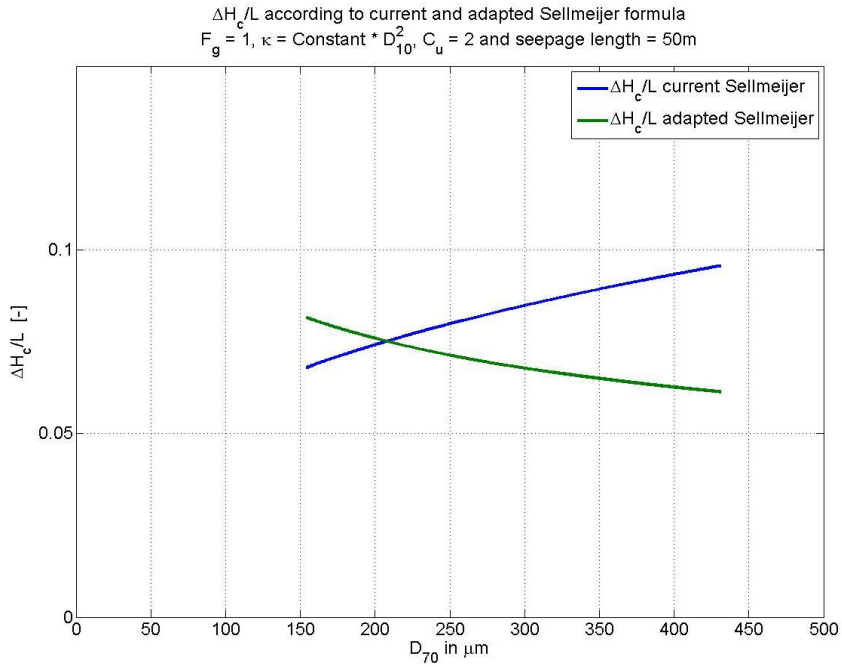

Figure 2-3 the current and the adapted Sellmeijer 2-forces formulas, for a constant RD, KAS and C_u

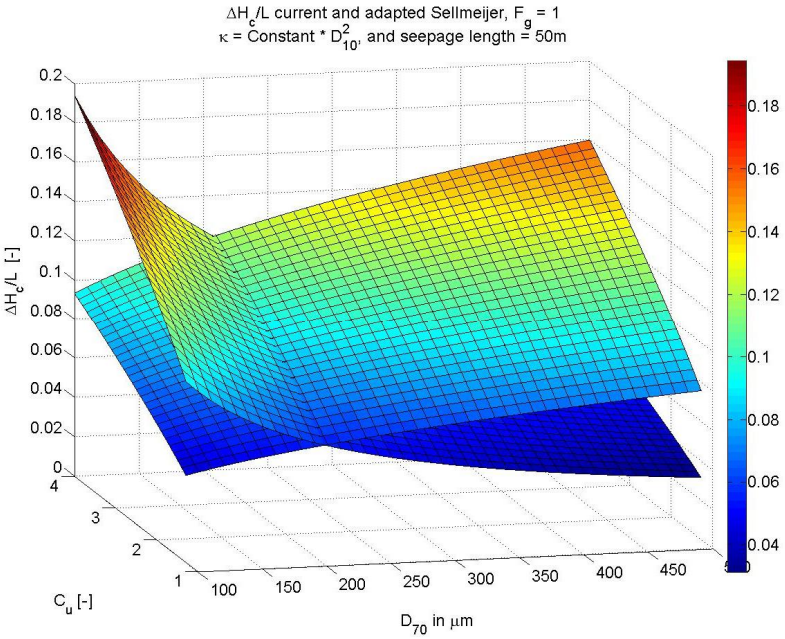

Figure 2-4 the critical gradient as a function of D_{70} and C_u according to the current and adapted Sellmeijer 2-forces formula, for a constant RD and KAS

It has been proposed by López de la Cruz that since the influence of KAS is negligible and the influence of C_u is also quite small, these factors can be left out of the proposed equation (López de la Cruz, 2009).
To derive a new piping formula based on a MVA, certain steps need to be followed. These steps are summarized in the flow chart shown in Figure 2-5. Formulation of a new piping formula is not the objective of this thesis, because this has already been done by Sellmeijer (Sellmeijer, 2010a). In this thesis, the influence of the grain size and other relevant variables on the critical head is researched. This can be done by following the same procedure as shown in Figure 2-5. First a MVA on the small-scale experiments has to be performed. The outcome of the MVA on medium-scale and full-scale experiments should not contradict the outcome of the MVA on the small-scale dataset. If the MVA is also done on the data of the experiments done by de Wit, a comparison can be made with the outcome of the MVA on SBW data.

The MVA on the SBW data has been redone in this thesis because of the following reasons.

- The constant is kept fixed in the MVA (López de la Cruz, 2009). It seems more appropriate to keep the constant not fixed in the MVA
- Three values of the critical head used by (López de la Cruz, 2009, Sellmeijer, 2010a) did not agree with the values in the factual reports

- The seepage length in the MVA was kept fixed as 34cm by (López de la Cruz, 2009, Sellmeijer, 2010a), while according to the factual reports the seepage length in the experiments of SBW varied between 32.5 and 34.5cm
- Variables which contribute only to a less extent according to the MVA, can be excluded, as can be done for the KAS and the C_u, but the MVA must be redone to redistribute the influence of the less important variable over the important variables and the constant. This has not been done by (López de la Cruz, 2009, Sellmeijer, 2010a)
- If more experiments are done and added to the dataset, the MVA must be redone anyway. It was the intention that, as part of this thesis, experiments should be performed on coarse grained sands. Unfortunately, during the period of the thesis, the sands were not delivered and experiments could not be carried out

By performing a MVA on the data of SBW, the influence of the variables on the critical gradient can be investigated. This may confirm or reject the negative trend between D_{70} and critical gradient found by López de la Cruz. A comparison with the de Wit data can also be done.

The experiments were performed on homogeneous sands, so that permeability and D_{70} are correlated. In reality multiple layers of sand can be present, so that the permeability of the lower layer and the D_{70} of the top layer can be less or even uncorrelated.

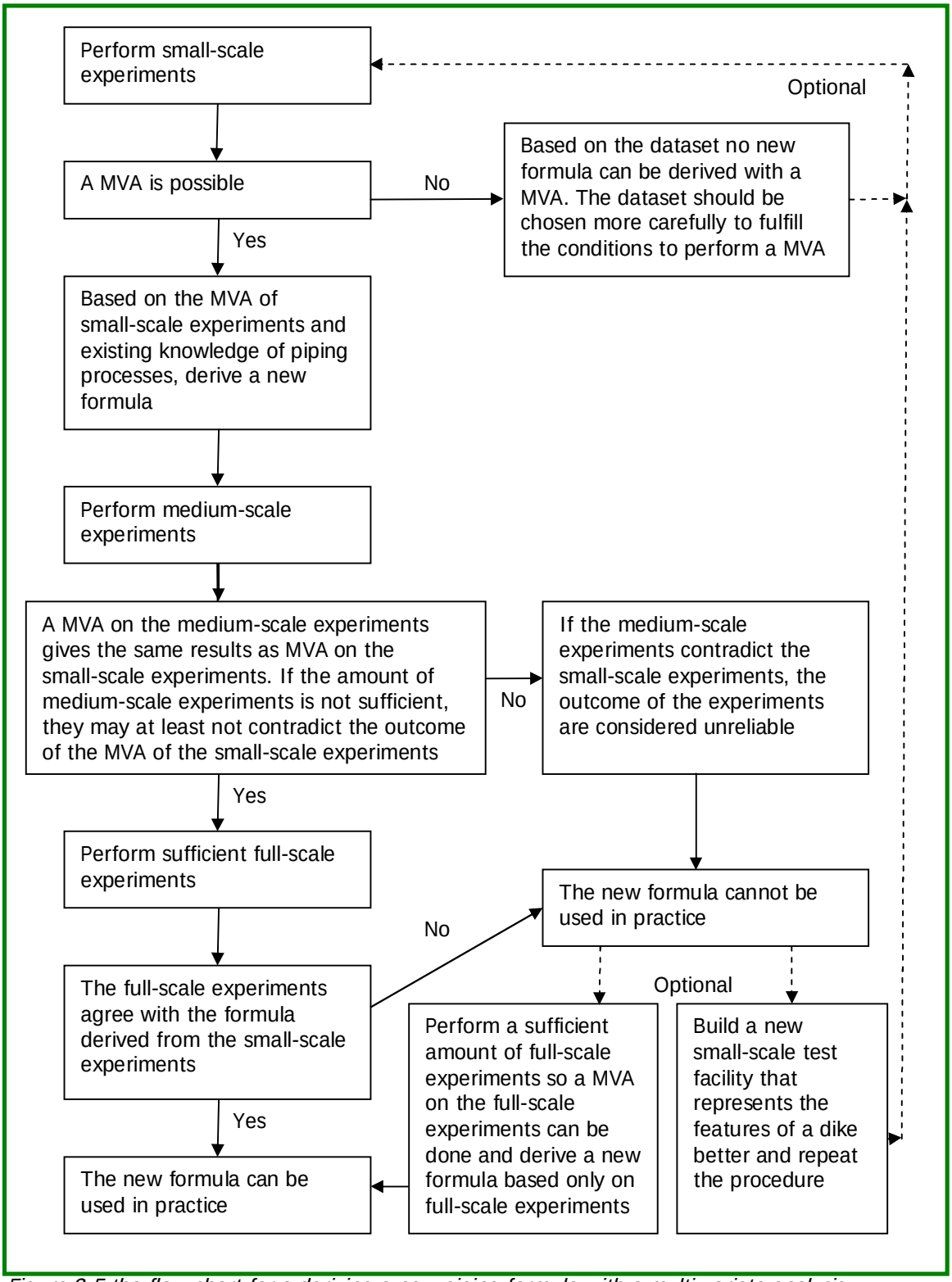

Figure 2-5 the flow chart for a deriving a new piping formula with a multi variate analysis

2.2 Statistical definitions used in this chapter

If y=f(x), y is called the dependent variable and x is called the independent variable in mathematics. Dependency between variables means something else, it has a statistical meaning. To clearly distinguish between the two meanings of dependency, the following nomenclature is used in this chapter.

- If y=f(x), the independent variable x is called the input parameter
- If y=f(x), the dependent variable y is called the output parameter
- By dependency and independency, statistical (in)dependency is meant

Statistical (in)dependency is defined as follows. If E[AB] = E[A]E[B], A and B are independent, where E is the expectation operator. If E[AB] ≠ E[A]E[B], A and B are dependent, and correlation is defined as linear dependency. The correlation coefficient $\rho(A,B) = \frac{\mathrm{cov}(A,B)}{\sigma(A)\sigma(B)}$ is a measure of linear dependency, where cov(A,B) is the covariance between A and B, cov(A,B) = E(A-E[A])E(B-E[B]) and σ is the standard deviation. Note: correlated variables are dependent, as uncorrelated variables need not to be independent. The interpretation of the correlation coefficients is somewhat arbitrary as it depends on the quality, quantity and the techniques used to gather the data. However, an indication how large the relation is between the variables can be interpreted as shown in Table 2-1.

Table 2-1 the interpretation of the correlation coefficient

influence	negative correlation coefficient	positive correlation coefficient
negligible	-0.1 to 0.0	0.0 to 0.1
small	-0.3 to -0.1	0.1 to 0.3
medium	-0.7 to -0.3	0.3 to 0.7
large	-1.0 to -0.7	0.7 to 1.0

In Figure 2-6 two fictitious datasets are plotted. Dataset A has uncorrelated variables and dataset B has correlated variables. By inspecting a plot where two variables are plotted against each other, it can be seen directly if the variables are correlated in a high extent or not.

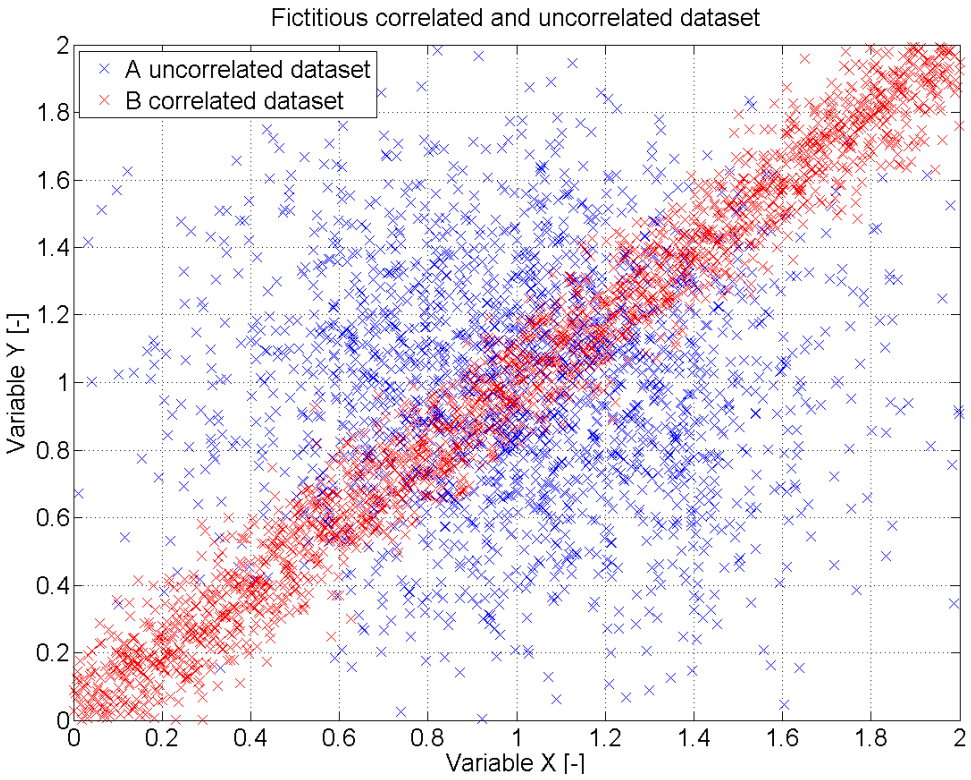

Figure 2-6 two fictitious datasets. The one has correlated variables, the other has not

2.3 Description of the variables

In this paragraph, an overview is given of the variables that are included in the study of variables in this thesis.

The following variables have been considered in the study of variables.

- The permeability based on Darcy's Law (k_{Darcy})
- The 70th percentile of the grain diameter (D_{70})
- The coefficient of uniformity, ($C_u = \frac{D_{60}}{D_{10}}$)
- The relative density (RD)
- The roundness of the grain particles (KAS)

These variables are chosen because there are known (but also unknown) physical influences (expected) of these variables on groundwater flow and erosion of the grains.

The physics behind the variables is explained further.

The grain size of the larger grain fraction (D_{70}) is a kind of a resistance variable. Coarser grains are more difficult to erode and transport, because of the higher mass. The D_{70} is defined as the 70th mass percentile of a sand sample passing through a sieve with mesh size D. The D_{70} is chosen as representation of the grain fraction which resists erosion. For a given sand sample, a sieve diagram can be made. In Figure 2-7 a sieve diagram of Baskarp sand is shown. Baskarp sand is used often in SBW experiments.

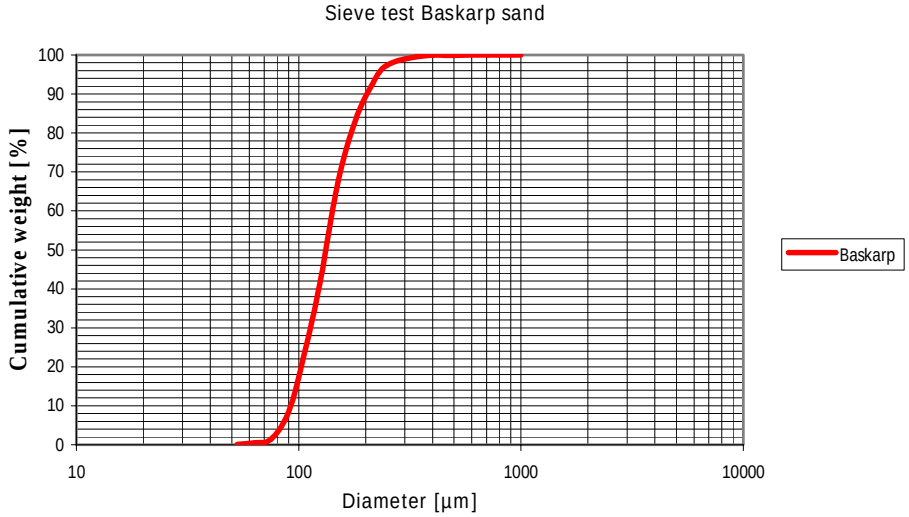

Figure 2-7 the sieve diagram of Baskarp sand

The permeability (k_{Darcy}) is a kind of load variable, as a higher permeability leads to a higher erosion capacity. The permeability k_{Darcy} of the samples of SBW is determined from Darcy's law, $Q = kA\frac{dh}{dx}$. The discharge was measured during the experiments. Together with the head difference and the dimensions of the test facility, k_{Darcy} can be determined. k_{Darcy} has the dimension m/s. This is not the average velocity of the pore water. The velocity is a factor $1/n$ higher, where n is the porosity. The intrinsic permeability κ, which is used in the Sellmeijer formula, can be calculated with the formula $\kappa = k\frac{\nu}{g}$ where g is the gravitational acceleration, g = 9.81m/s^2 and ν is the kinematic viscosity, which is in the order of 10^{-6}m^2/s for water, depending on the temperature. For the multi variate analysis (MVA) it does not matter if k or κ is used, since $\kappa = k\frac{\nu}{g}$, $\frac{\kappa}{\kappa_{mean}} = \frac{k\frac{\nu}{g}}{k_{mean}\frac{\nu}{g}} = \frac{k}{k_{mean}}$.

Arbitrarily, k is used for the MVA.

The coefficient of uniformity, $C_u = \frac{D_{60}}{D_{10}}$, is the ratio of the larger grain fraction and the smaller grain fraction, where D_{60} and D_{10} are defined as the 60th and 10th mass percentile of a sand sample passing through a sieve with mesh size D.

The relative density (RD) defines how tight or loose soil is packed. The relative density influences the resistance, as tighter packed grains are (presumably) more difficult to erode than loose packed grains. The RD is calculated by $RD = \frac{n_{max} - n}{n_{max} - n_{min}} * 100\%$ where n is the porosity. A RD of 100% represents a very tight packing and a RD of 0% represents a very loose packing. RD's of more than 100% or less than 0% are possible, because n_{max} and n_{min} are determined according to certain definitions, in the laboratory. In reality, other circumstances than those that are present in the laboratory are possible in nature, which can lead to RD's of more than 100% or less than 0% (Lubking, 2010).

In Figure 2-8 a loose and a tight packing are shown.

Figure 2-8 a very loose packing (left) and a very tight packing (right) (Verruijt, 2001)

The angularity (roundness) of the grain particles (KAS) is included in the study because round grains (presumably) roll easier over the bed of the channel than non-round grains, and non-round grains may interlock in each other, which may create some kind of extra resistance. The angularity of the grains is expressed in the value of KAS. A low value of KAS corresponds with very angular grains. A high value of KAS corresponds with very round grains. The KAS values range from 0 to 100. The determination of the KAS value of a sand sample is done visually. Kruse gives a more detailed description on how to determine the KAS value (Kruse, 2008). In Figure 2-9 the definition of KAS value is given.

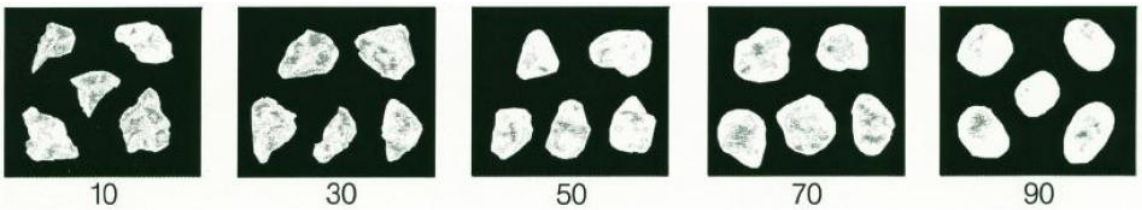

Figure 2-9 the definition of KAS value (van Beek, 2009a)

Some variables are related to each other, as for example permeability depends on grain size and RD. In the following text the dependency is explained in further detail.

Permeability is strongly dependent of the smaller grain fraction, the D_{10}. With the formula of Beyer or Hazen, the permeability can be calculated quite easily, $k \approx C * D_{10}^2$. It is the D_{70} of the sand which determines the resistance against erosion in the channel and the D_{10} determines the groundwater flow (load) in the sand.
Since D_{70} and D_{10} are correlated, load and resistance are also correlated. In Figure 2-10 a small and a big grained sand sample is shown (in reality the grains do not have a constant grain size, the figures are of illustrative use only). The big grains are heavier and are more difficult to transport with respect to the smaller grains, but the permeability is also higher with the big grains, as the pore dimensions are also larger than the pore dimensions of the finer grains. Note that in Figure 2-10 the sand samples shown have the same porosity, but not the same permeability.

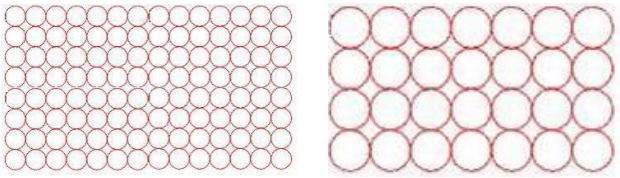

Figure 2-10 fine grained sand with a low permeability (left) and coarse grained sand with a high permeability (right) (Verruijt, 2001)

In Figure 2-11 a figure of a more realistic sand sample with diverse grain sizes is shown (although some of the grains appear to be “floating”, which in reality is obvious not the case).

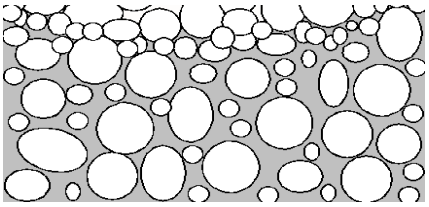

Figure 2-11 small and big sized grains in one sample (Schiereck, 2004)

The permeability is, besides the D_{10}, also dependent of RD, especially for fine grained sands, as can be seen in Figure 2-12. In this figure the permeability is shown as a function of D_{10} and relative density. The “C_r” and “type” mentioned in the figure refer to the gradation (defined differently than C_u) and the shape of the sieve curve respectively. (More information about these definitions can be found in (Hunt, 2005)).

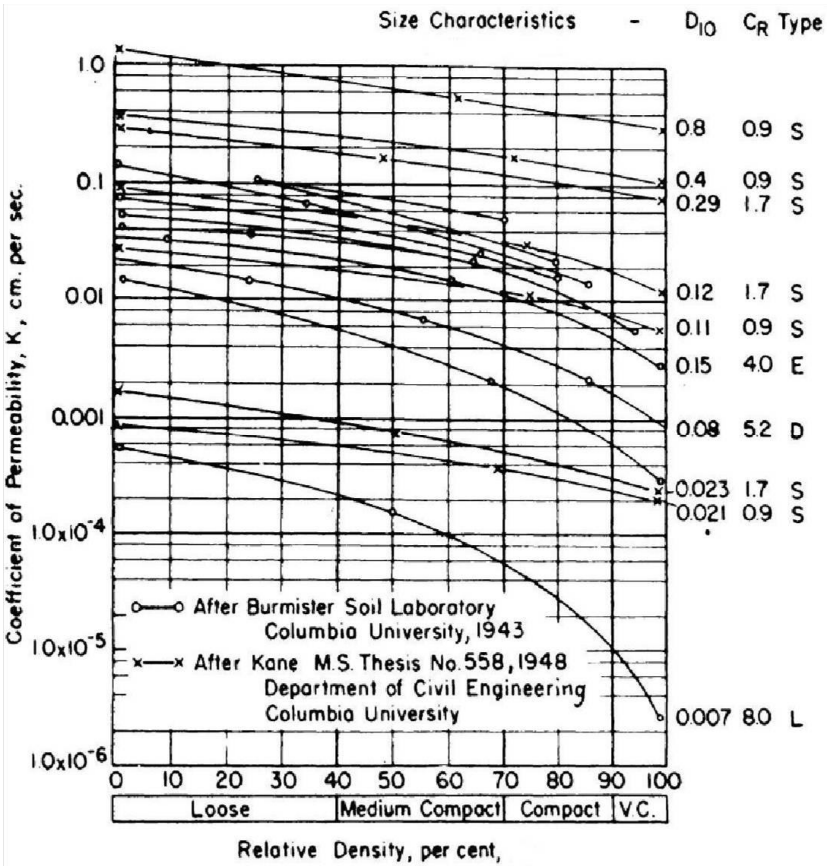

Figure 2-12 the permeability as a function of D_{10} and RD (Hunt, 2005)

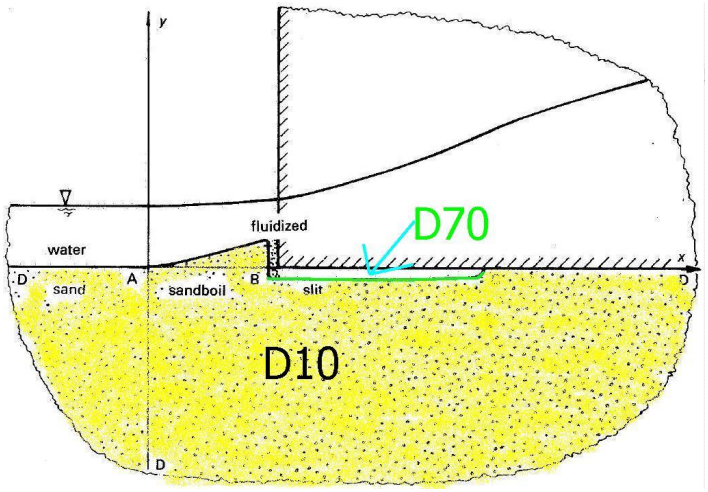

Figure 2-13 part of the model of the piping process under a dike (Sellmeijer, 1988, the colours are added in this thesis)

It is important to realize where the different grain sizes are determining the piping process. In Figure 2-13 a part of the model considered by Sellmeijer is shown. In

the sand body itself (yellow part), it is mostly the D_{10} which determines the piping process, since the D_{10} determines the ground water flow. In the slit, on the interface between the water flow and the sand (green line), it is mostly the D_{70} which determines the piping process, since the D_{70} determines the erosion process.

2.4 Multi variate analysis

(Sellmeijer, 2010a) proposes an adapted 2-forces Sellmeijer formula. In this adapted formula, the current 2-forces model is extended with several factors of variables as explained earlier. Some of these factors include the influence of several variables which were not included in the current model and some factors alter the influence of variables which were already present in the current Sellmeijer formula. These factors are determined from a multi variate analysis (MVA) on the SBW small-scale tests. With the MVA, the so-called regression coefficients of these variables were found. The dataset must fulfill certain requirements if a MVA is performed on it. The requirements are shown in the flow chart in Figure 2-14. The MVA is explained below. With a MVA, the exponential influence of a deviation of an input variable with respect to the input variable's mean on the output variable can be determined. A (linear) MVA has the following form.

$$Y = e^{\alpha}\left(\frac{X_1}{X_{1,\,mean}}\right)^{\beta}\left(\frac{X_2}{X_{2,\,mean}}\right)^{\gamma}\left(\frac{X_3}{X_{3,\,mean}}\right)^{\delta}\ldots + error\ term \qquad \textit{(eq 2-3).}$$

Where Y is the output variable and X_i are the input variables, e^{α} is a constant and the error term represents the variation in the output variable that cannot be captured by the input variables (Garson, 2009, López de la Cruz, 2009). α, β, γ and δ are the regression coefficients. In the formula of the MVA, X_i are present as linear terms. In this report, when X_i appear linearly in the formula, this is called a linear MVA.

If the formula has the following shape,

$$Y = e^{\alpha}\left(\frac{f(X_1)}{f(X_{1,\,mean})}\right)^{\beta}\left(\frac{g(X_2)}{g(X_{2,\,mean})}\right)^{\gamma}\left(\frac{h(X_3)}{h(X_{3,\,mean})}\right)^{\delta}\ldots + error\ term \qquad \textit{(eq 2-4).}$$

Where f, g and h are non-linear functions, this is called a non-linear MVA in this report. Non-linear MVA's are quite difficult and a lot of verifying is needed to ensure no errors are made.

When inserting the dataset in the formula of the MVA, with algebra the best fit of the formula with the dataset is determined with the least squares method. The outcome of the MVA is valid for the dataset it was performed on, thus in this case for the small-scale test facility and not for a real dike.

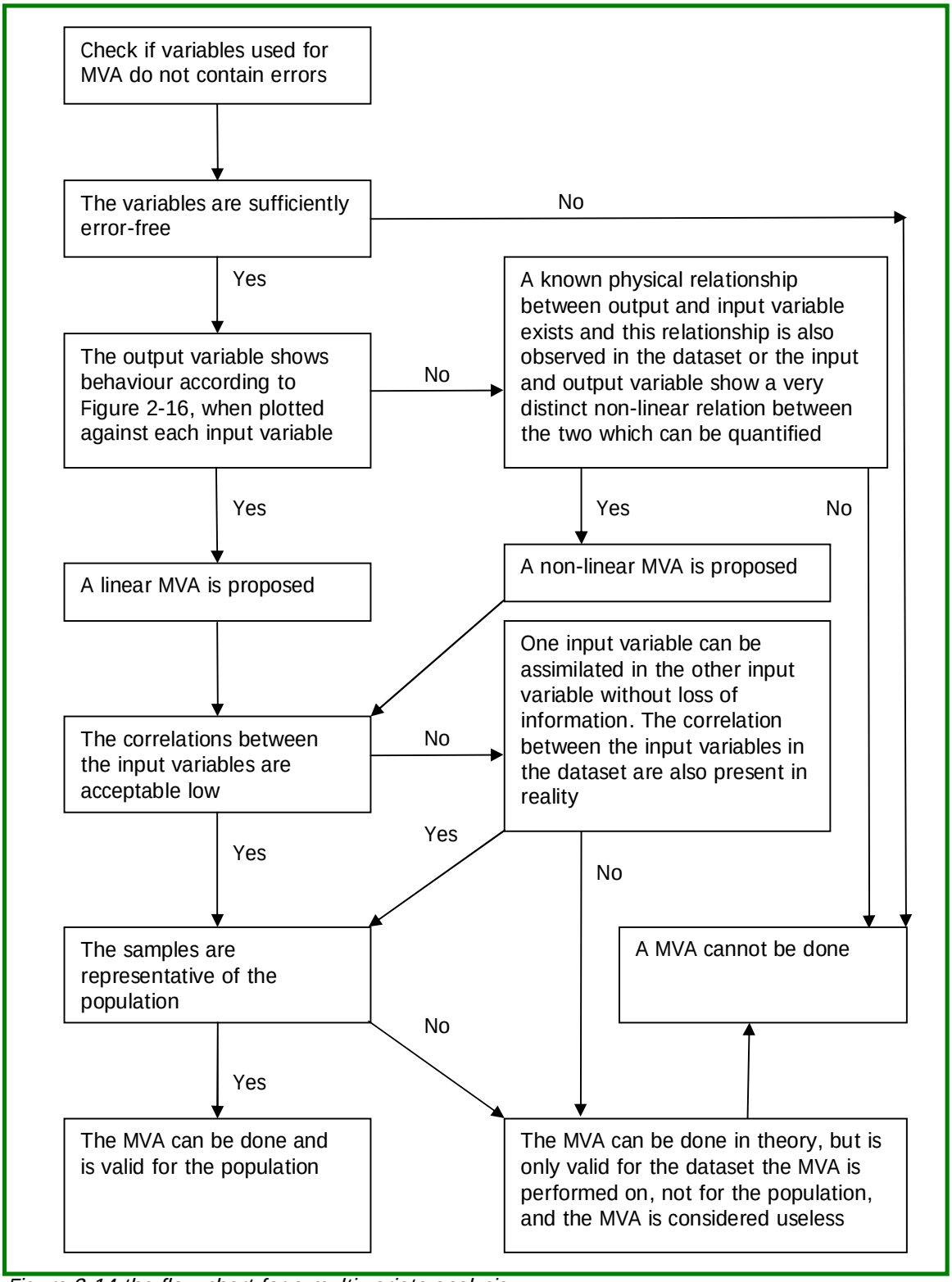

Figure 2-14 the flow chart for a multi variate analysis

It is clear, the outcome of the MVA on the small-scale dataset is valid only for the small-scale test facility. The model (test facility) and the reality (a real dike) may not be considered to be the same. The most important key concept of modeling is as follows: A model and its results should not be identified with reality. Allocating the outcome of the analysis of a model to a real problem can be (very) hazardous. Figure 2-15 shows the pitfall which should be avoided. Also the results of the SBW experiments are of an empirical nature as no physical foundation is available yet. Also the results are valid in the range of the variables which were used for the experiments.

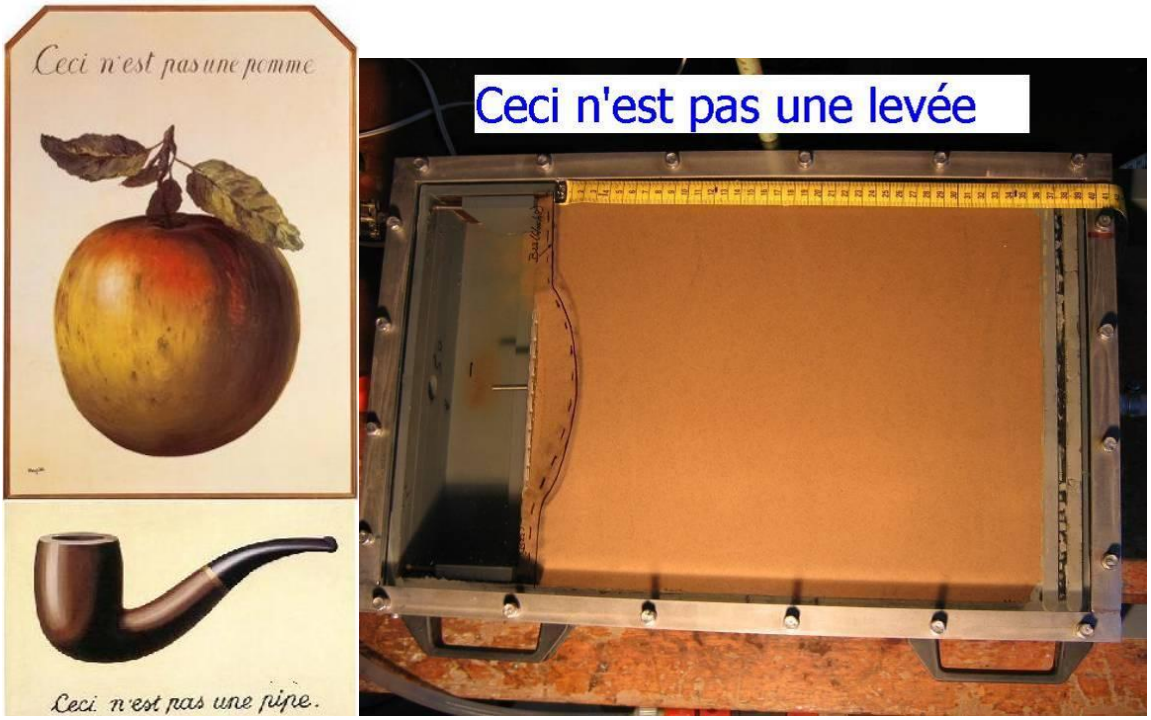

Figure 2-15 the test facility is not a dike, it is a model of a dike, and the outcome of the model may not be considered to be true for a real dike (picture of pipe and apple: René Magritte)

The small-scale experiments can be used to investigate if some unexpected behaviour occurs with respect to the current ideas about piping, such as the observed forward erosion, the decreased influence of D_{70} and the strong influence of the RD on H_c, but the numerical outcome of analysis on small-scale tests can not directly be used for a new rule for real dikes. The outcome of small-scale data analysis applies to the small-scale test facility, not to a real dike. However, a formula can be derived with a combination of existing knowledge about piping, and the outcome of small-scale, medium-scale and full-scale experiments, only this new formula should be verified by sufficient medium-scale and full-scale experiments. Only if the medium-scale and the full-scale experiments prove the new model is correct, the new formula may be used. Finding a new formula is not

the objective of this thesis, finding an explanation for the difference between the measured influence of the grain size and the theoretical influence of the grain size according to the current 2-forces Sellmeijer formula on the critical gradient is. However, the tools that can be used to find the influence of the variables on the critical gradient, are the same as the ones that are used for deriving a new formula. So to find the influence of variables on the critical gradient, the same procedure can be followed as the one to derive a new formula, which is the procedure shown in Figure 2-5.

As can be seen in the flow chart in Figure 2-14, the first thing that must be done is to check if the variables are error-free. Secondly, it must be researched if a linear MVA can be used. In Figure 2-16 the formula $y = (\frac{x}{x_{mean}})^{\alpha}$ for different values of α is shown. If the output variable, when plotted against every input variable, shows behaviour like the lines shown in Figure 2-16, a linear MVA is justified. If not, a non-linear MVA needs to be performed, or a MVA cannot per performed at al.

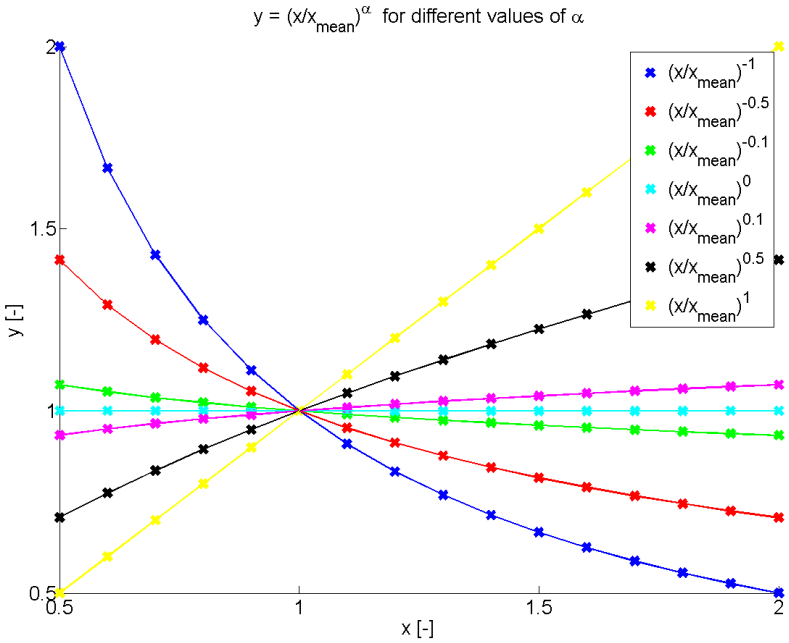

Figure 2-16 a graph of $y = (\frac{x}{x_{mean}})^{\alpha}$ *for different values of* α

In Figure 2-17 three different fictitious output variables y are plotted against the input variable x (these variables are not physical variables, they serve only as an example). When comparing Figure 2-17 with Figure 2-16, variable 1 and 3, the red and blue data points in Figure 2-17, show resemblance with the lines in Figure 2-16. For the dataset of variable 1 and 3, a linear MVA can be done. Variable 2,

the purple data points, does not resemble a line in Figure 2-16 at al. A linear MVA can not be done on this dataset. For a given dataset, the output variable must be plotted against every input variable and the plots must be compared with Figure 2-16 to judge if a linear MVA is justified.

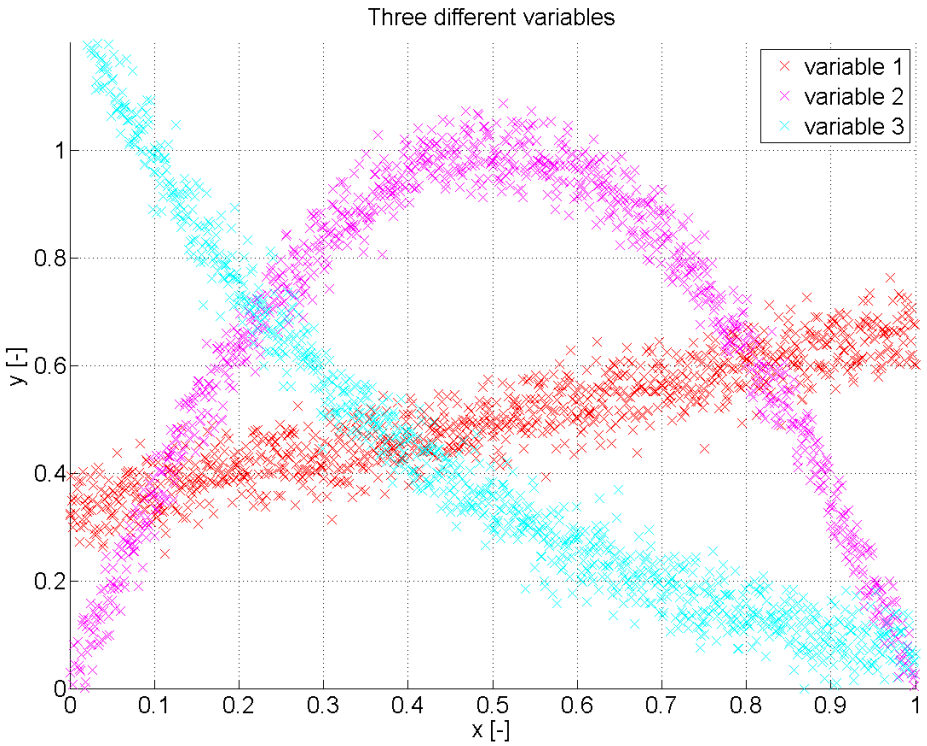

Figure 2-17 variable 1 and 3 show behaviour as is shown in Figure 2-16. A linear MVA can be done on these datasets. Variable 2 does not show behaviour as shown in Figure 2-16 at al. A linear MVA can not be done on the dataset of variable 2

Then the correlations between the input variables need to be investigated. If two input variables show a very strong correlation and this correlation is also present in reality, one of the variables can safely be assimilated in the other variable. As stated earlier, the linear MVA has the following shape:

$$Y = e^{\alpha}\left(\frac{X_1}{X_{1,\,mean}}\right)^{\beta}\left(\frac{X_2}{X_{2,\,mean}}\right)^{\gamma}\left(\frac{X_3}{X_{3,\,mean}}\right)^{\delta}\ldots + error\ term \qquad \textit{(eq 2-3).}$$

Where Y is the output variable and X_i are the input variables and e^{α} is a constant. The regression coefficients in this equation can be solved with the least squares method. To solve this equation for given Y, X_i and $X_{i,mean}$ the natural logarithm of the equations has to be taken, resulting in

$$\ln(Y) = \alpha + \beta * \ln\left(\frac{X_1}{X_{1,\,mean}}\right) + \gamma * \ln\left(\frac{X_2}{X_{2,\,mean}}\right) + \delta * \ln\left(\frac{X_3}{X_{3,\,mean}}\right) \qquad \textit{(eq 2-5).}$$

In matrix notation:

$$\begin{bmatrix} \ln(Y) \\ \vdots \end{bmatrix} = \begin{bmatrix} 1 & \ln(\frac{X_1}{X_{1,mean}}) & \ln(\frac{X_2}{X_{2,mean}}) & \ln(\frac{X_3}{X_{3,mean}}) \\ \vdots & \vdots & \vdots & \vdots \end{bmatrix} \begin{bmatrix} \alpha \\ \beta \\ \gamma \\ \delta \end{bmatrix} = \underline{\underline{A}}\,\underline{x} = \underline{b} \quad \textit{(eq 2-6).}$$

Where $\underline{\underline{A}}$ is in this case the matrix with the Ln of the normalized input variables, $\underline{b}$ is the Ln of the output variable and $\underline{x}$ is the vector containing the regression coefficients $\begin{bmatrix} \alpha & \beta & \gamma & \delta \end{bmatrix}^T$. Since there are more data samples than the amount of variables that are considered, there is generally no exact solution which fulfills the system of equations. Therefore a least squares method is used to find a best fit of the equation. The least square solution is determined as follows. $\underline{\underline{A}}^T \underline{\underline{A}}\,\hat{\underline{x}} = \underline{\underline{A}}^T \underline{b}$ $\hat{\underline{x}} = (\underline{\underline{A}}^T \underline{\underline{A}})^{-1} \underline{\underline{A}}^T \underline{b}$. The columns of matrix $\underline{\underline{A}}$ contain the Ln of the normalized input parameters. If these columns are strongly correlated, and this correlation is not present in reality, the MVA analysis will yield a formula which describes the dataset quite well, but performs very badly in reality. This means distinction between (statistical) correlations and causality has to be taken into account. High correlations between column vectors spoil the outcome of the calculation, because in the case of high correlations, it is not possible to account which input variable contributes to which amount to the output variable. This is called multicollinearity. Because the columns consist of the Ln of the normalized input variables, the correlations between the Ln of the normalized input variables are normative for the assessment if a MVA results in multicollinearity or not (Garson, 2009, López de la Cruz, 2009). The dataset must also be representative for the population, otherwise the outcome of the MVA does not apply to reality, only to the dataset.

2.5 Multi variate analysis on SBW data

In this paragraph the outcome of the multi variate analysis (MVA) on SBW data is treated. A MVA had already been done by (López de la Cruz, 2009), but because of the reasons mentioned on page 25, the MVA has been redone. This MVA is done so that the influence of the variables on the critical head in the small-scale test facility can be determined. The outcome of the MVA on SBW data can be compared with the outcome of the MVA on de Wit's dataset, to investigate if the variables in both datasets have the same influence on the critical head.

Small-scale, medium-scale and full-scale experiments have been performed in the framework of SBW. In this paragraph, also de Deltagoot experiments are considered.

2.5.1 Analysis of small-scale SBW data

In this subparagraph, the analysis of small-scale SBW data is shown. The first step in the MVA according to Figure 2-14 is to investigate if the variables are sufficient error-free. The input and output variables cannot be completely error-free. The D_{70}, the uniformity and the KAS can be determined quite accurately, but the relative density can only be determined with an accuracy of 5 percentage points. The permeability k cannot be determined very accurately. Determining k from the measured discharge and the head difference, will yield a permeability which is the total permeability of the sand and filter together. Other methods for determining the permeability do exist, such as Beyer's formula or Hazen's formula. This still does not gives an accurate answer. The value of k determined with Darcy is preferred. The critical head itself is determined quite accurately during the experiments. This value needs to be corrected for the resistance of the test facility, including the filter. This has been done for the SBW small-scale and medium-scale experiments.

In total, 48 small-scale experiments were performed in the framework of SBW. Ten experiments are excluded for the analysis of the multi variate analysis because of various reasons, mostly because of the forward erosion process or extreme outliers, see appendix F for more information about results of not used experiments. The variables of SBW's experiments were double-checked by means of the factual reports (van Beek, 2008a) and are considered sufficient error-free.

The second step according to Figure 2-14 is to investigate if the output variable against every single input variable shows the same kind of behaviour as is shown in Figure 2-16. In Figure 2-18 until Figure 2-22, $\frac{\Delta H_c}{L}$ is plotted against the input variables. As can be seen in Figure 2-18, the RD has a strong influence on the critical gradient.

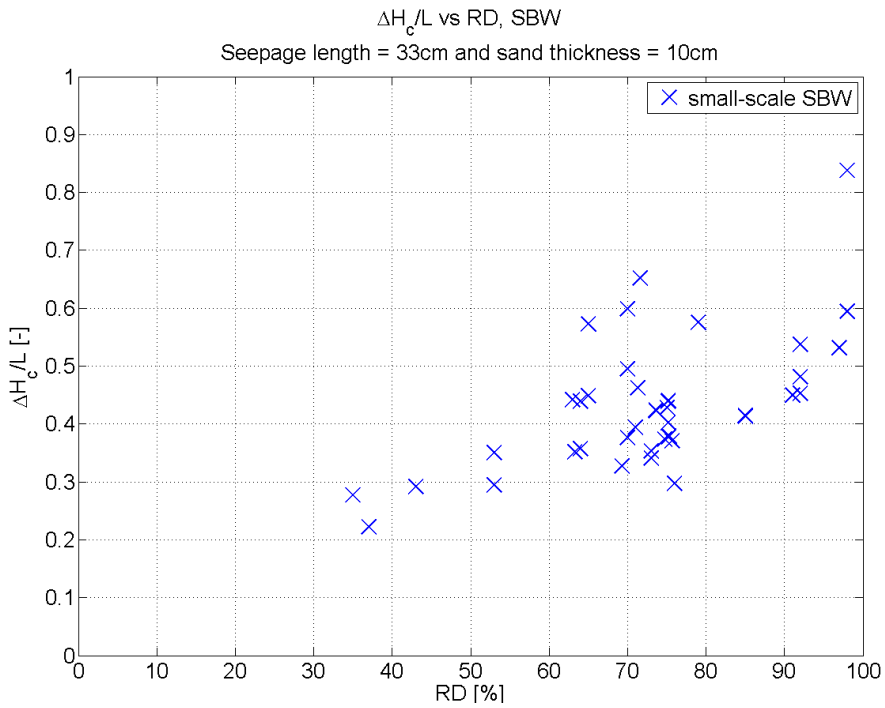

Figure 2-18 the plot of the critical gradient against RD for small-scale SBW measurements

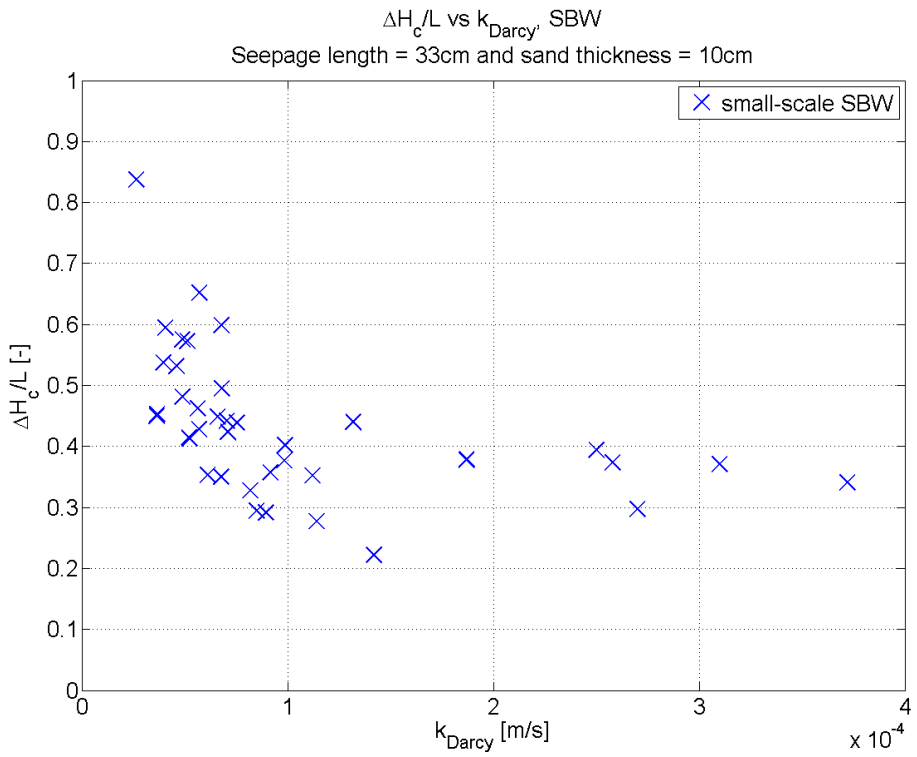

Figure 2-19 the plot of the critical gradient against k_{Darcy} for small-scale SBW measurements

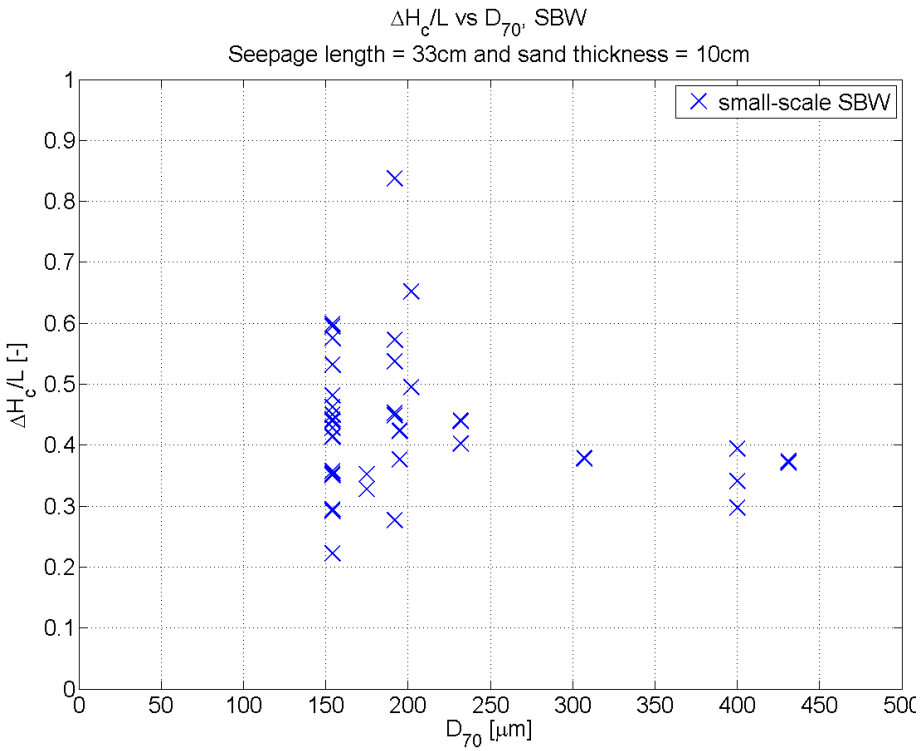

Figure 2-20 the plot of the critical gradient against D_{70} for small-scale SBW measurements

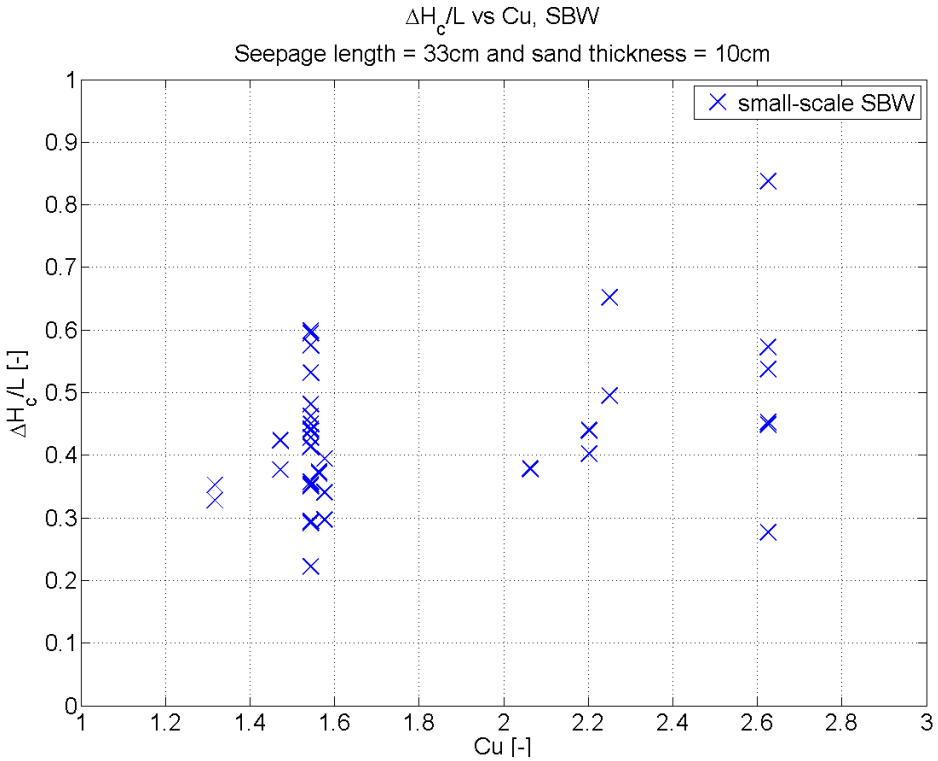

Figure 2-21 the plot of the critical gradient against C_u for small-scale SBW measurements

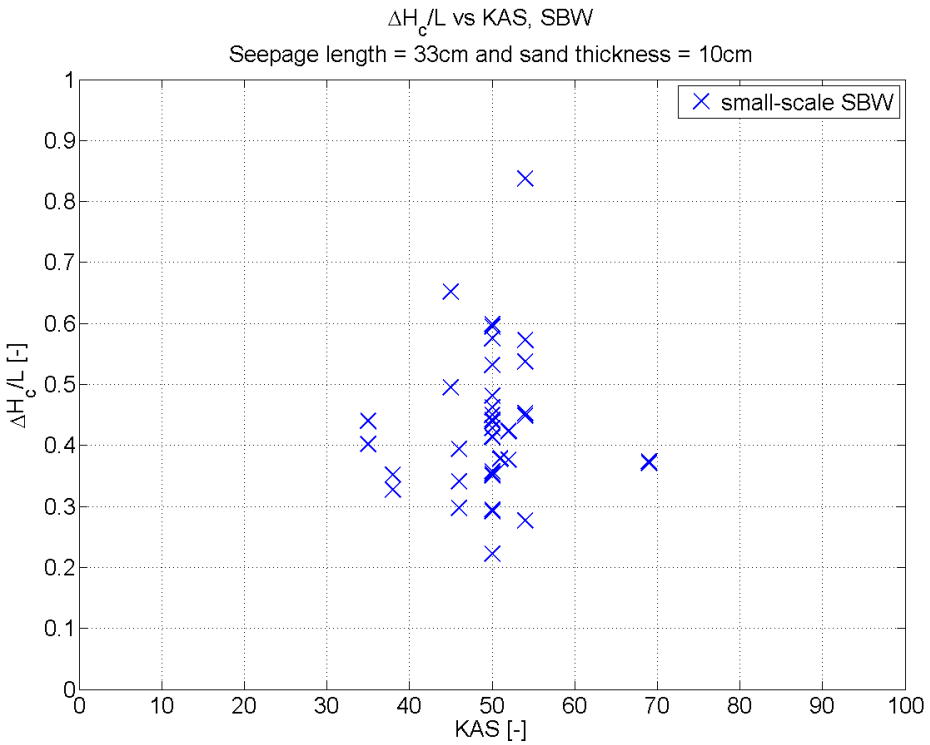

Figure 2-22 the plot of the critical gradient against KAS for small-scale SBW measurements

As can be seen in Figure 2-18 until Figure 2-21, the data points for the output variable against the input variables (RD, k_{Darcy}, D_{70}, and C_u) show more or less the kind of behaviour as the lines shown in Figure 2-16 except for one outlier ($\frac{H_c}{L}$ = 0.85), although a lot of scatter is present. The scatter does not indicate if a linear or a non-linear MVA should be used, it is the trend of the data points that is important for the decision to perform a linear or a non-linear MVA. As can be seen in Figure 2-22, the data points for $\frac{H_c}{L}$ against KAS show virtually no dependency at al. This means the KAS can actually be excluded from the MVA. It is decided to include the KAS in the MVA anyway to check if this is true. If the KAS does not influence $\frac{H_c}{L}$, the result of the MVA will give a negligible regression coefficient of the KAS. Based on Figure 2-18 until Figure 2-22 and the explanations of the figures, it is concluded that the input variables show roughly the behaviour as is shown in Figure 2-16 and a linear MVA is justified.

The third step according to Figure 2-14 is to investigate if the correlations between the input variables are acceptably low. The correlation coefficients between the normalized variables are calculated and are shown in Table 2-2.

Table 2-2 the correlation coefficients of the normalized variables of the SBW small-scale samples

	H_c	RD	k_{Darcy}	D_{70}	C_u	KAS
H_c	1.000	0.623	-0.452	-0.211	0.393	0.069
RD	0.623	1.000	-0.182	0.061	0.077	0.060
k_{Darcy}	-0.452	-0.182	1.000	0.915	-0.199	0.175
D_{70}	-0.211	0.061	0.915	1.000	0.011	0.278
C_u	0.393	0.077	-0.199	0.011	1.000	0.068
KAS	0.069	0.060	0.175	0.278	0.068	1.000

Most of the parameters are correlated as can be seen in Table 2-2. Unfortunately, most parameters cannot be varied independently of other parameters. E.g. changing the D_{70} or the RD also changes the permeability. The high correlation between k_{Darcy} and D_{70} is as expected, as permeability depends strongly on the grain size. H_c is the output variable, and according to Figure 2-14, only correlations between input variables need to be concerned here. That is why correlations between H_c and the input variables are not treated here. The only correlation between two input variables that is of significance, is the correlation between k_{Darcy} and D_{70}. In reality, these two variables are also quite strong correlated. Van Gelder states that when parameters are more than 70% correlated, one variable can safely be assimilated in the other variable without much loss of information (van Gelder, 2010). This means that based on the SBW data the permeability can be assimilated in the D_{70}. Still the parameters are both included in the MVA. The reason for this is that in reality, the correlation between permeability and D_{70} is not always predictable with formulas.

As stated before, the formula for a linear MVA is as follows.

$$Y = e^{\alpha}\left(\frac{X_1}{X_{1,\,mean}}\right)^{\beta}\left(\frac{X_2}{X_{2,\,mean}}\right)^{\gamma}\left(\frac{X_3}{X_{3,\,mean}}\right)^{\delta}\ldots + error\ term \qquad \textit{(eq 2.3)}.$$

In paragraph 2.3 the following variables were mentioned as having influence on the piping process:

- The permeability based on Darcy's Law (k_{Darcy})
- The 70th percentile of the grain diameter (D_{70})
- The coefficient of uniformity, ($C_u = \frac{D_{60}}{D_{10}}$)
- The relative density (RD)
- The roundness of the grain particles (KAS)

For these variables, the formula for the MVA for the small-scale test facility is as follows.

$$\frac{H_c}{L} = e^{\alpha}\left(\frac{RD}{RD_{mean}}\right)^{\beta}\left(\frac{k_{Darcy}}{k_{Darcy,mean}}\right)^{\gamma}\left(\frac{D_{70}}{D_{70,mean}}\right)^{\delta}\left(\frac{C_u}{C_{u,mean}}\right)^{\varepsilon}\left(\frac{KAS}{KAS_{mean}}\right)^{\theta} + error\ term \qquad \textit{(eq 2-7)}$$

(López de la Cruz, 2009, (besides the different constant, as mentioned on page

25)). It is mentioned that this is also a model, which can be used to find the exponential influence of a variable. The values for all of the used variables are given in appendix F. To minimize the error term in the equations, a least squares method is applied. To solve this system of equations, the natural logarithm of the equations has to be taken and this results in

$$\ln(\frac{H_c}{L}) = \alpha + \beta \ln(\frac{RD}{RD_{mean}}) + \gamma \ln(\frac{k_{Darcy}}{k_{Darcy,mean}}) + \delta \ln(\frac{D_{70}}{D_{70,mean}}) + \varepsilon \ln(\frac{C_u}{C_{u,mean}}) + \theta \ln(\frac{KAS}{KAS_{mean}})$$

(eq 2-8).

The equation is shown below in matrix notation.

$$\begin{bmatrix} 1 & \ln(\frac{RD}{RD_{mean}}) & \ln(\frac{k_{Darcy}}{k_{Darcy,mean}}) & \ln(\frac{D_{70}}{D_{70,mean}}) & \ln(\frac{C_u}{C_{u,mean}}) & \ln(\frac{KAS}{KAS_{mean}}) \\ \vdots & \vdots & \vdots & \vdots & \vdots & \vdots \end{bmatrix} \begin{bmatrix} \alpha \\ \beta \\ \gamma \\ \delta \\ \varepsilon \\ \theta \end{bmatrix} = \begin{bmatrix} \ln(\frac{Hc}{L}) \\ \vdots \end{bmatrix}$$

$= \underline{\underline{A}}\underline{x} = \underline{b}$ *(eq 2-9)*.

It is this system of equations which it's least squares solution gives the best fit for the proposed formula. In this system of equations, high correlations between column vectors spoil the outcome of the calculation, because in the case of high correlations, it is not possible to account which input variable contributes to which amount to the output variable. This is called multicollinearity (Garson, 2009, López de la Cruz, 2009). Multicollinearity will only occur if the correlations between the Ln of the column vectors of the input variables have a high correlation, because it are the Ln of the normalized input variables the least square solution method is performed on. As discussed in section 2.3 the correlations between the Ln of the normalized input parameters are normative for the assessment if a MVA results multicollinearity or not. The correlation coefficients between the Ln of the normalized variables is calculated and is shown in Table 2-3.

These correlations are used only to justify the use of the MVA.

Table 2-3 the correlation coefficients of the natural logarithms of the normalized variables of the SBW small-scale samples

	H_c	RD	k_{Darcy}	D_{70}	C_u	KAS
H_c	1.000	0.683	-0.610	-0.173	0.365	0.076
RD	0.683	1.000	-0.345	0.107	0.040	0.019
k_{Darcy}	-0.610	-0.345	1.000	0.801	-0.234	-0.001
D_{70}	-0.173	0.107	0.801	1.000	0.120	0.156
C_u	0.365	0.040	-0.234	0.120	1.000	0.060
KAS	0.076	0.019	-0.001	0.156	0.060	1.000

As can be seen the highest correlation present is between the permeability and the D_{70}. The value of the correlation is 0.80. This seems quite high, but according to (Garson, 2009, López de la Cruz, 2009), it has been empirically established that only correlations above 0.90 might translate into multicollinearity in the data.

The fourth step according to Figure 2-14 is verifying if the samples are representative of the population. Most samples of SBW have a D_{70} between 150 and 200µm and only a few samples have a D_{70} between 200 and 500µm. No samples from SBW have a D_{70} larger than 500µm. The MVA on the SBW samples is only valid for D_{70} between 150 and 500µm. More tests should be done on samples with a D_{70} between 200 and 500µm to have a more representative dataset. In Figure 2-23 a histogram of the D_{70} of the sand samples used for SBW is shown. Because of the little amount of coarse grained sand, some kind of lever effect can occur in the MVA. Advised is to do more experiments on coarse grained sand to make the dataset statistically more reliable.

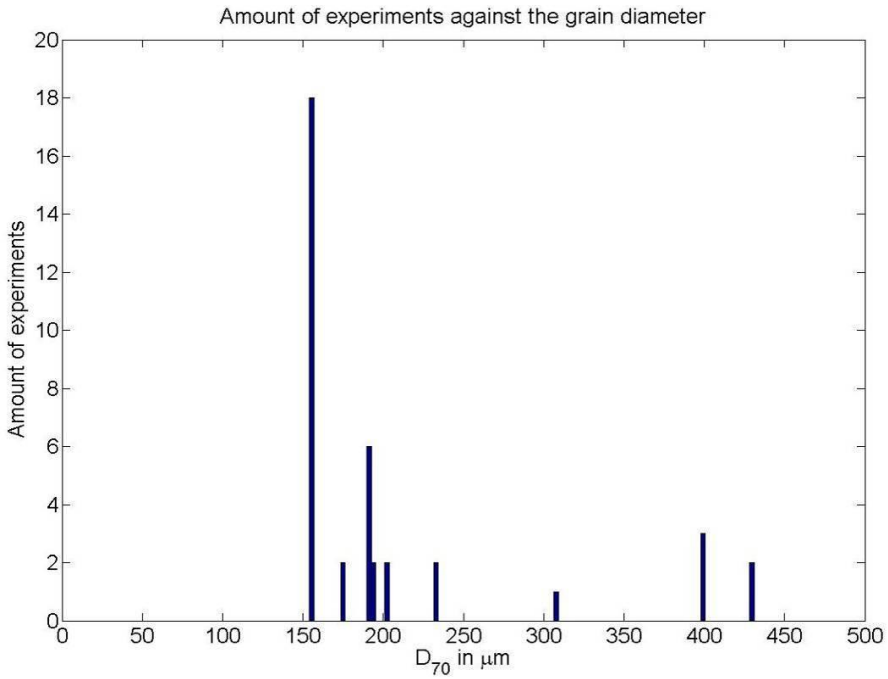

Figure 2-23 a histogram of the D_{70} of the sand samples used for the small-scale SBW experiments

To keep this chapter readable, several figures of paragraph 2.5 are presented in appendix K. In Figure K-1 till Figure K-4 respectively the histograms of RD, C_u, KAS and k_{Darcy} are shown. As can be seen in Figure 2-23, Figure K-2 and Figure K-3, the D_{70}, the C_u and the KAS show a very distinct spike. This is because of the choice of the sand samples used for SBW. For the succeeded experiments, in total 18 times Baskarp sand was used. With this choice the D_{70}, the C_u and the KAS are fixed. The RD is the only variable which can be truly varied in the experiments, if a

certain sand type is chosen. The k_{Darcy} is also not completely fixed if a certain sand type is chosen, but it is very dependent on the D_{10} (also fixed if a certain sand type is chosen) and the RD. Based on Figure 2-22, the critical gradient does not show any relation with the KAS, so more variation of KAS does probably not give better results in the MVA. Varying D_{70} and the C_u more is advised to get a more varied dataset. The RD is already varied enough. Although because of the selection of the sand samples, the dataset of SBW does not completely represent reality, the MVA is continued. Adding more variation to the dataset by doing more experiments with more varied sand characteristics will give a more accurate answer. Since outcomes with forward erosion, which occurs at the experiments with very low RD, was excluded from the MVA, the outcome of the MVA may not be used for low RD's.

The system of equations shown below need to be solved.

$$\begin{bmatrix} 1 & \ln(\frac{RD}{RD_{mean}}) & \ln(\frac{k_{Darcy}}{k_{Darcy,mean}}) & \ln(\frac{D_{70}}{D_{70,mean}}) & \ln(\frac{C_u}{C_{u,mean}}) & \ln(\frac{KAS}{KAS_{mean}}) \\ \vdots & \vdots & \vdots & \vdots & \vdots & \vdots \end{bmatrix} \begin{bmatrix} \alpha \\ \beta \\ \gamma \\ \delta \\ \varepsilon \\ \theta \end{bmatrix} = \begin{bmatrix} \ln(\frac{Hc}{L}) \\ \vdots \end{bmatrix}$$

$= \underline{\underline{A}}\underline{x} = \underline{b}$ *(eq 2.9)*.

The system of equations $\underline{\underline{A}}\underline{x} = \underline{b}$ needs to be solved. Because the amount of data is higher than the unknowns in the equation, there is no unique solution. The least squares method results in a best fit of the data.

$$\underline{\underline{A}}^T \underline{\underline{A}}\hat{\underline{x}} = \underline{\underline{A}}^T \underline{b} \qquad \hat{\underline{x}} = (\underline{\underline{A}}^T \underline{\underline{A}})^{-1} \underline{\underline{A}}^T \underline{b}$$

$$\hat{\underline{x}} = \begin{bmatrix} \alpha & \beta & \gamma & \delta & \varepsilon & \theta \end{bmatrix}^T = \begin{bmatrix} -0.91 & 0.41 & -0.31 & 0.29 & 0.16 & -0.005 \end{bmatrix}^T$$

The values of the regression coefficients are shown in Table 2-4.

Table 2-4 the regression coefficients are the outcome of the MVA

variable	symbol of regression coefficient	regression coefficient
constant	α	-0.91
RD	β	0.41
k_{Darcy}	γ	-0.31
D_{70}	δ	0.29
C_u	ε	0.16
KAS	θ	-0.005

The following can be concluded from Table 2-4. The regression coefficient of D_{70} is 0.29. According to the current 2-forces Sellmeijer formula (eq 1-4), the regression

coefficient of D_{70} should be 1. The outcome of analysis of the small-scale dataset from SBW and the Sellmeijer 2-forces formula do not support each other, and finding an explanation for this difference is the main objective of this master thesis. The high influence of the RD on the critical gradient is also notable. The value of the regression coefficients of k_{Darcy} is -0.31, and agrees with the theoretical value of $\frac{1}{\sqrt[3]{\kappa}}$ in the current Sellmeijer formula (eq 1-4). The regression coefficient of the KAS is negligible, as was already concluded based on Figure 1-18. The influence of C_u on the critical gradient is also quite low. This does not mean the uniformity itself has a very low influence since the uniformity is already represented via D_{70} and k in the MVA.
This results in the formula

$$\frac{H_c}{L} = e^{-0.91}\left(\frac{RD}{RD_{mean}}\right)^{0.41}\left(\frac{k_{Darcy}}{k_{Darcy,mean}}\right)^{-0.31}\left(\frac{D_{70}}{D_{70,mean}}\right)^{0.29}\left(\frac{C_u}{C_{u,mean}}\right)^{0.16}\left(\frac{KAS}{KAS_{mean}}\right)^{-0.005} \quad \textit{(eq 2-10)}.$$

This is a best fit solution for the data of the small-scale SBW test facility. It is emphasized again this formula is not valid for a real dike, but for the small-scale test facility only. The regression values corresponds with the regression coefficients found by López de la Cruz, shown in paragraph 2.1. The outcome of the MVA may only be used for cases with RD higher than 50%, a D_{70} between 150 and 430µm and a C_u between 1.3 and 2.6.

Because the influence of KAS is negligible and the influence of C_u is also low, these factors can be excluded from the formula. The regression coefficient of k_{Darcy} is -0.31. This resembles the value of -0.33, which is present in the Sellmeijer formula, a lot. Also, about this variable the least uncertainty was present.

The regression coefficient of the D_{70} is 0.29. If the permeability is taken into account, $\kappa \approx C * D_{70}^2$, $\frac{H_c}{L} \sim \frac{D_{70}^{0.29}}{\kappa^{0.31}} \sim \frac{D_{70}^{0.29}}{D_{70}^{0.62}} \sim D_{70}^{-0.33}$. This is the negative trend as is shown in Figure 1-17. The D_{70} itself actually has a positive influence on the critical gradient (0.29), but the permeability has a negative effect which results in a net negative influence (-0.33) for D_{70} (because increasing grain size leads to increasing permeability). According to the current 2-forces Sellmeijer model, $\frac{H_c}{L} \sim \frac{D_{70}}{\sqrt[3]{\kappa L}}$ which results in the increase of the critical gradient with the cubic root of the grain size (if a constant C_u is assumed). Research to find an explanation for the different outcomes of SBW and Sellmeijer's 2-forces model is the main topic of this master thesis.
Because the correlation between k and D_{70} is still considered as fairly large, and the regression coefficient of k agrees with the existing theory, the MVA is

performed again on the data set with the regression coefficient of $(\frac{k}{k_{mean}})$ kept as a constant value of -0.33. Also the C_u and KAS are not included in the MVA, so that the new MVA needs less variables, but still covers the most important variables. Repeating the same procedure yields the regression coefficients which are shown in Table 2-5.

Table 2-5 the regression coefficients are the outcome of the redone MVA

variable	symbol of regression coefficient	regression coefficient
constant	α	-0.92
RD	β	0.39
D_{70}	γ	0.34

This results in the formula

$$\frac{H_c}{L} = e^{-0.92}\left(\frac{k_{Darcy}}{k_{Darcy,mean}}\right)^{-0.33}\left(\frac{RD}{RD_{mean}}\right)^{0.39}\left(\frac{D_{70}}{D_{70,mean}}\right)^{0.34} \qquad \textit{(eq 2-11).}$$

The results of inserting the dataset of the small-scale experiments in the best fit formula derived in this thesis (eq 2-10), the best fit formula derived by López de la Cruz (eq 2-1) and the current (eq 1-4) and adapted 2-forces Sellmeijer formula (eq 2-2), and a comparison between the formulas is shown in appendix J in Table J-1. The formula of López de la Cruz and the formula derived in this paragraph have the lowest error as can be seen in Table J-2 and both are considered the best fit for the small-scale dataset. In this chapter, from now on, the formula derived in this paragraph (eq 2-10) is used when is referred to the MVA formula for SBW. As can be seen in Table J-1, the difference for the derived formula is in the order of 20%, when compared with the measured values, but several outliers are present.

2.5.2 Analysis of medium-scale SBW data

In this sub paragraph, the analysis of medium-scale SBW data is performed. As shown in Figure 2-5, the next step is to perform medium-scale experiments. The amount of medium-scale experiments is not enough to perform a MVA. So a MVA on medium-scale experiments can not be performed, and a comparison of a MVA on small-scale and medium-scale experiments can not be made. However, the medium-scale experiments may not contradict the MVA of the small-scale experiments, otherwise the outcome of the MVA on the small-scale experiments is considered invalid. In appendix D the medium-scale test facility is described. The results of the medium-scale experiments can be found in appendix F in Table F-3 and Table F-4. Eight medium-scale experiments were carried out. One of them failed due to failure of the pump during the experiment, so seven experimental outcomes are considered here. In Table J-3 a comparison between measured critical gradients and the critical gradient calculated with the formula's of the

outcome of the MVA of the small-scale experiments (eq 2-10) and the current (eq 2-4) and adapted 2-forces Sellmeijer model (eq 2-2) is shown. As can be seen, the difference between the measurements and the outcome of the formula of the MVA (eq 2-10) is between 30 and 40%. This may be because of the length effect, which is not present in the MVA. The adapted formula is more normative for a comparison. The adapted 2-forces (eq 2-2) model agrees quite well with the measured data, the difference is in the order of 20%, just as the MVA on the small-scale experiments, as is shown in Table J-1. However, there is a tendency for the adapted formula to overestimate the critical gradient.

Since the difference between the measurements and the MVA is in the same order as with the small-scale experiments, the medium-scale experiments do not contradict the outcome of the MVA of the small-scale experiments, but do not support it either, because of the tendency for the adapted formula to overestimate the critical gradient and the amount of experiments is quite low.

2.5.3 Analysis of full-scale SBW and Deltagoot data

In this sub paragraph, the analysis of full-scale SBW data and de Deltagoot is performed. According to Figure 2-5, it must be checked if the full-scale experiments also shows the same trend as the small-scale experiments do. Since there are not enough full-scale experiments, a MVA can not be done on these experiments. The values are inserted in (eq 2-10, eq 1-4 and eq 2-2) and compared if the outcome agrees with the measurements or not. Two datasets are available for the full-scale analysis, de Deltagoot tests, which are explained in appendix G and H, and de IJkdijk tests, which are explained in appendix E and F. The measured critical gradients and the calculated critical gradients of the available full-scale experiments are shown in Table 2-6 and Table 2-7. The measured values do not correspond with the outcome of the MVA formula (eq 2-10), but this is expected as the length effect is not in the MVA formula.

As can be seen in the tables, de Deltagoot agrees with the current 2-forces model (eq 1-4), but this is because the 2-forces model is fitted on de Deltagoot tests. De IJkdijk tests for fine sand agree also with the current 2-forces model, but not for coarse sand.

De Deltagoot tests agree less with the adapted 2-forces model (eq 2-2) than with the current 2-forces model. De IJkdijk tests agree a bit more with the adapted formula than the current formula, but not much. Based on above conclusions, it can not be concluded that for real dikes, as de Deltagoot and de IJkdijk, the influence of variables is the same as in the small-scale test facility. This means that also the validity of the adapted 2-forces model is questionable. It is unknown if the observed lower than expected influence of D_{70} on the critical head (with respect to

the current 2-forces Sellmeijer model) in the small-scale test facility is also present with real dikes. At test 2 of de IJkdijk, the critical gradient is indeed lower, but considering the huge scatter that is found in SBW data, but also in data from Bligh (Appendix N), this may be due to scatter.

Table 2-6 overview of de Deltagoot experiments

test number	D_{70} [µm]	H_c/L [-] measured	MVA outcome (eq 2-10)		current Sellmeijer 2-forces model (eq 1-4)		adapted Sellmeijer 2-forces model (eq 2-2)	
			H_c/L [-]	difference [%]	H_c/L [-]	difference [%]	H_c/L [-]	difference [%]
T2	247	0.188	0.466	-59.7	0.191	-1.4	0.157	19.6
T3	247	0.180	0.466	-61.4	0.182	-0.8	0.150	20.3
T4	247	0.175	0.466	-62.5	0.207	-15.5	0.171	2.5

Table 2-7 overview of de IJkdijk experiments

test number	D_{70} [µm]	H_c/L [-] measured	MVA outcome (eq 2-10)		current Sellmeijer 2-forces model (eq 1-4)		adapted Sellmeijer 2-forces model (eq 2-2)	
			H_c/L [-]	difference [%]	H_c/L [-]	difference [%]	H_c/L [-]	difference [%]
test 1	180	0.153	0.361	-57.5	0.153	0.0	0.149	2.9
test 2	260	0.117	0.371	-68.6	0.187	-37.5	0.157	-25.6
test 3	180	0.140	0.358	-60.9	0.152	-7.9	0.148	-5.3

Since there are only three Deltagoot tests and three IJkdijk tests, rigid conclusions can not be drawn, because there are not enough full-scale experiments performed.

2.5.4 Concluding remarks of analysis on SBW data

From analysis of the small-scale SBW experiments, it appears that the influence of grain size on the critical gradient is less than is expected from the Sellmeijer model. The grain size itself has a positive influence, but the permeability, which is correlated with the grain size has a even higher negative influence resulting in a net negative influence of grain size. The influence of permeability resembles the influence in the Sellmeijer formula. The influence of the RD is quite high and the influence of the KAS is negligible in the small-scale experiments. The influence of C_u is also quite small, this can be explained since both D_{70} and k_{Darcy} are already included in the MVA, the uniformity is already present in those two variables. The medium-scale and full-scale experiments do not contradict the small-scale experiments, but do not support it either because of the low amount of experiments performed and the large scatter that is present in the data.

In appendix J, amongst others, the following formulas are shown:

(eq J-1): the outcome of the MVA according to (López de la Cruz, 2009)

$$\frac{H_c}{L} = \left[\frac{H_c}{L}\right]_{mean}\left[\frac{RD}{RD_{mean}}\right]^{0.35}\left[\frac{C_u}{C_{u,mean}}\right]^{0.13}\left[\frac{KAS}{KAS_{mean}}\right]^{-0.02}\left[\frac{\kappa}{\kappa_{mean}}\right]^{-0.35}\left[\frac{D_{70}}{D_{70,mean}}\right]^{0.39}$$

(eq J-2): the outcome of the MVA according to the analysis in this thesis

$$\frac{H_c}{L} = e^{-0.91}\left(\frac{RD}{RD_{mean}}\right)^{0.41}\left(\frac{k_{Darcy}}{k_{Darcy,mean}}\right)^{-0.31}\left(\frac{D_{70}}{D_{70,mean}}\right)^{0.29}\left(\frac{C_u}{C_{u,mean}}\right)^{0.16}\left(\frac{KAS}{KAS_{mean}}\right)^{-0.005}$$

(eq J-3): the outcome of the MVA according to the analysis in this thesis, in simplified form

$$\frac{H_c}{L} = e^{-0.92}\left(\frac{k_{Darcy}}{k_{Darcy,mean}}\right)^{-0.33}\left(\frac{RD}{RD_{mean}}\right)^{0.39}\left(\frac{D_{70}}{D_{70,mean}}\right)^{0.34}$$

In Table 2-8 the regression coefficients and standard deviations for the three different MVA formulas are shown.

Table 2-8 the regression coefficients and standard deviations for three different MVA formulas

formula	α	β	γ	δ	ε	θ	σ [-]
	constant	RD	k_{Darcy}	D_{70}	C_u	KAS	standard deviation
Eq J-1	-	0.35	-0.35	0.39	0.13	-0.02	0.0703
Eq J-2	-0.91	0.41	-0.31	0.29	0.16	-0.005	0.0705
Eq J-3	-0.92	0.39	-0.33[*1]	0.34	-	-	0.0722

[*1] *the regression coefficient of k_{Darcy} was included in the MVA formula at forehand in eq J-3*

As can be seen in Table 2-8, the regression coefficients of the different MVA formulas agree quite well with each other. The standard deviation of the critical head, when measured and calculated values are compared, is almost identical for equation J-1 and J-2, although the regression coefficients are not identical. This can be allocated to multi-colinearity. Because of this multi-colinearity, there is a range of regressions coefficients which give the same least square error, as long as the product of $\left(\frac{k_{Darcy}}{k_{Darcy,mean}}\right)^{\gamma}\left(\frac{D_{70}}{D_{70,mean}}\right)^{\delta}$ results in this least square error, when compared with the outcome of the experiments. The regression coefficients in Table 2-8 of k_{Darcy} ranges from -0.31 to -0.35 and the regression coefficients of D_{70} ranges from 0.29 to 0.39.

Since the value of the regression coefficient of k_{Darcy} is very close to the value of -0.33 which is present in the Sellmeijer model, this value can be kept fixed at -0.33 in the MVA, so that the influence of D_{70} with this influence of permeability is calculated. This has been done with formula C in Table 2-8.

In paragraph 2.6, it is tried to perform a MVA on de Wit's data set, so a comparison can be made between outcomes of SBW and de Wit. A detailed conclusion about the outcome of the MVA on SBW data is treated in chapter 4.

2.6 Multi variate analysis on de Wit data

If a multi variate analysis is done on the dataset of de Wit, the influence of the variables discussed in paragraph 2.2 on the critical gradient can be researched. If this is done, a comparison with the outcome of the MVA on SBW's dataset can be made. De Wit performed small-scale and medium-scale experiments. In total 44 small-scale experiments (L=80cm), 24 medium-scale experiments (L=240cm) and 5 medium-scale experiments (L=450cm) were successful. As with SBW, the datasets of the small-scale and medium-scale experiments of de Wit are used to research the influence of the variables on the critical gradient. In Figure 2-24 an overview of de Wit's test facility is shown. More detailed information about the test facility of de Wit is given in appendix A.

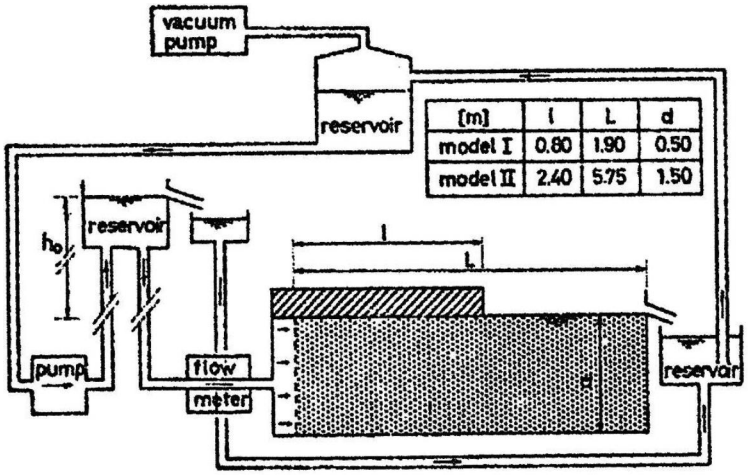

Figure 2-24 an overview of de Wit's test facility (de Wit, 1984)

2.6.1 Analysis of small-scale de Wit data

The procedure of the MVA is the same as the one that was performed on the MVA that was done on the SBW dataset. The data for the variables which was used can be found in appendix B. The first step is to check if the variables are sufficiently error-free. Unfortunately, this may not be the case. As can be seen in Figure 2-25 the test facility of de Wit has a filter. The test facility itself and the filter have a resistance, and the measured critical head should be corrected for the resistance. It is unknown whether de Wit corrected the critical head for the filter influence.

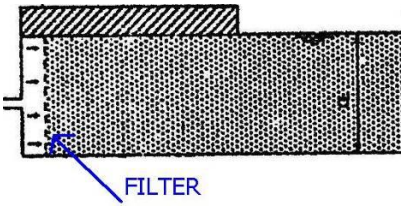

Figure 2-25 part of the test facility used by de Wit, where the location of the filter is pointed out with a blue arrow (de Wit, 1982, the blue arrow is added in this thesis)

The test facility itself is not present anymore, so the influence of the test facility and the filter can not be determined anymore, as it is unknown what filter de Wit used. The resistance of the filter for the SBW experiments was significant. The filter has the highest influence on the resistance, the rest of the test facility has only a minor influence. The resistance varied from only a few % to 10-15% for sands with a D_{70} around 200µm and between 30 to 40% for sands with a D_{70} around 400µm. The longer the seepage length is, the lower the resistance of the filter is relatively with respect to the measured critical gradient. (This has also been found in the experiments of SBW (van Beek, 2009b)). It is not sure if the resistance of the filter of de Wit's test facility is in the same order as SBW's filter. In the experiments of de Wit, grains with a D_{70} of 1390µm are used. No experiments have been performed in the framework of SBW with this size of grains, so no information about percentages of resistance is known, but it is expected to be quite high, since a larger grain size and a higher permeability leads to higher flow velocities and thus more resistance.

Since the seepage length of the small-scale de Wit experiments are longer than SBW small-scale experiments, the resistance of the filter is probably no more than 10% for sands with a D_{70} of 200µm and 20% for sands with a D_{70} of 400µm, but this is not sure. According to Figure 2-14 a MVA can only be performed if the variables are sufficiently error-free. Because it is not sure if the error made by (possibly) neglecting the filter resistance is reasonably small, the judgment if a MVA on de Wit's data is justified will be done later.

The second step according to Figure 2-14 is to investigate if the output variable against every single input variable shows the same kind of behaviour as is shown in Figure 2-16. In Figure 2-26 until Figure 2-30, $\frac{\Delta H_c}{L}$ is plotted against the input variables.

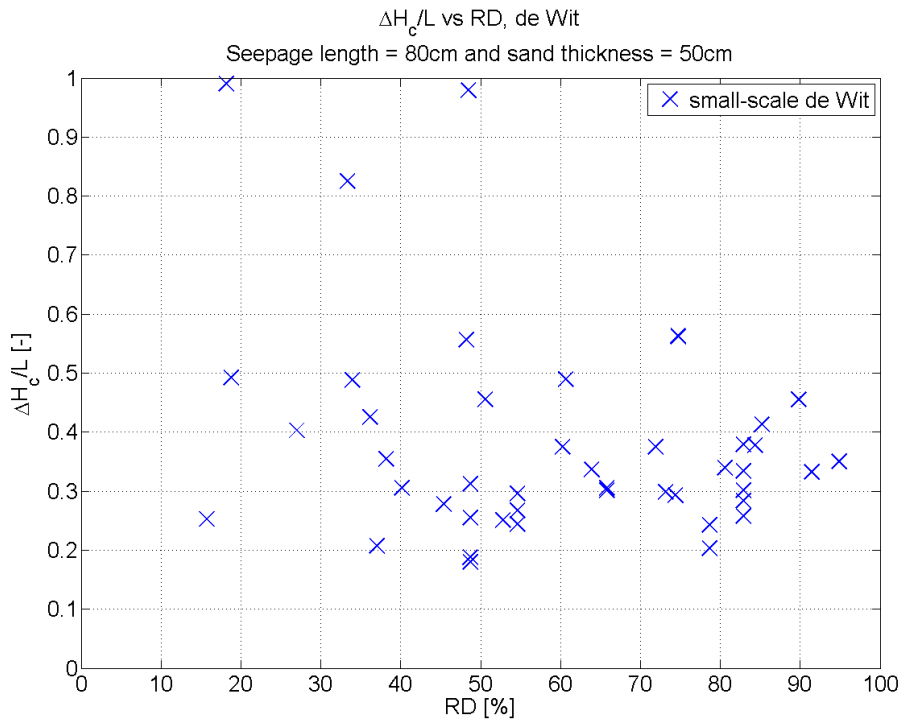

Figure 2-26 the plot of the critical gradient against RD for small-scale de Wit experiments

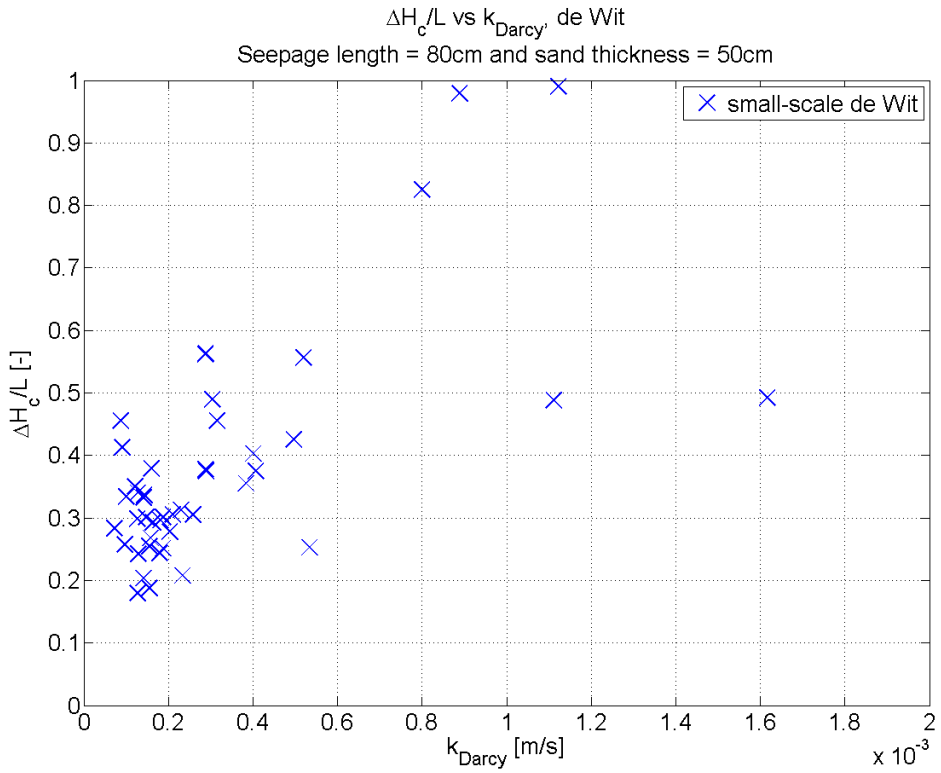

Figure 2-27 the plot of the critical gradient against k_{Darcy} for small-scale de Wit experiments

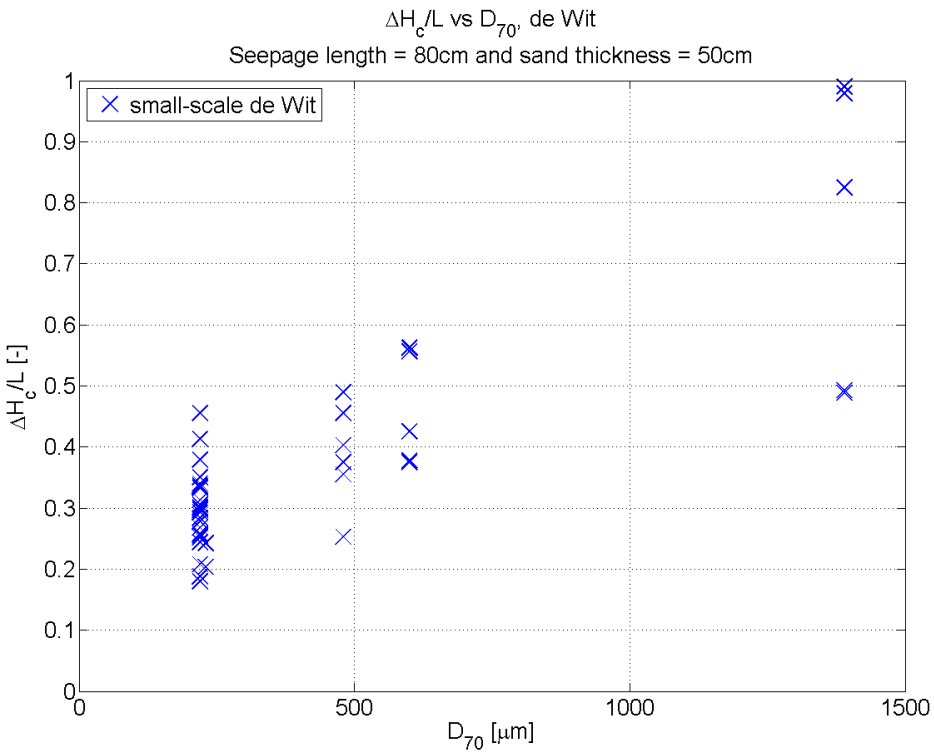

Figure 2-28 the plot of the critical gradient against D_{70} for small-scale de Wit experiments

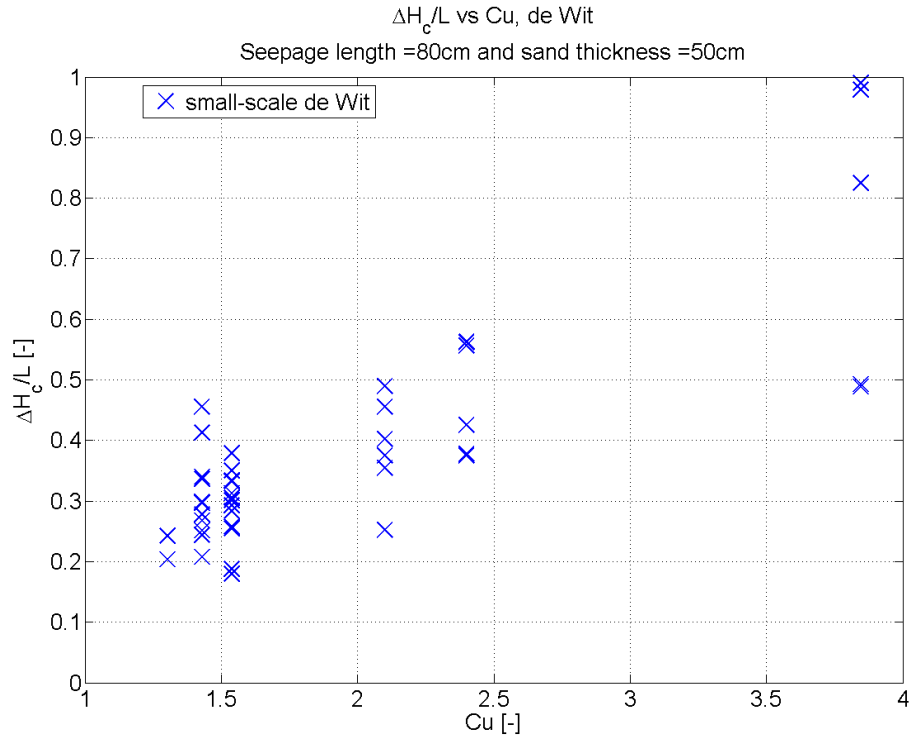

Figure 2-29 the plot of the critical gradient against C_u for small-scale de Wit experiments

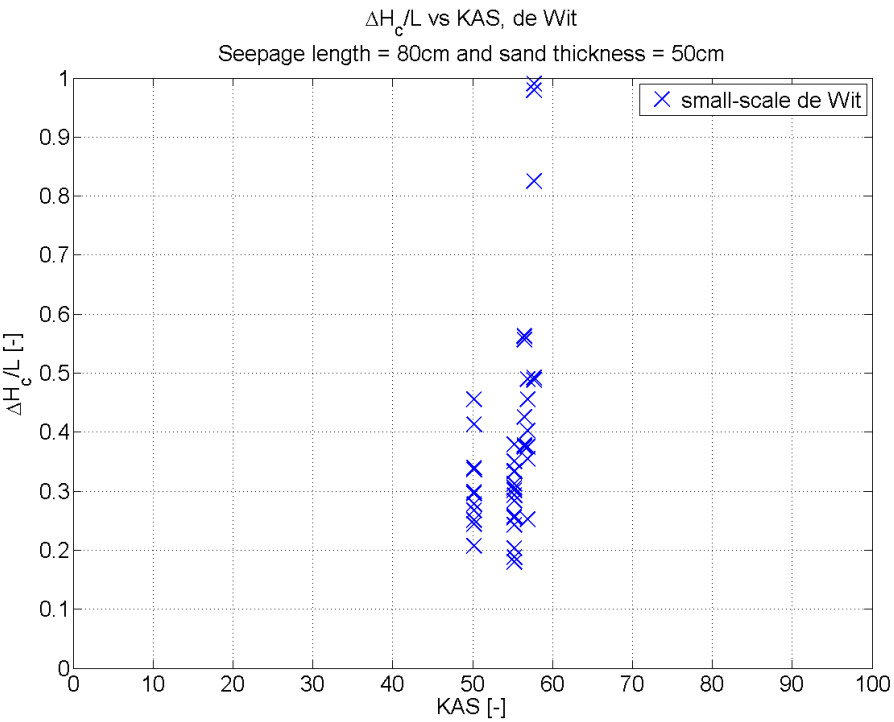

Figure 2-30 the plot of the critical gradient against KAS for small-scale de Wit experiments

As with SBW, the figures are compared with Figure 2-16. As can be seen in Figure 2-26 the RD shows reasonable the behaviour needed for a linear MVA, except for three outliers. In Figure 2-27, k_{Darcy} does not show a clear trend, and it is doubtful if a linear MVA gives a useful outcome. In Figure 2-28 the D_{70} shows a very clear trend which is very suited for a linear MVA. In Figure 2-29 the C_u also shows a very clear trend which is very suited for a linear MVA. As can be seen in Figure 2-30, the data points for $\frac{H_c}{L}$ against KAS show virtually no dependency at al. Based on Figure 2-25 until Figure 2-30 and the explanations of the figures, it is concluded that some of the input variables show roughly the behaviour as is shown in Figure 2-16, but for k_{Darcy} the behaviour is doubtful. Because it is doubtful if a MVA can be performed, the judgment if a MVA on de Wit's data is justified will be done later.

The third step according to Figure 2-14 is to investigate if the correlations between the input variables are acceptable low. The correlation coefficients between the normalized variables is calculated and is shown in Table 2-9. Comparing Table 2-9 with Table 2-2, it is striking the correlations do not agree with each other at al. This will be explained later.

Table 2-9 the correlation coefficients of the normalized variables of de Wit small-scale samples

	H_c	RD	k_{Darcy}	D_{70}	C_u	KAS
H_c	1.00	-0.29	0.67	0.83	0.83	0.44
RD	-0.29	1.00	-0.67	-0.55	-0.55	-0.28
k_{Darcy}	0.67	-0.67	1.00	0.93	0.93	0.53
D_{70}	0.83	-0.55	0.93	1.00	0.99	0.58
C_u	0.83	-0.55	0.93	0.99	1.00	0.63
KAS	0.44	-0.28	0.53	0.58	0.63	1.00

Most of the parameters are correlated as can be seen in Table 2-9. The high correlation between k_{Darcy} and D_{70} is as expected, as permeability depends strongly on the grain size. The high correlation between k_{Darcy} and C_u can also be expected, as a high C_u indicates a high amount of fines in the sample, and these fines are very important for the permeability. The extremely high correlation between D_{70} and C_u can not be explained by a physical law. A lot of medium correlations are present between input parameters. Some of these correlations can be expected based on physical background as the correlations between k_{Darcy} and RD. Medium correlations between RD and D_{70}, RD and C_u, k_{Darcy} and KAS, D_{70} and C_u, D_{70} and KAS and C_u with KAS are not expected. Based on a physical background, no (strong) relation is present between these variables. Variables with a very high correlation can be assimilated in the other variable, but this is only allowed if this correlation between variables is also present in reality. Based on the dataset of de Wit, the variable C_u can be assimilated in the D_{70}. In reality, this correlation does not occur, so assimilating the C_u in the D_{70} and then perform a MVA will give a result that fits the dataset of de Wit but does not agree with reality. Thus assimilating the C_u in the D_{70} should not be done. As with SBW, the proposed MVA formula has the following shape.

$$\frac{H_c}{L} = e^{\alpha}\left(\frac{RD}{RD_{mean}}\right)^{\beta}\left(\frac{k_{Darcy}}{k_{Darcy,mean}}\right)^{\gamma}\left(\frac{D_{70}}{D_{70,mean}}\right)^{\delta}\left(\frac{C_u}{C_{u,mean}}\right)^{\varepsilon}\left(\frac{KAS}{KAS_{mean}}\right)^{\theta} + error\ term \quad \text{(eq 2.7)}.$$

Applying the same procedure as was done in paragraph 2.5 results in the following. The correlation coefficients between the Ln of the normalized variables is calculated and is shown in Table 2-10. These correlations are used only to justify the use of the MVA.

Table 2-10 the correlation coefficients of the natural logarithms of the normalized variables of the de Wit small-scale samples

	H_c	RD	k_{Darcy}	D_{70}	C_u	KAS
H_c	1.00	-0.25	0.65	0.80	0.80	0.44
RD	-0.25	1.00	-0.78	-0.59	-0.59	-0.32
k_{Darcy}	0.65	-0.78	1.00	0.92	0.91	0.58
D_{70}	0.80	-0.59	0.92	1.00	0.99	0.64
C_u	0.80	-0.59	0.91	0.99	1.00	0.67
KAS	0.44	-0.32	0.58	0.64	0.67	1.00

As can be seen in Table 2-10 correlations between the Ln of D_{70} and k_{Darcy}, C_u and k_{Darcy}, and D_{70} and C_u is unacceptable high to perform a MVA on. A MVA will result in multicollinearity and the outcome of the MVA will fit the dataset of de Wit, but is not useful for reality. In Figure 2-31 and Figure M-1 till Figure M-6 several histograms and plots are shown. These histograms and their corresponding explanations reveal why the variables are correlated.

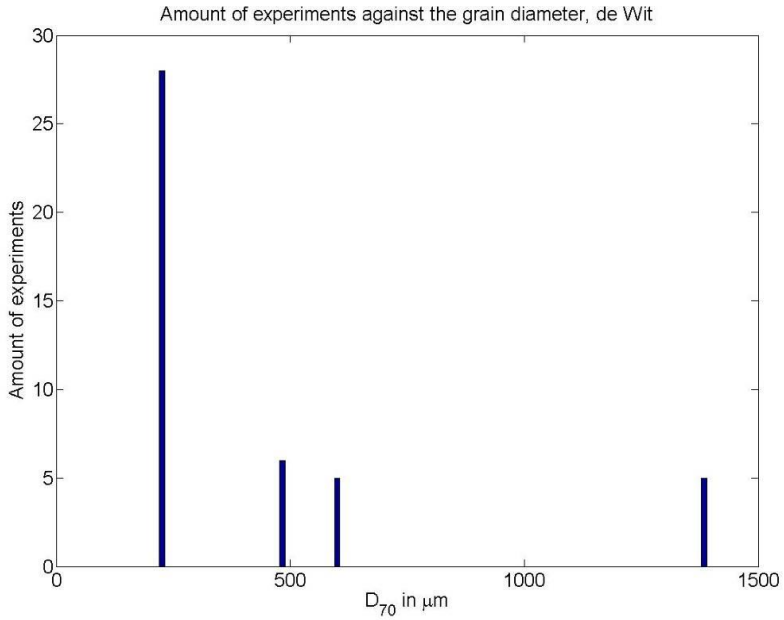

Figure 2-31 a histogram of the D_{70} of the sand samples used for the small-scale de Wit experiments

In Figure 2-31 and Figure M-1 till Figure M-4 histograms of the amount of experiments of the input variables are shown. As can be seen, only four different D_{70}'s are present. In Table 2-11 an overview is shown of the types of sand used by de Wit for the small-scale experiments. As can be seen, a higher D_{70} corresponds with a higher C_u and a higher KAS. This introduces very strong correlations between the variables, which are not present in reality.

Table 2-11 an overview of the types of sand used for the small-scale de Wit experiments

sand type	times used	D_{70}	C_u	KAS
dune sand	11	220	1.43	50.2
beach sand I	15	220	1.54	55.2
beach sand II	2	230	1.30	55.2
sieved river sand	6	480	2.10	56.9
river sand	5	600	2.40	56.5
coarse sand	5	1390	3.85	57.7

For a given sand sample the D_{70}, the C_u and the KAS are fixed values. Only the RD can still be varied. The k_{Darcy} is mostly determined from D_{70} and RD, and is thus partly fixed, partly free. By selecting only six different sand samples, and with

increasing grain size the C_u and the KAS also increases, very high correlations are present between variables in de Wit's dataset, which are not present in reality. In Figure 2-32, Figure M-5 and Figure M-6 certain variables are plotted against each other to investigate the correlation between the variables. As can be seen in Figure M-6, the higher the D_{70}, the lower the RD. This correlation is present because de Wit choices a low RD for the high D_{70}. This correlation is not present in reality. In Figure 2-32 the C_u against the grain size is plotted. A high D_{70} corresponds with a high C_u, and these variables are thus correlated in this dataset. In reality, these variables may be correlated to a certain extent, but not by a value of 0.99 as is shown in Table 2-9. Because of the poor choice of the dataset, between some input variables high correlations are present which do not occur in reality. This explains the difference between the correlations coefficients in Table 2-2 and Table 2-9.

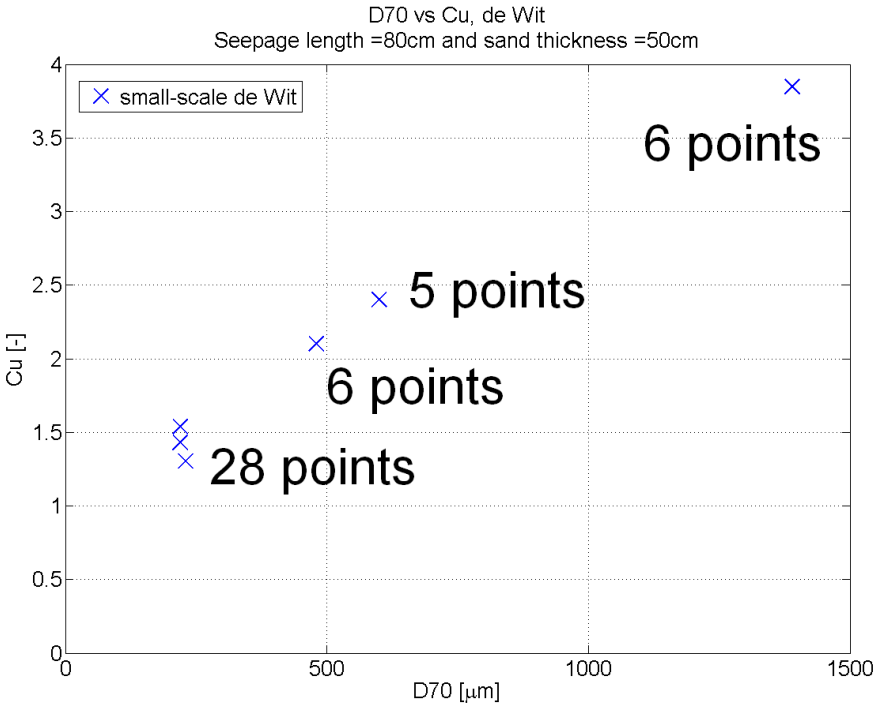

Figure 2-32 C_u plotted against the D_{70} for the small-scale de Wit experiments

To make a recapitulation,

- It is not sure if the error made by (possibly) neglecting the filter resistance is acceptably small, so it is not guaranteed the critical head is sufficient error-free
- The trend of the critical gradient against k_{Darcy} is not clear, as can be seen in Figure 2-27
- Extremely high correlations which are present in the dataset, but are not present in reality, prevent that a MVA can be done

Based on the above recapitulation, this means the small-scale data from de Wit's experiments can not be used for a MVA. It is not possible to perform a MVA on de Wit's dataset, but it is possible, that the variables from de Wit's experiments are substituted in the adapted Sellmeijer formula, to verify if the outcome agrees with the measured values or not.
The values of k_{Darcy}, RD, D_{70}, C_u and KAS of de Wit are inserted in the adapted Sellmeijer formula (eq 2-2), and the outcome can be compared with the measured values and a judgment about the agreement can be done. The results are shown in Table L-1 in appendix L. As can be seen in Figure 2-33, the measured and calculated critical heads with (eq 2-2) do not agree at al, especially for large sized grains. It should be noted that with the derivation of the MVA on SBW, it was stated the formula was derived on grain sizes with a D_{70} lower than 500µm, and the formula should be used with care for larger grains. The prediction with the current Sellmeijer model (eq 1-4) performs well, only for very coarse sand it does not give a very good prediction. The difference shown in Table L-1 shows some very high percentages, when compared with Table J-1. The data of de Wit agrees better with the current Sellmeijer formula, although for very coarse grains the Sellmeijer formula also over predicts the critical gradient. According to the error in Table L-2, the current Sellmeijer model performs the best for de Wit small-scale experiments.

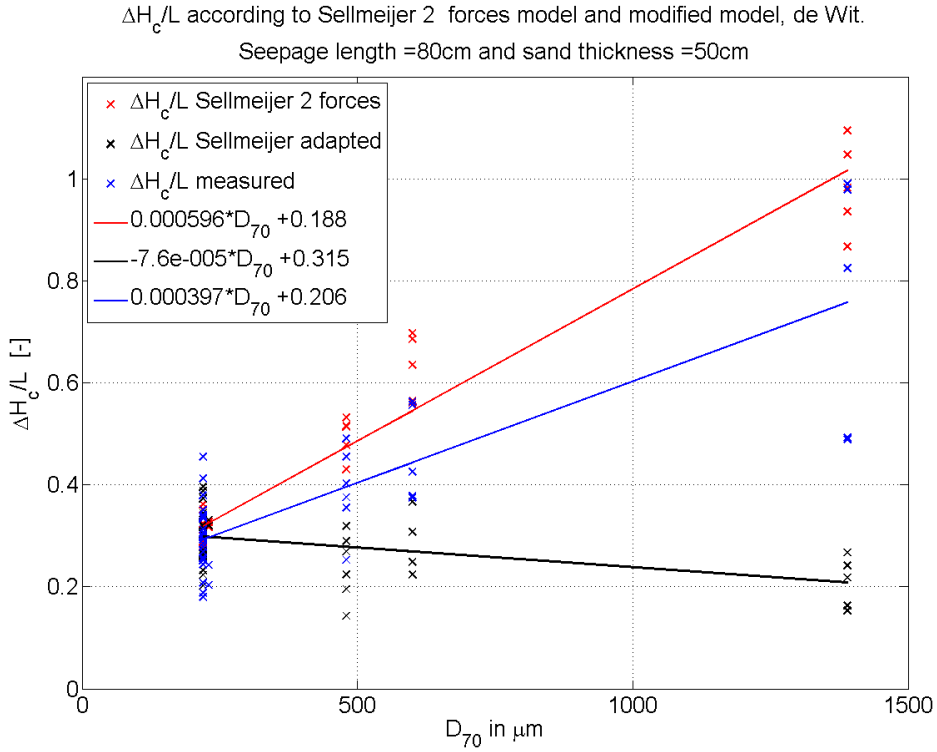

Figure 2-33 the measured critical head (small-scale de Wit experiments) and the critical head according to the prediction with the 2-forces and adapted Sellmeijer formula

From this the following can be concluded.

A MVA on de Wit's data can not be done, but when the data from de Wit is inserted in the adapted Sellmeijer formula (eq 2-2), the outcome does not agree with the observed critical heads at al. This means that the small-scale datasets of de Wit and SBW do not show the same behaviour. Since in Figure 2-33 the larger grains have a larger difference between measured and predicted values, the influence of grain diameter in de Wit's dataset on the critical gradient is higher than in SBW's dataset.

Possible explanations for this is that the two test facilities are not the same, or the range of variables in the datasets differ a lot. This will be explained further in chapter 4.

2.6.2 Analysis of medium-scale de Wit data

De Wit performed medium-scale tests with two different seepage lengths, 2.4m and 4.5m. According to Figure 2-14, the medium-scale experiments may not contradict the MVA of the small-scale experiments. Since a MVA on the small-scale experiments of de Wit is not possible, no comparison can be done. The amount of experiments of 2.4m is high enough to perform a MVA on it. Since only five medium-scale experiments of 4.5m have been done, no MVA or calculations of correlations have been done on the 4.5m experiments. The same procedure is followed as with the small-scale experiments. Again, it is unknown if the resistance of the filter was taken into account by de Wit, but since the seepage length is quite large, the relative error of (possibly) neglecting the filter resistance is probably quite low for the sands with a D_{70} around 200 and 400µm, but this is not certain. The second step according to Figure 2-14 is to investigate if the output variable against every single input variable shows the same kind of behaviour as is shown in Figure 2-16. Since most of the figures show the same behaviour as the small-scale experiments, the figures for the analysis are not treated here but are shown in appendix M. In Figure M-7 until Figure M-11, $\frac{\Delta H_c}{L}$ is plotted against the input variables.

As with SBW and the small-scale de Wit's experiments, the figures are compared with Figure 2-16. As can be seen in Figure M-7, it is very doubtful if the RD shows the behaviour needed for a linear MVA.

In Figure M-8, k_{Darcy} shows a clear trend and a linear MVA gives a useful outcome. In Figure M-9 and Figure M-10 the D_{70} and C_u show a very clear trend which is very suited for a linear MVA. In Figure M-11 the KAS is shown. This figure is not according to Figure 2-16. It is possible to use a very high exponential factor α for

the factor $\left[\frac{KAS}{KAS_{mean}}\right]^{\alpha}$, but this reduces the robustness of the MVA, and it is very unlikely that this very high influence of KAS is present in reality. It is more probable that a very high correlation is present between KAS and another input variable. The judgment if a MVA on de Wit's data is justified will be done later.

The third step according to Figure 2-14 is to investigate if the correlations between the input variables are acceptable low. The correlation coefficients between the normalized variables is calculated and is shown in Table 2-12. For the same reasons as discussed for the small-scale experiments, the correlation coefficients between the Ln of the normalized variables is calculated and is shown in Table 2-13.

Table 2-12 the correlation coefficients of the normalized variables of de Wit medium-scale samples

	H_c	RD	k_{Darcy}	D_{70}	C_u	KAS
H_c	1.00	-0.29	0.67	0.83	0.83	0.44
RD	-0.29	1.00	-0.67	-0.55	-0.55	-0.28
k_{Darcy}	0.67	-0.67	1.00	0.93	0.93	0.53
D_{70}	0.83	-0.55	0.93	1.00	0.99	0.58
C_u	0.83	-0.55	0.93	0.99	1.00	0.63
KAS	0.44	-0.28	0.53	0.58	0.63	1.00

Table 2-13 the correlation coefficients of the natural logarithms of the normalized variables of the de Wit medium-scale samples

	H_c	RD	k_{Darcy}	D_{70}	C_u	KAS
H_c	1.00	-0.25	0.65	0.80	0.80	0.44
RD	-0.25	1.00	-0.78	-0.59	-0.59	-0.32
k_{Darcy}	0.65	-0.78	1.00	0.92	0.91	0.58
D_{70}	0.80	-0.59	0.92	1.00	0.99	0.64
C_u	0.80	-0.59	0.91	0.99	1.00	0.67
KAS	0.44	-0.32	0.58	0.64	0.67	1.00

As can be seen in Table 2-12 and Table 2-13, correlations between input variables are sometimes extremely high, for the same reason as with the small-scale experiments of de Wit. Some of these correlations are present in reality as k_{Darcy} and D_{70}, k_{Darcy} and RD and C_u and k_{Darcy}, but most of the correlations are because of the choice of the dataset. Since the dataset contains such high correlations, and these correlations are not present in reality, assimilating one variable in the other can not be done. The high correlations between the input variables can be explained as follows. In Figure M-12 till Figure M-19 several histograms and plots are shown. These histograms and their corresponding explanations reveal why the variables are correlated.
The explanation of correlations is actually the same as for the small-scale experiments of de Wit. In Figure M-12 till Figure M-16 histograms of the amount of

experiments of the input variables are shown. As can be seen, only two different D_{70}'s are present. Also, just three different values of C_u and KAS are present. In Table 2-14 an overview is shown of the types of sand use by de Wit for the medium-scale experiments. As can be seen, a higher D_{70} corresponds with a higher C_u and a higher KAS. This introduces very strong correlations between the variables, which are not present in reality.

Table 2-14 an overview of the types of sand used for the medium-scale de Wit experiments

sand type	times used	D_{70}	C_u	KAS
dune sand	3	220	1.43	50.2
beach sand	12	220	1.54	55.2
coarse sand	9	1390	3.85	57.7

In Figure M-17 till Figure M-19 certain variables are plotted against each other to investigate the correlation between the variables. As can be seen in Figure M-17, the higher the D_{70}, the lower the RD. This correlation is present because de Wit choices a low RD for the high D_{70}. This correlation is not present in reality. In Figure M-18 the C_u against the grain size is plotted. A high D_{70} corresponds with a high C_u, and these variables are thus correlated in this dataset. In reality, these variables may be correlated to a certain extent, but not by a value of 0.99 as is shown in Table 2-9. Because of the poor choice of the dataset, between some input variables high correlations are present which do not occur in reality. In Figure M-19 the KAS against the grain size is shown.

To make a recapitulation,

- It is not known if a correction for the filter resistance has been done by de Wit, so it is not guaranteed the critical head is sufficient error-free
- The trend of the critical gradient against RD is not clear, as can be seen in Figure M-7. The KAS shown in Figure M-11 shows behaviour which can only be modeled with an extremely high exponential factor, which is undesired
- Extremely high correlations which are present in the dataset, but are not present in reality, prevent that a MVA can be done

Based on the above recapitulation, this means the medium-scale data from de Wit's experiments can not be used for a MVA.

Again as with the small-scale de Wit data, the dataset can be inserted in the adapted Sellmeijer formula and to verify if the outcome agrees with the measured values or not. In Figure 2-34 the measured and the prediction according to the current (eq 1-4) and adapted Sellmeijer formula (eq 2-2) is shown. As can be seen, both the current and adapted Sellmeijer formula do not agree with the measurements. The finer grains show an over prediction with the adapted Sellmeijer formula, the coarser grains show an under prediction.

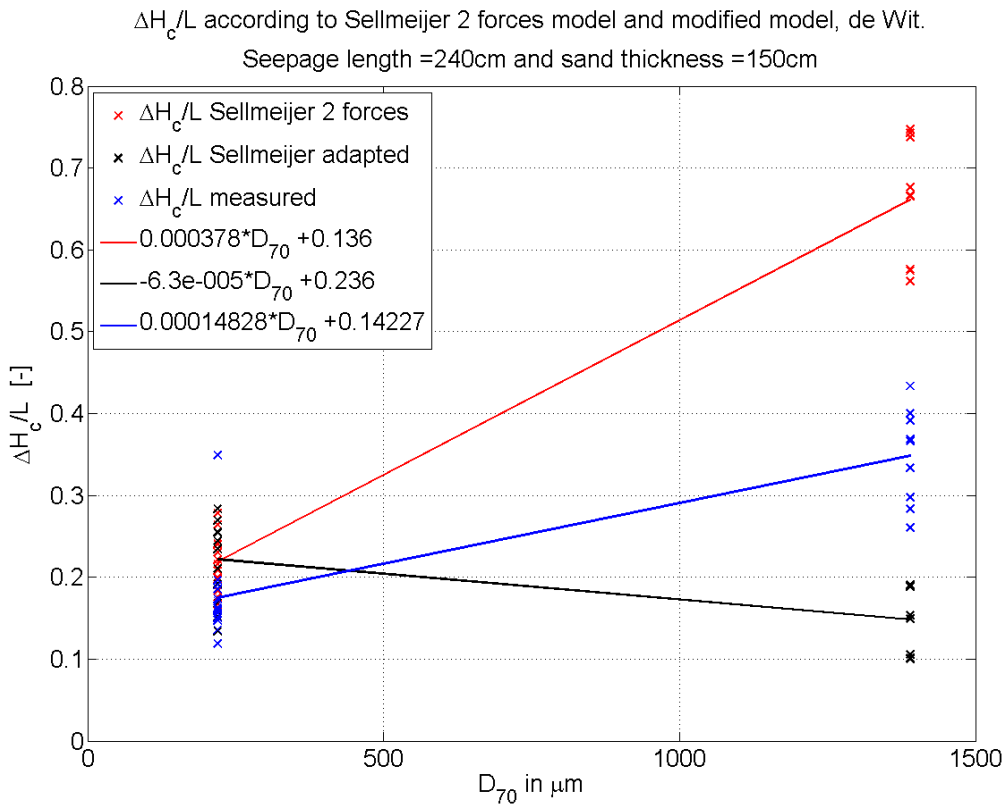

Figure 2-34 the measured critical head (medium-scale de Wit experiments) and the critical head according to the prediction with the 2-forces and adapted Sellmeijer formula

As can be seen in Figure 2-34, the measured (de Wit) and calculated critical heads with (eq 2-2) for medium-scale experiments do not agree at al. In Table L-3 the measured values and a comparison with the current and adapted 2-forces Sellmeijer models are shown. The differences are in the order of 100% or more. In Table L-4 the error is shown. As can be seen, the error is the smallest for the current 2-forces Sellmeijer formula. For seepage lengths of 450cm, 5 experiments have been performed with a D_{70} of 220μm. Results of calculation performed on this dataset is shown in Table L-5 and Table L-6. The adapted 2-forces Sellmeijer formula (eq 2-2) gives a very low error, but since only one D_{70} is involved, it does not give any information about a trend between D_{70} and critical gradient so the error shown in Table L-6 can not be used for comparison.

2.6.3 Concluding remarks of analysis on de Wit data

The following can be concluded. A MVA on de Wit's medium-scale data can not be done because of, amongst others, high correlations, but when the data from de Wit is inserted in the adapted Sellmeijer formula, the outcome does not agree with the observed critical heads at al. This means that the small-scale dataset of SBW and the medium-scale dataset of de Wit do not show the same behaviour. The

outcome of the experiments in de Wit's dataset show a higher influence of the grain size on the critical head than the experiments from SBW do.

It is concluded in this paragraph that both small-scale and medium-scale experimental outcome do not agree with the trend of SBW. The current Sellmeijer 2-forces model (eq 1-4) performs well for de Wit's dataset. In chapter 4, a detailed comparison between the SBW and de Wit outcome of the MVA is discussed.

In Figure 1-16 the trend between critical gradient and D_{70} is shown. The trend between critical gradient and D_{70} looks positive, but because of the correction of the filter resistance, which was possibly not performed, the critical head may not be correct. The resistance is dependent on the flow velocity, and because larger grains have a higher permeability and thus a higher flow velocity, the resistance is higher for the larger grains. And because the D_{70} is highly correlated with other variables, it is not sure to say if it is the D_{70} which causes the higher critical gradient. The D_{70} is extremely highly correlated with C_u in the dataset of de Wit. It may be that the higher C_u leads to a higher critical gradient, and when the critical gradient is plotted against the D_{70}, a positive trend between critical gradient and D_{70} is visible because of the strong correlation. This correlation is not present in reality, so the outcome is not valid for reality. It can not be stated that in de Wit's dataset a positive trend is present between D_{70} and critical head, which is purely present because of the D_{70}. The trend that is visible in Figure 1-16 may be present because of the D_{70}, or because of another variable that is correlated with D_{70}. Based on substituting the outcome of de Wit's experiment in the adapted Sellmeijer formula (eq 2-2), it is shown that in de Wit's experiments, the D_{70} has a higher influence of the critical gradient than the experiments of SBW do. For very coarse sand, the current Sellmeijer formula gives an overestimation when compared with the measurements of de Wit (Sellmeijer, 1993).

2.7 Conclusions and a summary about multi variate analysis on SBW and de Wit data

In this chapter a study of variables is performed. This study consists out of a multi variate analysis (MVA) on the datasets of SBW and de Wit. The adapted Sellmeijer formula is explained in paragraph 2.1. This adapted Sellmeijer formula consists out of the current Sellmeijer formula corrected with certain factors, which were the outcome of a multi variate analysis of López de la Cruz on the SBW small-scale dataset. In paragraph 2.2 and 2.3 it is explained which variables are taken into account in the MVA. In paragraph 2.4 the use of the MVA is explained.

In paragraph 2.5 a multivariate analysis was performed on the SBW data. The MVA was successful and influence of the variables on the critical head could be distinguished. The influence of the D_{70} is less than would be expected based on

the Sellmeijer model. The influence of permeability is just as is expected from theory, as vary little doubt is about the groundwater flow equation in the Sellmeijer formula. Also remarkable is the high influence of the relative density, which is not taken into account in the current Sellmeijer formula. The regression coefficients, which are the outcome of the MVA on the SBW data are shown in Table 2-15.

These regression coefficients confirm the regression coefficients found by López de la Cruz. The small differences between the two can be allocated to multi-colinearity, or to some of the arguments shown on page 25.

Table 2-15 the regression coefficients are the outcome of the MVA

variable	symbol of regression coefficient	regression coefficient from MVA performed in this thesis	regression coefficient from MVA performed by López de la Cruz
constant	α	-0.91	-
RD	β	0.41	0.35
k_{Darcy}	γ	-0.31	-0.35
D_{70}	δ	0.29	0.39
C_u	ε	0.16	0.13
KAS	θ	-0.005	-0.02

A MVA was tried on the data of de Wit. Unfortunately, because very strong correlations between variables in the dataset of de Wit were present, a MVA could not be performed. The data of de Wit is inserted in the adapted Sellmeijer formula. The difference of the measured values and the calculated values is shown in Figure 2-33, and Figure 2-34. As can be seen in the graphs, the fine grained sands in the de Wit dataset are overestimated with the adapted Sellmeijer formula, the coarse grained sands are underestimated. This means the influence of D_{70} on the critical head in the de Wit dataset is higher than the influence of the D_{70} in the SBW dataset. An explanation has to be found for this difference between influence of grain size on the critical gradient in the SBW and de Wit dataset. The current Sellmeijer formula agrees better with the data of de Wit, only not for very coarse sand. A possible reason why the trends are not the same is that in SBW the critical head is corrected for the resistance of the filter. This correction is significant. It is unknown if de Wit has performed this correction on his dataset. The test facility used by de Wit is also different from the test facility used by SBW. The variables in the datasets of SBW and de Wit do not have the same range. These arguments are elaborated on in more detail in chapter 4.

It should be kept in mind the experiments were performed on homogeneous sands, so that permeability and D_{70} are correlated. In reality multiple layers of sand can be present, so that the permeability of the lower layer and the D_{70} of the top layer can be less or even uncorrelated.

3. Research to the transport and erosion mechanism

The objective of this masters thesis is to research the influence of the grain size and other sand characteristics on the critical head of piping, and to find an explanation for the difference found between SBW results and the Sellmeijer formula.

One of the hypotheses of this thesis is that the found difference between SBW and the Sellmeijer formula is because the formula of White is not applicable as an erosion formula in a piping model. In this chapter, research to the erosion model of White in the Sellmeijer model is performed.

Sellmeijer's model consists out of three differential equations, continuity, Poiseuille flow and the equilibrium of grains according to White. The outcome of these differential equations is the Sellmeijer formula.

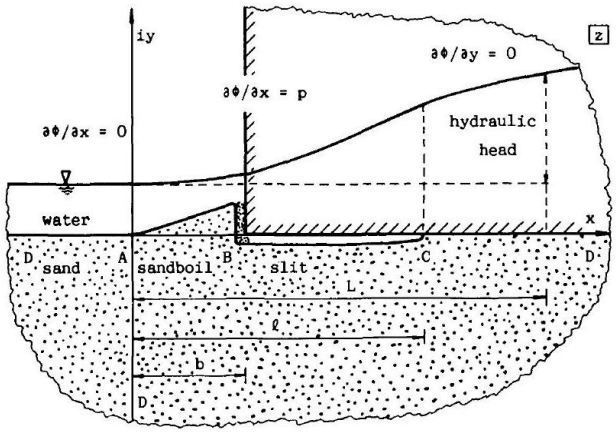

Figure 3-1 a picture of the geometrical plane of the Sellmeijer model (Sellmeijer, 1988)

In the Sellmeijer model, it is assumed a (short) channel is present under a dike (this is because of convergence of the streamlines). This can be seen in Figure 3-1. In this channel Poiseuille flow is assumed. This flow transfers a shear stress on the bed of the channel. The equilibrium of the grains on the bed of the channel with the shear stress caused by Poiseuille flow is assumed to be according to White's equilibrium formula. When the gradient is increased, the length of the channel increases, until a new quasi-static equilibrium is reached. This continues until a channel length of 0.5L is reached, where L is the seepage length. Then, no equilibrium is present anymore, and the channel grows very fast until the intake point of the flow is reached and a full pipe is present under the dike.

One of the hypotheses of this thesis is that the equilibrium of White is not applicable as an erosion formula for piping. White assumes individual grain transport, where the grains roll over each other.

In paragraph 3.1 the erosion model of White is explained. The implementation of White in the Sellmeijer model is shown in paragraph 3.2. From a theoretical background, the applicableness of the equilibrium of grains according to White is questioned in the flume and in the case of a pipe. This is treated in paragraph 3.3. To verify experimentally if the erosion process, and accordingly the equilibrium of grains, in the pipe is as White described, experiments were carried out in the laboratory of Deltares. For the experiments a test facility was constructed. The test facility and the set-up during the experiments is explained in paragraph 3.4. The results of the experiments are treated in paragraph 3.5. In paragraph 3.6 explanations and conclusions about the experimentally observed erosion mechanism are given. Conclusions about the use of the formula of White as an erosion mechanism in the piping model is treated in paragraph 3.7. In paragraph 3.8 the agreement of the outcome of the experiments with reality is discussed and some recommendations about the erosion mechanism is given. Conclusions about the erosion mechanism are given in paragraph 3.9.

3.1 The equilibrium of grains on a bed according to White

The theory of equilibrium of grains on a bed according to White was published in 1939 in an article called “The equilibrium of grains on the bed of a stream” (White, 1939). In this article the equilibrium of grains on a bed is researched experimentally in a flume. A summary (of the aspects that are considered relevant for piping, and used by Sellmeijer in his model) of that article is given in this paragraph. All statements, assumptions and conclusions in this paragraph represent the statements, assumptions and conclusions of White.

The relevant parts of the paper of White is summarized below:

A fluid moving over a loose flat granular bed tends to move the grains forward, and the conditions under which movement begins depend, not only on the speed but also on the nature of the motion itself: viscous steady motion, steady inviscid motion, and turbulent motion act somewhat differently, and the speed necessary to dislodge grains differs appreciably.

White states the shear stress exceeded by the flow in the flume is transmitted from flow to the bed by the more prominent grains in the uppermost layer only.

Two extreme cases are considered by White. At slow speeds and with small grains the pressure at the front does not appreciably exceed that at its rear, and the

force applied is the resultant of viscous stresses acting tangentially as shown in Figure 3-2.

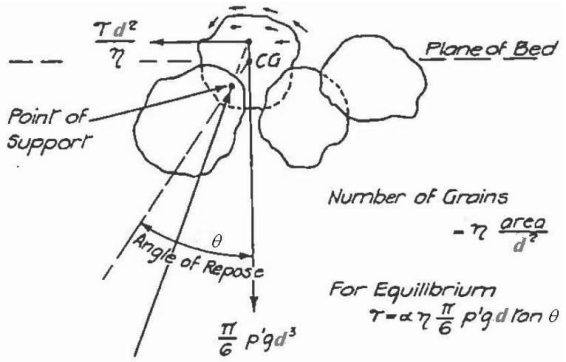

Figure 3-2 the equilibrium of an individual sand grain according to White when the tangential forces are of major importance (White, 1939)

White states that at high speed and with large grains such tangential drag becomes relatively unimportant compared with the drag due to pressure differences, which results in a pressure distribution that is not symmetrical but is less over the downstream half of the grain, so that when integrated it gives rise to a resultant force or form drag whose component resist the motion.

White states that at low speeds and at high speeds, if the main stream is turbulent, the force applied to the grains fluctuates irregularly. In the low speed case, if the main stream is steady, the force on the grain is also steady. In the high speed case, whatever the state of the main stream, eddies are shed from the back of the grains and grains farther downstream are at least subjected to the cumulative effect of the pulsations from upstream.

White introduces a so called packing coefficient η, defined as D^2 times the number of grains per unit area. When a mean stress τ is applied to the bed each exposed grain transmits a horizontal force $\frac{\tau D^2}{\eta}$ from fluid to bed. White states that in the high-speed case, when tangential forces components are negligible, the resultant force, if the grain be regarded as spherical, passes through it's centre, and the forces are in equilibrium and the grains about to move when, as in Figure 3-3, $\tau = \eta \frac{\pi}{6} \rho' g D \tan(\theta)$ *(eq 3-1)*.

Where ρ' is the effective density and θ is the angle of repose of the surface layer of the grains.

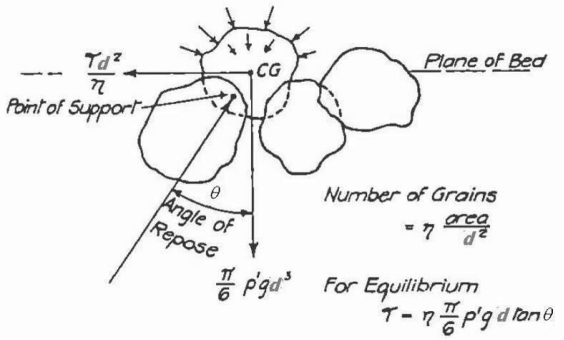

Figure 3-3 the equilibrium of an individual sand grain according to White when the fluid acts normally to the surface and tangential stresses are negligible (White, 1939)

For the slow-speed case the corresponding force system is shown in Figure 3-2, where it is seen that the line of action lies above the centre of gravity.

Since the height of at which the force acts cannot be predicted analytically, an experimental coefficient α must be included in the equation by white, which becomes $\tau = \alpha\eta\frac{\pi}{6}\rho' gD\tan(\theta)$ *(eq 3-2)*.

Both equations of the shear stress concern the equilibrium of grains just as they are about to move according to White, and in both the value of τ is a local and instantaneous one.

White performed several experiments, steady viscous flow, steady inviscous flow and turbulent flow were researched. Since Sellmeijer assumes slow-speed flow, only steady viscous flow is discussed in this paragraph in detail.

For the steady viscous flow, a flume has been used, and two types of sand are researched. According to Nikuradse, viscous or tangential stresses dominate when $u_*\frac{D}{\nu} < 3.5$, where $u_* = \sqrt{\frac{\tau}{\rho_w}}$. Because of this, the need for a fluid more viscous than water is needed. A lubricating oil with a viscosity of $0.16*10^{-3}m^2/s$ was used by White. Each type is tested two times, with different packing factors ($\eta = 0.3-0.4$ and $\eta = 0.8-1.0$). The (critical) stresses on the bottom of the bed are $\tau = \rho ghi$. From the experiments it appeared that the critical stresses are independent of the packing factor η. White explained this by suggesting that with a lower η, less grains are available to transfer the shear stresses, but the point of the resultant force on the grains is lower down. From that White concluded it is sufficient to calculate the product $\alpha\eta$. The α factor in the White model (eq 3-2) is defined as an empirical correction coefficient for the lever length, because the

resulting force of the friction forces does not go through the mass centre of the grain. Two figures have been made to clarify White's conclusion. In Figure 3-4, a tight packing is shown on the left and a loose packing is shown on the right (the grains are round and all have equal diameter, the stresses drawn are not on scale). The loose packed grains have a lower packing coefficient, and transfer higher stresses per grain, but the resulting force has a lower lever length to the bed, when compared with the tight packed grains. White concludes the product of the packing coefficient (η) and the correction coefficient of the lever length of the resulting force on a grain (α) is constant.

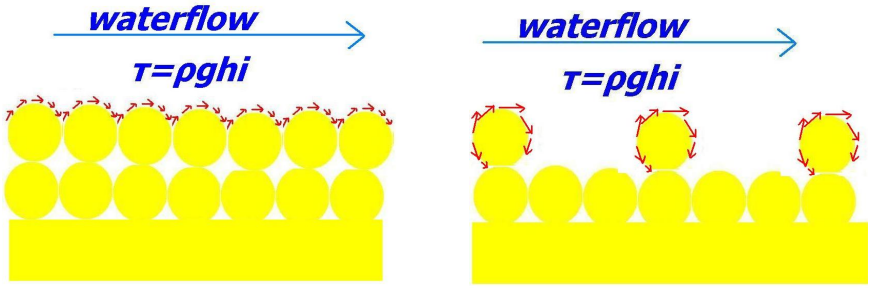

Figure 3-4 stresses on grains with a tight packing (left) and a loose packing (right) according to White

White concludes, based on two experiments, that tight packed grains transfer less stress per grain, but have a high lever length. Loose packed grains transfer more stress per grain, but have a lower lever length, and thus the product of stress per grain times the lever length is constant, and only the value $\alpha\eta$ has to be determined experimentally. In Table 3-1 values of $\alpha\eta$ for the two types of sand are shown.

Table 3-1 results of $\alpha\eta$ according to experiments of White for steady viscous motion (White, 1939)

exp. no.	sand type	D [µm]	tan(θ) (in oil) [-]	τ_c [Pa]	$\alpha\eta$ [-]
1	no. 2 Aylesford	210	1.40	0.95	0.37
2	no. 3 Leighton Buzzard	900	1.05	2.60	0.31

White suggested the value of $\alpha\eta = 0.31$ is the most reliable, as the individual grains of the finer sand were almost invisible in oil. White performed also experiments for steady inviscous flow and turbulent flow. Since Sellmeijer did not use these experimental outcomes, these are not described here in detail. But an interesting remark about the steady inviscous flow experiment is given.
The steady inviscous flow is researched in one single experiment with a nozzle, and water is used as fluid. The outcome is $\alpha\eta = 0.39$. Allowing for uncertainty in D and tan(θ), White states the outcome is consisted with the outcome of the steady viscous flow. With the water and oil experiment White covers values of $u_* \frac{D}{\nu} = 0.04$

to 2.1, and he states the $\alpha\eta$ value does not show significant change as function of $u_* \frac{D}{\nu}$. White states that this conclusion is in contradiction with the findings of Shields, who concludes that $\frac{\tau}{\rho' gD}$ varies inversely with $u_* \frac{D}{\nu}$. White concludes that this is because his results are based on a much wider experimental range.

White states that several researchers have tried to explain the very large differences between flume values and the static force required to dislodged a grain. This has been attributed by several researchers as the lift force, as this was found in several experiments. White is convinced this lift force is negligible in his experiments, because water overpressure can easily flow out of the spaces between the grains. White did a experiment with a 5.6mm grain made out of wax. The downstream movement of the wax grain was prevented because it was fastened by a piece of cotton. Flowing up of the wax grain was not prevented. Still the grain remained on it's place, and White concluded lift forces are negligible.

3.2 Use of the equation of White in the Sellmeijer model

Sellmeijer used as a starting point for equilibrium of grains on the bottom of the slit the η parameter, as according to Sellmeijer only the more prominent grains on the bed transfer shear stress from the flow to the grains.

The α factor in the White model is defined as an empirical correction coefficient for the lever length, because the resulting force of the friction forces does not go through the mass centre of the grain. The factor $\alpha\eta$ is constant according to White. Sellmeijer uses the factor η and does not take into account the α factor. (The use of the α factor in White should not be confused with the α factor in the Sellmeijer formula. In the Sellmeijer formula α is the layer thickness parameter which is a function of the length over width ratio of the sand layer).

The shear stress on the bottom in a flume is $\tau = \rho_w ghi$, in the slit in a piping channel the shear stress on the bottom is $\tau = 0.5\rho_w gai$, where a is used as slit height in stead of the water depth h. Assumed is bottom and top of the slit contribute equal to the shear stress. This results in $0.5\rho_w gai = \eta \frac{\pi}{6} \rho_p' gD\tan(\theta)$. The equation $i = \frac{d\varphi}{dx}$ can be substituted. This results in $\frac{a}{D}\frac{d\varphi}{dx} = \frac{\pi}{3}\eta \frac{\gamma_p'}{\gamma_w}\tan(\theta)$ *(eq 3-3)*. This is basically the same formula shown in Figure 3-2, only in a different notation. This is the equation used by Sellmeijer as is shown in paragraph 1.4 and 5.1.

A value of $\alpha\eta$ is 0.31 is suggested by White. Since there is some uncertainty in this value, and α is not taken into account in the Sellmeijer model, a safe value of 0.25 is suggested by Sellmeijer. The value of 0.31 corresponds to a grain diameter, of which 65 to 75% of the grains have a smaller diameter (Sellmeijer, 1988). Because of this Sellmeijer chooses the D_{70} as the characteristic grain size which represents the resistance against erosion in the channel.

3.3 Theoretical arguments against the use of White in a piping model

In this paragraph the correctness of the equilibrium of grains according to White is questioned from a theoretical background. Several of the assumptions and conclusions made by White in paragraph 3.1 are questioned and show that White may possibly not be a correct model, or is possibly not applicable, for calculating equilibrium of the grains. The use of White in a flume and the use of the equation of White in the Sellmeijer piping model are treated separately.

The arguments why the equilibrium of grains in the erosion model of White may possibly be incorrect, or possibly not applicable, in case of a flume are shown below. The arguments are summarized first, later a more detailed explanation is given. Since not all arguments are equally convincing, the degree of convincingness is also discussed.

a) Only a very few amount of experiments have been performed by White
b) The results of the fine grained experiments are considered less reliable by White, because the individual grains were almost not visible
c) The experiments with viscous steady motion are performed with a lubrication oil
d) A spherical grain is assumed
e) With the formula $\tau = \rho g h i$, equilibrium of the grains is calculated. Only the prominent larger grains that stick out of the channel bed are assumed to transfer stresses from flow to grain according to White
f) Lift forces (because of pressure fluctuations) are assumed negligible, based on one experiment
g) White concludes the $\alpha\eta$ value does not show significant change as function of $u_* \frac{D}{\nu}$, this is in contradiction with the findings of Shields
h) The force on the grain is horizontal according to White

The arguments why the erosion model of White is incorrect in case of piping specific are shown below.

i) The resistance of individual grains is considered by White
j) The resistance of grains against transport is modeled with the rolling resistance angle
k) The experiments of White are performed in a flume
l) Shields is not valid for water depths shallower than 100*D
m) With the formula $\tau = \rho ghi$, equilibrium of the grains is calculated

The arguments are explained further below

a) For the viscous steady motion, only four experiments have been performed. A coarse sand and a fine sand was tested, both with a loose packed and a tight packed layer of grains on the bed of the flume. The amount of experiments is to few to make rigid conclusions
b) The results of the fine grained experiments are considered less reliable by White, because the individual grains were almost not visible. That is why only the two experiments with coarse grained sand are considered reliable by White, so the value of $\alpha\eta$ = 0.31 is only based on two experiments on coarse grained sand. Since the shear stress found by White for loose and tight packed sand was roughly the same, White concluded the product of α (correction coefficient for the lever length) and η (packing coefficient) is always constant. This is based on two experiments with coarse grains. It is very doubtful if this is indeed correct
c) The experiments with viscous steady motion are performed with a lubrication oil. This means the outcome of White's experiments is only valid for lubrication oils. Since in normal conditions, it is water that is the fluid that drives erosion, the outcome for the experiment with lubrication oil may not be applicable to erosion by water. Besides the viscosity, also the density and the surface tension is of the oil is different than that of water. In Figure 3-2 the formula of the shear stress is shown. In the formula, ρ' is present, which is 1650kg/m^3 for quartz sand. Since the lubrication oil has a different density than water, the outcome of the experiment may not be applicable to erosion by water
d) A spherical grain is assumed for the calculation of equilibrium of the grains, in reality grains are not spherical
e) White assumes only the larger more prominent grains that stick out of the bed transfer shear stress of the water. It is unknown if this is true
f) Lift forces are assumed negligible by White, based on one experiment, while other researchers claim lift forces are present (Schiereck, 2004)
g) White contradicts Shields when comparing the viscous steady motion experiments (with lubrication oil) and the steady inviscid motion (one experiment with water in a nozzle) with the outcomes of Shields, and White

claims that this is because of a much wider experimental range in the experiments of White is present. Since only one experiment was done with the nozzle, the amount of experiments is to few to make this conclusion

h) The force on the grain is horizontal according to White. On a grain, normally it is considered a drag, shear and lift force is present in a flow (with piping an additional force from the up flow of seepage water in the channel is present, which is included in the Sellmeijer 4-forces model). This means the resulting force on the grains is in general not horizontal
i) Resistance of individual grains is considered by White. It is still unclear if this is true. Grains may move as mass transport
j) The resistance of grains against transport is modeled with the rolling resistance angle. It is unclear if the grains roll indeed over each other like is assumed by White
k) The experiments of White are performed in a flume, and this does not mean the results are also valid for piping
l) Shields is not valid for water depths shallower than 100 grain diameters. It is unknown if White has the same restriction, since White did not perform experiments in shallow water. (In stead of Shields, Ashida can be used for very shallow water in a flume)
m) With the formula $\tau = \rho ghi$, equilibrium of the grains is calculated. Since both top and bottom contribute to the shear stress, $\tau = 0.5\rho ghi$ is assumed for top and bottom. It is not clear if this is true, since the sandy bottom and the clay top have a different (Nikuradse) roughness

The arguments of a, b, c, d, f, i, j, k and l are strong arguments why the equilibrium of grains on a bed according to the erosion model of White is possibly incorrect or possibly not applicable as a formula for erosion in a flume in general, or for erosion in the piping channel. The arguments of e, g, h and m are not very strong arguments, but are worth noting.

Based on the arguments in this paragraph it is argued from theory that it is questionable that the equilibrium of grains on a bed according to the erosion model of White is applicable for piping.

3.4 Set-up of the experiments with the one-dimensional test facility

To investigate the erosion process, and accordingly the dislodging process of grains, a test facility has been constructed to observe the piping process from the side. In this paragraph the test facility and the set-up of the experiments with the test facility is treated. The test facility is shown in Figure 3-5. This test facility is referred to as the one-dimensional test facility. The test facility is 50cm long, 1cm

thick and 10cm deep (inner dimensions). The seepage length of the sand is roughly 33cm.

Figure 3-5 the test facility

The test facility is filled from the side. With a metallic pounder the sand is compacted until the wanted relative density is reached. The first few centimeters of the test facility is filled with filter gravel at the inflow side, as can be seen in Figure 3-6 on the left, to prevent the inflow of water to act like a jet on the sand. At the outflow side a filter is present, to support the sand. This filter is not present over the whole height. The top 2cm is open, as can be seen in Figure 3-6 in the middle. The filter is supported with two struts. Whenever in this chapter is referred to the exit point of grains, the point shown in Figure 3-6 (right side) is meant. The erosion process is filmed from close by with a video camera. This is shown in Figure 3-7. As can be seen the lens of the video camera is at a distance of about 1cm from the test facility. A frame of roughly 3cm wide is recorded from this distance. After the test facility is filled, the filter shown in Figure 3-6 (middle) and the lit is placed and the test facility is tilted.

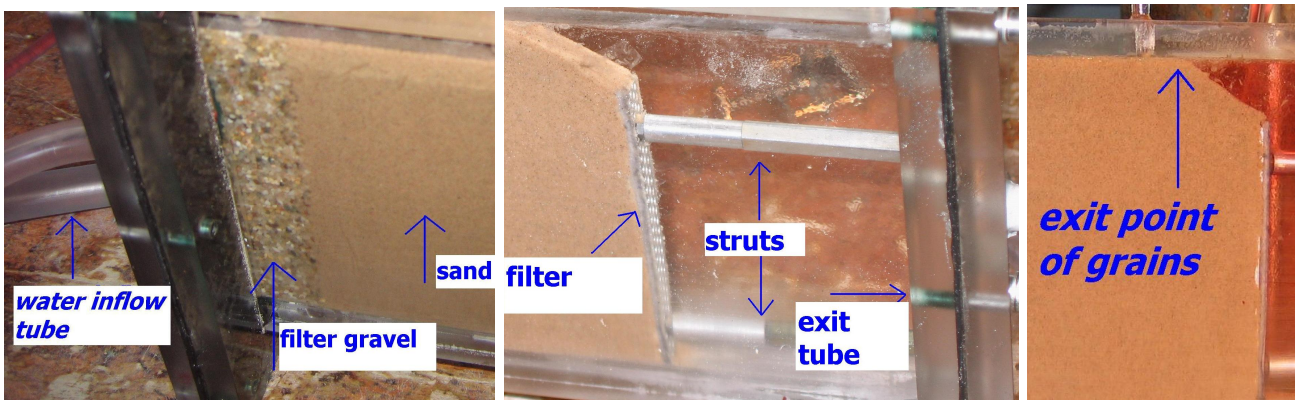

Figure 3-6 the filter gravel at the inflow side (left) the filter at the outflow side (middle) and the exit point of the grains (right)

Figure 3-7 the set-up for the video camera

Every recording has been done with high resolution. These recordings use a lot of memory, that's why every recording has been copied with a medium resolution. The high resolution recordings are available at Deltares. For the medium resolution, the complete recordings and summary's of a few minutes are available. Whenever referred to a timeframe in this chapter, it is referred to the complete recording of the medium resolution recording.

3.5 Results of the experiments with the one-dimensional test facility

In total 18 experiments were performed. For every experiment a factual report is made. These can be found in appendix P. In this paragraph the results of these experiments are treated. The interpretation of these experiments follow in paragraph 3.6.

Most of the experiments were performed with the sand "Ringstrasse Itterbeck Enschede", with a D_{70} of 431µm the coarsest sand used in SBW. The reason for the use of this coarse sand is that it is easier to film the individual grains with a video camera. Different relative densities were used.

The relative densities used were in the orders of

- 25%
- 40-50%
- 60%
- 80%

Each of the different relative densities gave a somehow different result. These different results are treated separately. The measured critical gradients during experiments were in general higher than in the small-scale test facility used by van Beek in SBW. This can be explained by the following.

- In the small-scale test facility, piping searches for the route with the least resistance. In the one-dimensional test facility, piping can only follow one path
- In the small-scale test facility, three dimensional flow in the sand body to the channel occurs, this three dimensional flow is not present in the one-dimensional test facility
- In the one-dimensional test facility, arching effects may occur. This can happen when the width (1cm in case of the test facility) is less than 100 times the grain diameter (Schenkeveld, 2010)
- Some boundary effects are different, as putty was used on the inside of the test facility in the experiments of van Beek, to create roughness

Since the critical gradients with low relative densities were between 0.35 and 0.55, the erosion process of the experiments with low relative densities are considered most normative as erosion mechanism of piping, as they resemble the outcome of the small-scale SBW experiments the most.
The experiments are meant only for observations. The measured numerical values for the critical gradient should not be used for calculations or fittings. In all figures in this chapter, the water flows from the left side to the right side.

The dislodging of grains that is observed during the growing of the erosion channel is normative for the assessment what the behaviour of the erosion mechanism is. Once the channel is through all the way, the erosion mechanism is not normative for the equilibrium against piping.

Results of the experiments with a relative density of 40-50% are treated first, since most of the experiments were performed with this relative density, and most of the video footage of these experiments are of the best quality. After that, the experiments with a relative density of 60%, 80% and 25% is treated. More detailed information about the measured values can be found in appendix I and in the factual reports in appendix P.

3.5.1 Results of the experiments with a RD of 40-50%

In this subparagraph the results of the experiments with a relative density of 40-50% is treated. Ten experiments with this relative density were performed. The sand type Ringstrasse Itterbeck Enschede was used. Most of the critical heads with these relative densities varied between 15 to 25cm. When the head applied to the sand is gradually increased, the first thing that happens to the sand is that, from the exit point of the grains (this point is defined in Figure 3-6), seen from the top, over a length of roughly 4 or 5cm a sinusoidal channel of roughly 1 or 2mm thick and 1 or 2 grain diameters deep appears. In Figure 3-8 this sinusoidal channel is

shown from the top. The picture is not very clear, so the picture is shown two times, where on the second picture the channel is drawn with a red line.

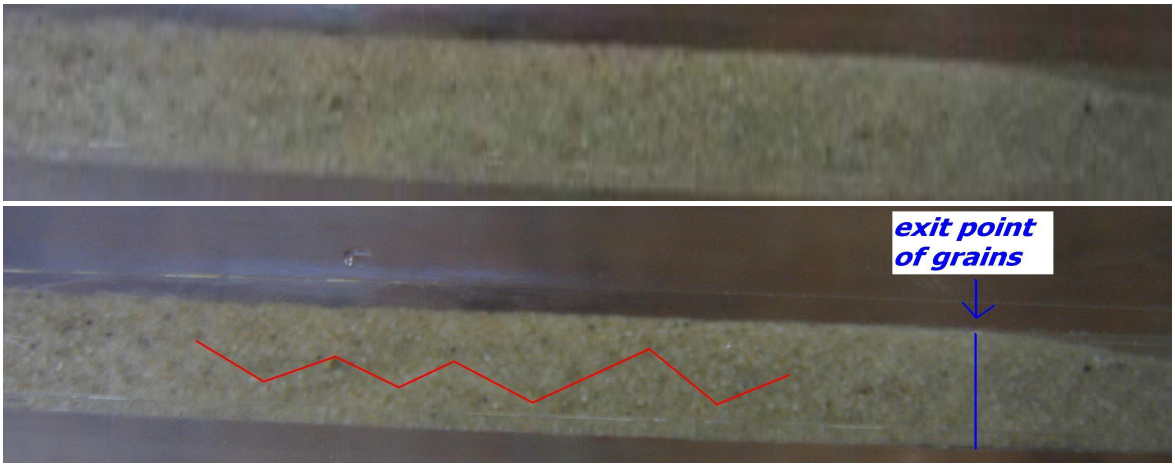

Figure 3-8 a top view of the sinusoidal channel, with a length of 4cm

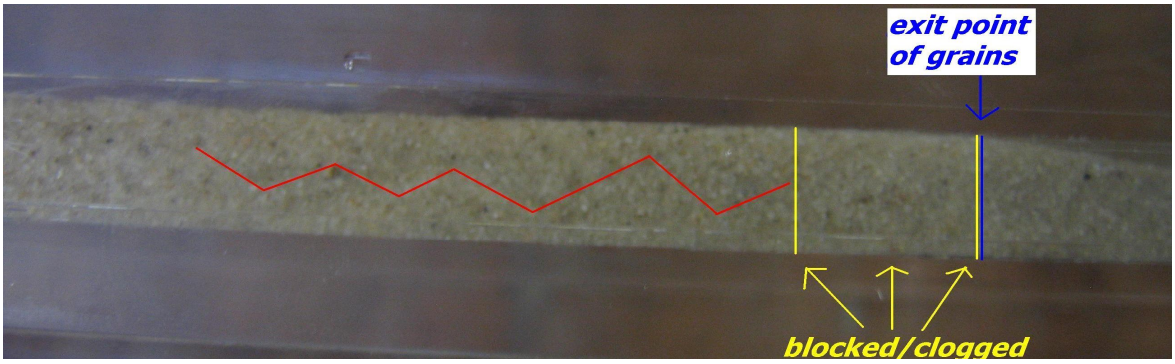

Figure 3-9 a top view of the part what is blocked after a sinusoidal channel is formed

After the occurrence of the sinusoidal channel, at the exit point of the grains, the sinusoidal channel is often blocked again with grains. This is shown in Figure 3-9. A new equilibrium situation occurs. Then the head is increased again. Then at the top side, it can be seen certain “clouds” of grains, with a surface of roughly 0.5 by 1cm^2 and 1 grain diameter thick, travel to the exit point. This process is observed in all of the experiments and is recorded during experiment Q9 and Q10 from the top. In Figure 3-10 a picture of the transport is shown, from the top. The grains between the yellow lines move together, as mass transport, as a “cloud” of one grain diameter thick, to the right. The movement can best be seen on the video of Q9 or Q10 itself. These clouds are sometimes in combination of transport of grains in sinusoidal shaped erosion channels.

Figure 3-10 a picture from the top, the grains between the yellow lines move as a cloud to the right

The movements of these clouds of grains continue for a while. From the side these clouds are in most of the experiments not visible, since most of the times just the grain that lies against the Perspex wall does not move, or the cloud is not present over the whole width of the test facility, and tends to develop at the other side of the test facility, which is not filmed. In experiment Q16, this process is visible from the side. This is shown in Figure 3-11. The grains are dislodged and move together as mass transport of roughly 1 grain diameter thick to the right. This process is relatively slow.

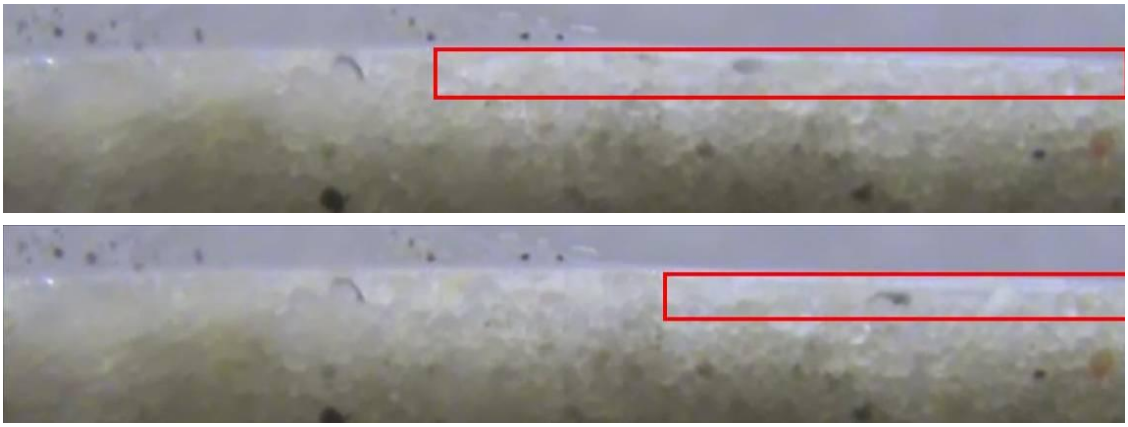

Figure 3-11 the slow movement of a layer what is called a "cloud" in this chapter

After several of these clouds passed by, at certain places the channel gets clogged, or blocked by grains. This is shown in the red box in Figure 3-12. In the blue box, no grains are present.

Figure 3-12 the blocking of a channel

The grains in the red box are stable for several seconds, then the plugged sand grains are pushed through the channel in a "wave". The grains are dislodged from

the granular matrix with hundreds of grains together, with a layer thickness of roughly 7 grains. This transport of grains in “waves” is as mass transport. These waves are seen in all the experiments with a relative density of 40-50%. The sand waves are explained by means of several screen shots right after each other of the video of experiments Q14 and Q17, shown in Figure 3-13 to Figure 3-15. The process can best be seen in the videos itself. More figures of waves can be found in appendix O. The front of the wave is pointed out by a blue arrow in the figures.

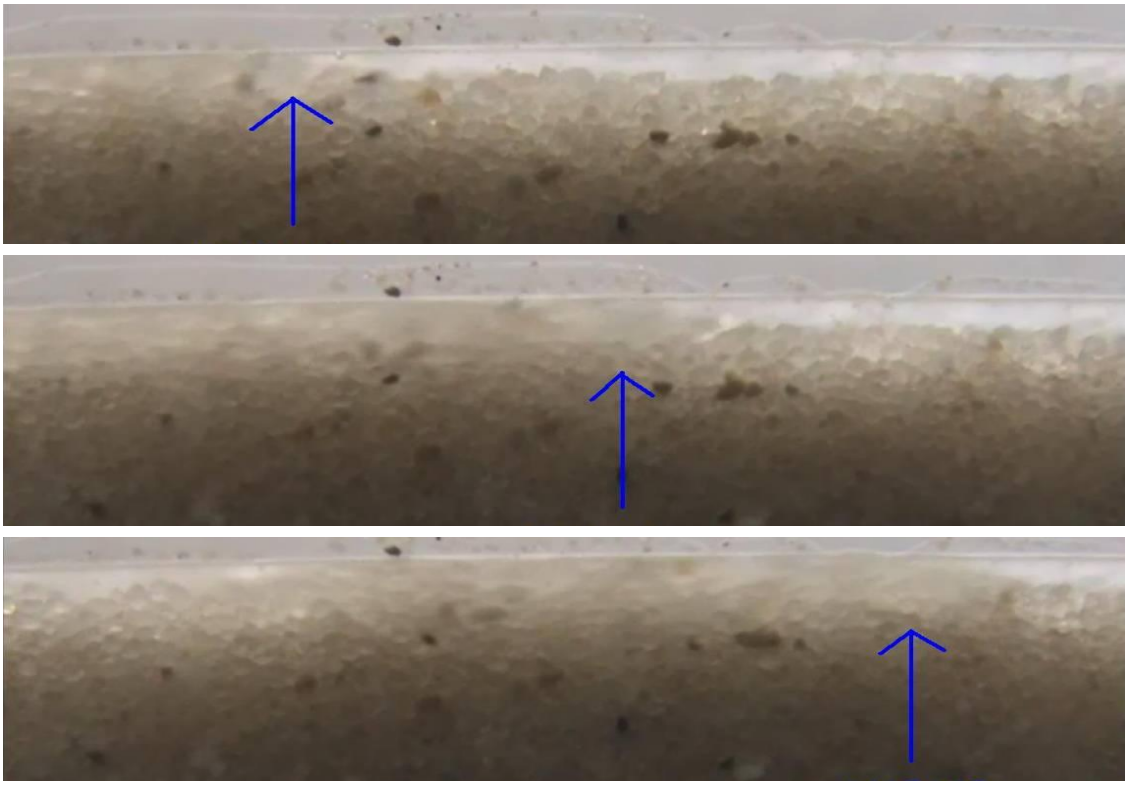

Figure 3-13 the movement of a wave of grains in experiment Q17 03:00

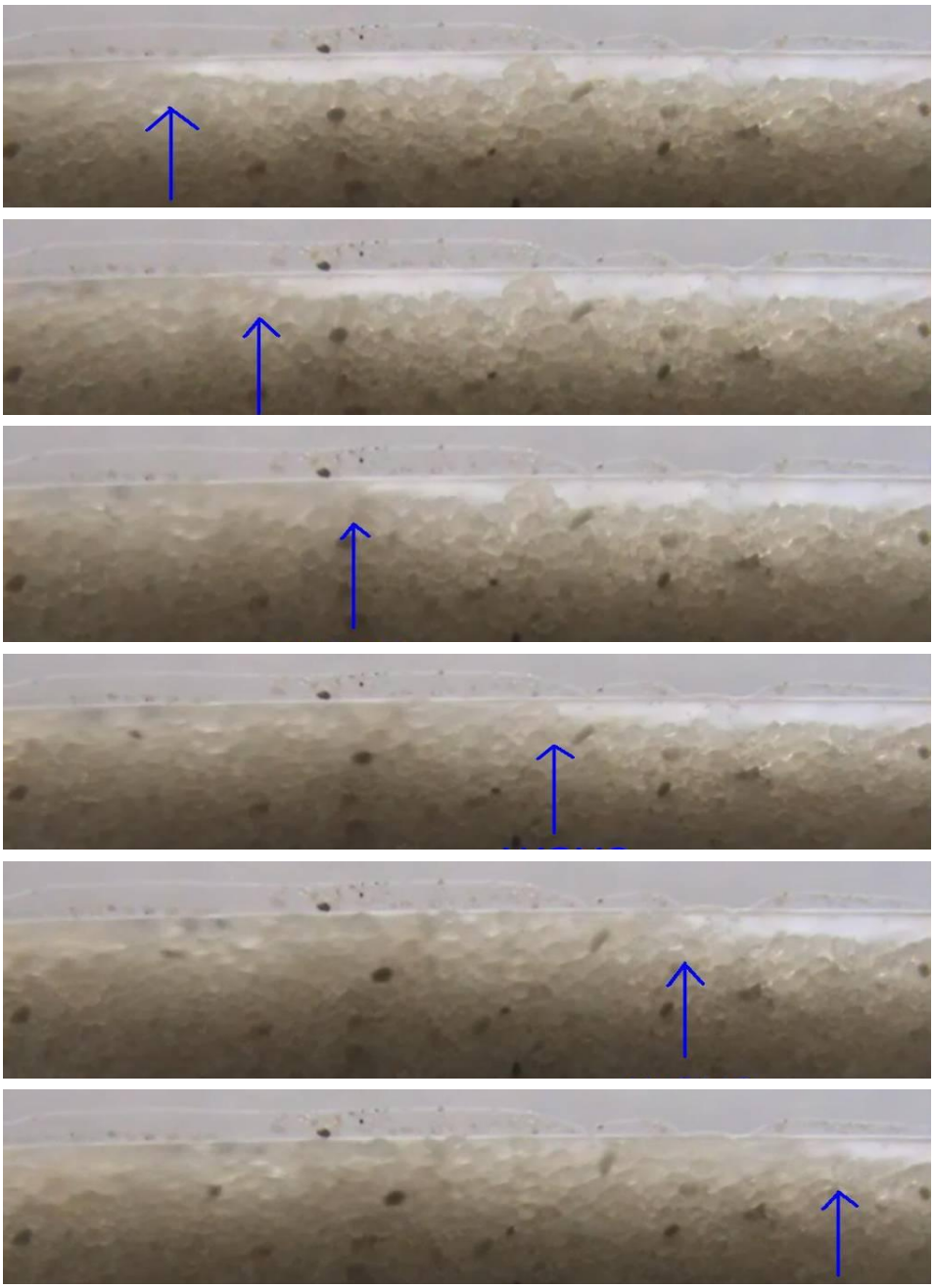

Figure 3-14 six screen shots of the wave in experiment Q17 at 3:10

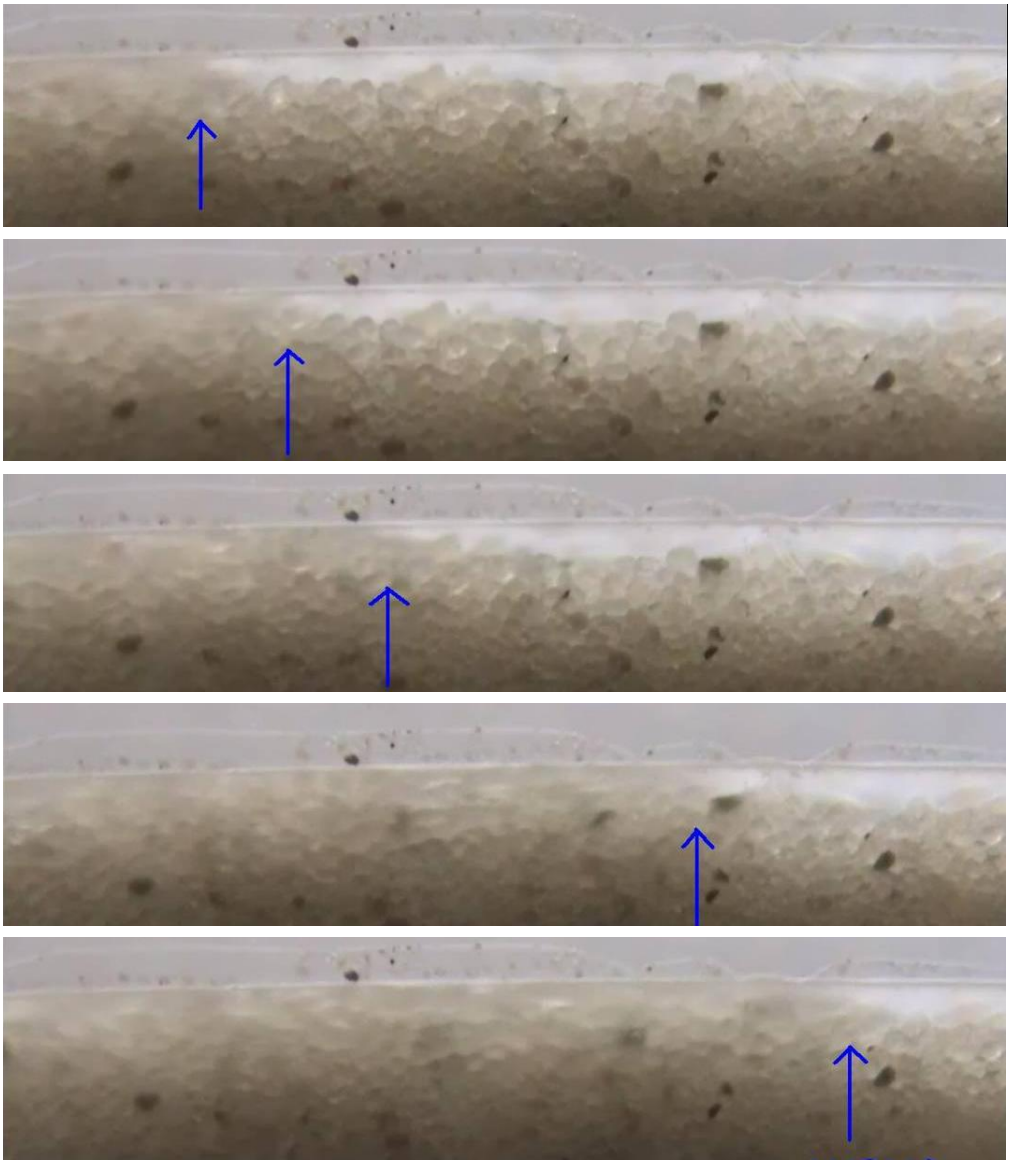

Figure 3-15 the movement of a wave of grains in experiment Q17 03:32

The dislodging of the grains is mass erosion, not individual grain movement as White assumes. Dislodging is defined in this thesis as the dislodging from the original sand matrix. A more detailed explanation of the sand plug is given in paragraph 3.6. This plug of sand consists of several hundreds of sand grains, and these grains are pushed through the channel together in a wave, as mass transport.

On the video, the layer which is transported in the channel like a wave appears to be roughly seven grains deep, but this is not completely correct. When examining more closely, it appears the top three grains are transported through the channel (shown in the red box in Figure 3-16) and the layer of four grains (shown in the

blue box in Figure 3-16) is dragged with the top layer along a certain distance, but the top layer travels faster. When the top layer (red box) is passed, the grains in the blue box remain on their place, until the following wave of grains passes by and the grains in the blue box are displaced again by a certain distance.

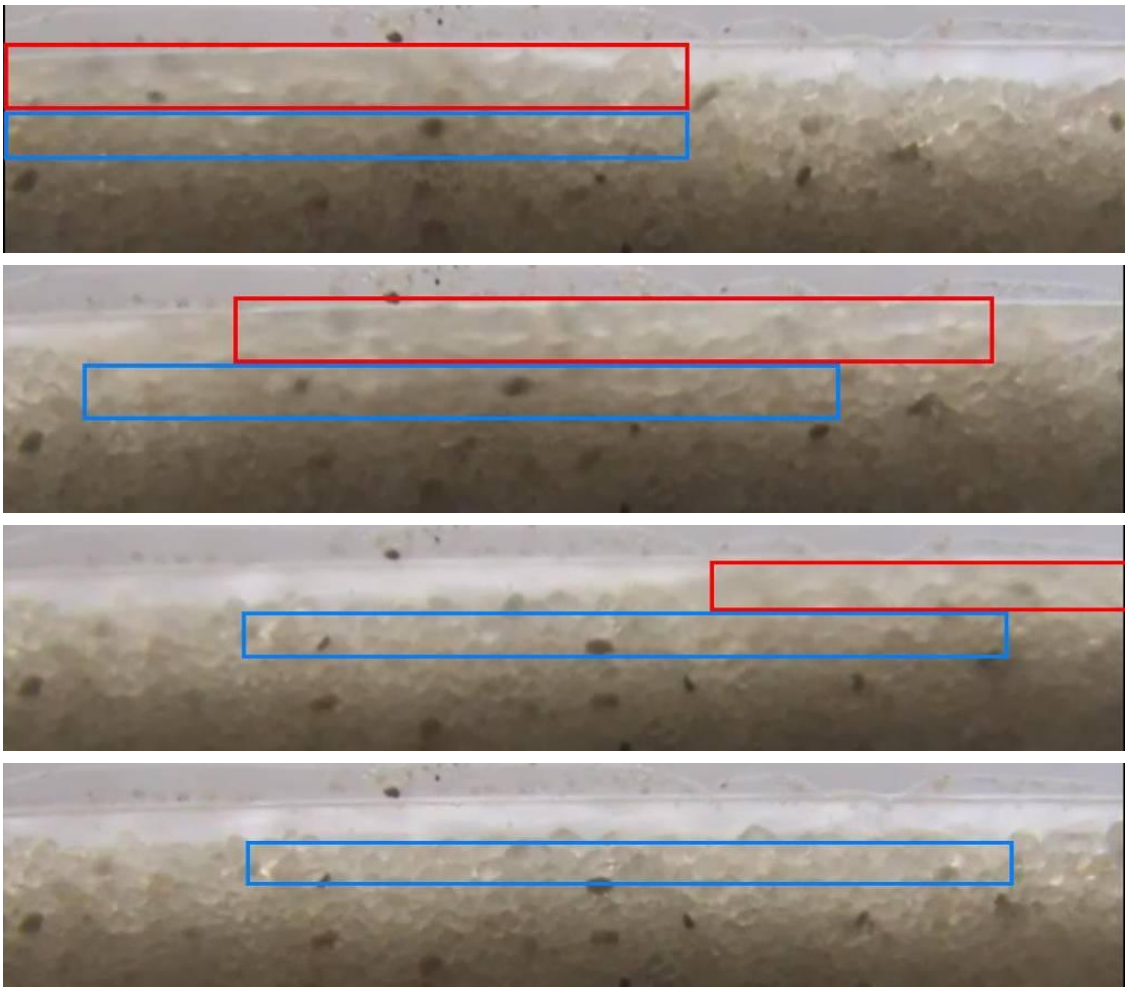

Figure 3-16 the displacement of the top layer (red box) and the layer beneath that layer (blue box) in a wave in video Q17 03:10

In video Q17, about 20 of these waves pass by the camera. The time between the waves decrease every time a wave passes. At first the waves appear to have a frequency of 0.2 to 0.25Hz. Later the frequency increases to 0.5Hz. In the time between the waves, some individual grains are also dislodged and transported, but the majority of the grains are dislodged as mass erosion and transported in a wave. After about 20 waves, the erosion increases very fast. This is shown in Figure 3-17 (the picture is blurry because of the high speed of the grains). The grains in the red box are transported at very high speed with a burst. The grains are mostly suspended in the water. This water-grain mixture behaves as a very

thick fluid, with high density. Since the particles in the water also hit the bottom of the channel, because of inertia of the suspended grains, the grains of the bottom are also absorbed in the flow.

Figure 3-17 the erosion process which occurs when the channel is almost cleared Q17 03:45

This type of erosion occurs when the channel is almost fully developed. This erosion type is present when the channel length has grown so far, the erosion process is a process which is not representative for the dislodging of grains. This is not the erosion mechanism which should be incorporated in a piping model.

After several of these bursts, the channel is completely developed, and a situation shown in Figure 3-18 is present. Water flows directly through the filter layer (shown in brown) and then flows over the sand bed directly to the outflow point of the water. A print screen is shown in Figure 3-19. Most of the grains present in the bed in the picture are stable and are not transported. Still transport (sheet flow) is visible, but this is from grains which come from upstream. These grains roll over the bottom very fast. Again is mentioned, since the channel is completely developed, this is not the erosion process which is representative for the dislodging of grains.

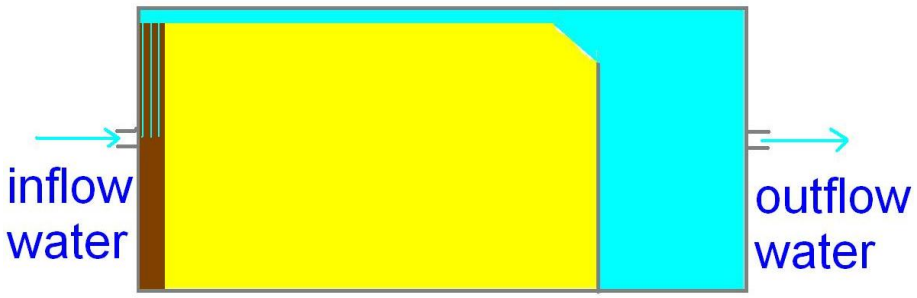

Figure 3-18 a sketch of the situation after the channel is completely cleared

Figure 3-19 the bottom of the channel after the channel is completely cleared Q17 04:04

3.5.2 Results of the experiments with a RD of 60%

The experiments Q6 and Q7 were performed with a relative density of approximately 60%. The sand type Ringstrasse Itterbeck Enschede was used. The results are treated in this subparagraph. The critical heads with these relative densities was around 33cm.

The erosion process starts with the sinus shaped channel of 4cm long (just as the experiments with a RD of 50%). This channel is not visible from the side. Then the dislodging of a layer of grains of 1 grain diameter starts. This is followed rapidly by the movement of a layer of two grains thick. This movement is shown in Figure 3-20. The thickness of the layer of transport increases from two grains to three grains to four grains.

Figure 3-20 the movement of a layer of two grains thick of experiment Q06 7:05

Then the formation of waves of sand begins. These waves look the same as the waves treated in subparagraph 3.5.1. One such a wave is shown in Figure 3-21.

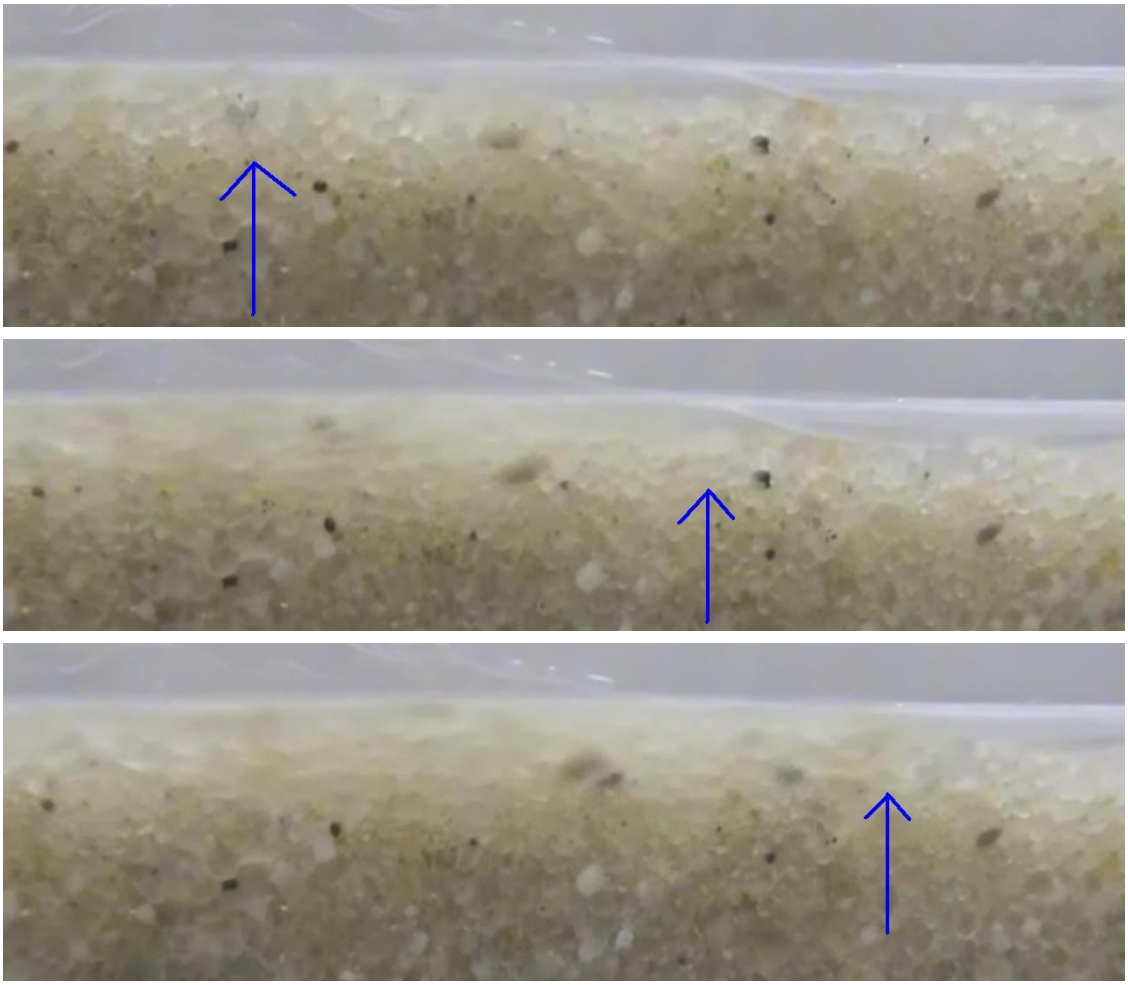

Figure 3-21 the movement of a wave of grains in experiment Q06 07:18

When the channel is almost completely through, very fast dislodging and transport takes place. This is shown in Figure 3-22 (the picture is blurry because of the high speed of the grains). The grains travel very fast and are mostly suspended in the water. Most of the properties of the erosion mechanism of the sand with a relative density of 60% is the same as the erosion mechanism of sand with a relative density of 50%, which is treated in subparagraph 3.5.1. The mayor difference that was observed between the erosion processes with the two relative densities is the time dependent behaviour. With a relative density of 60%, the erosion process goes much faster than with a relative density of 50%. The waves travel by with a frequency of 1Hz.

Figure 3-22 the erosion process which occurs when the channel is almost cleared Q06 07:28

3.5.3 Results of the experiments with a relative density of 80%

The experiments Q1 until Q4 were performed with a relative density of approximately 80%. The results are treated in this subparagraph. The critical heads with these relative densities varied between 18 and 42 cm for Baskarp sand and was 53cm for Ringstrasse Itterbeck Enschede. The reason the critical heads were so high, is probably because of the arching effect (Schenkeveld, 2010). Because the grains were densified a lot, and because the test facility is only 1cm wide, the grains experience an arching effect. The measured critical heads are not the critical heads which would be present if the test facility was wider. When the critical head is reached, the sand is transported very fast, much faster than was measured at relative densities of 60%. In a matter of seconds the entire channel is through. Because of the arching effect, the head when the erosion process starts is higher than when no arching process takes place. Also, because of the high gradients involved, fluidization of the sand can be present. That's why the erosion process goes so fast, and the erosion process might not be representative of what happens at a relative density of 80% without arching effect.

3.5.4 Results of the experiments with a RD of 25%

Experiment Q12 was performed with a relative density of approximately 25%. The sand type Baskarp was used. The results are treated in this subparagraph. The critical head with this relative density was 16cm.

Since the relative density was very low, the erosion mechanism forward erosion appeared, because of the absence of effective stresses. Because the critical head was very low the erosion process took much longer, when compared with the other experiments.

First the erosion process was as follows. The grains dislodged and flowed slowly as a sheet of seven grain diameter thick for several minutes long. This is shown in Figure 3-23. Later some small waves occurred, but these were not very dominant. The sheet flow determined the erosion process.

Figure 3-23 the sheet flow in Q12 14:29

Since the erosion process is forward erosion, the erosion process is not normative for backward erosion piping.

3.5.5 Additional remarks about the experiments

During the experiments, no quasi-static equilibrium was observed, although this is predicted by the Sellmeijer model.

In the first experiment a red dye was added to the water. This can be seen in Figure 3-24. It can be seen that after a while, when erosion has not started yet but a significant amount of water has flown out of the test facility, at the lower side the water with the dye remains. This means the water that flows out of the test facility comes from the upper part. This means most of the water that flows through the test facility flows through the top two cm that is not covered with the filter.

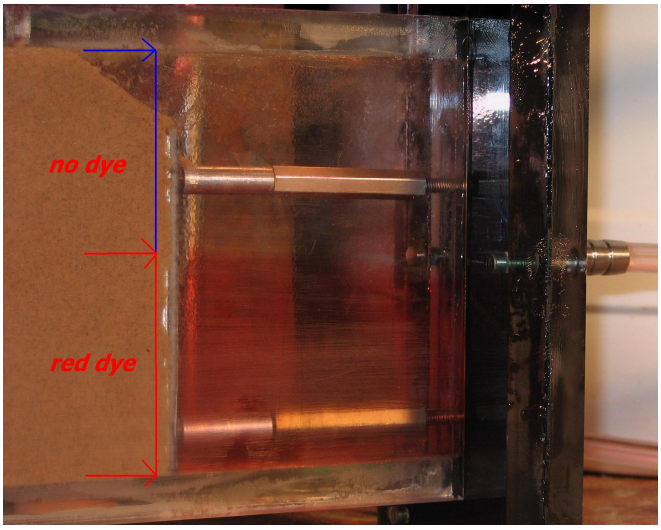

Figure 3-24 the filter at the outflow side. The red dye is only present in the lower part

This can be explained by the fact that it is easier for water to flow out of the sand, instead of flowing though the filter. The filter does not perform well, as it should

let water flow through easily. This means contraction of flow lines is present at the exit point of the grains.

3.6 Explanations and conclusions about the experimentally observed erosion mechanism

In this paragraph interpretations and conclusions about the observations made during the experiments with the one-dimensional test facility is treated.

In almost all the experiments, a sinus shaped channel of roughly 4cm appears when observed form the top (shown in Figure 3-8). Then a cloud of grains is eroded which creates a slit of one grain diameter thick (shown in Figure 3-10 and Figure 3-11). This cloud of grains consists presumably out of the finer fraction of the sand. Then the slit is clogged with grains (shown in Figure 3-12). This creates a plug. The creation of the plug can be explained as follows. The transport of the grains in clouds, as is shown in Figure 3-11, creates a slit of roughly one grain diameter at some places. Then because of the flow one (or more) grains is transported up in the channel, and is then jammed and blocks the channel. This is visualized in Figure 3-25 and Figure 3-26. At the blocking of the channel, a pressure is build up. This building up of pressure takes some time since the water must first flow from the sand body into the channel. After enough pressure is build up, the grains in the sand plug is dislodged from the granular matrix as a mass, as a layer of 7 grains thick, and is pushed in a wave through the channel.

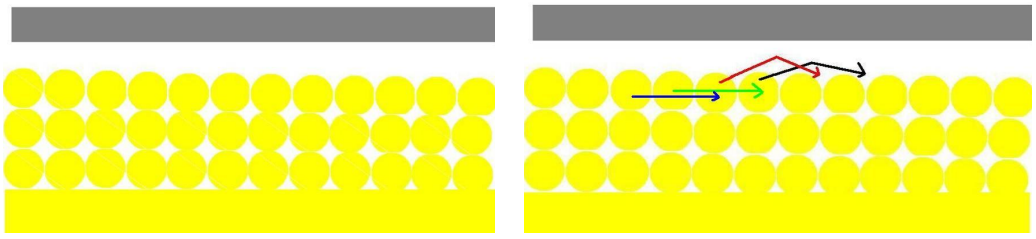

Figure 3-25 the presence of a slit because of the transport of grains in clouds (left) and some grains are transported (right)

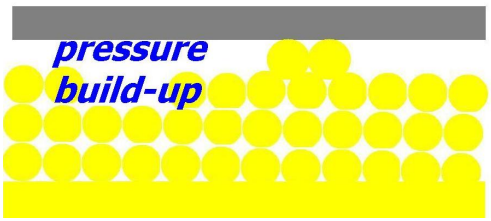

Figure 3-26 the transported grains get jammed and a pressure builds up behind it

Since the channel is blocked, a pressure builds up behind it and the plug of sand is pushed like a wave through the channel. These waves are shown in several figures in subparagraph 3.5.1, 3.5.2 and appendix O. The waves can best be viewed on

the videos made during the experiments. The transport is clearly mass transport, not individual transport.

Since there is very little room for the grains to move to, this creates a lot of resistance of the grains against moving. With a higher relative density, the erosion process is faster than with a low relative density. The inter arrival time between the waves is smaller when the relative density is higher. This is important for the time dependent behaviour of piping. With a higher RD, the critical head is higher (as was also found in the SBW experiments), but when the critical head is reached, the erosion process goes much faster, when compared with experiments with a lower RD. With a relative high critical head, the water flows faster through the sand layer according to Darcy's law, which may result in a faster build-up of pressure behind the sand plug, and because of the higher gradient, the pressure may also be higher when compared with experiments with lower critical gradients. This is a possible explanation of the faster erosion process of the sand, when experiments with a relative high critical gradient is compared with experiments with a lower critical gradient.

The sand waves has been identified by Barends as "sludge flow" (Barends, 2011). Mastbergen identified the waves as "slurry flow" (Mastbergen, 2011), as sludge flow refers to suspended fine sediment in wastewater, and slurry flow is associated with transport of sand (or ore) in high concentrations in a pipeline. Since the sand waves in the test facility consists out of high concentrations of sand, the transport of the grains is called slurry flow in this thesis.

With a relative density of 80% the measured critical head is much higher as is expected based on the SBW experiments, because of arching effects. Because of that, when the critical head is reached, the channel is cleared in a few seconds. Also fluidization may take place because of the high gradient. The erosion process is not normative for a real dike. The one-dimensional test facility is not suited for experiments on high relative densities.

With a relative density of 25%, the forward erosion mechanism appeared. The sand transport was very slow, when compared with the transport velocity of experiments with relative densities of 40-50%. Sand was mainly transport in sheet flow, in a layer of roughly seven grains thick. Some small sand waves appeared, but the sheet flow was the main transport mechanism. Since forward erosion only appears in the absence of effective stresses, and the forward erosion mechanism is not part of this thesis, the erosion process with very low relative densities is not researched further.

At the small-scale test facility, it was found that whenever a channel was blocked, the channel started to meander, as is shown in Figure 3-27. This is not possible in the one-dimensional test facility. This means the blocking of the channel in the small-scale test facility, and the following waves may show some difference with the one-dimensional test facility, but it is unknown if there is a difference or not, or how much this potential difference is.

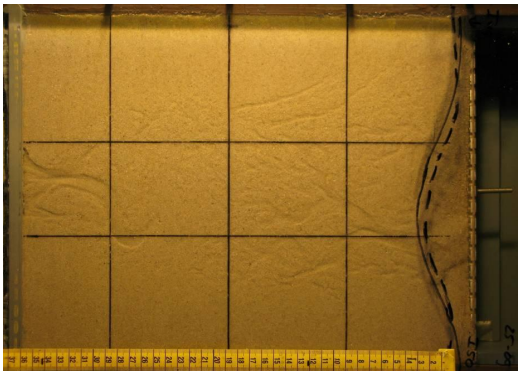

Figure 3-27 the meandering of the channels (van Beek, 2009a)

3.7 Agreement of experiments with reality

In this paragraph the agreement of the outcome with reality is discussed, as the key concept of modeling is shown again in Figure 3-28.

Figure 3-28 the one-dimensional test facility is not a dike, it is a model of a dike

The one-dimensional test facility is not a dike, it is a model of a dike. It must be researched in what extent the outcomes of the experiments agree with reality. Several aspects in the test facility are different than in reality. Several of these aspects are:

- A different seepage length is present in the test facility with respect to reality
- A higher critical gradient is present in the test facility with respect to reality
- In the test facility the pipe cannot meander, in reality it can meander
- A higher vertical pressure gradient is present in the test facility with respect to reality

Since in the test facility a quite high gradient and low seepage length is present with respect to reality the erosion process and dislodging of grains in reality may be slower than was observed in the test facility, or the erosion process and dislodging may even be different than is observed in the test facility. It can not be concluded for sure that in reality the erosion process is the same as was observed in the test facility. Still, because some basic processes are the same, as groundwater flow through a sand layer under a rigid “roof” by a head difference, which erodes grains at the exit point and a channel grows in downstream direction, the behaviour under a real dike may be somewhat similar as the observed behaviour in the test facility. The process observed with relative densities of 40-50% are considered normative for the erosion process, since the critical gradient in those experiments were, of all experiments (except for forward erosion), the closest to the ones observed in the small-scale SBW experiments. In the Sellmeijer model the erosion process of White was assumed to be always applicable as an erosion formula in piping. If this would be true, this would also been observed in the test facility. The absence of the ability to meander will probably not have a mayor impact on the erosion process.

In Figure 3-29 the location is shown where the erosion process is filmed. This is not near the exit point of the grains, because the inclined plane which is present in the test facility, is not present in reality, and the erosion process going on near the exit point of the grains, may not be the erosion processes going on in reality.

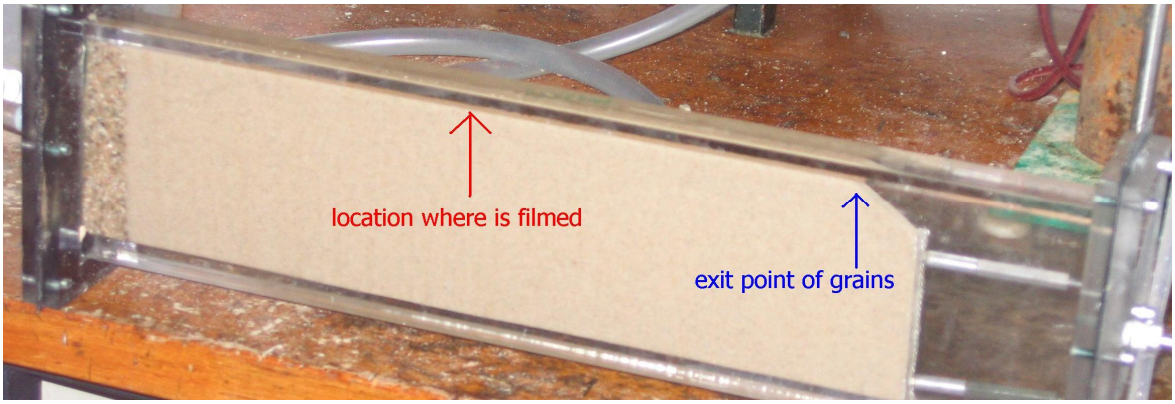

Figure 3-29 the location where the erosion process is filmed

The Sellmeijer model predicts a quasi-static equilibrium, until a channel length of roughly half the seepage length is reached. This is not observed during the experiments. It is not sure that the observed erosion (and transport) processes are the processes that are normative for describing the critical head of piping. It may be that the observed erosion processes in the test facility occurs also in reality, however only when the critical gradient already has been reached. It is not sure if the observed erosion is normative for determining the critical gradient or not, this

is still under discussion. Although it is not sure if the erosion processes is normative for determining the critical gradient, it is concluded the observed processes are important for the time dependent behaviour, with respect to the erosion rate.

The following is concluded about the vertical pressure gradient. In Figure 3-30 the pressure distribution in the sand is shown according to the Sellmeijer 4-forces model. For the length of a real dike the right one of the three graphs is applicable. The ratio of L/1000d is equal to 2.3 for Baskarp sand and 0.8 for Ringstrasse Itterbeck Enschede in the one-dimensional (and also the small-scale) test facility. This corresponds to the left graph in Figure 3-30. Note that p and q are defined as

$p = \frac{d\varphi}{dx}$ *(eq 3-4)* and $q = -\frac{d\varphi}{dy}$ *(eq 3-5)*

It can be seen in Figure 3-30, that q is quite large for small seepage lengths, around 0.5-0.6 (values at the side are unreliable because of mathematical singularities). This graph is derived for an infinitely deep sand layer. There are currently no graphs available for finite thick layers. Two MSEEP calculations have been performed on the small-scale test facility on coarse and fine sand. The maximum value of q was 0.43 for coarse sand and 0.29 for fine sand. It is emphasized the calculated values of q are just an indication, for a certain given head, more detailed research is needed to calculate the influence of the critical gradient for the small-scale test facility. In the 4-forces model, the equilibrium of grains according to White changes in $\frac{p(\frac{3}{\pi}\frac{1}{\eta}\frac{a}{d}+1)}{\frac{\gamma_p'}{\gamma_w}-Cq} = \frac{\sin(\beta+\theta)}{\cos(\theta)} = \tan(\theta)$ *(eq 3-6)*.

C is the coefficient of Martin, which takes into account the collapse of the pressure gradient across the top particles. Values of C ranging from 0.35 to 0.50 are determined (Sellmeijer, 1988). In the 2-forces model the -Cq term is absent, (just as the value +1). For a C value of 0.50, the numerator of the equation of White (4-forces) reduces from 1.65 to 1.43 for coarse sand and to 1.50 for fine sand. This means that if the values of the measured critical gradient in the small-scale test facility need to be compared or extrapolated to scales of a real dike, where the influence of the vertical gradient is much lower, results of experiments must be corrected. Experiments on coarse grained sands need to be corrected with a multiplication factor 1.15 and for fine sands the multiplication factor is 1.10. This means the negative trend shown in Figure 1-17 is a bit less negative in case of a real dike. It is emphasized again the calculated values of q are just an indication. More research is needed. This is very time consuming and falls outside of the scope of this thesis.

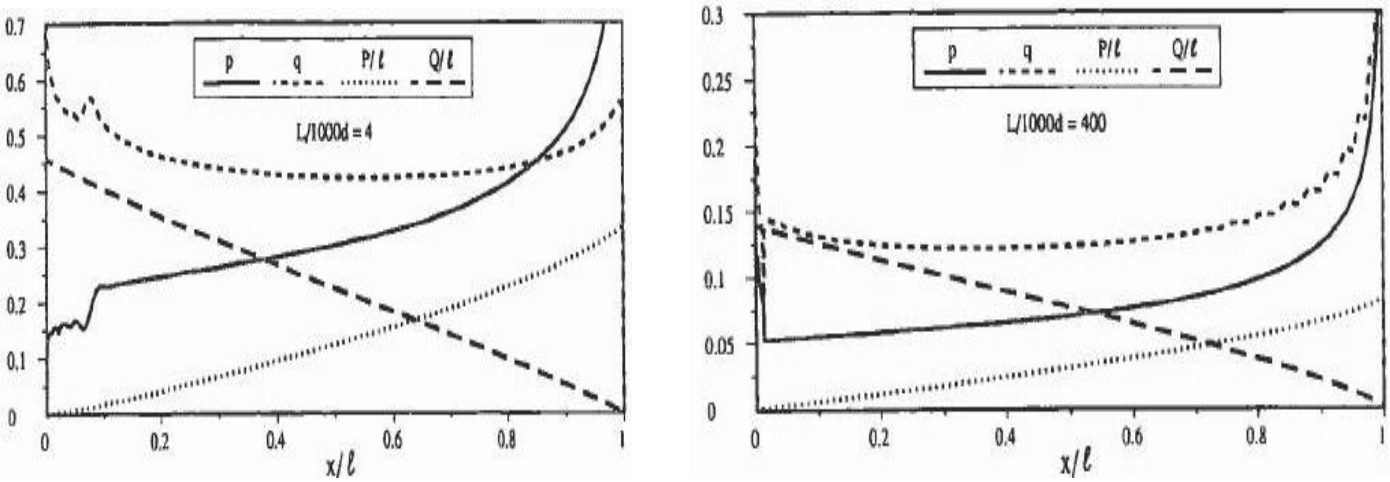

Figure 3-30 pressure gradients in the sand according to the Sellmeijer 4-forces model for l/L=0.4 (Sellmeijer, 1988

This vertical pressure gradient q, can make the sand bottom fluidized, if it reaches a value of 1.0 (Verruijt, 2001). This effect is not included in the Sellmeijer 2- and 4-forces model. Since the calculated values of q are 0.43 and 0.29, this process is not present based on this values. More research is needed to validate this.

It is noted that during the experiments of de Deltagoot, the slurry flow was not observed.

3.8 Implications of the found results on the Sellmeijer model

In this paragraph, the implications of the found results on the Sellmeijer model is treated. In paragraph 3.3 the correctness of the implementation of White as an equilibrium model of the grains in the Sellmeijer model is questioned from a theoretical background. In paragraph 3.6 and 3.7 the correctness of the implementation of White as an erosion mechanism in the Sellmeijer model is questioned with the use of experimental outcomes. It was concluded it is not sure if the observed erosion mechanism is normative for the erosion of grains for calculating the critical gradient. This is still under discussion. More research is needed. This research falls outside of the scope of this thesis.

The Sellmeijer model consists out of three differential equations, with certain boundary conditions. These differential equations are

- LaPlace equation (continuity and Darcy)
- Poiseuille flow in the channel
- The erosion formula of White

These differential equations are explained in paragraph 1.4.

In paragraph 3.3, it was argued from a theoretical background that it is doubtful that the erosion mechanism of White is applicable as an piping erosion mechanism. In paragraph 3.6 and 3.7 it was shown in a test facility that the dislodging of grains from the granular matrix is as mass erosion. The transport of sand occurred in waves, named slurry flow by Mastbergen (Mastbergen, 2011). If the erosion mechanism is also applicable in a piping model is not sure, this must be verified.

Based on the three differential equations mentioned above, Sellmeijer derived with the use of dimensional arguments that $\frac{H_c}{L} = \alpha\eta \tan(\theta)\frac{\gamma'_p}{\gamma_w}\frac{D_{70}}{\sqrt[3]{\kappa L}}$ (eq 1.4).

The numerical value of θ is fitted on de Deltagoot experiments. The Deltagoot experiments are elaborated further in appendix G. The length scale factor in $\frac{H_c}{L} \sim \frac{D_{70}}{\sqrt[3]{\kappa L}}$ is validated with the outcome of experiments in de Deltagoot.

The influence of the permeability, $\frac{H_c}{L} \sim \frac{D_{70}}{\sqrt[3]{\kappa L}}$ is based on the equation of continuity and Poiseuille. Since very little doubt is about the groundwater flow equation, and the same influence of the permeability on the critical gradient was also found in the multivariate analysis on the SBW dataset, as is explained in paragraph 2.5, this part of the model of Sellmeijer is considered correct. The α factor, which is the variable which takes into account the sand layer thickness, is also based on groundwater flow equations, and this is also considered correct.

The influence of the remaining variables, $\frac{H_c}{L} \sim \eta \tan(\theta)\frac{\gamma'_p}{\gamma_w}D_{70}$, is based on the equation of White. The correctness of the implementation of the equilibrium of grains on a bed according to the erosion model of White is questioned in this thesis both from theoretical as experimental point of view. The experiments performed with the one-dimensional test facility showed that the erosion process, the dislodging of grains from the granular matrix is mass erosion. It is not sure if the observed mass erosion is applicable for a piping model. If erosion of grains in reality is indeed different than in the model of White, it may be concluded that the equilibrium of grains according to the erosion model of White, may not be applicable in a piping model. It is still not verified if the erosion is indeed applicable or not. It is recommended to research the starting of the erosion mechanism. A test facility can be constructed where the initial erosion processes represent reality better than the inclined plane which is present in the one-dimensional test facility.

The observed transport process (slurry flow) is also present in pipelines, where a sand-water mixture is pumped through the pipeline. From dredging engineering, knowledge and experience about this transport is available. Formulas for slurry flow are available from dredging engineering.
If it is shown that the observed erosion process (mass erosion) and transport (slurry flow) is also applicable in a piping model, it can be tried to incorporate this in a new piping model. If this is tried, a lot of verifying should be done to check if these formulas are indeed applicable to the piping process, since the formula's for slurry flow were derived for pipeline flow, not piping, and also different boundary conditions are present in a pipeline than that are present in the case of piping. The slurry is a Bingham plastic, a non-Newtonian fluid (Mines, 2010, Rabah, 2010). The behaviour of a Bingham plastic is shown in Figure 3-31.

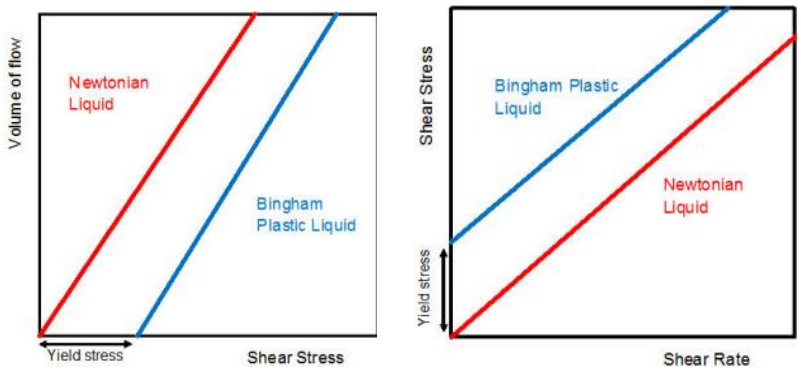

Figure 3-31 the behaviour of a Bingham plastic (Wikipedia, 2010)

As can be seen, the fluid will only start to move when the applied shear stress reaches a certain threshold. For slurry flow, distinction has to be made between turbulent and laminar flow. Mines states that for slurry flow, turbulent flow initiates at a higher velocity than with water alone (Mines, 2010). It must be researched if the flow in the one-dimensional test facility and also in case of a real dike is laminar or turbulent. An important parameter for slurry flow is the so called modulus of rigidity of the sand (η), which is the modulus of elasticity in shear. The Reynolds number for slurry flow is $\mathrm{Re} = \frac{\rho u D}{\eta}$, where ρ is the slurry density and u and D the velocity and the diameter of the pipe. For both turbulent as laminar flow, formula's are present to calculate the velocity in the pipeline (Rabah, 2010). Since these formula's were derived for pipelines, it must be verified if these formula's are also valid in case of piping. If the formula's are not valid for piping, these formula's may not be used for a piping model. Too often a erosion mechanism (White, Shields) has been assumed without verifying if equilibrium of grains according to these formulas are indeed applicable to piping. In the case of piping, the size of the channel and the length of the channel is not fixed, as it grows as a function of the amount of transported sediment. A

mathematical formula has to be derived for this. Since the channel is blocked regularly, as was demonstrated with the one-dimensional test facility, no continuous pipe is present and the thickness of the channel varies locally.

This makes it very difficult to make a mathematical model. With piping, the discharge begins at zero and increases gradually until it reaches a maximum at the exit point of the channel, because the water flows in from the bed of the channel. This flow also causes an additional uplift force on the particles.

Note that deriving a model like this is difficult and very time consuming, and is not part of this thesis.

The Sellmeijer formula has been used on the outcome of the experiments in de Deltagoot, to fit the variable θ. The D_{70} of the sand used in de Deltagoot is 247µm. This means that, if the equilibrium of grains according to the erosion model of White is indeed not applicable for piping, the Sellmeijer formula itself may not describe the piping process in a proper way, but because of the fitting of θ on the experiments performed in de Deltagoot, the outcome of the Sellmeijer formula gives a reasonable correct numerical outcome for piping calculations on medium fine sands (sands with a D_{70} in the order of 247µm), but performs less well for coarser sands. This may explain why the outcome of small-scale experiments of SBW on fine and medium fine sands agrees reasonable well with the current Sellmeijer formula, and experiments on coarse sands (D_{70} of 400µm) do not. In the medium-scale and full-scale experiments the outcome on fine sands agrees quite well with the formula, the medium fine and coarse sands agree less. This may be explained by the fact that only few medium-scale and full-scale experiments were performed, and with the high scatter that is observed in piping experiments, no rigid conclusion can be drawn. The adapted Sellmeijer formula is introduced in paragraph 2.1. This adapted Sellmeijer formula consists out of the current Sellmeijer formula, extended with several factors which were determined with a multi variate analysis on the small-scale SBW data, without a solid understanding why the influence of the D_{70} is lower than is predicted with the current Sellmeijer formula.

From a scientific point of view it is important to know how a process works, otherwise it is (partly) a black box model. If a formula has been derived based on known physical laws, and experiments support the formula, a lot of confidence about the correctness of the formula is present.
If a formula has been derived based on experiments, and especially when the amount of experiments is low, or the range of variables that is varied is insufficient compared with the range in which variables are present in reality, and no or insufficient knowledge is present about the physical processes that are determining

the piping process, the confidence about the correctness of the formula is quite low. Especially when the experimental set-up is a model of reality, care should be taken that the outcome of the experiments are not directly used in a formula without the proper verification. The importance of Figure 2-15 is emphasized again.

Also when the formula is fitted on experiments, some or even all of the restrictions in what cases the formula is applicable and in what cases it is not applicable, may be overlooked, and this may result is quite dangerous situations.

The current Sellmeijer formula may possibly not describe the piping process in a proper way. By fitting the numerical value of the rolling resistance angle of the sand grains on experiments performed in de Deltagoot, the formula gives quite reasonable correct numerical outcomes for fine and medium fine sand, but not for coarse sand. To correct for this, the current Sellmeijer formula is extended with factors to create an adapted formula, but this is based on fitting on small-scale SBW data, without knowing enough about physical processes that are governing the piping process. This makes the adapted Sellmeijer formula partly a black box model. This model is fitted on laboratory experiments, however also a few full-scale experiments have been performed to validate the outcome of the adapted formula.

Application of formula's based on (partly) black box models should be done with care. A proper insight in the processes governing the piping process is essential. With the proper insight in the governing processes, the experimental outcomes can be understood and judged better, the applicableness of formulas and it's restrictions are much better understood and more confidence about the formulas is present.
As was stated in paragraph 1.2, piping is considered the most dangerous failure mechanism of dikes in the Netherlands and the net present value of the risk of piping and also the costs of preventive measurements to prevent piping is several billions of euros. Since the adapted Sellmeijer formula is going to be used in performing the safety assessment of the Dutch dikes, it is certainly worthwhile to invest money in research to piping, since a better understanding of the piping process can lead to a better formula, based on physics, where a lot of confidence is in, where more is known about restrictions and applicableness of the formula.

3.9 Conclusions and a summary about the erosion mechanism and flow in the channel

In this paragraph conclusions and a summary about the use of the equation of White in the Sellmeijer model is treated.

In the Sellmeijer model, it is assumed a channel is present under a dike where Poiseuille flow is assumed. The equilibrium of the grains on the bed of the channel is assumed to be according to White's erosion formula.

In paragraph 3.1 and 3.2 the theory of White and it's implementation in the Sellmeijer model is explained. From theory it is argued that the erosion mechanism of White may possibly not be applicable to the piping process, as is discussed in paragraph 3.3.

In paragraph 3.4 the experimental set-up of the one-dimensional test facility is treated. In paragraph 3.5 and 3.6 the results and explanations of the experiments with the test facility is treated respectively. Based on the experiments with the one-dimensional test facility, the erosion mechanism of White may not be applicable to the piping process in the test facility. White assumes the equilibrium of grains can be modeled with individual grain transport, the experiments show the grains are dislodged as mass erosion in a layer of 7 grains thick. The transport occurs in waves, called slurry flow. The sand continuously blocks the channel like a plug and a pressure builds up, until the pressure reaches a value where the grains are eroded and the plug is pushed through like a wave. This can best be seen in the videos.

In paragraph 3.7 the agreement of the experiments with reality is discussed. Since the one-dimensional test facility is not a dike, it is a model of a dike, it is not sure if the erosion in reality is as in the test facility. Since the basic processes, as groundwater flow through a sand layer under a rigid "roof" by a head difference, which erodes grains at the exit point and a channel grows in downstream direction are both present in reality as in the test facility, it is quite reasonable that the erosion mechanism is also present in reality, maybe on a different (time)scale, but probably mass erosion is present, not individual grain erosion. This must be validated first. It must also be researched if the observed erosion is the erosion type which is normative for calculating the critical gradient. It may be that the observed erosion is the erosion type that occurs after the critical gradient has been reached and progressive failure takes place. Since no quasi-static equilibrium was observed, it is unknown and still under discussion what type of erosion was observed during the experiments.

Also the influence of the vertical pressure gradient in the test facility is compared with a real dike and a correction is needed if the outcome of the small-scale experiments are compared or extrapolated to real dike dimensions. The negative trend show in Figure 1-17, is then a bit less negative.

In paragraph 3.8 the implications of the found results on the Sellmeijer model is treated. Since the current Sellmeijer model is based on the equilibrium of grains according to the erosion mechanism of White, the Sellmeijer formula may possibly be improper. Since the Sellmeijer formula is fitted on the outcome of de Deltagoot experiments, the numerical value of calculations on sands with a grain size in the same range as the grain size used in de Deltagoot experiments, may give an reasonable correct answer. Other ranges of grain sizes will give an incorrect answer. The adapted Sellmeijer formula consists out of the current Sellmeijer formula, multiplied with correction factors which were determined with a multi variate analysis on the small-scale SBW data. The adapted Sellmeijer formula is partly a black box model. Part of the model is based on a correct and applicable process (groundwater flow), another part is possibly based on a not applicable process (White), and the correction factors are not based on physical processes and little insight is present regarding restrictions and applicableness, since it is fitted on a dataset with a quite limited amount of data, the confidence in the model is not very high.

Since the observations in the test facility show mass erosion, this is the mechanism that should be modeled, if this erosion is indeed applicable (this should be researched first). There are formula's for the observed slurry flow. These formula's were derived in the field of dredging engineering.

4. Possible explanations of differences between SBW experiments and the Sellmeijer model

The objective of this masters thesis is to research the influence of the grain size and other sand characteristics on the critical head of piping, and to find an explanation for the difference found between SBW results and the Sellmeijer formula.

In this chapter, possible explanations for the differences in outcome between the experiments of SBW and the current Sellmeijer 2-forces model are treated, and the data of Bligh and de Wit are also taken into account. Several explanations for the difference between SBW and the Sellmeijer formula are found.

These explanations are:

1) The small-scale and medium-scale test facility may not represent the piping behaviour correctly, this is treated in paragraph 4.2.

2) The results of the experiments are interpreted incorrectly, or the amount of experiments performed are to few to draw rigid conclusions, this is treated in paragraph 4.3.

3) The equilibrium of the grains and the flow in the channel in the Sellmeijer model may be different than was assumed, this is treated in paragraph 4.4.

4) The Sellmeijer model is a 2D model, in reality the piping process is 3D.

Or a combination of above mentioned explanations. Other explanations are also possible, as the above mentioned possible explanations are not exhaustive.

4.1 The results of SBW

In this paragraph the results of SBW are shown. In Figure 4-1 the results of the small-scale SBW experiments are shown, together with the values of the critical gradient according to the current Sellmeijer formula. According to the Sellmeijer formula $\frac{H_c}{L} \sim \frac{D_{70}}{\sqrt[3]{\kappa L}}$, while the SBW dataset show $\frac{H_c}{L} \sim \frac{D_{70,mean}}{\sqrt[3]{\kappa L}} (\frac{D_{70}}{D_{70,mean}})^{0.34}$, where the exponent 0.34 is not completely fixed, it is more of an indication of the order of the influence, as several different values between 0.29 and 0.39 were found, the values of these regression coefficient can be found in Table 2-8.

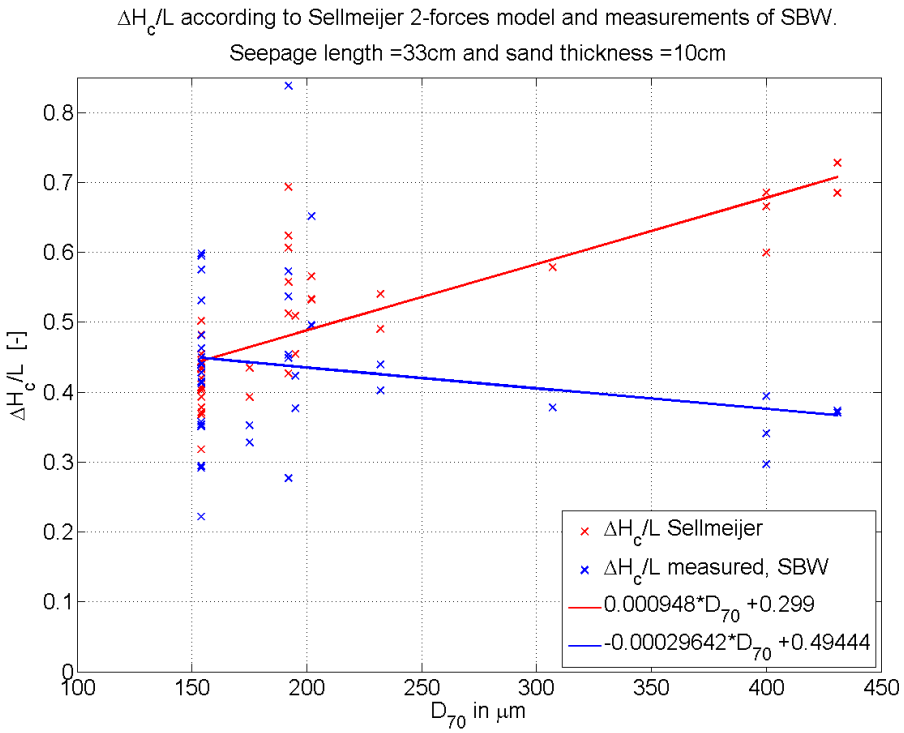

Figure 4-1 the critical gradient as function of D_{70} according to the small-scale SBW experiments and the current Sellmeijer formula

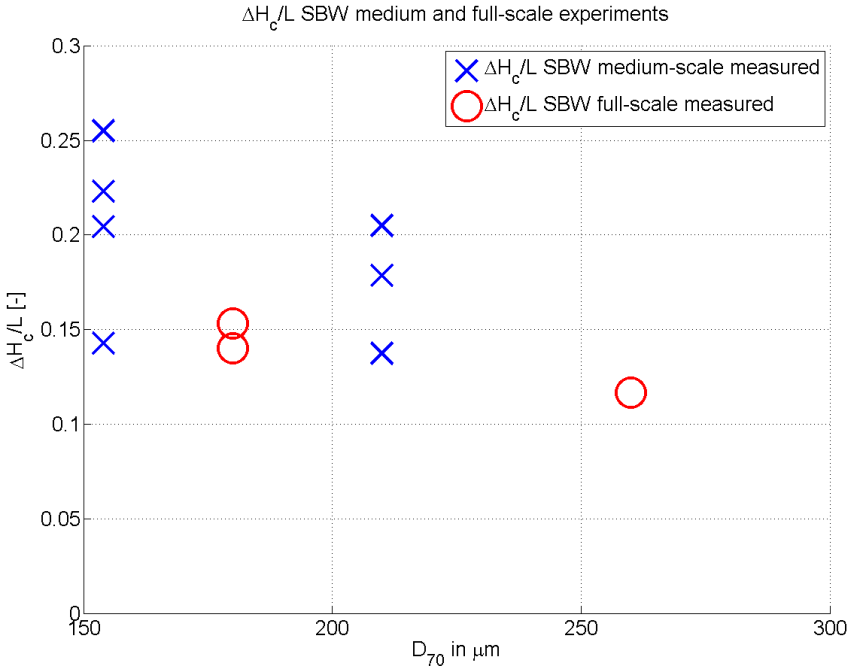

Figure 4-2 the critical gradient as function of D_{70} according to the medium- and full-scale SBW experiments

As can be seen in Figure 4-1, for fine sands the current Sellmeijer formula predicts the critical gradient quite well. For coarser sands, the current Sellmeijer formula gives an unsafe predication. In Figure 4-2 the critical gradients as a function of D_{70} for the medium-scale and full-scale experiments is shown. These also show a negative trend.

In this chapter possible explanations are presented for the difference between the influence of the grain diameter on the critical gradient according to SBW and the current Sellmeijer formula.

4.2 The possible incorrect modeling of piping in the small-scale and medium-scale test facility

One of the possible explanations of the difference between the Sellmeijer model and the SBW measurements is that the small-scale and medium-scale test facility may not model the piping behaviour correctly. The importance of Figure 2-15 is emphasized again. In paragraph 3.7 it was shown that in the test facility a high vertical gradient was present, which is much lower in case of a real dike. It was shown that the critical gradient in the test facility should be multiplied with a factor of 1.10 for fine sands and 1.15 for coarse sands, if the critical gradients are compared or extrapolated to real dike dimensions (these value are just an indication). The negative trend shown in Figure 1-17 is then a bit less negative, but still a negative trend is present. The effect of the vertical pressure gradient on the piping process in the test facility must be researched further.
In Figure 4-3 a cross-section of the small-scale SBW test facility is shown on the left. On the right of Figure 4-3 a part of the model is shown, where Sellmeijer based his model on. The medium-scale test facility has the same basic shape as the small-scale test facility, only other dimensions.

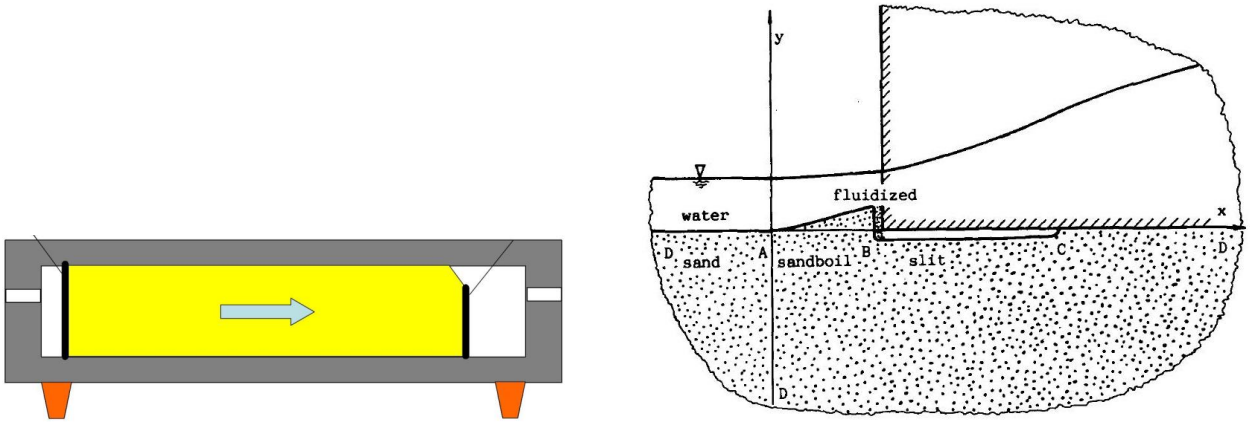

Figure 4-3 a cross-section of the small-scale test facility (left) (Knoeff, 2008) and part of the geometrical plane on which the Sellmeijer model is derived on (right) (Sellmeijer, 1988)

As can be seen Figure 4-3, the two models are not exactly the same. However, MSEEP calculation have shown the difference between the two models are small.

In paragraph 3.5.5 it is mentioned that with the first experiment with the one-dimensional test facility, a red dye is added. This can be seen in Figure 4-4.

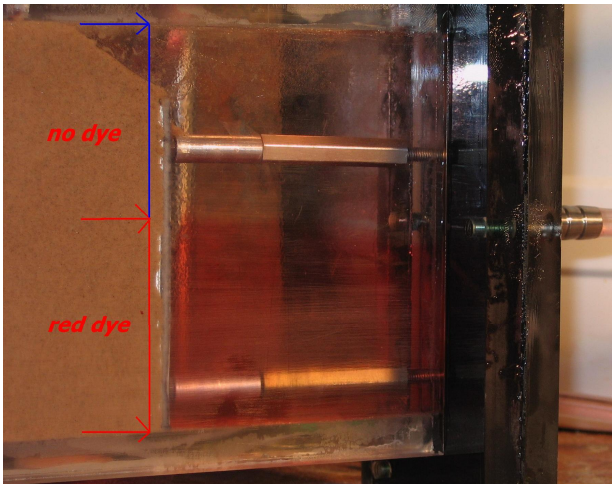

Figure 4-4 the downstream filter at the outflow side. The red dye is only present in the lower part

It can be seen that only the top half of the water flows of in the exit tube. This was explained in paragraph 3.5.5 by because it is easier for water to flow out of the sand at the top, instead of flowing though the downstream filter. The filter does not perform well, as it should let water flow through easily. This means contraction of flow lines is present at the exit point of the grains. In Figure 4-5 the contraction of flow lines is sketched for the one-dimensional test facility. The flow avoids the filter.

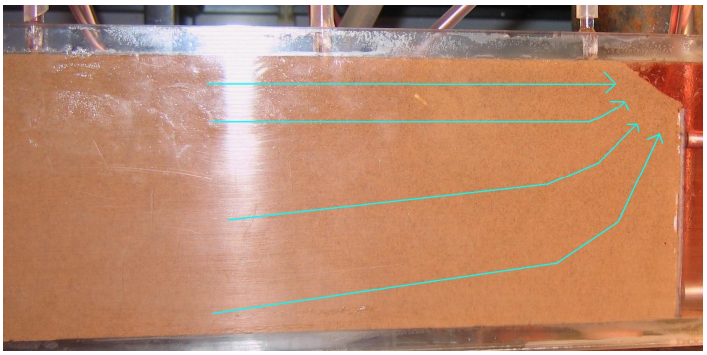

Figure 4-5 contraction of flow lines in the one-dimensional test facility

The experiments of SBW were not performed with this test facility, but with the small-scale test facility shown in Figure 4-3, but the same principle of the flow

lines avoiding the filter holds. In Figure 4-6 the flow lines under a dike is roughly sketched. Also some contraction is present, but not full contraction.

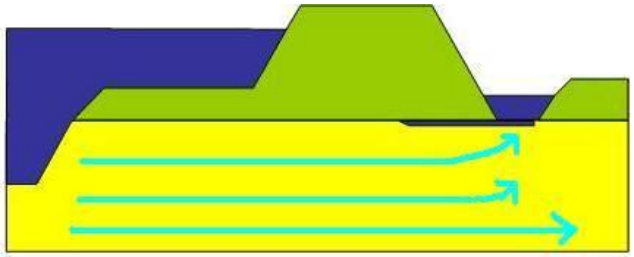

Figure 4-6 contraction of flow lines under a real dike (van Beek, 2009d, the flow lines are added)

The downstream filter in the small-scale, medium-scale and one-dimensional test facility works as a semi-impermeable boundary, which influences the flow lines. Since coarser sand has a higher permeability than fine sand, flow lines in coarse sand are more attracted to the exit point where no filter is present than in the case of fine sand. This might also be a reason why with coarse sand the piping process starts with a lower critical gradient than the finer grained sands in the SBW small-scale and medium-scale experiments. It is unknown how much the influence of the contraction of the flow lines on the critical gradient is.

The filter on the upstream side causes a resistance on the water flow (the resistance of the rest of the test facility is small compared to the filter influence). The critical gradient can be corrected for this. This has been done for SBW experiments, but possibly not for de Wit. The resistance is a function of the flow velocity, and thus the discharge through the test facility, as was found in SBW. Since discharge and flow velocity in the test facility depends on permeability, and thus on the grain size, the resistance of the filter is plotted against the D_{70} in Figure 4-7. Resistance is defined here as

$$\text{Resistance} = \left[\frac{(H_c \text{without correction}) - (H_c \text{with correction})}{(H_c \text{without correction})} \right] * 100\% \qquad (eq\ 4\text{-}1).$$

As can be seen in Figure 4-7, sand samples with a higher D_{70} have a higher percentage of filter resistance in the small-scale SBW experiments than the sand samples with a lower D_{70}. Since the filter resistance for coarse grained sand is quite high, the calculated critical gradient with filter resistance may be unreliable, as the filter dominates the outcome quite a lot. The used filter may be unsuitable for experiments with the test facility. The critical gradients of the small-scale SBW experiments without filter correction are shown in Figure 4-8 as function of D_{70}.

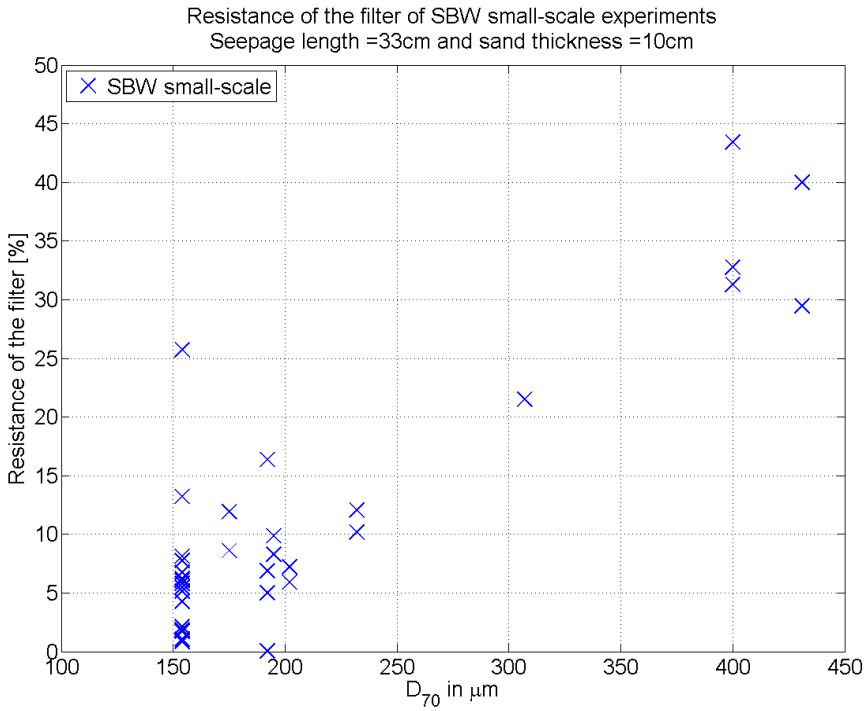

Figure 4-7 the resistance of the filter (and the rest of the test facility) as a function of D_{70} of the small-scale experiments of SBW

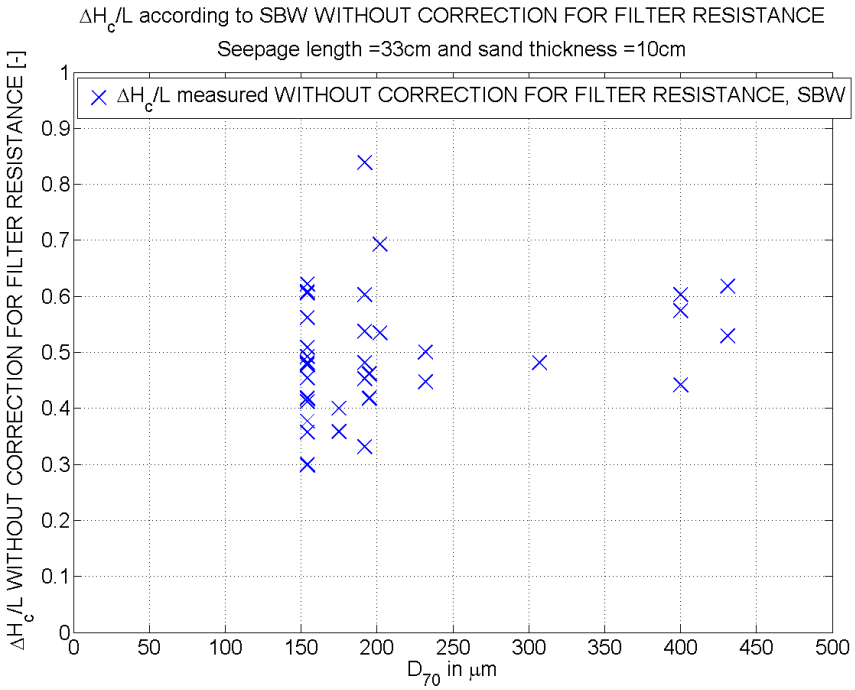

Figure 4-8 the critical gradient as function of D_{70} according to the small-scale SBW experiments without the filter correction applied

As can be seen in Figure 4-8 the trend is more like a neutral trend. This graph is without filter correction, so this graph may not be correct. It is advised to perform experiments with coarse grained sands with a filter with less resistance, or with a different type of filter, e.g. a gravel filter to find out if the results are like Figure 4-7 or like Figure 4-8. Even without correction for the filter resistance, the outcome is still not as the current Sellmeijer formula predicts, the filter correction can thus not be the reason why the Sellmeijer formula and SBW do not agree. However, performing experiments with a filter which has a lower resistance will give more accurate results.

Another explanation for the found difference between the current Sellmeijer formula and the SBW results is that in case of a real dike, some initial process (which may have a lot of influence) happens, prior to the piping process itself. This process may have an erosion length of, say, several decimeters. If this process also starts in our test facility, the experiment is over before the real piping process starts, since the seepage length is 33cm. It is unknown if this happens or not.

When regarding the SBW full-scale experiments (de IJkdijk), the experiments are performed on a real dike. Still some modeling errors can be present, as in reality the sand is deposited during several thousands of years, a process of nature. In de IJkdijk (also in de Deltagoot) the sand is deposited by men in several days.

Regarding the explanation that the Sellmeijer model is a 2D model and in reality the piping process is 3D, it is unknown how much the 2D schematization differs from the 3D behaviour of piping.

4.3 The interpretation of the experiments

In this paragraph the interpretation of the experiments is treated. As can be seen in Figure 4-10, only five experiments on coarse grains have been performed in the framework of SBW with the small-scale. The negative trend shown may be because the amount of performed experiments is to insufficient in combination with the high variance. The smaller grained sands show a high scatter. Not enough experiments on coarse grained sands were performed to make a rigid conclusion about the influence of grain size on the critical gradient. It is recommended more experiments should be done on coarse grained sand to make a more rigid conclusion about the trend in SBW experiments.

In Figure 4-11 the negative trend between grain size and critical gradient is shown for the medium-scale and full-scale (IJkdijk) SBW experiments. Only seven medium-scale experiments were performed successfully. If the measurement of

$\frac{\Delta H_c}{L} = 0.255$ would be taken away from the dataset, the negative trend would change to an almost neutral trend. This is not robust. This means the amount of experiments performed is not enough.

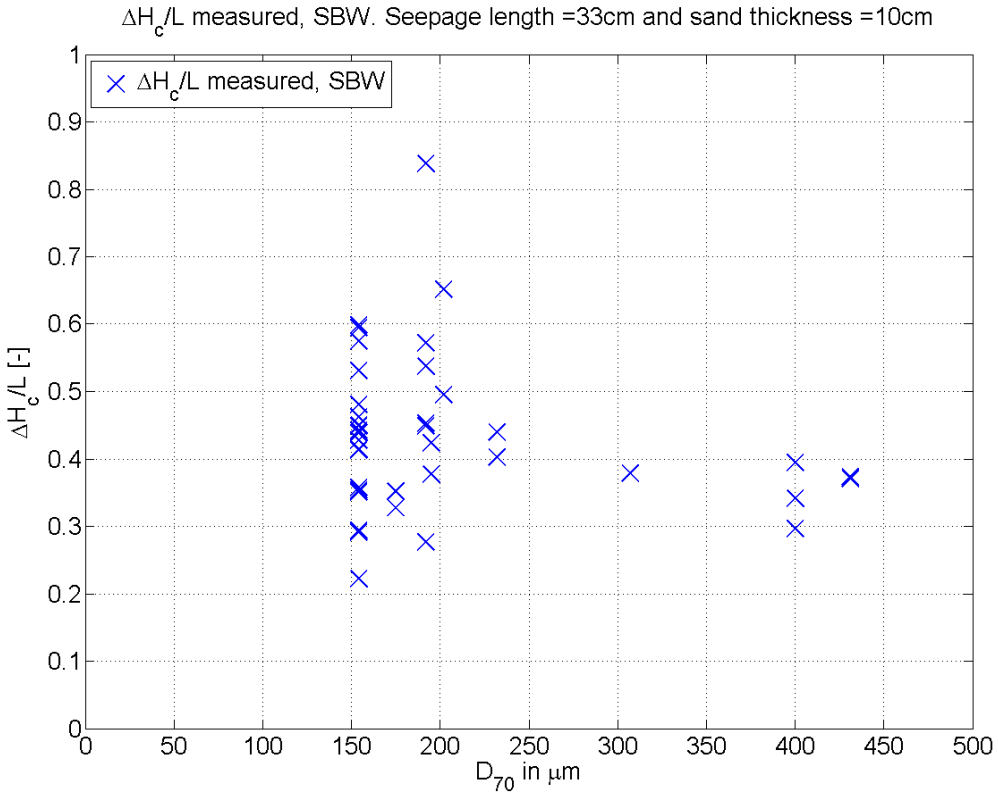

Figure 4-9 the critical gradient versus the D_{70} of the small-scale SBW experiments

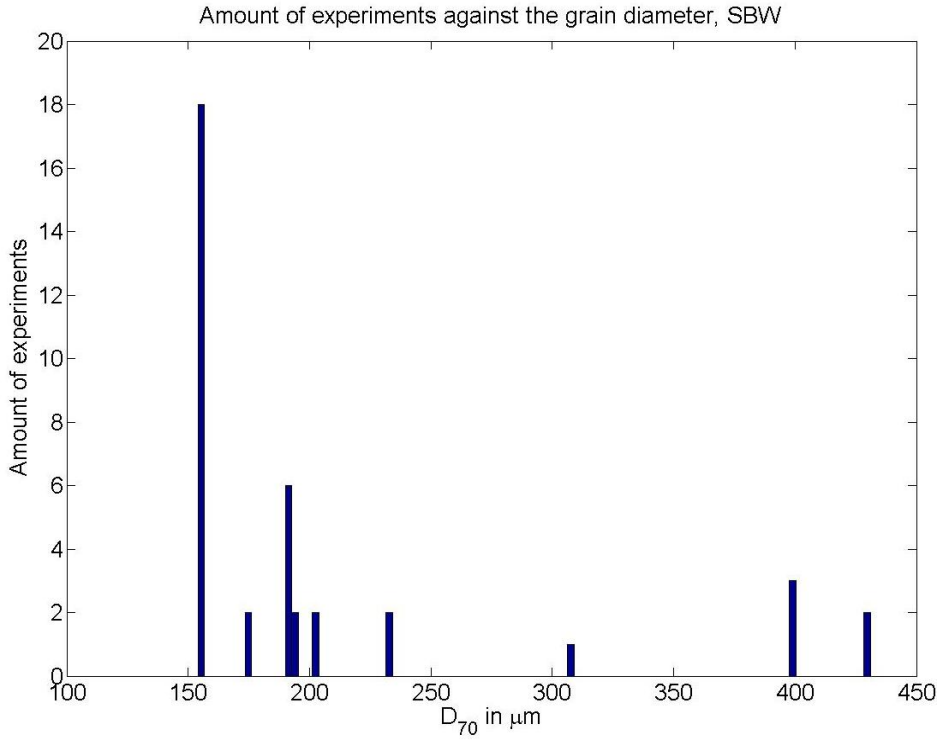

Figure 4-10 a histogram of the sand samples used for the small-scale SBW experiments

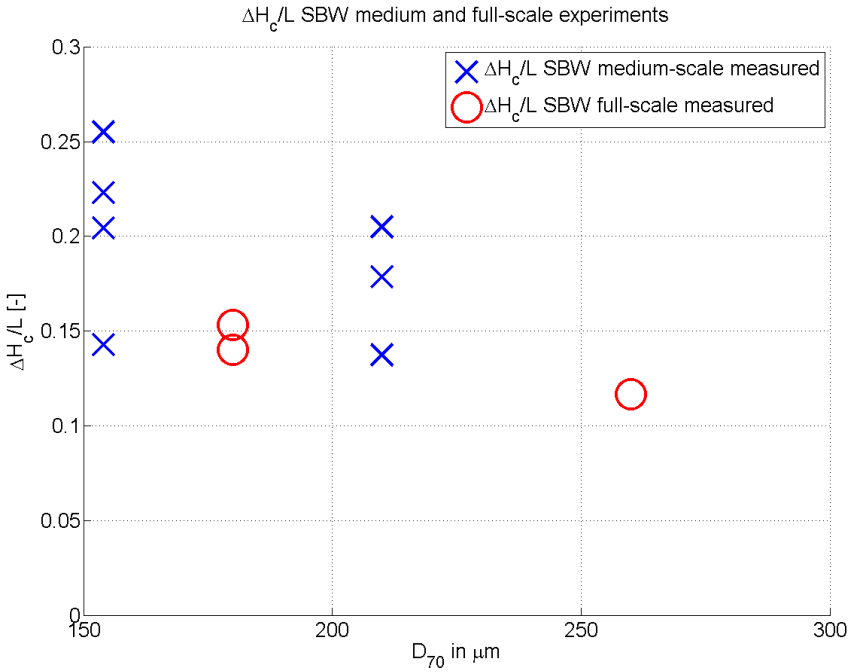

Figure 4-11 the negative trend between D_{70} and critical gradient for medium-scale and full-scale (IJkdijk) tests in SBW

There were three successful experiments with de IJkdijk, of which one was performed on coarse sand. For de IJkdijk, a negative trend between grain size and critical head is visible. Again, since only three experiments were performed, and only one on coarse sand, this is to few to make a rigid conclusion. The small, medium and full-scale experiments have a different seepage length, so they may not be compared directly. Full-scale experiments were also performed in de Deltagoot, although only one sand type was used, so no information about a trend between grain size and critical gradient can be obtained from de Deltagoot experiments.

In appendix N, several figures of the observations of Bligh for fine and coarse sand is shown. It can be seen that the scatter is very high. Two of these figures are also shown in Figure 4-12. It must be noted that the grain size is not determined very accurately, as Bligh did not specify the grain size accurately. Bligh specified the sands as fine sand, coarse sand or gravel/cobbles. Kanning suggested this classification is best represented by a grain size of 200µm, 700µm or 3000µm respectively. The data was extracted from an article of Lane (Lane, 1935) by Kanning (Kanning, 2010). As can be seen in Figure 4-12, a negative trend is present when considering the averages of the failures, but the lower boundary shows a positive trend. This is also shown in the SBW results show in Figure 4-1.

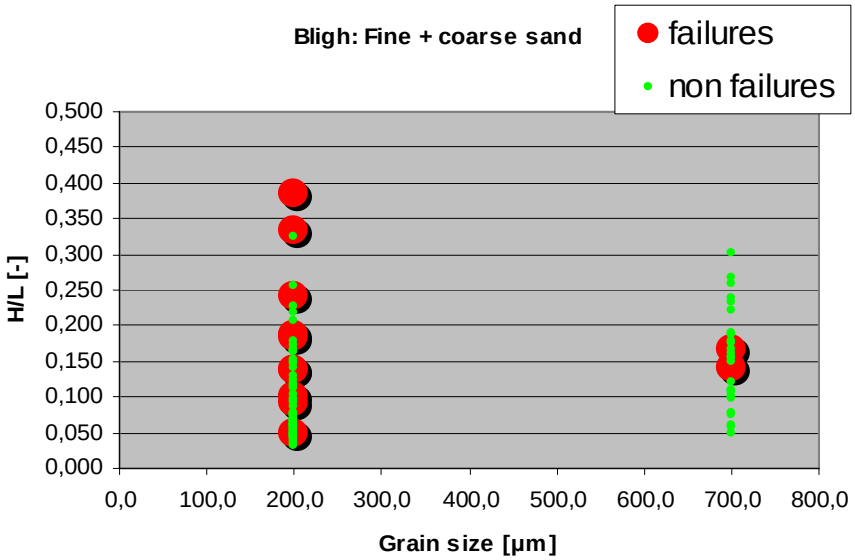

Figure 4-12 the estimated gradient of failures and non-failures as a function of grain size (coarse and fine sand and gravel) according to Bligh data (Kanning, 2010, adapted)

Conclusions about the Bligh data supporting the SBW data should not be done to hasty. The same can be said about the observations of Bligh an Lane as was said about the experiments of SBW. Only two failure observations for coarse sand is

available, as can be seen in Figure 4-12. Also Bligh distinguished only between “fine sand” and “coarse sand”. By (Kanning, 2010) this was interpreted as roughly a grain size of 200µm and 700µm respectively, but this is not sure, so the values shown in Figure 4-12 can deviate to the left or right substantially. Also only the grain size was taken into account by Bligh.

This is not sufficient, as the critical gradient depends beside grain size strong on the following variables.

- Permeability
- Relative density
- Layer thickness of the sand
- Coefficient of uniformity (dependency of critical gradient on C_u is not very strong, if both grain size and permeability is already taken into account)

These variables were not taken into account by Bligh, and the individual data of Bligh may be incomparable. As a matter of fact, Bligh did not take into account all existing variables, except for the grain size. Also, because the sand is deposited in nature, non-homogeneous layers of sand may be present, which can influence the piping behaviour substantially (van Beek, 2008b).

In the formula of Bligh a safe lower boundary was chosen for the piping formula, hence the positive trend in the critical gradient as a function of the grain size in the Bligh formula. On average the trend in the Bligh data is negative. Just as in the SBW dataset. However, since not enough information about variables in the Bligh dataset is available, a full comparison can not be made between SBW and Bligh. At least SBW data is not contradictory to the Bligh data.

As can be seen in Figure 4-11 and Figure 4-12, both in SBW and Bligh datasets, the finer sands shows a higher variation of the critical gradient than the coarser sands. This can be explained by the fact that the permeability is not taken into account in these graphs and, as is shown in Figure 2-12, permeability has a high variation for fine sand, but coarse sand has a lower variation, when the relative density is varied.

In Figure 4-13 the outcome of the small-scale and medium-scale experiments of de Wit are shown. A positive trend is visible. It is unknown if it is actually the D_{70} that causes the positive trend, as the D_{70} is correlated for 99% with the coefficient of uniformity in de Wit’s experiments. The small and medium-scale experiments have a different seepage length, so they may not be compared directly.

As was already stated in chapter 2, de Wit has a filter in the test facility, which causes a resistance, and it is unknown if the critical head is corrected for this resistance by de Wit. This filter is shown in Figure 2-25.

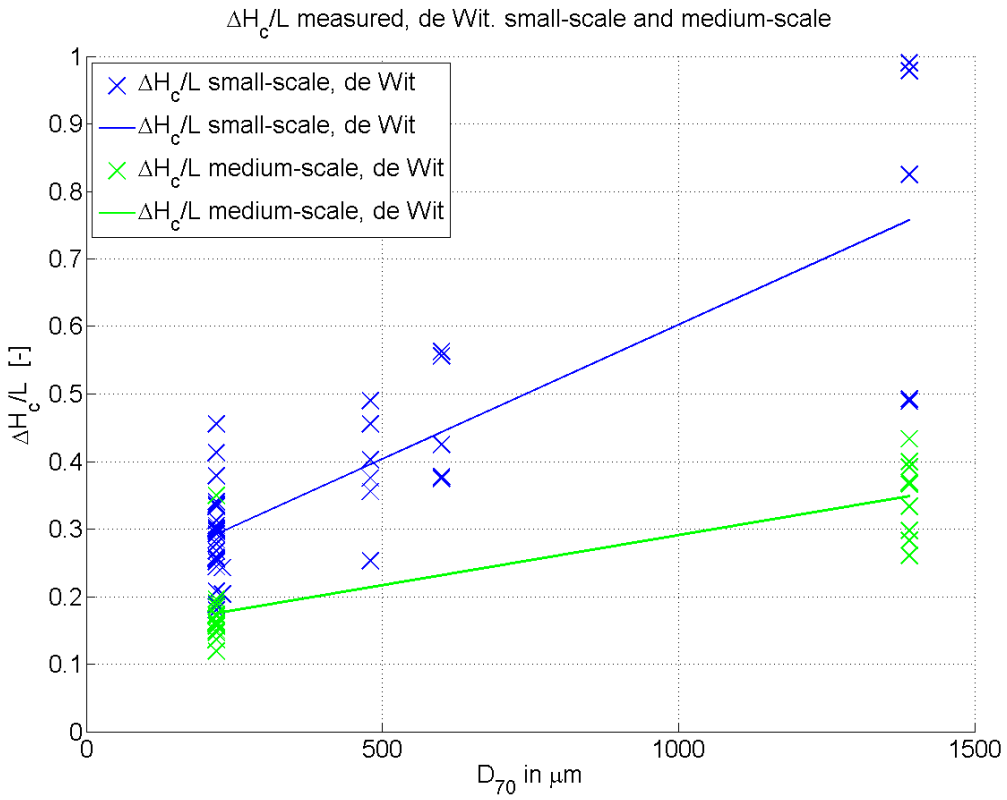

Figure 4-13 the data of the small-scale and medium-scale experiments of de Wit

In paragraph 2.6 is shown that the data from the experiments of de Wit does not agree with the dataset of SBW. One of the possible explanations is that because the resistance of the filter may not be taken into account by de Wit, the measured critical gradients are to high. The resistance of the filter depends on the flow velocity. Since coarser grains have a higher permeability, the critical gradient has a higher correction for the coarser grains as the finer grains. The resistance of the filter in SBW varied from only a few % to 10-15% for sands with a D_{70} around 200μm and between 30 to 40% for sands with a D_{70} around 400μm. No experiments were done in SBW with a D_{70} around 1390μm, as de Wit did. The resistance of the filter is likely to be even higher with this grain size. Therefore no conclusions can be drawn about the influence of the D_{70} on the critical gradient in de Wit's experiments. The experiments of de Wit are observational experiments. The experiments were not meant for finding numerical values of critical gradients.

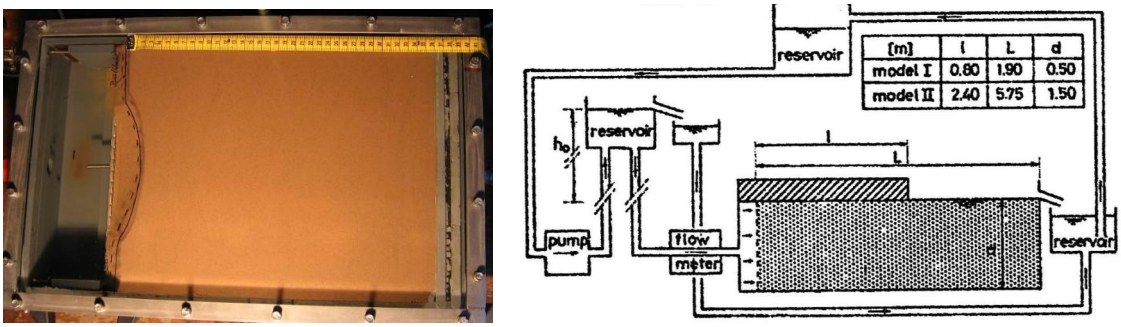

Figure 4-14 the test facility of SBW (left) and the test facility of de Wit (right)

The range of D_{70}'s used by de Wit is also much higher than is used in SBW. Also the test facility of de Wit is different than the test facility used by SBW as shown in Figure 4-14. This may also be a reason for the different findings.

4.4 The possible not applicableness of White in the Sellmeijer model

In this paragraph the possible not applicableness of White in the Sellmeijer model is treated. In chapter 3, the correctness of the implementation of the erosion model of white in the Sellmeijer formula was questioned both from theory and from experimental view. From a theoretical background, in paragraph 3.3 it is argued the use of the erosion model of White for the equilibrium of grains in the Sellmeijer model is questionable. With the one-dimensional test facility, it was shown experimentally that the grains in the piping process are eroded as mass, in a layer of roughly 7 grains thick in the test facility. The transport occurs in waves, as is shown in paragraph 3.5. In paragraph 3.8 it was concluded that it is not sure if the observed erosion is representative for determining the critical gradient, as the observed erosion may be the erosion type when the critical gradient has already been exceeded. This is still under discussion.

4.5 Evaluation of the found possible explanations

In paragraph 4.2 the possible correctness of the small-scale and medium-scale test facility was questioned. The possible incorrect interpretation of the experiments was treated in paragraph 4.3, as was the explanation that the amount of experiments was to few to make rigid conclusions. In paragraph 4.4 the possible not applicableness of White in the Sellmeijer model was treated. The found explanations for the difference between the current Sellmeijer formula and the results found in SBW is not exhaustive. More explanations are possible.

It was found that the small-scale and medium-scale test facilities do not agree exactly with the model of Sellmeijer, but the differences are small, so this is not a

likely explanation for the differences between SBW and the current Sellmeijer formula. However, more experiments on coarse grained sands with a different filter should be done to research the influence of the grain size more accurate. It was found that the vertical gradient in the test facilities is much higher than in case of a real dike. The influence of this vertical gradient influences the outcomes of the experiments moderately, this may explain part of the difference between SBW and the current Sellmeijer formula. More research is needed to the influence of the vertical gradient on the piping behaviour.

The Sellmeijer model consists out of the three following differential equations.

$\nabla^2\phi = 0$ continuity of flow in the sand layer (LaPlace) (eq 1-5).

$a^3 \frac{\partial\phi}{\partial x} = 12\kappa \int \frac{\partial\phi}{\partial y}\,\mathrm{d}x$ continuity of flow in the pipe (Poiseuille) (eq 1-6).

$\frac{a}{d}\frac{\partial\phi}{\partial x} = \frac{\pi}{3}\eta\frac{\gamma'_{\mathrm{p}}}{\gamma_{\mathrm{w}}}\frac{\sin(\theta+\beta)}{\cos\theta}$ equilibrium of the sand particles in the pipe (White) (eq 1-7).

The symbols have been explained in paragraph 1.4.

The solution of this set of differential equations is $\frac{H_c}{L} = \alpha\eta\tan(\theta)\frac{\gamma'_p}{\gamma_w}\frac{D_{70}}{\sqrt[3]{\kappa L}}$ (eq 1-4).

The influence of the grain size is linear in the current Sellmeijer formula. This is because the grain diameter is also linear present in the equation of White which describes the equilibrium of grains before erosion starts.

Based on the observations of the experiments in the one-dimensional test facility, it was shown the model of White is possibly not applicable for piping. It must be researched further if the observed erosion is normative for determining the critical gradient. The experiments with the test facility showed the transport of grains is a mass erosion process. Since the observed erosion in the one-dimensional test facility is different than the erosion mechanism of White, the influence of the grain diameter may also be different as is described in the current Sellmeijer formula. This is a possible explanation for the difference found between the current Sellmeijer formula and the results of SBW.

It is concluded that the equation of White, which may possibly not be applicable in the piping model (more research is needed to prove this), is a plausible cause of the difference found between SBW and the current Sellmeijer formula.

4.6 Conclusions and a summary about the found possible explanations

In this chapter a possible explanation for the difference between the current Sellmeijer formula and the results found by SBW is given.
In paragraph 4.1 the data of SBW is shown. In paragraph 4.2 the possible incorrect modeling of piping in the small-scale and medium-scale test facility is treated. It is unknown how much the 2D schematization differs from the 3D behaviour of piping. In paragraph 4.3 the interpretation of the experiments and the amount of experiments is treated.

The influence of the grain size on the critical gradient in the SBW experiments is questioned, since the test facility does not represent all of the features a real dike has. Also the influence of the filter is discussed, and the amount of coarse grained small-scale experiments and the amount of medium-scale and full-scale experiments is quite low. If the results of the small-scale test facility are compared or extrapolated to real dike dimensions, a correction needs to be made because of the influence of the vertical gradient.

The possible not applicableness of White in the Sellmeijer model is treated in paragraph 4.4. In the Sellmeijer model equilibrium of grains is assumed to be according to the erosion model of White. Because it was shown that the equilibrium of grains according to the erosion model of White may possibly not be applicable to piping (this must be researched further), it is concluded that a possible explanation for the difference of the influence of grain size on the critical gradient between the Sellmeijer model and SBW experiments may be because the model of White is implemented in the piping model, while White may not be applicable in a piping model.

5. Theoretical research of the relation between variables in the channel

In this chapter theoretical research of the relation between variables in the channel is done. This is not part of the main objective of this thesis, but an important relationship is found between grain size and velocity in the channel. The investigation is based on the Sellmeijer 2-forces model.

In paragraph 5.1 the normalized model of Sellmeijer is discussed. In paragraph 5.2 theoretical research to the velocity in the slit is performed. Conclusions and a summary is given in paragraph 5.3.

5.1 The normalized model of Sellmeijer

In this paragraph the normalized model of Sellmeijer is explained. The model of Sellmeijer consists of the equations of groundwater flow (LaPlace), flow in the slit (Poiseuille) and the equilibrium of grains on the bed of the slit (White), which are derived by Sellmeijer for the current 2-forces model. These equations are explained in paragraph 1.4. These equations are

$\nabla^2\phi = 0$ continuity of flow in the sand layer (LaPlace) (eq 1-5).

$a^3 \frac{\partial\phi}{\partial x} = 12\kappa \int \frac{\partial\phi}{\partial y}\,\mathrm{d}x$ continuity of flow in the pipe (Poiseuille) (eq 1-6).

$\frac{a}{d}\frac{\partial\phi}{\partial x} = \frac{\pi}{3}\eta \frac{\gamma'_{\mathrm{p}}}{\gamma_{\mathrm{w}}} \frac{\sin(\theta+\beta)}{\cos\theta}$ equilibrium of the sand particles in the pipe (White) (eq 1-7).

The symbols have been explained in paragraph 1.4.

Since the derivation in paragraph 5.2 is based on the Sellmeijer model, the outcome is only valid if the Sellmeijer model is valid, including all the assumptions and simplifications that Sellmeijer did in his model.

Sellmeijer recently made a blueprint for piping models (Sellmeijer, 2010b). This blueprint contain the above mentioned formula's, but are normalized to make certain computations easier. These normalized equations serve as a basis for a model that makes use of the Sellmeijer model.

These equations are normalized as follows.

$$X = \frac{x}{L} \qquad \textit{(eq 5-1).}$$

$$Y = \frac{y}{L} \qquad \textit{(eq 5-2)}.$$

$$\Phi = \frac{1}{\lambda}\frac{\varphi}{L} \qquad \textit{(eq 5-3)}.$$

The normalized equations of LaPlace, Poiseuille and White are as follows

$$\nabla^2\Phi = 0 \qquad \text{(LaPlace)} \qquad \textit{(eq 5-4)}$$

$$\frac{a^3}{\delta^3}\frac{\partial\Phi}{\partial X} = \int\frac{\partial\Phi}{\partial Y}\,\mathrm{d}X \qquad \text{(Poiseuille)} \qquad \textit{(eq 5-5)}$$

$$\frac{a}{\delta}\frac{\partial\Phi}{\partial X} = 1 \qquad \text{(White)} \qquad \textit{(eq 5-6)}$$

With $$\lambda = \frac{\pi}{3}\eta\frac{\gamma'_{\mathrm{p}}}{\gamma_{\mathrm{w}}}\frac{\sin(\theta+\alpha)}{\cos\theta}\frac{d}{\delta} \qquad \textit{(eq 5-7)}$$

$$\delta = \sqrt[3]{12\kappa L} \qquad \textit{(eq 5-8)}$$

$$\Phi = \Phi(X, Y(X), \frac{D}{L}) \qquad \textit{(eq 5-9)}$$

The statement Φ is a function of X, Y(X) and $\frac{D}{L}$ is only valid for the idealized geometry which is shown in Figure 1-5, for another geometry Φ is dependent on more variables. In this chapter, the idealized geometry is taken as starting point. Since the idealized geometry is analyzed, $\beta = 0$ and the $\frac{\sin(\theta+\beta)}{\cos\theta}$ factor reduces to tan(θ).

The following quantity's can be normalized

$$\hat{Q} = \frac{1}{\lambda}\frac{Q}{k\,L} \qquad \text{where } \hat{Q} = \hat{Q}(X, Y(X), \frac{D}{L}) \qquad \textit{(eq 5-10).}$$

$$\hat{a} = \frac{a}{\delta} \qquad \text{where } \hat{a} = \hat{a}(X, Y(X), \frac{D}{L}) \qquad \textit{(eq 5-11).}$$

$$\hat{V} = \frac{V}{\delta\,L} \qquad \text{where } \hat{V} = \hat{V}(X, Y(X), \frac{D}{L}) \qquad \textit{(eq 5-12).}$$

The author of this thesis tried to find an analytical solution for Φ. Unfortunately, the attempt was not successful.

5.2 Theoretical research of the velocity in the slit

In this paragraph the velocity as function of the grain size is researched based on the normalizations shown in paragraph 5.1.
First, several other normalizations besides the one mentioned in paragraph 5.2 have to be made.

$$\hat{p} = \frac{d\Phi}{dX} \qquad \textit{(eq 5-13).}$$

$$\hat{a} = \frac{1}{\hat{p}} \qquad \textit{(eq 5-14).}$$

$$\hat{q} = \frac{d\Phi}{dY} \qquad \textit{(eq 5-15).}$$

$$\hat{Q} = \int \hat{q}\, dX = \int \frac{d\Phi}{dY} dX \qquad \textit{(eq 5-16).}$$

Since $\frac{a^3}{\delta^3}\hat{p} = \int \frac{\partial \Phi}{\partial Y} \mathrm{d}X$, multiplying the first formula with $\hat{p}^2$ yields

$$(\frac{a}{\delta}\hat{p})^3 = \hat{p}^2 \int \frac{\partial \Phi}{\partial Y} \mathrm{d}X = \hat{p}^2 \hat{Q} \qquad \textit{(eq 5-17).}$$

Since $\frac{a}{\delta}\hat{p} = 1$, $\qquad \hat{p}^2 \hat{Q} = 1$ *(eq 5-18).*

$$\frac{a}{\delta} = \frac{1}{\hat{p}}, \text{ so } a = \frac{\delta}{\hat{p}} = \frac{\sqrt[3]{12\kappa L}}{\hat{p}} \qquad \textit{(eq 5-19).}$$

Also $(\frac{a}{\delta})^2 = \hat{a}^2 = \int \frac{\partial \Phi}{\partial Y} \mathrm{d}X = \hat{Q}$ *(eq 5-20).*

Since $\frac{1}{\lambda}\frac{Q}{k\,L} = \hat{Q}$, $Q = \hat{Q}\lambda k\, L$ *(eq 5-21).*

and because $\lambda = \frac{\pi}{3}\eta \frac{\gamma'_{\mathrm{p}}}{\gamma_{\mathrm{w}}} \tan\theta \frac{d}{\delta}$, $Q = \frac{\hat{Q}\, k\, L d}{\delta} F_r$ *(eq 5-22).*

where $F_r = \frac{\pi}{3}\eta \frac{\gamma'_{\mathrm{p}}}{\gamma_{\mathrm{w}}} \tan\theta$, the same as the resistance factor in the current 2-forces Sellmeijer model, except a factor $\frac{\pi}{3}$ is added. This factor is also present in the current 2-forces model, but there this factor is assimilated in the geometry factor.

$$Q = \frac{\hat{Q} k\, Ld}{\delta} F_r = \frac{\hat{Q}\kappa \frac{g}{\upsilon} Ld}{\sqrt[3]{12\kappa L}} F_r = \frac{\hat{Q}(\kappa L)^{\frac{2}{3}} \frac{g}{\upsilon} d}{\sqrt[3]{12}} F_r = \frac{F_r}{12} \hat{Q} \frac{g}{\upsilon} \delta^2 d = \frac{F_r}{12} \hat{Q} \frac{g}{\upsilon} da^2 \hat{p}^2 \quad \textit{(eq 5-23).}$$

$$u = \frac{Q}{a} = \frac{F_r}{12} \frac{g}{\upsilon} \left[\hat{Q} \hat{p}^2 \right] da \quad \textit{(eq 5-24).}$$

since $\hat{p}^2 \hat{Q} = 1$ *(eq 5-18).*

$$u = \frac{Q}{a} = \frac{F_r}{12} \frac{g}{\upsilon} da \quad \textit{(eq 5-25).}$$

$$Q = \frac{F_r}{12} \frac{g}{\upsilon} da^2 \quad \textit{(eq 5-26).}$$

Note the Sellmeijer model is derived per running meter, so u is the velocity in the slit, in m/s in (eq 5-25).

It is emphasized again that the above formulas are based on the Sellmeijer model and they are only valid if the Sellmeijer model is valid, including all the assumptions and simplifications that Sellmeijer did in his model, and the idealized geometry is regarded.

From this can be concluded the velocity in the slit (according to the Sellmeijer model) is a constant times the grain size times the channel depth (eq 5-25). This formula can be very convenient if one researches the properties of the channel. The formula is valid in the entire channel. This formula (eq 5-25) is named the van der Zee equation.

5.3 Conclusions and a summary about the theoretical research of the relation between variables in the channel

In paragraph 5.1 the equations of the Sellmeijer formula (continuity, Poiseuille and White) are normalized.

In paragraph 5.2, the velocity in the channel (according to the current Sellmeijer model) is derived. The velocity is: $u = \frac{Q}{a} = \frac{F_r}{12} \frac{g}{\upsilon} da$ (eq 5-25), with $F_r = \frac{\pi}{3} \eta \frac{\gamma'_{\mathrm{p}}}{\gamma_{\mathrm{w}}} \tan\theta$. The velocity in the slit is a constant times the grain size times the channel depth. This formula (eq 5-25) is named the van der Zee equation. The equation is based on the Sellmeijer model and it is only valid if the Sellmeijer model is valid.

6. Conclusions

The objective of this masters thesis is to investigate the influence of the grain size and other sand characteristics on the critical head of piping, and to find an explanation for the difference found between SBW results and the Sellmeijer formula. This chapter presents the conclusions as a result of the research.

A study of variables has been performed. A multi variate analysis (MVA) was performed successfully on the SBW data. From this it was concluded the influence of the D_{70} was less than in the Sellmeijer model, and the influence of the permeability agreed well. The outcome of the MVA confirmed the results found by López de la Cruz. A MVA could not be performed on de Wit data because of, amongst others, high correlations between variables. When the de Wit dataset is inserted in the adapted Sellmeijer formula, the outcome did not agree, this may be because the data of de Wit may possibly not be corrected for the filter resistance, or because of the different range of variables in the de Wit dataset, when compared with the SBW dataset.

One of the hypothesis of this thesis is that the erosion of grains is as mass erosion, not as individual erosion, as is in the model of White, which is the erosion model assumed in the Sellmeijer model. From a theoretical background, it was found that it is doubtful that modeling the equilibrium of grains according to the model of White is applicable in a piping model. Some objections against using White in a piping model are: the formula is derived for a flume and not for a piping model, very little amount of experiments were performed, White used lubrication oil in his experiments instead of water, only the more prominent grains are assumed to transfer the shear stresses from the water to the bed and according to White the product of correction factor of the lever length and the packing coefficient is always constant, which is very doubtful.

Based on observations in the one-dimensional test facility, it was found that the grains are dislodged from the (original) granular matrix with hundreds of grains together, with a layer thickness of roughly 7 grains. The dislodging of grains is different than the model of White describes and the equilibrium of grains according to the model of White is possibly not applicable in a piping model. The transport of grains is mass transport, in waves, called slurry flow. The sand waves are pushed through the channel by a pressure difference.

It is not certain that the observed dislodging of grains from the sand matrix is normative for describing the critical gradient of piping. Since no quasi-static equilibrium was observed and the transport is observed halfway the test facility, it may be that the observed erosion mechanism is the erosion mechanism that

occurs after the critical gradient has been reached. More research is needed to prove or disprove that the observed erosion mechanism is normative for calculation the critical gradient.

If this erosion process is also in reality present under a real dike is not sure. However, some basic processes are the same, as groundwater flow through a sand layer under a rigid “roof” by a head difference, which erodes grains at the exit point and a channel grows in downstream direction, it is concluded the behaviour under a real dike is probably somewhat similar as the observed behaviour in the test facility. More research is needed to the erosion process.

Since Sellmeijer based his piping model on the equations of continuity, White and Poiseuille, it is concluded this model may possibly not describe the piping process in a proper way, as it does not describe the real processes going on. However, for fine and medium fine sands, it gives a numerical correct answer for the small-scale SBW experiments, but not for coarser sands. This may be because of the fitting on de Deltagoot experiments. For the medium-scale and full-scale experiments, the current Sellmeijer formula performs well for fine sands, but less for medium fine sands and coarse sands. This may be due to the low amount of medium-scale and full-scale experiments performed, in combination with a high scatter of results.

It is concluded the adapted Sellmeijer formula is partly a black box model. Part of the model is based on a correct and applicable process (groundwater flow), another part is based on a (possible) not applicable process (White), and the correction factors are not based on physical processes but on fitting on empirical data and little insight is present regarding restrictions and applicableness.

It is concluded the flow in the test facility is slurry flow, and the dislodging of grains may not be according to the model of White. From dredging engineering, experience is present about slurry flow.

It was concluded the vertical pressure gradient in the one-dimensional and small-scale test facility is higher when compared with real dike dimensions. If the calculated critical gradients are compared or extrapolated to real dike dimensions, a correction has to be made. This has not been done for SBW small-scale results. More research is needed to the vertical pressure gradient. The influence of the filter on the critical gradient in the test facility is not known precisely.

It is concluded that the outcome of SBW does not contradict the data of Bligh, as Bligh did only take into account the grain size, not the other relevant variables, and Bligh took an safe lower value of the observations.

It is concluded that a likely reason for the difference between critical gradient between SBW and the Sellmeijer model is because the dislodging of grains from the granular matrix in reality may be different than the model of White, which is assumed in the Sellmeijer model. This is not sure as it is unclear if the observed erosion process is normative for determining the critical gradient.

Several minor reasons for the difference between SBW and Sellmeijer are the high influence of the vertical gradient in the test facility, the possible improper modeling of the filter resistance, and the low amount of coarse grained small-scale experiments, in combination with a high scatter.

A relation between the velocity in the channel and the grain size has been found. This relation is only valid when the Sellmeijer formula is valid.

7. Recommendations

This chapter presents the recommendations as a result of the research.

Since only a few experiments on coarse grained sands were performed in the small-scale test facility of SBW, it is advised to perform more experiments on coarse grained sands. Also a different kind of filter is advised for experiments on coarse grained sands, as the filter resistance is high for coarse sand, and this lessens the robustness of the outcomes of the experiments. A filter of gravel may be considered instead of a geotextiel for the experiments on coarse grained sands.

Only a few experiments were performed in the medium-scale and full-scale test facilities. Performing more experiments would increase the confidence in the outcome of these experiments.

It is unknown whether the critical head is corrected for the influence of the filter in the experiments of de Wit. It is recommended that, based on the charts of the hydraulic head, which were made by de Wit based on pressure tubes measurements, it is tried to retrieve information about the head difference, to determine the true critical gradient.

It is not sure if the observed erosion process is normative for the determination of the critical gradient. Further research is needed to prove or disprove that the observed erosion mechanism is normative for determining the critical gradient.

It is recommended to research if the erosion process that was observed in the one-dimensional test facility (mass erosion) is also present if the vertical gradient is lower than in the used one-dimensional test facility, e.g. by increasing the seepage length of the test facility and/or decreasing the depth of the aquifer.

The sand transport that was observed in the one-dimensional test facility is slurry flow. From dredging engineering, a lot of research has been done at slurry flow in pipelines. It is recommended that information is shared and discussed between the disciplines of dredging engineering and dike technology.

It is recommended that with data imaging techniques on the high-resolution recordings of the experiments performed with the one-dimensional test facility, the motion of the grains is determined more accurately. This may help with deriving a new piping model.

For the SBW small-scale test facility, (which has a seepage length of 33cm) the seepage of water flow to the pipe is several centimeters. In case of a real dike

with a seepage length of an order 200 times longer than the SBW small-scale test facility, the seepage of water flow may be more than a few centimeters, but probably not 200 times as much. Research to the influence of three-dimensional water flow as a function of pipe dimensions and seepage length is recommended.

Performing research to the time dependent processes, as for example the erosion rate, that was observed in the one-dimensional test facility is recommended, since the load on a dike is time dependent, and to perform a detailed safety analysis, the time dependent strength of a dike must also be known. This knowledge is also useful if mitigating measures are considered.

The Sellmeijer model predicts a quasi-static equilibrium. The quasi-static equilibrium is predicted because of converge of streamlines near the exit point, and the equilibrium of grains according to White. This equilibrium was not found in the small-scale, medium-scale and IJkdijk experiments. It is recommended that further research is performed to the quasi-static equilibrium, since mitigating measures, as “opkisten”, are used in the Netherlands against piping and these measures depend on the quasi-static equilibrium.

References

Written documents / presentations:

(Achmus, 2006) Achmus, M., *Considerations and Model Tests on the Design of River Barrages with Respect to Piping*, 2006

(Ammerlaan, 2007) Ammerlaan, P.R.M., Levees and levee evaluation The Dutch and US practice compared, MSc thesis, Delft University of Technology, Delft, 2007

(Barends, 2003) Barends, F.B.J., Uffink, G.J.M., *lecture notes CT3320, Groundwater mechanics, flow and transport,* Delft University of Technology, Delft, 2003

(Bligh, 1910) Bligh, W.G., *Dams Barrages and Weirs on Porous Foundations, Engineering news*, p 708, 1910

(Boon, 2007) Boon, M.J.J., *Water Controlling Water, Emergency flood protection,* MSc thesis, Delft University of Technology, Delft, 2007

(Clibborn, 1902) Clibborn, J., Beresford, J.S., *Experiments on the Passage of Water through Sand*, Govt. of India, Central Printing Office, 1902

(de Bruijn, 2009) De Bruijn, H.T.J. et al, *SBW Piping Hervalidatie Piping HP 5.4b Full-scale proeven (factual report proef 3),* Deltares, Delft, 2010

(de Rijke, 1991) De Rijke, W.G., *Verificatie piping model, proeven in de Deltagoot,* Delft, 1991

(de Wit, 1984) De Wit, J.M., laboratorium voor grondmechanica Delft, *onderzoek zandmeevoerende wellen,* Delft, 1984

(ENW, 2010) Expertise Netwerk Waterveiligheid (ENW), *Piping, Realiteit of Rekenfout?,* ENW, Delft, 2010

(Garson, 2009) Garson, G., *Multiple regression*. Statistical notes, North Carolina State University, 2009

(Griffith, 1913) Griffith, W.M., *the Stability of Weir Foundations on Sand and Soil subject to Hydrostatic Pressure*. Minutes of proceedings J.C.E., vol 197 pt III, p 221, 1913

(Harza, 1935) Harza, L.F., *Uplift and Seepage under Dams on Sand*, proceedings American Society of Civil Engineers, paper no 1920, 1935

(Hoffmans, 2009) Hoffmans, G.J.C.M., *Backward erosion in cohesion less soils beneath dikes,* Deltares, Delft, 2009

(Hunt, 2005) Hunt, R.E., *geotechnical engineering investigation handbook, second edition,* CRC Press, Boca Raton, 2005

(Kanning, 2010) Kanning, W., *excel sheet based on the data of Bligh and Lane*, 2010

(Knoeff, 2008) Knoeff, J.G. et al, *SBW piping, Vooronderzoek kleine schaal laboratoriumproeven (A1 literatuurstudie),* Deltares, Delft, 2008

(Koelewijn, 2010) Koelewijn, A.R., *PowerPoint presentation: Performance of detection techniques at four full-scale seepage erosion tests, EWG Internal Erosion, Granada, 2010*

(Kohno, 1987) Kohno, L., *Levee failure caused by seepage and preventive measurements*, natural disaster science, volume 9, number 2, Okayama, 1987

(Kruse, 2008) Kruse, G.A.M. et al., *SBW Hervalidatie Piping. Bureaustudie zandeigenschappen (factual report) (zandsoorten gebruikt in kleinschalige proeven)', Rapport CO-433380.0012,* Deltares, Delft, 2008

(Lane, 1935) Lane, A.W., *Security from Under-Seepage Masonry Dams on Earth Foundations*, Transactions American Society of Civil Engineers, vol. 100 paper no. 1919, 1935

(López de la Cruz, 2009)	López de la Cruz, J. et al., *SBW Piping - Hervalidatie piping HP1 and HP1.2,* Deltares, Delft, 2009
(Lubking, 2010)	Lubking, P., *Aan de grond zitten,* Deltares Academy, Delft, 2010
(Mines, 2010)	Mines, R.O., *Sludge Pumping*, Mercer University School of Engineering, Macon, 2010
(Müller-Kirchenbauer, 1978)	Müller-Kirchenbauer, H. von, *Zum zeitlichen Verlauf der rückschreitenden Erosion in geschichtetem Untergrund unter Dämmen und Stauanlagen,* Berlin, 1978
(Ojha, 2001)	Ojha, C.S.P., *Influence of porosity on piping models of levee failure,* Journal of geotechnical and environmental engineering, December 2001
(Polubarinova-Kochina, 1962)	Polubarinova-Kochina, P.Y., *Theory of Groundwater Movement*, Princeton University Press, Princeton, New Jersey, 1962
(Rabah, 2010)	Rabah, F., *Pumping Stations Design For Infrastructure Master Program Engineering Faculty-IUG Lecture 7: Design of sludge pumping stations, Gaza, 2010*
(Rietdijk, 2009)	Rietdijk, J., *SBW piping, Hervalidatie piping HP 2.1 Medium-schaal proeven (factual report),* Deltares, Delft, 2009
(Schiereck, 2004)	Schiereck, G.J., *Introduction to bed, bank and shore protection*, Delft University Press, Delft, 2004
(Schmertmann, 2000)	Schmertmann, J.H., *The no filter factor of safety against piping through sands,* Gainesville, 2000
(Schmertmann, 2002)	Schmertmann, J.H., *A method for assessing the relative likelihood of failure of embankment dams by piping,* Gainesville, 2002

(Sellmeijer, 1988) Sellmeijer, J.B., *on the mechanism of piping under impervious structures,* Delft University of Technology, Delft, 1988

(Sellmeijer, 1989) Sellmeijer, J.B. et al, *influence of aquifer thickness on piping below dikes and dams,* Delft geotechnics, Delft, 1989

(Sellmeijer, 1991) Sellmeijer, J.B. et al, *A mathematical model for piping,* Delft geotechnics, Delft, 1991

(Sellmeijer, 1993) Sellmeijer, J.B. et al, *A new model to deal with the piping mechanism,* Delft geotechnics, Delft, 1991

(Sellmeijer, 2003) Sellmeijer, J.B., *engineering tools for piping – neural networks created using FEM*, Deltares, Delft, 2003

(Sellmeijer, 2010a) Sellmeijer, J.B. et al, *Fine-tuning of the piping model trough small-scale, medium-scale and IJkdijk experiments*, Deltares, Delft, 2010

(Sellmeijer, 2010b) Sellmeijer, J.B., *Piping geschaald,* Deltares, Delft, 2010

(TAW, 1999) Technical Advisory Committee on Flood Defences (TAW), *Technical Report on Sand Boils (piping)*, TAW, Delft, 1999

(ter Horst, 2005) Ter Horst, W.L.A., *An analysis of the failure probability of dike ring areas in flood wave situations,* MSc thesis, Delft University of Technology, Delft, 2005

(Terzaghi, 1948) Terzaghi, K. von et al., *Mechanics of piping,* 1948, published in "*Soil mechanics in engineering practice*", Wiley, New York, 1996

(van Beek, 2008a) Van Beek, V.M., et al *various factual reports of SBW experiments with piping*, Deltares, Delft, 2008-2010

(van Beek, 2008b) Van Beek, V.M. et al, *Piping phenomena in heterogeneous sands – experiments and simulations*, Deltares, Delft, 2008

(van Beek, 2009a) Van Beek, V.M. et al, *SBW piping Hervalidatie piping B3 analyse kleinschalige laboratorium proeven*, Deltares, Delft, 2009

(van Beek, 2009b) Van Beek, V.M. et al, *SBW Hervalidatie piping H.P. 2.2 Medium-schaal proeven (Analysereport)*, Deltares, Delft, 2009

(van Beek, 2009c) Van Beek, V.M., *Powerpoint presentation: SBW piping small-scale experiments* , Deltares, Delft, 2009

(van Beek, 2009d) Van Beek, V.M., *Powerpoint presentation: Research on piping, Lab experiments and IJkdijk*, Deltares, Delft, 2009

(van Beek, 2010a) Van Beek, V.M. et al, *SBW piping Hervalidatie piping H.P. 5.5a analyse en validatie full-scale proeven*, Deltares, Delft, 2010

(van Beek, 2010b) Van Beek, V.M. *SBW Hervalidatie Piping H.P. 12 Afbakening relevantie displacement piping bij losse pakking,* Deltares, Delft, 2010

(Verruijt, 2001) Verruijt, A., *Soil mechanics*, Delft University Press, Delft, 2001

(Weijers, 2009) Weijers, J.B.A., *lecture notes CT5314, Flood defences,* Delft University of Technology*,* Delft, 2009

(Weijers, 2010) Weijers, J.B.A., *PowerPoint presentation: lecture CT5314, Flood defences,* Delft University of Technology*,* Delft, 2010

(White, 1939) White, C.W., *the Equilibrium of Grains on the Bed of a Stream*, Proceedings Royal Society London, vol 174A, 1939

(Zeping, 2001) Zeping, X., *Seepage Problems of River Dikes and Cost Effective Solutions*, Beijing, 2001

Personal conversations:

(Barends, 2011)	Barends, F.B.J. emeritus professor Delft University of Technology, scientist at Deltares, personal conversation, January 6th 2011
(Mastbergen, 2011)	Mastbergen, D.R., scientist at Deltares, e-mailing, January 10th 2011
(Schenkeveld, 2010)	Schenkeveld, F.M., laboratory employee at Deltares, personal conversation, September 29th 2010
(van Gelder, 2010)	Van Gelder, P.H.A.J.M., associate professor probabilistic design, Delft University of Technology, personal conversation, August 31st 2010

Web based resources:

(Wikipedia, 2011)	http://en.wikipedia.org/wiki/Bingham_plastic

A) Appendix A – The test facility used by de Wit

De Wit has done extensive research on piping. The experiments were conducted between 1974 and 1982 at GeoDelft (now part of Deltares). In this appendix the test facility that has been used is described. In Figure A-1 the test facility is shown. As can be seen, the model corresponds with the situation where no impervious layer is present at the hinterland. This model does not correspond with the model of the idealized geometry shown in Figure 1-5.

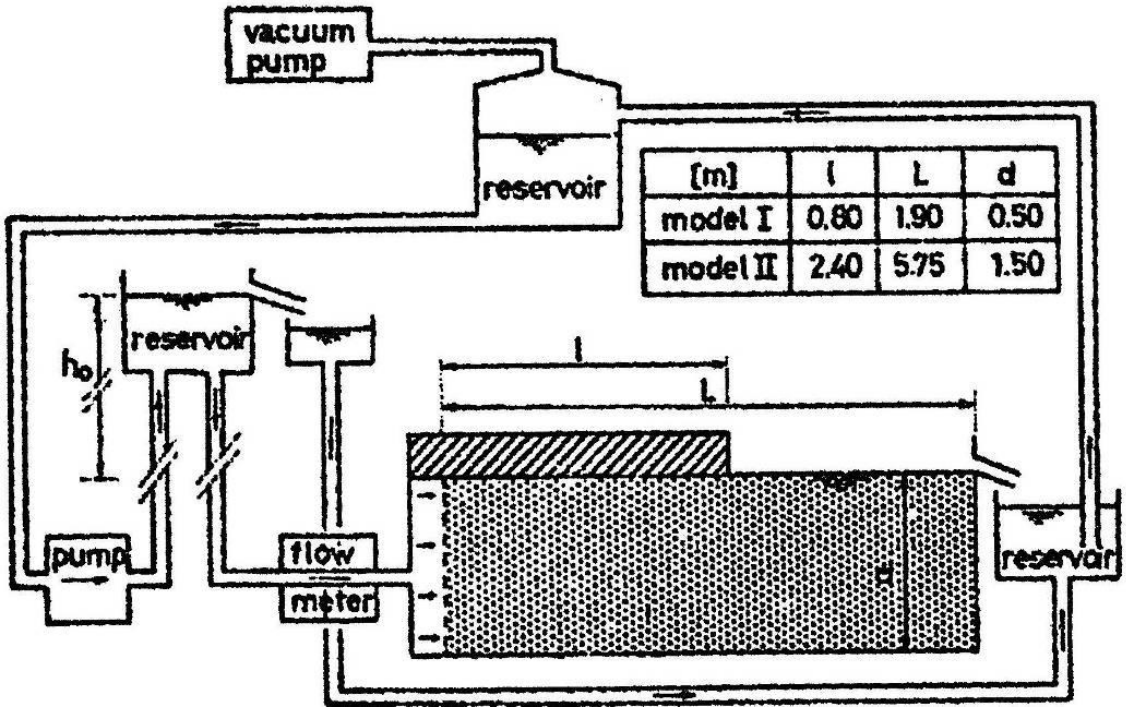

Figure A-1 the test facility that was used by de Wit (de Wit, 1984)

De Wit used several seepage lengths for the tests. Most of the seepage lengths measured 0.80m and 2.40m, although some tests have been done on seepage lengths of 0.40m, 0.70m, 1.20m and 4.50m. Unlike the SBW tests, no correction for the resistance of the filter and the facility itself has been made with respect to the critical head. Some dimensions of the test facility are shown in Figure A-1. As can be seen in the figure, a head difference is applied over a sand body. The head difference is increased until piping begins. For a more detailed description of the used test facility is referred to (de Wit, 1984). Several different sand samples with each its own characteristics were tested. The outcome of the experiments and the relevant sand characteristics are shown in appendix B.

B) Appendix B – The test data from de Wit's experiments

In this appendix, the outcome of the experiments of de Wit and the relevant sand characteristics are shown. As was already mentioned in appendix A, no correction for the resistance of the filter and the facility itself has been made with respect to the critical head. Not all the results of de Wit have been used. Some of the results were considered invalid because of influence of vibrations near or leakages in the test facility. Also, the first six tests were used as orientation tests and are not included in the analysis. The results of de Wit's experiments which were considered valid and were used for the analysis are shown in Table B-1 till Table B-6. The experiments that were considered unsuitable, are shown in Table B-7 and Table B-8. Unfortunately, the temperature was not measured (or reported) in a few cases. A viscosity of $1.002*10^{-6} m^2/s$ (standard value for water if T = 20°C) is used in that case. The data can be found in (de Wit, 1982) and the corresponding factual reports.

The permeability k is calculated with the use of Darcy's law. $Q = kA\frac{dh}{dx}$, the discharge is measured during the experiments. From the permeability, the intrinsic permeability can be calculated by the formula of $\kappa = \frac{k}{g}\nu$. The relative density is calculated by $RD = \frac{n_{max} - n}{n_{max} - n_{min}}$.

Table B-1 the results and sand characteristics of de Wit's experiments for L = 80cm part 1

test number	L [cm]	D [cm]	W [cm]	L/D [-]	sand type	D_{10} [µm]	D_{50} [µm]	D_{60} [µm]	D_{70} [µm]	D_{90} [µm]	C_u [-]
220880-I-1	80	50	50	1.60	dune	140	190	200	220	300	1.43
220880-I-2	80	50	50	1.60	dune	140	190	200	220	300	1.43
220880-I-4	80	50	50	1.60	dune	140	190	200	220	300	1.43
220880-I-5	80	50	50	1.60	dune	140	190	200	220	300	1.43
220880-I-6	80	50	50	1.60	dune	140	190	200	220	300	1.43
220880-I-7	80	50	50	1.60	dune	140	190	200	220	300	1.43
220880-I-8	80	50	50	1.60	dune	140	190	200	220	300	1.43
220880-I-9	80	50	50	1.60	dune	140	190	200	220	300	1.43
220880-II-1	80	50	50	1.60	river	200	420	480	600	1200	2.40
220880-II-2	80	50	50	1.60	river	200	420	480	600	1200	2.40
220880-II-3	80	50	50	1.60	river	200	420	480	600	1200	2.40
220880-II-4	80	50	50	1.60	river	200	420	480	600	1200	2.40
220880-II-5	80	50	50	1.60	river	200	420	480	600	1200	2.40
220880-III-1	80	50	50	1.60	river[*1]	200	380	420	480	680	2.10
220880-III-2	80	50	50	1.60	river[*1]	200	380	420	480	680	2.10
220880-III-3	80	50	50	1.60	river[*1]	200	380	420	480	680	2.10
220880-III-4	80	50	50	1.60	river[*1]	200	380	420	480	680	2.10
220880-III-5	80	50	50	1.60	river[*1]	200	380	420	480	680	2.10
220880-III-6	80	50	50	1.60	river[*1]	200	380	420	480	680	2.10
220880-V-1	80	50	50	1.60	beach	130	190	200	220	300	1.54
220880-V-2	80	50	50	1.60	beach	130	190	200	220	300	1.54
220880-V-3	80	50	50	1.60	beach	130	190	200	220	300	1.54
220880-V-4	80	50	50	1.60	beach	130	190	200	220	300	1.54
220880-V-6	80	50	50	1.60	beach	130	190	200	220	300	1.54
220880-V-7	80	50	50	1.60	beach	130	190	200	220	300	1.54
220880-VII-1	80	50	50	1.60	beach	130	190	200	220	300	1.54
220880-VII-2	80	50	50	1.60	beach	130	190	200	220	300	1.54
220880-VII-3	80	50	50	1.60	beach	130	190	200	220	300	1.54
220883-6-1	80	50	50	1.60	beach	165	200	215	230	310	1.30
220883-6-1	80	50	50	1.60	beach	165	200	215	230	310	1.30
220883-39-1	80	50	50	1.60	dune	140	190	200	220	300	1.43
220883-39-2	80	50	50	1.60	dune	140	190	200	220	300	1.43
220883-39-3	80	50	50	1.60	dune	140	190	200	220	300	1.43
220884-26-1	80	50	50	1.60	coarse	260	770	1000	1390	2900	3.85
220884-26-2	80	50	50	1.60	coarse	260	770	1000	1390	2900	3.85
220884-26-3	80	50	50	1.60	coarse	260	770	1000	1390	2900	3.85
220884-26-4	80	50	50	1.60	coarse	260	770	1000	1390	2900	3.85
220884-26-5	80	50	50	1.60	coarse	260	770	1000	1390	2900	3.85
220885-10-1	80	50	50	1.60	beach	130	190	200	220	300	1.54
220885-10-2	80	50	50	1.60	beach	130	190	200	220	300	1.54
220885-10-3	80	50	50	1.60	beach	130	190	200	220	300	1.54
220885-10-4	80	50	50	1.60	beach	130	190	200	220	300	1.54
220885-10-5	80	50	50	1.60	beach	130	190	200	220	300	1.54
220885-10-6	80	50	50	1.60	beach	130	190	200	220	300	1.54

[*1] the river sand is sieved

Table B-2 the results and sand characteristics of de Wit's experiments for L = 80cm part 2

test number	packing	k_{Darcy} 10^{-3} [m/s]	T (°C)	v 10^{-6} [m^2/s]	κ_{Darcy} 10^{-11} [m^2]	n [%]	n_{min} [%]	n_{max} [%]	RD [%]	KAS [-]	H_c [cm]	H_c/L [-]
220880-I-1	loose	0.091	20.7	0.983	1.749	35.7	34.1	44.9	64.0	50.2	33.0	0.41
220880-I-2	loose	0.087	19.3	1.025	2.240	35.2	34.1	44.9	98.0	50.2	36.4	0.46
220880-I-4	loose	0.126	18.6	1.046	2.030	37.0	34.1	44.9	97.0	50.2	23.9	0.30
220880-I-5	loose	0.142	18.8	1.040	2.690	38.0	34.1	44.9	37.0	50.2	26.9	0.34
220880-I-6	loose	0.128	21.2	0.968	2.547	36.2	34.1	44.9	65.0	50.2	27.2	0.34
220880-I-7	loose	0.187	22.8	0.919	3.381	39.2	34.1	44.9	65.0	50.2	20.1	0.25
220880-I-8	loose	0.233	22.0	0.943	4.904	40.9	34.1	44.9	35.0	50.2	16.6	0.21
220880-I-9	loose	0.203	20.7	0.983	4.831	40.0	34.1	44.9	64.0	50.2	22.2	0.28
220880-II-1	tight	0.288	22.9	0.916	2.952	33.0	31.7	40.0	63.0	56.5	30.2	0.38
220880-II-2	medium	0.288	24.5	0.868	3.233	33.8	31.7	40.0	98.0	56.5	45.0	0.56
220880-II-3	medium	0.406	26.2	0.816	3.279	35.0	31.7	40.0	92.0	56.5	30.0	0.38
220880-II-4	loose	0.520	22.6	0.925	4.084	36.0	31.7	40.0	92.0	56.5	44.5	0.56
220880-II-5	loose	0.496	21.6	0.956	4.097	37.0	31.7	40.0	91.0	56.5	34.0	0.43
220880-III-1	medium	0.289	20.1	1.001	5.590	34.0	31.5	40.4	92.0	56.9	30.0	0.38
220880-III-2	medium	0.304	18.7	1.043	1.407	35.0	31.5	40.4	75.3	56.9	39.2	0.49
220880-III-3	loose	0.315	19.4	1.022	1.603	35.9	31.5	40.4	71.6	56.9	36.4	0.46
220880-III-4	loose	0.384	18.7	1.043	1.625	37.0	31.5	40.4	70.0	56.9	28.4	0.36
220880-III-5	loose	0.400	20.0	1.004	2.013	38.0	31.5	40.4	74.7	56.9	32.2	0.40
220880-III-6	loose	0.533	19.2	1.028	2.479	39.0	31.5	40.4	75.7	56.9	20.2	0.25
220880-V-1	medium	0.141	20.9	0.977	2.679	34.0	33.0	44.7	76.0	55.2	26.6	0.33
220880-V-2	medium	0.160	20.7	0.983	1.398	35.0	33.0	44.7	73.0	55.2	30.3	0.38
220880-V-3	loose	0.163	20.8	0.980	1.616	36.0	33.0	44.7	70.0	55.2	23.4	0.29
220880-V-4	loose	0.211	22.2	0.937	1.951	37.0	33.0	44.7	71.0	55.2	24.4	0.31
220880-V-6	loose	0.230	18.3	1.056	1.448	39.0	33.0	44.7	73.6	55.2	25.0	0.31
220880-V-7	loose	0.259	19.6	1.016	1.316	40.0	33.0	44.7	79.0	55.2	24.4	0.31
220880-VII-1	medium	0.122	15.9	1.128	1.962	33.6	33.0	44.7	71.3	55.2	28.0	0.35
220880-VII-2	medium	0.147	17.6	1.077	1.834	35.0	33.0	44.7	69.3	55.2	24.1	0.30
220880-VII-3	loose	0.187	19.3	1.025	1.769	37.0	33.0	44.7	75.0	55.2	24.1	0.30
220883-6-1	loose	0.142		1.002	16.541	35.5	33.0	44.7	70.0	55.2	18.1	0.20
220883-6-1	loose	0.129		1.002	11.349	35.5	33.0	44.7	73.0	55.2	21.6	0.24
220883-39-1	loose	0.181	18.0	1.065	9.372	39.0	34.1	44.9	63.3	50.2	23.7	0.30
220883-39-2	loose	0.179	20.0	1.004	13.156	39.0	34.1	44.9	75.2	50.2	19.5	0.24
220883-39-3	loose	0.158	16.9	1.098	8.212	39.0	34.1	44.9	75.2	50.2	21.4	0.27
220884-26-1	loose	1.616	20.0	1.004	1.487	36.9	23.5	40.0	85.0	57.7	39.4	0.49
220884-26-2	medium	1.111		1.002	0.992	34.4	23.5	40.0	85.0	57.7	39.1	0.49
220884-26-3	tight	0.889	19.0	1.034	1.293	32.0	23.5	40.0	53.0	57.7	78.3	0.98
220884-26-4	loose	1.123	15.2	1.149	0.732	37.0	23.5	40.0	53.0	57.7	79.2	0.99
220884-26-5	medium	0.800	19.9	1.007	1.532	34.5	23.5	40.0	43.0	57.7	66.0	0.83
220885-10-1	loose	0.155	22.0	0.943	0.980	39.0	33.0	44.7	64.0	55.2	20.4	0.26
220885-10-2	medium	0.097	20.1	1.001	1.749	35.0	33.0	44.7	98.0	55.2	20.6	0.26
220885-10-3	loose	0.127	20.2	0.998	2.240	39.0	33.0	44.7	97.0	55.2	14.4	0.18
220885-10-4	medium	0.072	20.3	0.995	2.030	35.0	33.0	44.7	37.0	55.2	22.7	0.28
220885-10-5	loose	0.155	21.1	0.971	2.690	39.0	33.0	44.7	65.0	55.2	15.0	0.19
220885-10-6	medium	0.100	21.4	0.962	2.547	35.0	33.0	44.7	65.0	55.2	26.7	0.33

Table B-3 the results and sand characteristics of de Wit's experiments for L = 240cm part 1

test Number	L [cm]	D [cm]	W [cm]	L/D [-]	sand type	D_{10} [µm]	D_{50} [µm]	D_{60} [µm]	D_{70} [µm]	D_{90} [µm]	C_u [-]
220880-IV-1	240	150	50	1.60	dune	140	190	200	220	300	1.43
220880-IV-2	240	150	50	1.60	dune	140	190	200	220	300	1.43
220880-IV-3	240	150	50	1.60	dune	140	190	200	220	300	1.43
220880-VI-1	240	150	50	1.60	beach	130	190	200	220	300	1.54
220880-VI-2	240	150	50	1.60	beach	130	190	200	220	300	1.54
220880-VI-3	240	150	50	1.60	beach	130	190	200	220	300	1.54
220880-VI-4	240	150	50	1.60	beach	130	190	200	220	300	1.54
220880-VI-5	240	150	50	1.60	beach	130	190	200	220	300	1.54
220880-VI-6	240	150	50	1.60	beach	130	190	200	220	300	1.54
220880-VI-7	240	150	50	1.60	beach	130	190	200	220	300	1.54
220883-4-1	240	150	50	1.60	beach	130	190	200	220	300	1.54
220883-4-1	240	150	50	1.60	beach	130	190	200	220	300	1.54
220883-35-1	240	150	50	1.60	coarse	260	770	1000	1390	2900	3.85
220883-35-2	240	150	50	1.60	coarse	260	770	1000	1390	2900	3.85
220883-35-3	240	150	50	1.60	coarse	260	770	1000	1390	2900	3.85
220883-35-4	240	150	50	1.60	coarse	260	770	1000	1390	2900	3.85
220883-35-5	240	150	50	1.60	coarse	260	770	1000	1390	2900	3.85
220883-35-6	240	150	50	1.60	coarse	260	770	1000	1390	2900	3.85
220883-35-7	240	150	50	1.60	coarse	260	770	1000	1390	2900	3.85
220883-35-8	240	150	50	1.60	coarse	260	770	1000	1390	2900	3.85
220883-35-8	240	150	50	1.60	coarse	260	770	1000	1390	2900	3.85
220885-10-6	245	150	50	1.63	beach	130	190	200	220	300	1.54
220885-10-6	245	150	50	1.63	beach	130	190	200	220	300	1.54
220885-10-6	245	150	50	1.63	beach	130	190	200	220	300	1.54

Table B-4 the results and sand characteristics of de Wit's experiments for L = 240cm part 2

Test number	packing	k_{Darcy} 10^{-3} [m/s]	T (°C)	v 10^{-6} m^2/s	κ_{Darcy} 10^{-11} $[m^2]$	n [%]	n_{min} [%]	n_{max} [%]	RD [%]	KAS [-]	H_c [cm]	H_c/L [-]
220880-IV-1	tight	0.112	15.0	1.156	1.319	35.0	34.1	44.9	91.7	50.2	83.8	0.35
220880-IV-2	tight	0.140	22.6	0.925	1.325	36.0	34.1	44.9	82.4	50.2	37.4	0.16
220880-IV-3	tight	0.161	21.3	0.965	1.586	37.0	34.1	44.9	73.2	50.2	40.9	0.17
220880-VI-1	tight	0.156	23.9	0.886	1.411	34.4	33.0	44.7	88.0	55.2	41.5	0.17
220880-VI-2	tight	0.132	24.4	0.871	1.169	35.0	33.0	44.7	82.9	55.2	35.2	0.15
220880-VI-3	tight	0.197	23.8	0.889	1.788	36.8	33.0	44.7	67.5	55.2	41.4	0.17
220880-VI-4	tight	0.181	20.0	1.004	1.856	37.0	33.0	44.7	65.8	55.2	44.4	0.19
220880-VI-5	tight	0.229	20.4	0.992	2.319	38.0	33.0	44.7	57.3	55.2	36.0	0.15
220880-VI-6	medium	0.242	18.1	1.062	2.620	39.0	33.0	44.7	48.7	55.2	38.1	0.16
220880-VI-7	medium	0.283	18.0	1.065	3.068	40.0	33.0	44.7	40.2	55.2	28.5	0.12
220883-4-1	tight	0.065		1.002	0.661	36.0	33.0	44.7	74.4	55.2	47.0	0.20
220883-4-1	tight	0.076		1.002	0.772	36.0	33.0	44.7	74.4	55.2	45.6	0.19
220883-35-1	loose	1.796	19.0	1.034	18.941	37.0	23.5	40.0	18.2	57.7	88.0	0.37
220883-35-2	loose	1.768	16.0	1.125	20.284	36.7	23.5	40.0	20.0	57.7	96.0	0.40
220883-35-3	loose	1.634	16.0	1.125	18.740	36.6	23.5	40.0	20.6	57.7	80.0	0.33
220883-35-4	medium	1.087	17.1	1.092	12.102	34.3	23.5	40.0	34.6	57.7	68.0	0.28
220883-35-5	medium	1.085	16.7	1.104	12.213	34.3	23.5	40.0	34.6	57.7	71.4	0.30
220883-35-6	medium	1.013	16.1	1.122	11.582	34.1	23.5	40.0	35.8	57.7	88.5	0.37
220883-35-7	medium	0.830	18.2	1.059	8.953	32.0	23.5	40.0	48.5	57.7	62.6	0.26
220883-35-8	medium	0.763	16.7	1.104	8.592	32.0	23.5	40.0	48.5	57.7	104.0	0.43
220883-35-8	medium	0.773	16.4	1.113	8.765	32.0	23.5	40.0	48.5	57.7	94.0	0.39
220885-10-6	tight	0.096	18.9	1.037	1.013	35.0	33.0	44.7	82.9	55.2	39.7	0.16
220885-10-6	tight	0.093	17.5	1.080	1.028	35.0	33.0	44.7	82.9	55.2	39.2	0.16
220885-10-6	tight	0.091	17.1	1.092	1.010	35.0	33.0	44.7	82.9	55.2	33.2	0.14

Table B-5 the results and sand characteristics of de Wit's experiments for L = 450cm part 1

test number	L [cm]	D [cm]	W [cm]	L/D [-]	sand type	D_{10} [µm]	D_{50} [µm]	D_{60} [µm]	D_{70} [µm]	D_{90} [µm]	C_u [-]
220881-40-1	450	150	50	3	beach	130	190	200	220	300	1.54
220881-40-2	450	150	50	3	beach	130	190	200	220	300	1.54
220881-40-3	450	150	50	3	beach	130	190	200	220	300	1.54
220883-4-1	450	150	50	3	beach	130	190	200	220	300	1.54
220883-4-1	450	150	50	3	beach	130	190	200	220	300	1.54

Table B-6 the results and sand characteristics of de Wit's experiments for L = 450cm part 2

test number	packing	k_{Darcy} 10^{-3} [m/s]	T (°C)	v 10^{-6} m^2/s	κ_{Darcy} 10^{-11} $[m^2]$	n [%]	n_{min} [%]	n_{max} [%]	RD [%]	KAS [-]	H_c [cm]	H_c/L [-]
220881-40-1	tight	0.195		1.002	1.996	36.0	33.0	44.7	74.4	55.2	80.9	0.18
220881-40-2	tight	0.187		1.002	1.905	36.0	33.0	44.7	74.4	55.2	71.5	0.16
220881-40-3	tight	0.190		1.002	1.939	36.0	33.0	44.7	74.4	55.2	62.4	0.14
220883-4-1	tight	0.126		1.002	1.289	36.0	33.0	44.7	74.4	55.2	86.2	0.19
220883-4-1	tight	0.111		1.002	1.136	36.0	33.0	44.7	74.4	55.2	78.0	0.17

Table B-7 the results and sand characteristics of de Wit's experiments which are not used part 1

test number	reason not used[*1]	L [cm]	D [cm]	W [cm]	L/D [-]	sand type	D_{10} [µm]	D_{50} [µm]	D_{60} [µm]	D_{70} [µm]	D_{90} [µm]	C_u [-]
220880-6-1	or. test, leakage	40	50.8	49.9	0.79	dune	140	190	200	220	300	1.43
220880-6-2	or. test, unknown compaction sand	40	50.8	49.9	0.79	dune	140	190	200	220	300	1.43
220880-6-3	or. test, piping did not occur	40	50.8	49.9	0.79	dune	140	190	200	220	300	1.43
220880-6-4	or. test, piping did not occur	40	50.8	49.9	0.79	dune	140	190	200	220	300	1.43
220880-43-1	or. test, unknown compaction sand	70	50.0	50.0	1.40	dune	140	190	200	220	300	1.43
220880-43-2	or. test, unknown compaction sand	70	50.0	50.0	1.40	dune	140	190	200	220	300	1.43
220880-I-3	vibrations	80	50.0	50.0	1.60	dune	140	190	200	220	300	1.43
220880-II-6	vibrations	80	50.0	50.0	1.60	river	200	420	480	600	1200	2.40
220880-V-5	leakage	80	50.0	50.0	1.60	beach	130	190	200	220	300	1.54
220884-26-6	critical head not recorded	80	50.0	50.0	1.60	coarse	260	770	1000	1390	2900	3.85

[*1] *or. test means the experiment was an orientating test*

Table B-8 the results and sand characteristics of de Wit's experiments which are not used part 2

test number	packing	k_{Darcy} 10^{-3} [m/s]	T (°C)	v 10^{-6} m^2/s	κ_{Darcy} 10^{-11} $[m^2]$	n [%]	n_{min} [%]	n_{max} [%]	RD [-]	KAS [-]	H_c [cm]	H_c/L [-]
220880-6-1	loose	0.274[*1]		1.002	2.800[*1]	42.0	34.1	44.9	26.9	50.2	13.0	0.325
220880-6-2	tight	0.103		1.002	1.050	37.5	34.1	44.9	68.5	50.2	16.5	0.413
220880-6-3	tight	0.178[*1]		1.002	1.815[*1]	37.0	34.1	44.9	73.2	50.2	>0.41	>0.010
220880-6-4	tight	0.178[*1]		1.002	1.815[*1]	37.0	34.1	44.9	73.2	50.2	>0.42	>0.011
220880-43-1	tight	0.105		1.002	1.076	37.6	34.1	44.9	67.6	50.2	29.0	0.414
220880-43-2	tight	0.124		1.002	1.263	37.6	34.1	44.9	67.6	50.2	31.5	0.450
220880-I-3	tight	0.083	19.7	1.013	0.855	35.3	34.1	44.9	88.9	50.2	33.1	0.414
220880-II-6	loose	0.611	21.2	0.967	6.022	38.0	31.7	40.0	24.1	56.5	22.5	0.281
220880-V-5	tight	0.198	20.3	0.995	2.007	38.0	33.0	44.7	57.3	55.2	20.8	0.260
220884-26-6	medium	0.561	18.9	1.037	5.936	32.0	23.5	40.0	48.5	57.7	[*2]	[*2]

[*1] The discharge Q was not recorded, so k_{Darcy} and κ_{Darcy} could not be calculated, k_{Beyer} and κ_{Beyer} are used instead

[*2] The critical head was not measured or recorded

C) Appendix C – The small-scale test facility used for SBW by Deltares

Deltares has done extensive research on piping in the framework of SBW. The experiments were conducted between 2008 and 2010 in the laboratory at Deltares. Small-scale, medium-scale and full-scale tests have been done (the full-scale experiments were not performed at Deltares, but at Booneschans, see appendix E). In this appendix the small-scale test facility that has been used is described. In appendix D and E the medium-scale and full-scale test facility's are described. In Appendix F the outcome of the experiments of SBW are shown. In Figure C-1 till Figure C-4 (part of) the small-scale test facility is shown. The part of the test facility where the sand is placed in, is called "the box". The figures in this appendix were obtained via (Knoeff, 2008). A more detailed description of the small-scale test facility can also be found there. The inner dimensions of the test facility are approximately l = 50cm, b = 30cm and h = 10cm. The top of the box is made out of polymethyl methacrylate (trade name Plexiglas) so that this part is transparent. The cover of the box has a layer of putty (silicone material) on the inside to give the surface some roughness, so that the piping mechanism is not influenced by a smooth surface, which is also not present in reality under a real dike. For the same reason, at the sides of the test facility sandpaper is used. The test facility must be filled with sand from the side, so that the test facility is turned 90° during the filling procedure.

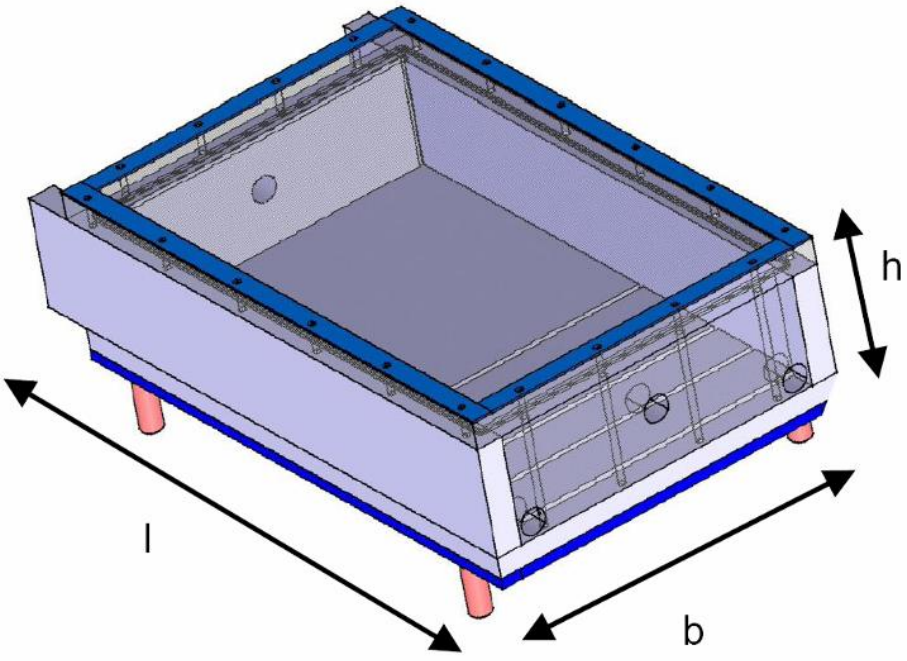

Figure C-1 a 3D illustration of the small-scale box (Knoeff, 2008)

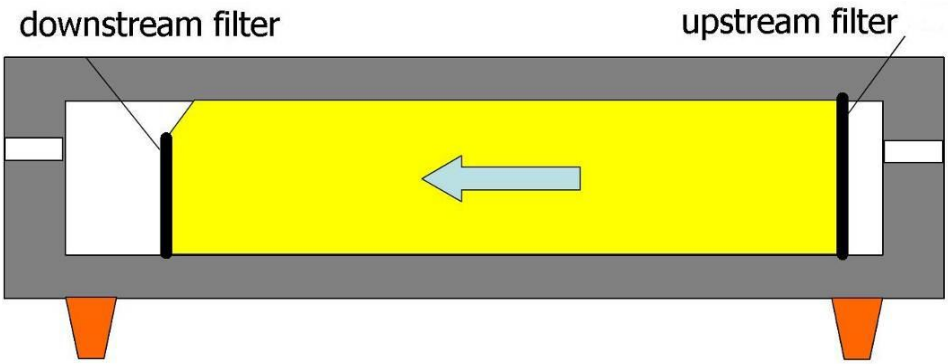

Figure C-2 a cross-section of the small-scale box (Knoeff, 2008)

As can be seen in Figure C-2, an upstream filter and a downstream filter is used. The resistance of the filters and the test facility is dependent on the discharge. This resistance has been measured and the critical heads are corrected for this. The seepage length of the sand in the small-scale box is usually between 34 and 36cm.

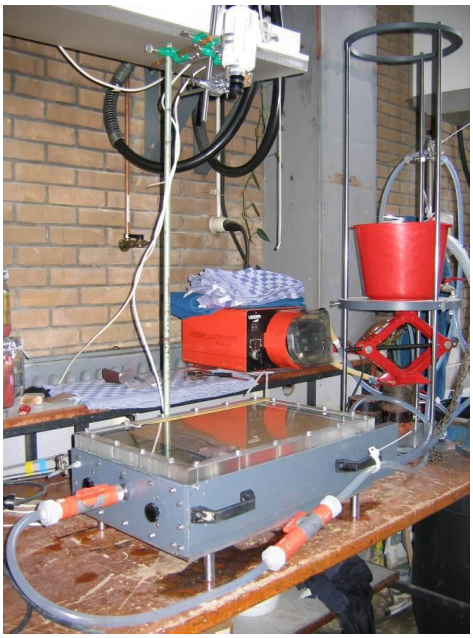

The small-scale box with the sand is shown on the bottom of the figure. The red bucket is used for applying a head difference on the box. The orange pump makes sure the bucket is always filled completely. Above the box, a camera is placed to make pictures during the experiments. The box, bucket and pump are all connected with hoses. The head difference can be adjusted by lowering the exit hose.

Figure C-3 an overview of the small-scale test facility, which includes the box, the bucket, the camera and the pump (Knoeff, 2008)

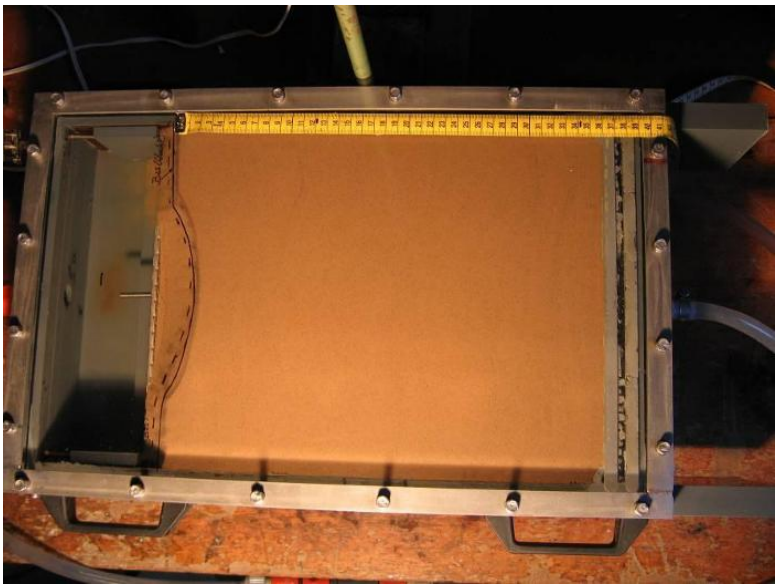

Figure C-4 a top view of the box filled with sand (Knoeff, 2008)

For a standard dike configuration, the constant in the geometry factor is 0.91. According to MSEEP calculations, the value used for this constant for the small-scale test facility should be 0.867.

D) Appendix D – The medium-scale test facility used for SBW by Deltares

In this appendix, the medium-scale test facility is described. In Appendix F the outcome of the experiments of SBW are shown. In Figure D-1 till Figure D-4 the medium-scale test facility is shown. The figures in this appendix were obtained via (Rietdijk, 2009) and (van Beek, 2009b). More detailed information about the medium-scale test facility can be found in these reports. The sand sample in the box has the following dimensions. The length of sand sample is 1.5m, the width is 0.88m and the depth is 0.4m. The box can be rotated 90° as can be seen in Figure D-2 and Figure D-4, so that the box can be filled with sand when standing upright. The cover of the box is made out of a plate of acrylate. Under this plate, another plate with pressure sensors is placed. As with the small-scale test facility, putty is used on the inside of the cover and sandpaper is used at the inner side of the box to increase the surface roughness. Above the test facility, two camera's are placed. During the experiments, the pressure is measured with pressure meters and also the temperature and discharge through the system is measured. As with the small-scale test facility, no effective stresses can be applied with the medium-scale test facility. The inflow and outflow of water is according the same procedure as with the small-scale test facility. A pump fills the input barrel and due to a head difference between input and output barrel, a flow through the sand in the test facility is present.


Figure D-1 a top view of the medium-scale test facility (Rietdijk, 2009)

Figure D-2 a side view of the medium-scale test facility, where the box is turned 90° (Rietdijk, 2009)

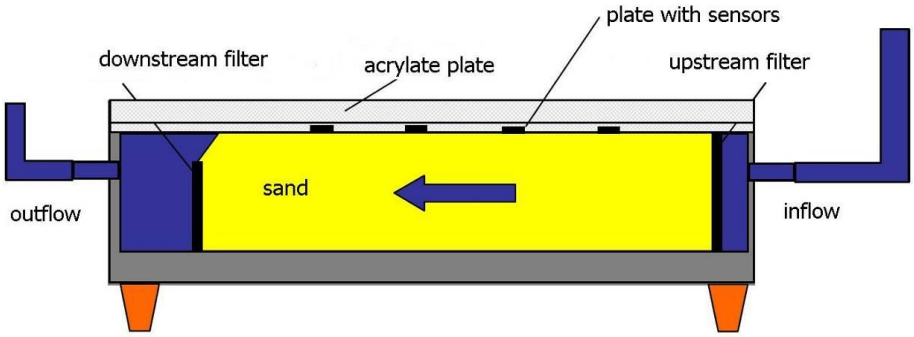

Figure D-3 a cross-section of the medium-scale box (van Beek, 2009b)

As can be seen in Figure D-3, an upstream filter and a downstream filter is used. The resistance of the filters and the test facility is dependent on the discharge. This resistance has been measured and the critical heads are corrected for this.

Figure D-4 a schematic overview of the medium-scale test facility (van Beek, 2009b)

E) Appendix E – The full-scale test facility (IJkdijk) used for SBW by Deltares

Near the city Booneschans, in the north-east of the Netherlands, a full-scale test facility has been constructed. This full-scale test facility is called de IJkdijk. De IJkdijk is treated in this appendix. Another full-scale test facility is de Deltagoot, which is treated in appendix G. Several failure mechanisms were tested at the site of de IJkdijk. One of the failure mechanisms was piping. In total four experiments with piping were carried out. Besides the need for research of the piping mechanisms itself, also a lot of measuring devices which were deployed during the experiments were tested out during the experiments and evaluated afterwards. In Figure E-1 a cross-section of de IJkdijk is shown. More detailed information can be found in (van Beek, 2010a).

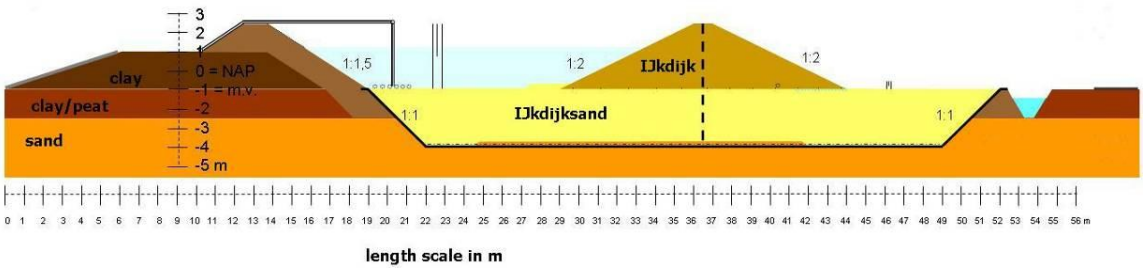

Figure E-1 a cross-section of de IJkdijk (van Beek, 2010a)

In Figure E-2 a top view of the location of de IJkdijk is shown.

Two of the four tests that were conducted were done on fine sand, the other two on coarse sand. Two tests were done explicitly for research in the framework of SBW. The two other tests were conducted to test the measuring equipment. In one of the two tests which was conducted to test the measuring equipment, it was found the equipment did not influence the result much. This experiment can also be used for SBW. The other test which was conducted to test the measuring equipment, influenced the outcome in such an extent, the outcome can not be used for SBW. In Table E-1 a summary of the three used full-scale experiments is shown. In appendix F more detailed information about the sand characteristics can be found.

Figure E-2 a top view of the location of de IJkdijk (Koelewijn, 2010)

Table E-1 a summary of the three used full-scale experiments (van Beek, 2010a)

test number	sand type	thickness sand layer [m]	seepage length [m]	width [m]	k_{Darcy} 10^{-3} [m/s]	RD [%]
IJkdijk test1	fine	3.00	15	17	0.078	60
IJkdijk test2	coarse	2.85	15	19	0.135	75
IJkdijk test3	fine	3.00	15	17	0.080	60

In Figure E-3 and Figure E-4 the construction of the sand layer and the clay dike of de IJkdijk is shown.

Figure E-3 the construction of the sand layer in de IJkdijk (de Bruijn, 2009)

Figure E-4 the construction of the clay dike in de IJkdijk (de Bruijn, 2009)

In Figure E-5 a sand boil at de IJkdijk is shown. In Figure E-6 the failure of de IJkdijk because of piping is shown.

Figure E-5 a sand boil at de IJkdijk (de Bruijn, 2009)

Figure E-6 failure of de IJkdijk because of piping (de Bruijn, 2009)

F) Appendix F – The test data from SBW's experiments

In this appendix, the outcome of the experiments of SBW and the relevant sand characteristics are shown. As was already mentioned in appendix C, a correction for the resistance of the filter and the facility itself has been made with respect to the critical head for the small-scale and medium-scale experiments. Not all the results of SBW have been used for data analysis. In total 48 small-scale experiments were done. Seven experiments were done on samples with a relative density lower than 35%, resulting in so called forward erosion. This erosion mechanism is not the classic backward erosion mechanism described by Sellmeijer's model and forward erosion falls outside the scope of this thesis. The forward erosion process was explained later by van Beek. Forward erosion takes place in the test facility because of the absence of effective stresses (van Beek, 2010b). Eight medium-scale experiments were done, and one experiment was excluded from the analysis because of a pump failure. Four full-scale experiments were performed, and one experiment was excluded from the analysis because of a very strong influence of the measurement equipment. The formulas used are the same as in appendix B. Unfortunately, the temperature was not measured. A viscosity of $1.002*10^{-6}$ m^2/s (standard value for water if T = 20°C) is used. The data can be found in the corresponding factual reports (van Beek, 2008a).

Table F-1 the results and sand characteristics of SBW's small-scale experiments part 1

test number	L [cm]	D [cm]	W [cm]	L/D [-]	sand type	D_{10} [µm]	D_{20} [µm]	D_{30} [µm]	D_{40} [µm]	D_{50} [µm]
B19	34.0	9.95	29.9	3.42	Baskarp	92	103	113	123	132
B23	33.8	9.95	29.9	3.40	Baskarp	92	103	113	123	132
B24	33.8	9.95	29.9	3.40	Baskarp	92	103	113	123	132
B28	33.5	9.95	29.9	3.37	Baskarp	92	103	113	123	132
D31	33.2	9.95	29.9	3.34	dekzand	64	95	118	133	148
D32	33.2	9.95	29.9	3.34	dekzand	64	95	118	133	148
D33	33.2	9.95	29.9	3.34	dekzand	64	95	118	133	148
B35	33.5	9.95	29.9	3.37	Baskarp	92	103	113	123	132
B36	33.4	9.95	29.9	3.36	Baskarp	92	103	113	123	132
D37	33.4	9.95	29.9	3.36	dekzand	64	95	118	133	148
D38	33.5	9.95	29.9	3.37	dekzand	64	95	118	133	148
D39	33.1	9.95	29.9	3.33	dekzand	64	95	118	133	148
B40	33.2	9.95	29.9	3.34	Baskarp	92	103	113	123	132
B41	33.4	9.95	29.9	3.36	Baskarp	92	103	113	123	132
O43	33.2	9.95	29.9	3.34	oostelijke rivierenzand	127	156	184	212	233
I45	33.2	9.95	29.9	3.34	Boxtel Ringstraat Itterbecke	80	108	126	139	155
I46	33.7	9.95	29.9	3.39	Boxtel Ringstraat Itterbecke	80	108	126	139	155
I47	34.0	9.95	29.9	3.42	Enschede Ringstraat Itterbecke	261	296	325	355	380
I48	34.0	9.95	29.9	3.42	Enschede Ringstraat Itterbecke	261	296	325	355	380
I49	34.0	9.95	29.9	3.42	Hoherstall Waalre	236	272	293	316	341
I50	33.2	9.95	29.9	3.34	Hoherstall Waalre	236	272	293	316	341
I51	33.5	9.95	29.9	3.37	ringstrasse Itterbecke Sandr	125	137	148	160	171
I52	33.1	9.95	29.9	3.33	Hoherstall Waalre	236	272	293	316	341
I53	32.5	9.95	29.9	3.27	Sandr	125	137	148	160	171
B54	33.0	9.95	29.9	3.32	Baskarp	92	103	113	123	132
B55	32.5	9.95	29.9	3.27	Baskarp	92	103	113	123	132
I56	33.5	9.95	29.9	3.37	Schemda Itterbecke	126	135	141	148	157
B57	33.0	9.95	29.9	3.32	Baskarp	92	103	113	123	132
B58	34.5	9.95	29.9	3.47	Baskarp	92	103	113	123	132
B61	34.5	9.95	29.9	3.47	Baskarp	92	103	113	123	132
I62	32.5	9.95	29.9	3.27	Schemda Itterbecke	126	135	141	148	157
S63	34.0	9.95	29.9	3.42	Sterksel	99	135	162	186	200
S64	33.5	9.95	29.9	3.37	Sterksel	99	135	162	186	200
B82	33.6	9.95	29.9	3.38	Baskarp	92	103	113	123	132
B83	33.4	9.95	29.9	3.36	Baskarp	92	103	113	123	132
B84	33.4	9.95	29.9	3.36	Baskarp	92	103	113	123	132
B85	33.6	9.95	29.9	3.38	Baskarp	92	103	113	123	132
B86	33.6	9.95	29.9	3.38	Baskarp	92	103	113	123	132

Table F-2 the results and sand characteristics of SBW's small-scale experiments part 2

test number	D_{60} [µm]	D_{70} [µm]	C_u [-]	packing	k_{Darcy} 10^{-3} [m/s]	v 10^{-6} [m^2/s]	κ_{Darcy} 10^{-11} [m^2]	n_{min} [%]	n_{max} [%]	RD [%]	KAS [-]	H_c [cm]	H_c/L [-]
B19	142	154	1.54	tight	0.092	1.002	0.937	34.6	45.8	64.0	50	12.15	0.357
B23	142	154	1.54	tight	0.041	1.002	0.416	34.6	45.8	98.0	50	20.10	0.595
B24	142	154	1.54	tight	0.046	1.002	0.471	34.6	45.8	97.0	50	17.96	0.531
B28	142	154	1.54	medium	0.142	1.002	1.446	34.6	45.8	37.0	50	7.43	0.222
D31	168	192	2.63	tight	0.051	1.002	0.524	28.4	42.8	65.0	54	19.00	0.572
D32	168	192	2.63	tight	0.066	1.002	0.675	28.4	42.8	65.0	54	14.90	0.449
D33	168	192	2.63	medium	0.114	1.002	1.164	28.4	42.8	35.0	54	9.20	0.279
B35	142	154	1.54	tight	0.075	1.002	0.770	34.6	45.8	64.0	50	14.70	0.439
B36	142	154	1.54	tight	0.070	1.002	0.719	34.6	45.8	63.0	50	14.76	0.442
D37	168	192	2.63	tight	0.027	1.002	0.272	28.4	42.8	98.0	54	27.98	0.848
D38	168	192	2.63	tight	0.040	1.002	0.404	28.4	42.8	92.0	54	17.99	0.537
D39	168	192	2.63	tight	0.037	1.002	0.374	28.4	42.8	92.0	54	14.99	0.453
B40	142	154	1.54	tight	0.036	1.002	0.371	34.6	45.8	91.0	50	14.92	0.449
B41	142	154	1.54	tight	0.049	1.002	0.498	34.6	45.8	92.0	50	16.07	0.481
O43	262	307	2.06	tight	0.187	1.002	1.910	32.2	42.3	75.3	51	12.56	0.378
I45	180	202	2.25	tight	0.057	1.002	0.584	32.3	46.1	71.6	45	21.64	0.652
I46	180	202	2.25	tight	0.068	1.002	0.695	32.3	46.1	70.0	45	16.70	0.496
I47	408	431	1.56	tight	0.258	1.002	2.635	32.01	41.06	74.7	69	12.70	0.374
I48	408	431	1.56	tight	0.310	1.002	3.166	32.01	41.06	75.7	69	12.60	0.371
I49	372	400	1.58	tight	0.270	1.002	2.758	35.03	45.0	76.0	46	10.09	0.297
I50	372	400	1.58	tight	0.372	1.002	3.800	35.03	45.0	73.0	46	10.29	0.310
I51	184	195	1.47	tight	0.099	1.002	1.006	33.13	44.1	70.0	52	12.62	0.377
I52	372	400	1.58	tight	0.250	1.002	2.554	35.03	45.0	710.	46	13.06	0.395
I53	184	195	1.47	tight	0.071	1.002	0.725	33.13	44.1	73.6	52	13.76	0.423
B54	142	154	1.54	tight	0.049	1.002	0.499	34.6	45.8	79.0	50	18.97	0.575
B55	142	154	1.54	tight	0.056	1.002	0.576	34.6	45.8	71.3	50	15.03	0.462
I56	166	175	1.32	tight	0.082	1.002	0.836	37.2	47.3	69.3	38	10.97	0.327
B57	142	154	1.54	tight	0.057	1.002	0.581	34.6	45.8	75.0	50	14.13	0.428
B58	142	154	1.54	tight	0.068	1.002	0.693	34.6	45.8	70.0	50	12.00	0.348
B61	142	154	1.54	tight	0.061	1.002	0.624	34.6	45.8	73.0	50	12.19	0.353
I62	166	175	1.32	tight	0.112	1.002	1.144	37.2	47.3	63.3	38	11.45	0.352
S63	218	232	2.20	tight	0.132	1.002	1.348	37.9	50.4	75.2	35	14.95	0.440
S64	218	232	2.20	tight	0.099	1.002	1.008	37.9	50.4	75.2	35	13.47	0.402
B82	142	154	1.54	tight	0.052	1.002	0.534	34.6	45.8	85.0	50	13.88	0.413
B83	142	154	1.54	tight	0.052	1.002	0.533	34.6	45.8	85.0	50	13.85	0.415
B84	142	154	1.54	tight	0.085	1.002	0.867	34.6	45.8	53.0	50	9.82	0.294
B85	142	154	1.54	tight	0.068	1.002	0.691	34.6	45.8	53.0	50	11.78	0.351
B86	142	154	1.54	medium	0.089	1.002	0.913	34.6	45.8	43.0	50	9.79	0.291

Table F-3 the results and sand characteristics of SBW's medium-scale experiments part 1

test number	L [cm]	D [cm]	W [cm]	L/D [-]	sand type	D_{10} [µm]	D_{20} [µm]	D_{30} [µm]	D_{40} [µm]	D_{50} [µm]	D_{60} [µm]	D_{70} [µm]	C_u [-]
Bms1	137.0	40	100	3.43	Baskarp	92	103	113	123	132	142	154	1.54
Bms2	145.0	40	100	3.63	Baskarp	92	103	113	123	132	142	154	1.54
Ims3	145.5	40	100	3.64	Itterbeck	130	140	150	160	170	190	210	1.46
Ims4	145.5	40	100	3.64	Itterbeck	130	140	150	160	170	190	210	1.46
Ims5	141.5	40	100	3.54	Itterbeck	130	140	150	160	170	190	210	1.46
Bms7[*1]	130.0	40	100	3.25	Baskarp	92	103	113	123	132	142	154	1.54
Bms8[*1]	133.0	40	100	3.33	Baskarp	92	103	113	123	132	142	154	1.54

[*1] *Bms7 and Bms8 are mistakenly in some SBW reports called Ims7 and Ims8*

Table F-4 the results and sand characteristics of SBW's medium-scale experiments part 2

test number	packing	k_{Darcy} 10^{-3} [m/s]	v 10^{-6} [m^2/s]	κ_{Darcy} 10^{-11} [m^2]	n_{min} [%]	n_{max} [%]	RD [%]	KAS [-]	H_c [cm]	H_c/L [-]
Bms1	medium	0.115	1.002	1.173	34.6	45.8	60	50	28	0.204
Bms2	tight	0.137	1.002	1.398	34.6	45.8	50	50	37	0.255
Ims3	tight	0.188	1.002	1.921	33.13	44.1	64	52	26	0.179
Ims4	tight	0.344	1.002	3.517	33.13	44.1	51	52	20	0.137
Ims5	tight	0.210	1.002	2.143	33.13	44.1	75	52	29	0.205
Bms7	tight	0.137	1.002	1.402	34.6	45.8	64	50	29	0.223
Bms8	tight	0.237	1.002	1.421	34.6	45.8	50	50	19	0.143

Table F-5 the results and sand characteristics of SBW's full-scale experiments part 1

test number	L [cm]	D [cm]	W [cm]	L/D [-]	sand type	D_{70} [µm]	C_u [-]	packing
IJkdijk test1	1500	300	1700	5.00	fine IJkdijk sand	180	1.60	tight
IJkdijk test2	1500	285	1900	5.26	coarse IJkdijk sand	260	1.80	tight
IJkdijk test3	1500	300	1700	5.00	fine IJkdijk sand	180	1.60	tight

Table F-6 the results and sand characteristics of SBW's full-scale experiments part 2

test number	k_{Darcy} 10^{-3} [m/s]	T (°C)	v 10^{-6} [m^2/s]	κ_{Darcy} 10^{-11} [m^2]	RD [%]	H_c [cm]	H_c/L [-]
IJkdijk test1	0.078	10.0	1.307	1.039	60	230	0.153
IJkdijk test2	0.135	10.0	1.307	1.799	75	175	0.117
IJkdijk test3	0.080	10.0	1.307	1.066	60	210	0.140

Table F-7 the results and sand characteristics of SBW's experiments which are not used part 1

test number	reason not used	L [cm]	D [cm]	W [cm]	L/D [-]	sand type	D_{10} [µm]	D_{20} [µm]	D_{30} [µm]	D_{40} [µm]	D_{50} [µm]
B22	forward erosion	34.0	9.95	29.9	3.417	Baskarp	92	103	113	123	132
B25	forward erosion	33.8	9.95	29.9	3.397	Baskarp	92	103	113	123	132
B26	forward erosion	33.8	9.95	29.9	3.397	Baskarp	92	103	113	123	132
B27	forward erosion	33.4	9.95	29.9	3.357	Baskarp	92	103	113	123	132
B29	forward erosion	33.5	9.95	29.9	3.367	Baskarp	92	103	113	123	132
B30	forward erosion	33.0	9.95	29.9	3.317	Baskarp	92	103	113	123	132
D34	forward erosion	33.2	9.95	29.9	3.337	dekzand	64	95	118	133	148
O42	very high permeability	33.2	9.95	29.9	3.337	oostelijke rivierenzand	127	156	184	212	233
O44	very high permeability	33.0	9.95	29.9	3.317	oostelijke rivierenzand	127	156	184	212	233
B87	performed later	33.6	9.95	29.9	3.377	Baskarp	92	103	113	123	132
Ims6	very high permeability. pump failure	146.5	40.00	100.0	3.663	Itterbeck	130	140	150	160	170
proef4	test data may be unreliable because of strong influence of sensors	1500	285	1900	5.263	coarse IJkdijk sand					199

Table F-8 the results and sand characteristics of SBW's experiments which are not used part 2

test number	D_{60} [µm]	D_{70} [µm]	C_u [-]	packing	k_{Darcy} 10^{-3} [m/s]	v 10^{-6} [m^2/s]	κ_{Darcy} 10^{-11} [m^2]	n_{min} [%]	n_{max} [%]	RD [%]	KAS [-]	H_c [cm]	H_c/L [-]
B22	142	154	1.54	tight	0.091	1.002	0.928	34.6	45.8	67.0	50	13.26	0.390
B25	142	154	1.54	medium	0.207	1.002	2.114	34.6	45.8	31.0	50	2.38	0.070
B26	142	154	1.54	medium	0.297	1.002	3.034	34.6	45.8	35.0	50	0.00	0.000
B27	142	154	1.54	medium	0.218	1.002	2.227	34.6	45.8	34.0	50	1.42	0.043
B29	142	154	1.54	medium	0.154	1.002	1.573	34.6	45.8	39.0	50	1.13	0.034
B30	142	154	1.54	medium	0.184	1.002	1.879	34.6	45.8	35.0	50	4.50	0.136
D34	168	192	2.63	medium	0.097	1.002	0.987	28.4	42.8	33.0	54	7.80	0.235
O42	262	307	2.06	tight	1.160	1.002	11.848	32.2	42.3	74.5	51	17.24	0.519
O44	262	307	2.06	tight	1.340	1.002	13.687	32.2	42.3	72.9	51	13.65	0.414
B87	142	154	1.54	medium	0.016	1.002	0.160	34.6	45.8	42.0	50	4.60	0.137
Ims6	190	210	1.46	medium	1.330	1.002	13.585	33.1	44.1	30.0	52	16.00	0.109
proef4		260	1.80	tight	0.120	1.002	1.599			70		203	0.135

In Figure F-1 the sieve diagrams of the sands that were used for SBW are shown.

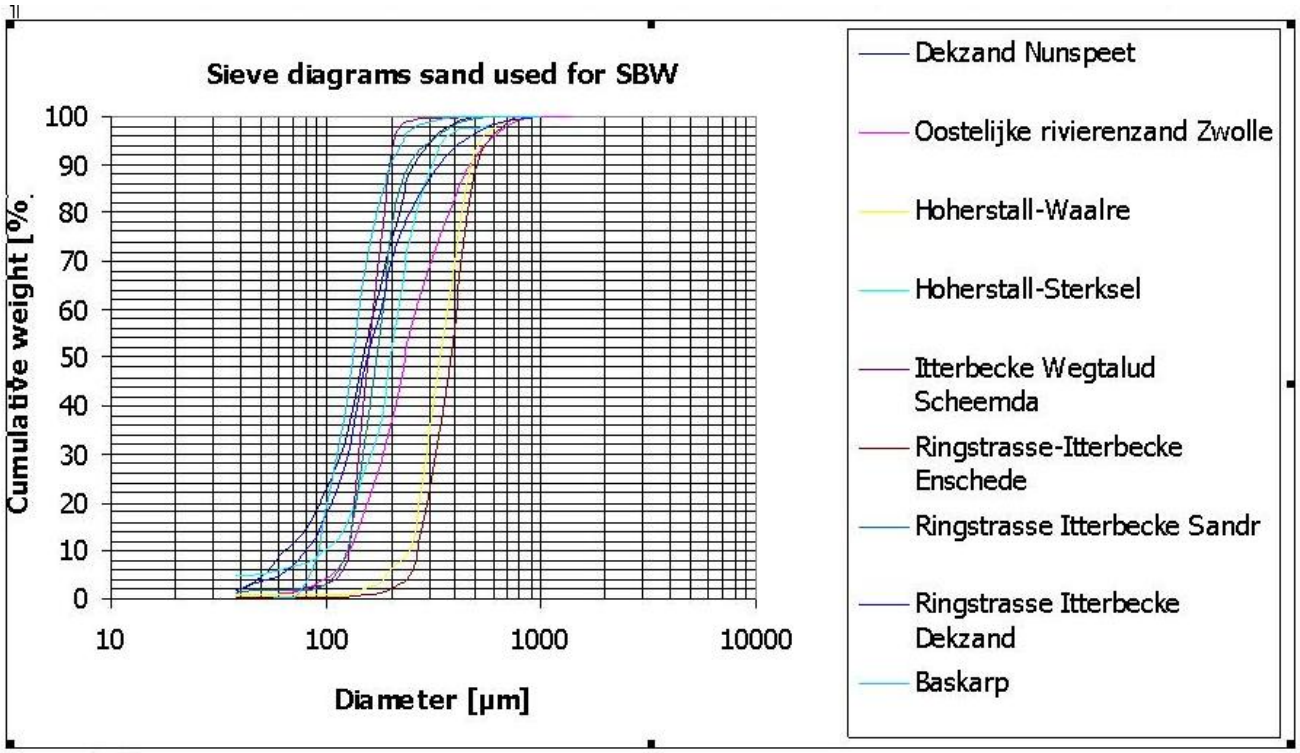

Figure F-1 the sieve curves of the sands that were used for SBW

G) Appendix G – De Deltagoot test facility

In 1991, four full-scale tests on piping have been performed in de Deltagoot. De Deltagoot is a test facility in Voorst, the Netherlands. The research has been done by ir. W.G. de Rijke, ir. W.B.A. Weijers and ir. F. Silvis et al. In this appendix the test facility that has been used is described. In Figure G-1 and Figure G-2 an overview and a photo of the test facility is shown.

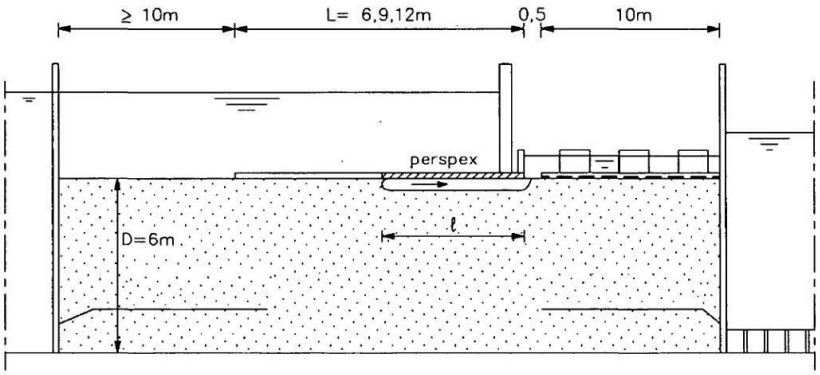

Figure G-1 an overview of the test facility in de Deltagoot

Figure G-2 a photo of de Deltagoot

For a more detailed description of the used test facility is referred to (de Rijke, 1991). Seepage lengths of 6, 9 and 12m were tested. The sand used came from the Marsdiep, a tidal gully between Texel and Den Helder, the Netherlands. The sand particles have a density of 2530 kg/m^3, which is lower than the value of 2650 kg/m^3, which is considered normal for quartz sand. The low density was attributed to the presence of shell fragments in the sand. The outcome of the tests and the relevant sand characteristics are shown in appendix H. Sellmeijer used the results of de Deltagoot to fit the rolling resistance angle used in his formula. The outcome of these experiments were used to fit the rolling resistance angle of the sand. In appendix H the outcome of the experiments of de Deltagoot are shown.

H) Appendix H – The test data from de Deltagoot

In this appendix, the outcome of the experiments de Deltagoot and the relevant sand characteristics are shown. The data can be found in (de Rijke, 1991). The results of experiment T1 are rejected because piping occurred along the side of the test facility during the experiment.

Table H-1 the results and sand characteristics of de Deltagoot experiments part 1

test number	L [cm]	D [cm]	W [cm]	L/D [-]	sand type	D_{10} [µm]	D_{50} [µm]	D_{60} [µm]	D_{70} [µm]	D_{90} [µm]
T2	900	601	500	1.498	Marsdiep sand	143	209	225	241	298
T3	1200	601	500	1.997	Marsdiep sand	143	209	225	241	298
T4	600	601	500	0.998	Marsdiep sand	143	209	225	241	298

Table H-2 the results and sand characteristics of de Deltagoot experiments part 2

test number	C_u [-]	packing	k_{Darcy} 10^{-3} [m/s]	T (°C)	v 10^{-6} m^2/s]	κ_{Darcy} 10^{-11} [m^2]	RD [%]	H_c [cm]	H_c/L [-]
T2	1.58	tight	0.0511	8.5	1.352	0.704	65.0	169.0	0.188
T3	1.58	tight	0.0511	8.5	1.352	0.704	65.0	216.0	0.180
T4	1.58	tight	0.0511	8.5	1.352	0.704	65.0	105.0	0.175

Table H-3 the result and sand characteristics of de Deltagoot's experiments which are not used part 1

test number	reason not used	L [cm]	D [cm]	W [cm]	L/D [-]	sand type	D_{10} [µm]	D_{50} [µm]	D_{60} [µm]	D_{70} [µm]	D_{90} [µm]
T1	Piping along side	600	601	500	0.998	Marsdiep sand	143	209	225	241	298

Table H-4 the result and sand characteristics of de Deltagoot's experiments which are not used part 2

test number	C_u [-]	packing	k_{Darcy} 10^{-3} [m/s]	T (°C)	v 10^{-6} m^2/s]	κ_{Darcy} 10^{-11} [m^2]	RD [%]	H_c [cm]	H_c/L [-]
T1	1.58	tight	0.0511	8.5	1.352	0.704	65.0	82.6	0.138

I) Appendix I – The test data from the one-dimensional test facility

In this appendix, the outcome of the experiments of the one-dimensional test facility and the relevant sand characteristics are shown. The formulas used are the same as in appendix B. The temperature was measured one time (21°C). More detailed information about the experimental outcomes can be found in the factual reports in appendix P.

Table I-1 the results and sand characteristics of the experiments with the one-dimensional test facility part 1

test number	L [cm]	D [cm]	W [cm]	L/D [-]	sand type	D_{10} [µm]	D_{20} [µm]	D_{30} [µm]	D_{40} [µm]	D_{50} [µm]
Q01	37.0	9.96	1	3.71	Baskarp	92	103	113	123	132
Q02	36.5	9.96	1	3.66	Baskarp	92	103	113	123	132
Q03	37.2	9.96	1	3.73	Baskarp	92	103	113	123	132
Q04	37.2	9.96	1	3.73	Enschede Ringstraat Itterbecke	261	296	325	355	380
Q05	35.4	9.96	1	3.55	Enschede Ringstraat Itterbecke	261	296	325	355	380
Q06	36.5	9.96	1	3.66	Enschede Ringstraat Itterbecke	261	296	325	355	380
Q07	36.5	9.96	1	3.66	Enschede Ringstraat Itterbecke	261	296	325	355	380
Q08	35.2	9.96	1	3.53	Enschede Ringstraat Itterbecke	261	296	325	355	380
Q09	38.5	9.96	1	3.87	Enschede Ringstraat Itterbecke	261	296	325	355	380
Q10	34.5	9.96	1	3.46	Enschede Ringstraat Itterbecke	261	296	325	355	380
Q11	34.0	9.96	1	3.41	Enschede Ringstraat Itterbecke	261	296	325	355	380
Q12	34.5	9.96	1	3.46	Baskarp	92	103	113	123	132
Q13	35.0	9.96	1	3.51	Enschede Ringstraat Itterbecke	261	296	325	355	380
Q14	35.5	9.96	1	3.56	Enschede Ringstraat Itterbecke	261	296	325	355	380
Q15	36.5	9.96	1	3.66	Enschede Ringstraat Itterbecke	261	296	325	355	380
Q16	33.0	9.96	1	3.31	Enschede Ringstraat Itterbecke	261	296	325	355	380
Q17	35.5	9.96	1	3.56	Enschede Ringstraat Itterbecke	261	296	325	355	380
Q18	36.5	9.96	1	3.66	Enschede Ringstraat Itterbecke	261	296	325	355	380

Table I-2 the results and sand characteristics of the experiments with the one-dimensional test facility part 2

test number	D_{60} [µm]	D_{70} [µm]	C_u [-]	packing	k_{Darcy} 10^{-3} [m/s]	κ_{Darcy} 10^{-11} [m^2]	n_{min} [%]	n_{max} [%]	RD [%]	KAS [-]	H_c [cm]	H_c/L [-]
Q1	142	154	1.54	tight	0.066	0.675	34.6	45.8	80	50	42	1.135
Q2	142	154	1.54	tight	0.189	1.934	34.6	45.8	70	50	18	0.493
Q3	142	154	1.54	tight	0.064	0.649	34.6	45.8	70	50	39	1.048
Q4	408	431	1.56	tight	0.325	3.318	32.01	41.06	78	69	53	1.425
Q5	408	431	1.56	medium	0.480	4.903	32.01	41.06	43	69	27	0.763
Q6	408	431	1.56	tight	0.446	4.556	32.01	41.06	60[*1]	69	33	0.904
Q7	408	431	1.56	tight	0.529	5.399	32.01	41.06	60[*1]	69	32	0.877
Q8	408	431	1.56	tight	0.410	4.189	32.01	41.06	40-50[*1]	69	33	0.938
Q9	408	431	1.56	tight	0.587	5.998	32.01	41.06	40-50[*1]	69	26	0.675
Q10	408	431	1.56	medium	0.658	6.724	32.01	41.06	40-50[*1]	69	20	0.580
Q11	408	431	1.56	medium	0.658	6.724	32.01	41.06	40-50[*1]	69	21	0.618
Q12	142	154	1.54	loose	0.137	1.398	34.6	45.8	25[*1]	50	16	0.464
Q13	408	431	1.56	medium	0.682	6.962	32.01	41.06	40-50[*1]	69	19	0.543
Q14	408	431	1.56	medium	0.689	7.041	32.01	41.06	40-50[*1]	69	19	0.535
Q15	408	431	1.56	medium	0.701	7.159	32.01	41.06	40-50[*1]	69	17	0.466
Q16	408	431	1.56	medium	0.799	8.158	32.01	41.06	40-50[*1]	69	14	0.424
Q17	408	431	1.56	medium	0.853	8.711	32.01	41.06	40-50[*1]	69	15	0.423
Q18	408	431	1.56	medium	1.353	13.818	32.01	41.06	40-50[*1]	69	13	0.356

[*1] *the relative density is estimated*

J) Appendix J – Comparison between measured and calculated SBW experiments

For five different formula's, the critical gradient is calculated and compared with the measured values for the small-scale and medium-scale SBW experiments. These formulas are shown below.

Formula *(eq J-1)*: the outcome of the MVA according to (López de la Cruz, 2009)

$$\frac{H_c}{L} = \left[\frac{H_c}{L}\right]_{mean}\left[\frac{RD}{RD_{mean}}\right]^{0.35}\left[\frac{C_u}{C_{u,mean}}\right]^{0.13}\left[\frac{KAS}{KAS_{mean}}\right]^{-0.02}\left[\frac{\kappa}{\kappa_{mean}}\right]^{-0.35}\left[\frac{D_{70}}{D_{70,mean}}\right]^{0.39}$$

Formula *(eq J-2)*: the outcome of the MVA according to the analysis in this thesis

$$\frac{H_c}{L} = e^{-0.91}\left(\frac{RD}{RD_{mean}}\right)^{0.41}\left(\frac{k_{Darcy}}{k_{Darcy,mean}}\right)^{-0.31}\left(\frac{D_{70}}{D_{70,mean}}\right)^{0.29}\left(\frac{C_u}{C_{u,mean}}\right)^{0.16}\left(\frac{KAS}{KAS_{mean}}\right)^{-0.005}$$

Formula *(eq J-3)*: the outcome of the MVA according to the analysis in this thesis, in simplified form

$$\frac{H_c}{L} = e^{-0.92}\left(\frac{k_{Darcy}}{k_{Darcy,mean}}\right)^{-0.33}\left(\frac{RD}{RD_{mean}}\right)^{0.39}\left(\frac{D_{70}}{D_{70,mean}}\right)^{0.34}$$

Formula *(eq J-4)*: the current Sellmeijer 2-forces model

$$\frac{H_c}{L} = F_R\, F_S\, F_G \qquad F_R = \frac{\gamma'_p}{\gamma_w}\eta\tan(\theta) \qquad F_S = \frac{D_{70}}{\sqrt[3]{\kappa L}} \qquad F_G = 0.867\left(\frac{D}{L}\right)^{\frac{0.28}{\left(\frac{D}{L}\right)^{2.8}-1}+0.04}$$

Formula *(eq J-5)*: the adapted Sellmeijer 2-forces model

$$\frac{H}{L} = F_R\, F_S\, F_G$$

$$F_R = \eta\frac{\gamma'_p}{\gamma_w}\tan\theta\left(\frac{RD}{RD_{mean}}\right)^{0.35}\left(\frac{U}{U_{mean}}\right)^{0.13}\left(\frac{KAS}{KAS_{mean}}\right)^{-0.02}$$

$$F_S = \frac{d_{70,mean}}{\sqrt[3]{\kappa L}}\left(\frac{d_{70}}{d_{70,mean}}\right)^{0.39} = \frac{d_{70}}{\sqrt[3]{\kappa L}}\left(\frac{d_{70,mean}}{d_{70}}\right)^{0.61}$$

$$F_G = 0.91\left(\frac{D}{L}\right)^{\frac{0.28}{\left(\frac{D}{L}\right)^{2.8}-1}+0.04}$$

In Table J-1 the measured and calculated critical gradients are shown, and the difference between the measured and calculated values. The difference is defined

as $\left[\frac{[H_c / L]_{measured}}{H_c / L_{calculated}} - 1\right] * 100\%$ *(eq J-6)*. In Table J-2 the error and standard deviation is shown.

Table J-1 the measured and calculated critical gradients and the difference for the small-scale SBW experiments

		equation J-1		equation J-2		equation J-3		equation J-4		equation J-5	
test number	H_c/L [-] measured	H_c/L [-]	difference [%]	H_c/L [-]	difference [%]	H_c/L [-]	difference [%]	H_c/L [-]	difference [%]	H_c/L [-]	difference [%]
B19	0.357	0.347	2.9	0.354	0.9	0.356	0.5	0.349	2.5	0.401	-11.0
B23	0.595	0.536	11.0	0.543	9.6	0.549	8.4	0.457	30.0	0.611	-2.7
B24	0.531	0.511	4.0	0.520	2.2	0.525	1.3	0.439	21.1	0.584	-9.1
B28	0.222	0.246	-9.8	0.247	-10.3	0.249	-10.7	0.302	-26.5	0.287	-22.7
D31	0.572	0.499	14.7	0.495	15.5	0.467	22.6	0.529	8.2	0.535	6.9
D32	0.449	0.456	-1.7	0.458	-2.0	0.429	4.5	0.486	-7.7	0.492	-8.8
D33	0.279	0.304	-8.8	0.300	-7.6	0.282	-1.7	0.405	-31.6	0.330	-16.1
B35	0.439	0.372	18.0	0.377	16.6	0.379	15.7	0.373	17.7	0.429	2.2
B36	0.442	0.379	16.7	0.382	15.7	0.386	14.6	0.382	15.8	0.437	1.1
D37	0.848	0.725	15.6	0.719	16.6	0.681	23.1	0.658	27.3	0.769	9.0
D38	0.537	0.617	-12.9	0.619	-13.2	0.582	-7.8	0.576	-6.8	0.658	-18.4
D39	0.453	0.634	-28.6	0.634	-28.6	0.598	-24.2	0.592	-23.5	0.677	-33.1
B40	0.449	0.543	-17.3	0.546	-17.6	0.554	-18.8	0.476	-5.6	0.620	-27.5
B41	0.481	0.492	-2.1	0.500	-3.8	0.504	-4.6	0.431	11.6	0.564	-14.6
O43	0.378	0.389	-2.8	0.389	-2.6	0.379	-0.1	0.550	-31.2	0.440	-14.0
I45	0.652	0.498	30.8	0.494	32.0	0.476	37.0	0.537	21.4	0.545	19.7
I46	0.496	0.465	6.5	0.464	6.9	0.446	11.2	0.506	-2.0	0.509	-2.7
I47	0.374	0.379	-1.5	0.369	1.1	0.381	-1.9	0.691	-46.0	0.448	-16.7
I48	0.371	0.357	3.7	0.351	5.6	0.360	2.9	0.650	-43.0	0.424	-12.5
I49	0.297	0.368	-19.4	0.360	-17.6	0.368	-19.4	0.632	-53.0	0.432	-31.2
I50	0.310	0.325	5.1	0.321	6.3	0.326	4.6	0.570	-40.1	0.384	-11.1
I51	0.377	0.380	-1.0	0.382	-1.4	0.390	-3.3	0.432	-12.8	0.444	-15.2
I52	0.395	0.369	6.8	0.359	10.0	0.368	7.3	0.650	-39.3	0.434	-9.0
I53	0.423	0.434	-2.5	0.432	-1.9	0.443	-4.3	0.483	-12.4	0.506	-16.3
B54	0.575	0.466	23.4	0.469	22.5	0.475	21.1	0.432	33.2	0.535	7.5
B55	0.462	0.427	8.2	0.431	7.4	0.435	6.2	0.412	12.2	0.493	-6.2
I56	0.327	0.385	-14.9	0.384	-14.8	0.398	-17.7	0.412	-20.6	0.452	-27.5
B57	0.428	0.434	-1.3	0.438	-2.3	0.443	-3.3	0.410	4.4	0.499	-14.2
B58	0.348	0.398	50.2	0.404	48.2	0.407	47.1	0.385	55.4	0.457	30.8
B61	0.353	0.419	-15.7	0.424	-16.7	0.428	-17.4	0.399	-11.3	0.481	-26.5
I62	0.352	0.334	5.5	0.336	4.9	0.346	1.8	0.373	-5.5	0.395	-10.9
S63	0.440	0.400	9.9	0.404	8.9	0.386	14.0	0.465	-5.5	0.441	-0.4
S64	0.402	0.443	-9.3	0.442	-9.0	0.425	-5.3	0.514	-21.7	0.487	-17.5
B82	0.413	0.467	-11.5	0.474	-12.8	0.478	-13.6	0.421	-1.9	0.535	-22.8
B83	0.415	0.467	-11.2	0.474	-12.5	0.478	-13.3	0.422	-1.6	0.536	-22.6
B84	0.294	0.334	-11.9	0.336	-12.5	0.339	-13.2	0.359	-18.0	0.386	-23.9
B85	0.351	0.361	-3.0	0.360	-2.7	0.365	-4.0	0.386	-9.2	0.416	-15.8
B86	0.291	0.305	-4.4	0.303	-4.0	0.307	-5.1	0.352	-17.3	0.353	-17.4

The error is defined as: error = $\sum_{i=1}^{38}\left[\left[\frac{H_c}{L}\right]_{calculated,i} - \left[\frac{H_c}{L}\right]_{measured,i}\right]^2$ *(eq J-7)*. The standard deviation is defined as $\sigma = \sqrt{\frac{error}{n-1}}$

Table J-2 the error and standard deviation of the formula's for the small-scale SBW experiments

	error [-]	σ [-]
equation J-1	0.1828	0.0703
equation J-2	0.1838	0.0705
equation J-3	0.1926	0.0722
equation J-4	0.6773	0.1470
equation J-5	0.2922	0.0889

As can be seen in Table J-2 the error of equation J-1 and J-2 are almost the same, and the lowest of all. The error of equation J-3 is also low, compared with equation J-1 and J-2, and is easier to use because of the lower amount of variables needed. equation J-4 shows a quite high error. equation J-5 shows a much lower error than equation J-4. In Table J-3 and Table J-4 the measured and calculated critical gradients and the errors and standard deviations for equation J-2 (MVA on SBW small-scale from this thesis), formula equation J-4 (current Sellmeijer 2-forces model) and equation J-5 (adapted Sellmeijer 2-forces model) are shown.

Table J-3 comparison of H_c /L for the medium-scale experiments with the MVA derived from small-scale experiments and the Sellmeijer models and the measured values

test number	H_c/L [-] measurements	equation J-2 H_c/L [-]	equation J-2 difference [%]	equation J-4 H_c/L [-]	equation J-4 difference [%]	equation J-5 H_c/L [-]	equation J-5 difference [%]
Bms1	0.204	0.322	-36.5	0.223	-8.5	0.252	-18.7
Bms2	0.255	0.283	-9.8	0.209	21.9	0.221	15.4
Ims3	0.179	0.308	-41.9	0.257	-30.4	0.245	-27.0
Ims4	0.137	0.232	-40.8	0.210	-34.5	0.185	-25.6
Ims5	0.205	0.317	-35.4	0.248	-17.5	0.250	-18.1
Bms7	0.223	0.313	-28.7	0.212	5.2	0.244	-8.6
Bms8	0.143	0.239	-40.1	0.176	-18.9	0.186	-23.2

Table J-4 the error and standard deviation of the formula's

	error [-]	σ [-]
equation J-2	0.1838	0.0705
equation J-4	0.7995	0.1470
equation J-5	0.2922	0.0889

It shows the MVA formula has the smallest standard deviation, and the adapted Sellmeijer model gives also quite accurate results. The current 2-forces Sellmeijer model does not give good results for the medium-scale SBW experiments.

K) Appendix K – Plots of the dataset of SBW

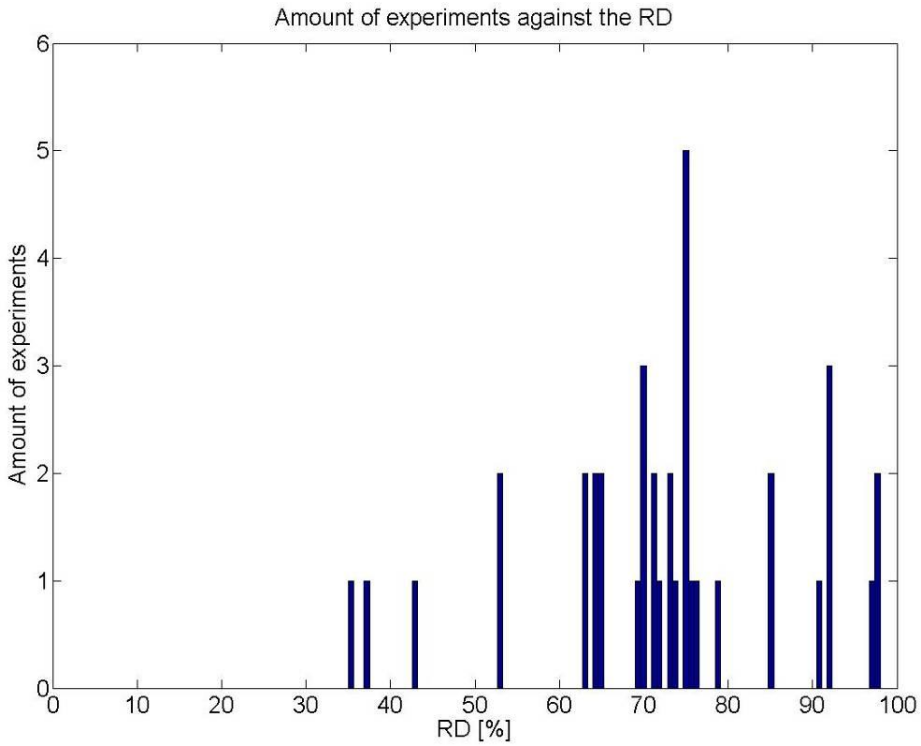

Figure K-1 a histogram of the RD of the sand samples used for the small-scale SBW experiments

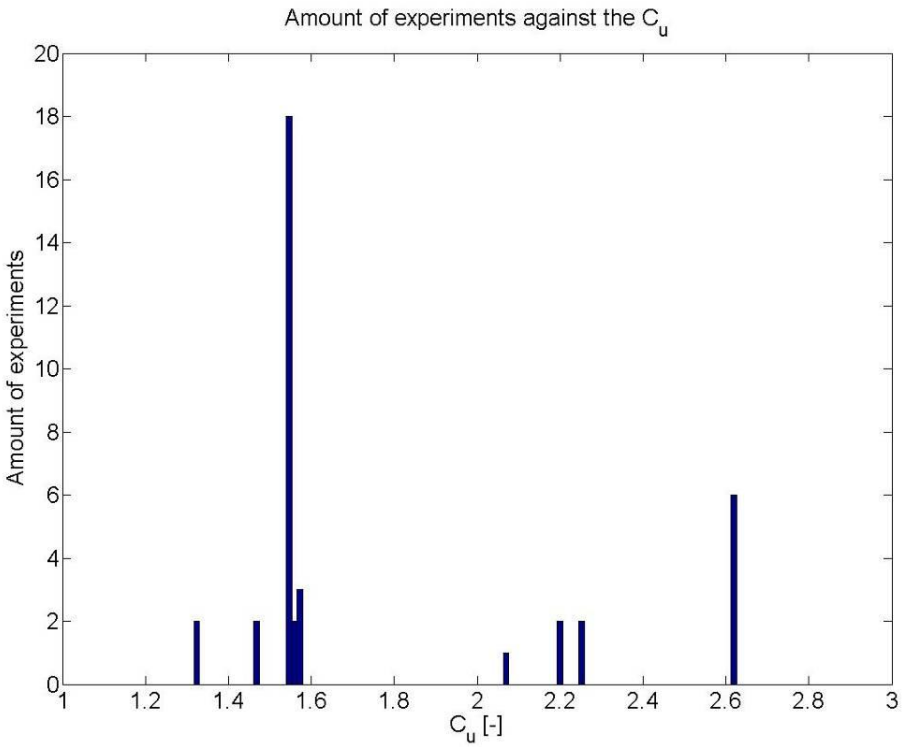

Figure K-2 a histogram of the C_u of the sand samples used for the small-scale SBW experiments

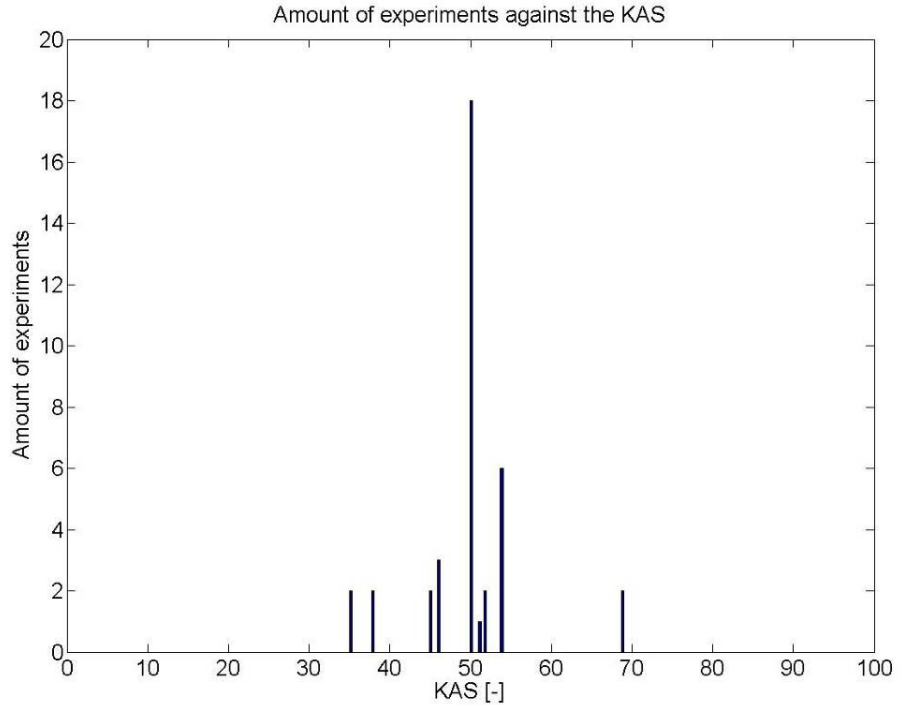

Figure K-3 a histogram of the KAS of the sand samples used for the small-scale SBW experiments

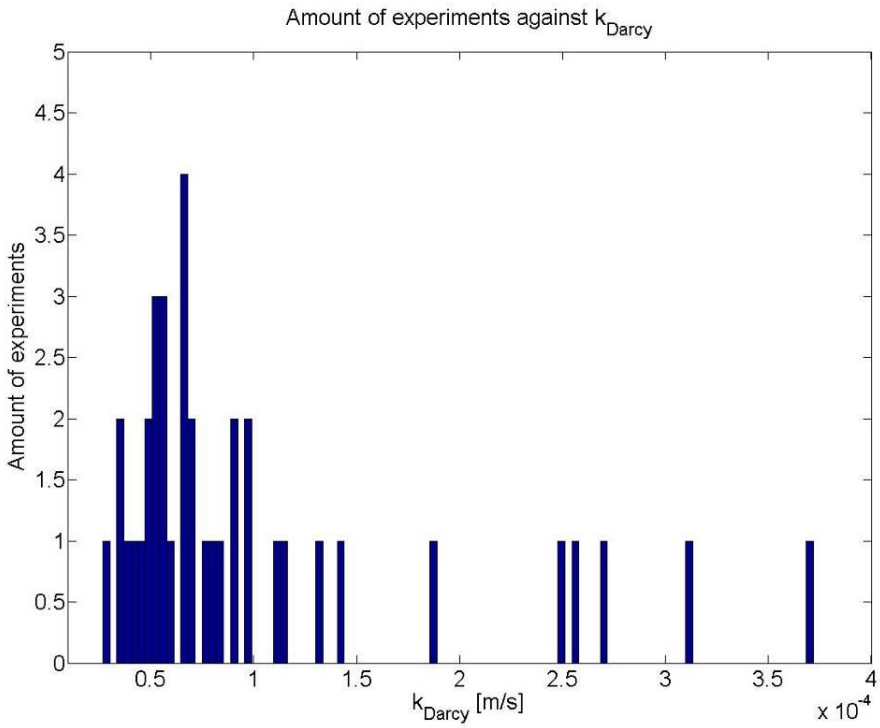

Figure K-4 a histogram of k_{Darcy} of the sand samples used for the small-scale SBW experiments

L) Appendix L – Comparison between measured and calculated de Wit experiments

For three different formula's, the critical gradient is calculated and compared with the measured values for the small-scale and medium-scale de Wit experiments. These formula's are equation J-2 (MVA on SBW small-scale from this thesis), equation J-4 (current Sellmeijer 2-forces model) and formula equation J-5 (adapted Sellmeijer 2-forces model), just as in appendix J.

In Table L-1 and Table L-2 the measured and calculated critical gradients and the errors and standard deviation are shown. Again, it is noted the measured critical head is not corrected for the resistance of the filter, as this resistance is unknown.

Table L-1 the measured and calculated critical gradients and the difference for the small-scale de Wit experiments

test number	H_c/L [-]	equation J-2		equation J-4		equation J-5	
	measured	H_c/L	difference	H_c/L	difference	H_c/L	Difference
		[-]	[%]	[-]	[%]	[-]	[%]
220880-I-1	0.413	0.438	-5.8	0.361	14.3	0.368	12.0
220880-I-2	0.455	0.453	0.4	0.361	26.2	0.375	21.4
220880-I-4	0.299	0.371	-19.5	0.317	-5.6	0.306	-2.5
220880-I-5	0.336	0.339	-0.7	0.305	10.3	0.281	19.6
220880-I-6	0.340	0.385	-11.6	0.323	5.2	0.324	5.1
220880-I-7	0.251	0.288	-12.7	0.290	-13.4	0.250	0.3
220880-I-8	0.208	0.232	-10.7	0.267	-22.3	0.204	1.9
220880-I-9	0.278	0.264	5.3	0.276	0.6	0.226	22.8
220880-II-1	0.378	0.443	-14.7	0.685	-44.9	0.382	-1.1
220880-II-2	0.563	0.421	33.5	0.698	-19.4	0.373	51.0
220880-II-3	0.375	0.347	8.2	0.635	-40.9	0.315	19.2
220880-II-4	0.556	0.293	89.8	0.561	-0.8	0.257	116.5
220880-II-5	0.425	0.264	60.8	0.564	-24.6	0.234	82.0
220880-III-1	0.375	0.380	-1.3	0.532	-29.4	0.320	17.1
220880-III-2	0.490	0.349	40.4	0.516	-5.0	0.293	67.4
220880-III-3	0.455	0.320	42.0	0.513	-11.3	0.273	66.5
220880-III-4	0.355	0.269	32.2	0.477	-25.6	0.230	54.2
220880-III-5	0.403	0.230	75.1	0.477	-15.5	0.204	97.7
220880-III-6	0.253	0.169	49.8	0.430	-41.2	0.152	66.1
220880-V-1	0.333	0.397	-16.3	0.312	6.6	0.326	1.9
220880-V-2	0.379	0.367	3.1	0.299	26.8	0.302	25.5
220880-V-3	0.293	0.350	-16.3	0.297	-1.6	0.289	1.1
220880-V-4	0.305	0.307	-0.6	0.277	10.2	0.258	18.2
220880-V-6	0.313	0.264	18.5	0.258	21.0	0.217	44.2
220880-V-7	0.305	0.235	29.7	0.252	21.2	0.197	54.5
220880-VII-1	0.350	0.423	-17.2	0.313	12.0	0.331	5.7
220880-VII-2	0.301	0.377	-20.1	0.298	1.2	0.301	0.0
220880-VII-3	0.301	0.319	-5.4	0.280	7.7	0.261	15.5
220883-6-1	0.203	0.368	-44.8	0.317	-35.9	0.307	-33.6
220883-6-1	0.243	0.379	-36.0	0.327	-25.9	0.316	-23.3
220883-39-1	0.296	0.295	0.5	0.279	6.1	0.244	21.5
220883-39-2	0.244	0.296	-17.5	0.286	-14.6	0.249	-2.3
220883-39-3	0.268	0.307	-12.9	0.289	-7.4	0.253	6.0
220884-26-1	0.493	0.193	155.5	0.867	-43.2	0.172	185.6
220884-26-2	0.489	0.276	77.1	0.983	-50.3	0.240	103.3
220884-26-3	0.979	0.342	185.9	1.047	-6.5	0.290	237.1
220884-26-4	0.990	0.213	364.9	0.935	5.9	0.184	438.1
220884-26-5	0.825	0.303	172.0	1.094	-24.6	0.266	210.0
220885-10-1	0.255	0.299	-14.6	0.306	-16.7	0.257	-0.8
220885-10-2	0.258	0.429	-39.9	0.350	-26.5	0.354	-27.3
220885-10-3	0.180	0.317	-43.3	0.321	-43.9	0.269	-33.2
220885-10-4	0.284	0.470	-39.6	0.388	-26.8	0.392	-27.6
220885-10-5	0.188	0.298	-37.2	0.303	-38.1	0.254	-26.3
220885-10-6	0.334	0.425	-21.5	0.352	-5.1	0.356	-6.2

Table L-2 the error and standard deviation of the formula's for the small-scale de Wit experiments

	error [-]	σ [-]
equation J-2	1.8102	0.2052
equation J-4	0.8559	0.1411
equation J-5	2.0046	0.2159

As can be seen in Table L-2, the error is very large, especially when compared with the values in Table J-2. From formula D, the current 2-forces Sellmeijer model, performs the best. The MVA formula and the adapted 2-forces Sellmeijer model perform not good.

Table L-3 the measured and calculated critical gradients and the difference for the medium-scale (L=240cm) de Wit experiments

test number	H_c /L [-] measured	equation J-2 H_c/L [-]	equation J-2 difference [%]	equation J-4 H_c/L [-]	equation J-4 difference [%]	equation J-5 H_c/L [-]	equation J-5 Difference [%]
220880-IV-1	0.349	0.423	-17.4	0.221	58.0	0.231	50.9
220880-IV-2	0.156	0.377	-58.7	0.221	-29.4	0.223	-30.0
220880-IV-3	0.170	0.344	-50.5	0.208	-18.0	0.201	-15.2
220880-VI-1	0.173	0.379	-54.4	0.216	-20.0	0.223	-22.5
220880-VI-2	0.147	0.390	-62.4	0.230	-36.2	0.233	-36.9
220880-VI-3	0.173	0.316	-45.5	0.200	-13.6	0.188	-8.2
220880-VI-4	0.185	0.321	-42.4	0.197	-6.2	0.184	0.6
220880-VI-5	0.150	0.282	-46.9	0.183	-18.1	0.163	-7.8
220880-VI-6	0.159	0.260	-38.9	0.176	-9.7	0.148	7.6
220880-VI-7	0.119	0.229	-48.1	0.167	-28.8	0.131	-9.2
220883-4-1	0.196	0.465	-57.9	0.278	-29.6	0.271	-27.7
220883-4-1	0.190	0.443	-57.1	0.264	-28.1	0.257	-26.1
220883-35-1	0.367	0.184	99.2	0.574	-36.2	0.113	224.6
220883-35-2	0.400	0.192	108.0	0.561	-28.7	0.114	250.4
220883-35-3	0.333	0.200	67.0	0.576	-42.2	0.118	181.4
220883-35-4	0.283	0.280	1.3	0.667	-57.5	0.164	72.6
220883-35-5	0.298	0.280	6.3	0.665	-55.2	0.164	81.7
220883-35-6	0.369	0.290	27.1	0.677	-45.5	0.169	118.7
220883-35-7	0.261	0.350	-25.4	0.737	-64.6	0.204	27.6
220883-35-8	0.433	0.359	20.8	0.747	-42.0	0.207	109.1
220883-35-8	0.392	0.358	9.6	0.743	-47.2	0.206	90.3
220885-10-6	0.162	0.431	-62.4	0.240	-32.6	0.243	-33.3
220885-10-6	0.160	0.434	-63.1	0.239	-33.1	0.242	-33.8
220885-10-6	0.136	0.438	-69.1	0.241	-43.7	0.243	-44.3

Table L-4 the error and standard deviation of the formula's for the medium-scale (L=240cm) de Wit experiments

	error [-]	σ [-]
equation J-2	1.8102	0.2052
equation J-4	0.8559	0.1411
equation J-5	2.0046	0.2159

Table L-5 the measured and calculated critical gradients and the difference for the medium-scale (L= 450cm) de Wit experiments

test number	H_c /L [-] measured	equation J-2		equation J-4		equation J-5	
		H_c/L [-]	difference [%]	H_c/L [-]	difference [%]	H_c/L [-]	Difference [%]
220881-40-1	0.180	0.330	-45.5	0.176	2.4	0.171	5.2
220881-40-2	0.159	0.335	-52.6	0.178	-10.9	0.174	-8.5
220881-40-3	0.139	0.333	-58.4	0.177	-21.8	0.173	-19.6
220883-4-1	0.192	0.378	-49.3	0.203	-5.7	0.198	-3.1
220883-4-1	0.173	0.393	-55.9	0.212	-18.2	0.206	-15.9

Table L-6 the error and standard deviation of the formula's for the medium-scale (L=450cm) de Wit experiments

	error [-]	σ [-]
equation J-2	0.1746	0.2089
equation J-4	0.0035	0.0296
equation J-5	0.0026	0.0253

M) Appendix M –Plots of the dataset of de Wit

In Figure M-7 until Figure M-11 $\frac{\Delta H_c}{L}$ is plotted against the input variables for the medium-scale de Wit experiments (L=240cm). In Figure M-12 until Figure M-16 the histograms of the medium-scale de Wit experiments are shown. In Figure M-17 until Figure M-19 several input variables are plotted against each other to show the correlations between those variables. From paragraph 2.6 is referred to these figures.

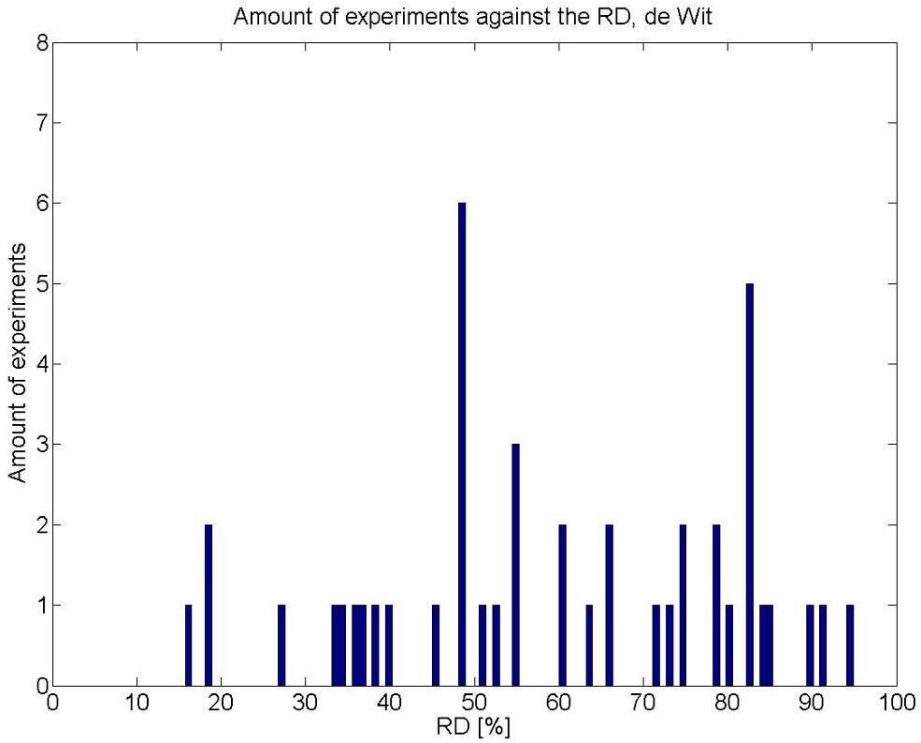

Figure M-1 a histogram of the RD of the sand samples used for the small-scale de Wit experiments

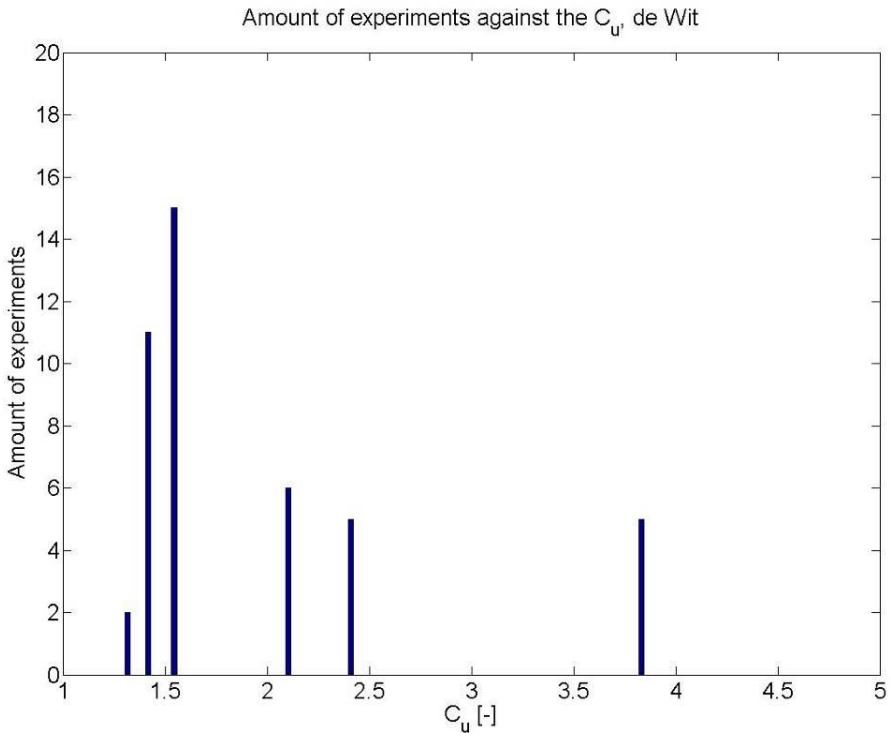

Figure M-2 a histogram of the C_u of the sand samples used for the small-scale de Wit experiments

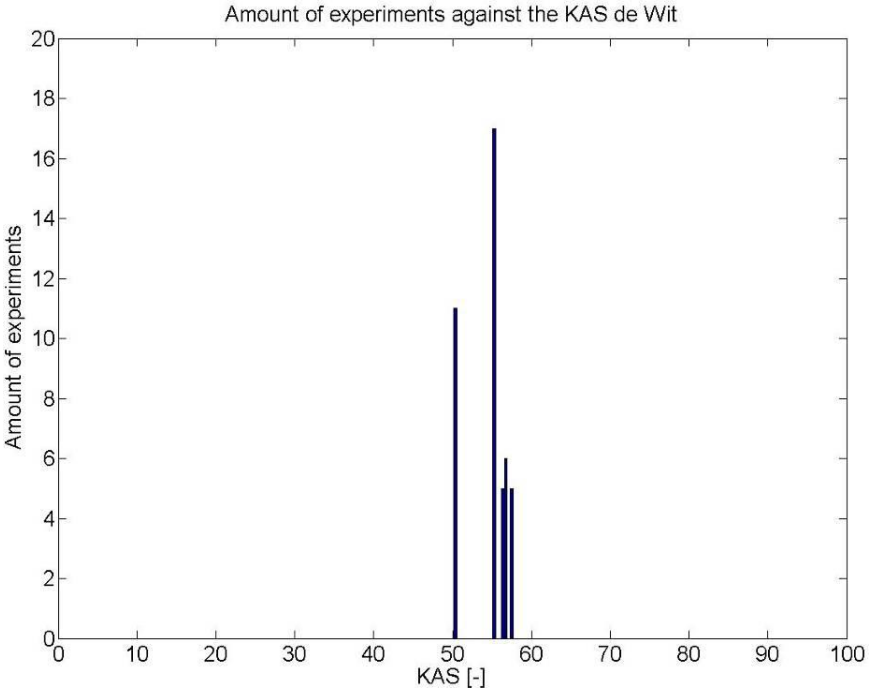

Figure M-3 a histogram of the KAS of the sand samples used for the small-scale de Wit experiments

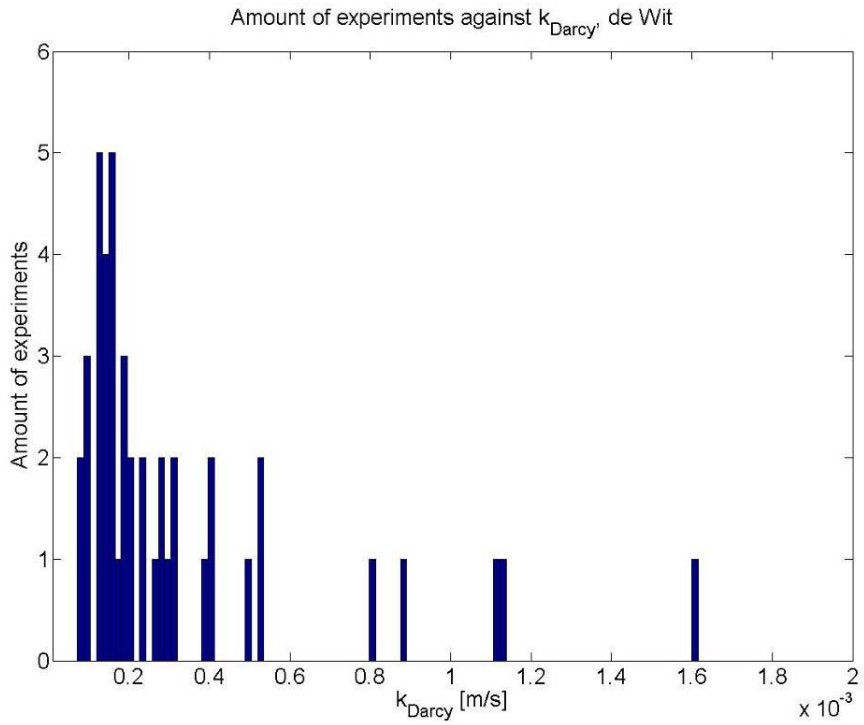

Figure M-4 a histogram of K_{Darcy} of the sand samples used for the small-scale de Wit experiments

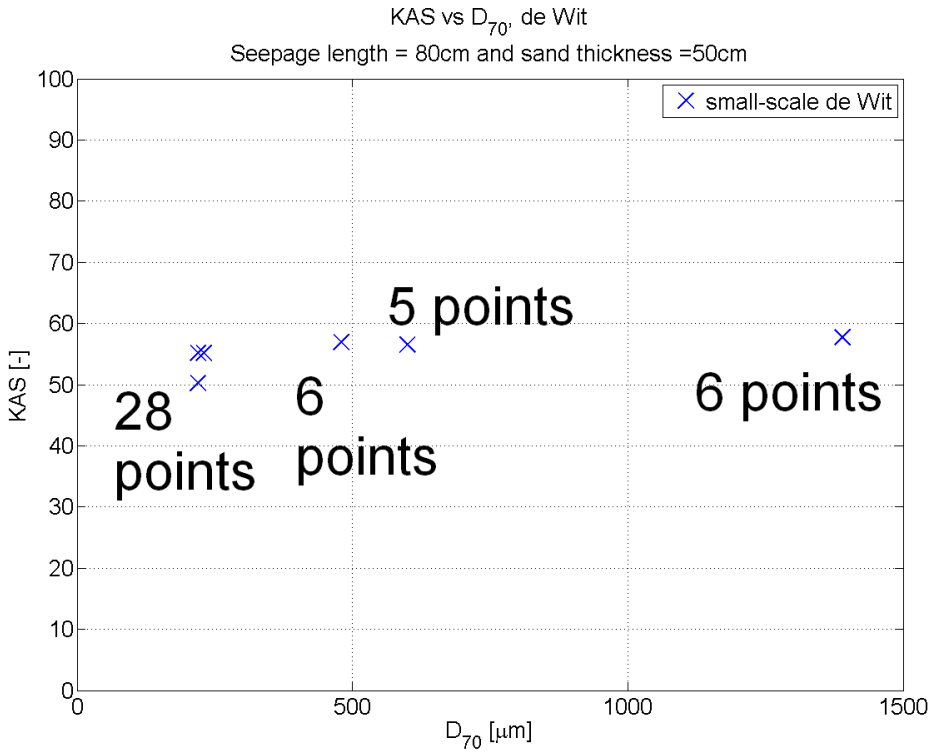

Figure M-5 KAS plotted against the D_{70} for the small-scale de Wit experiments

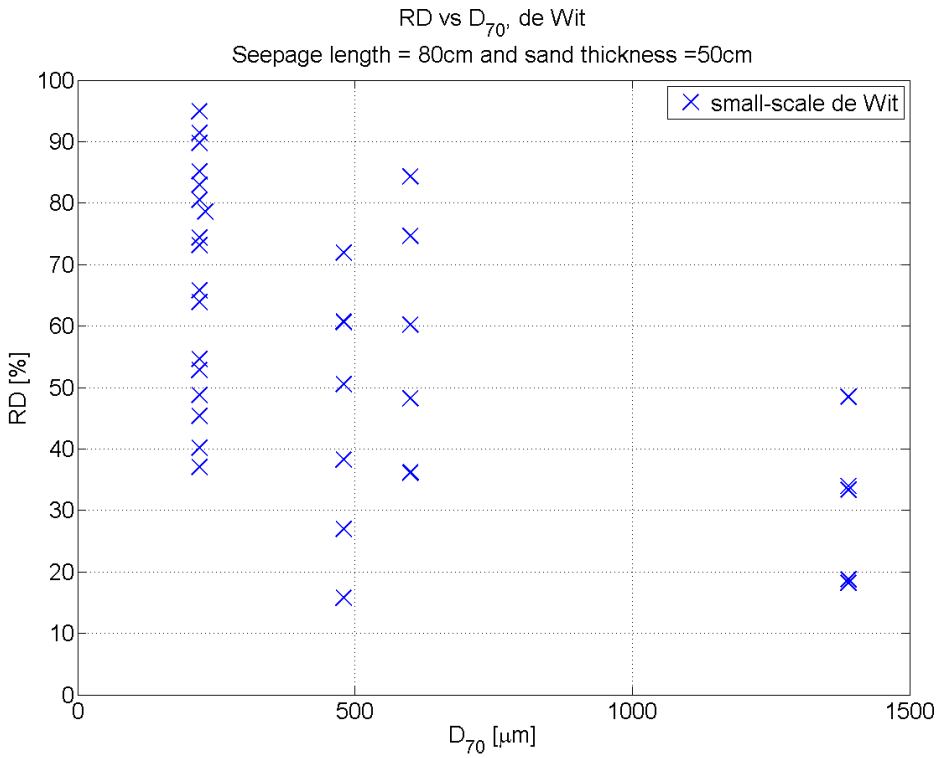

Figure M-6 RD plotted against the D_{70} for the small-scale de Wit experiments

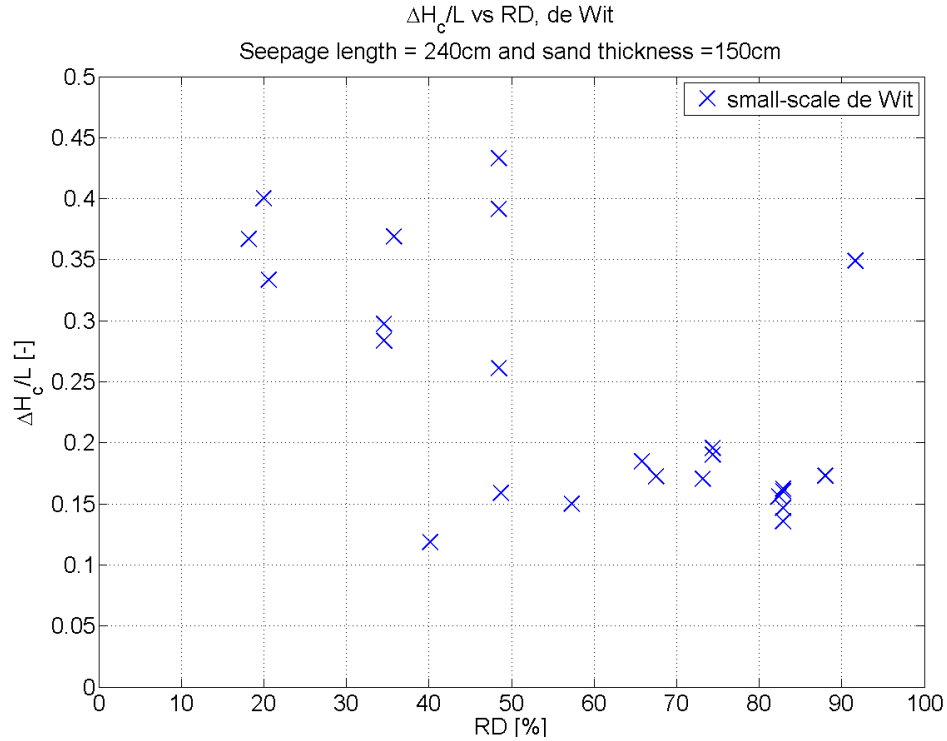

Figure M-7 the plot of the critical gradient against RD for medium-scale de Wit measurements

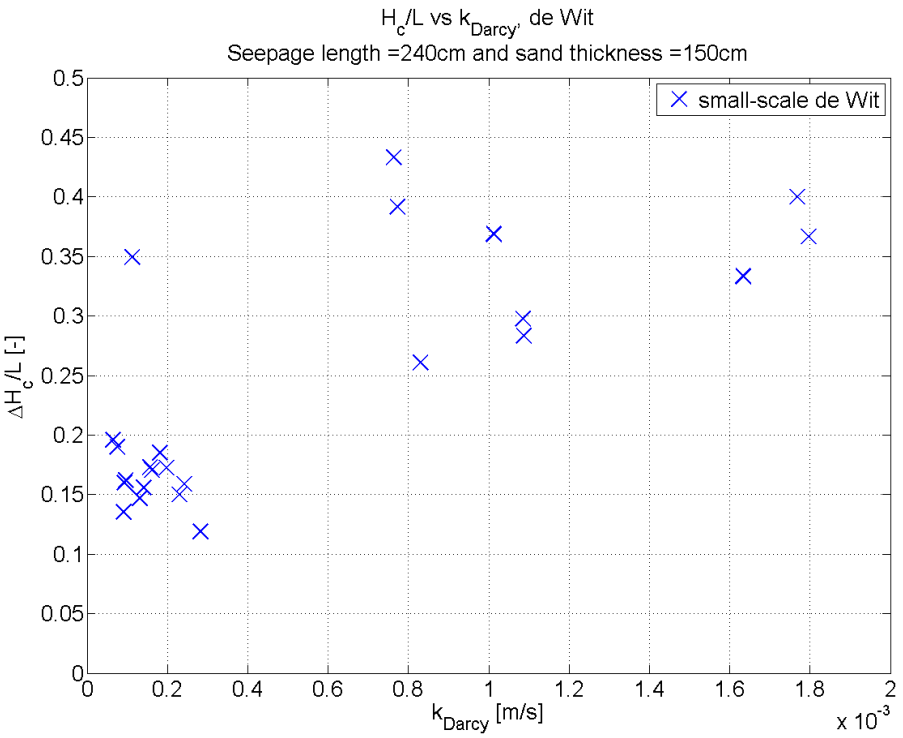

Figure M-8 the plot of the critical gradient against k_{Darcy} for medium-scale de Wit measurements

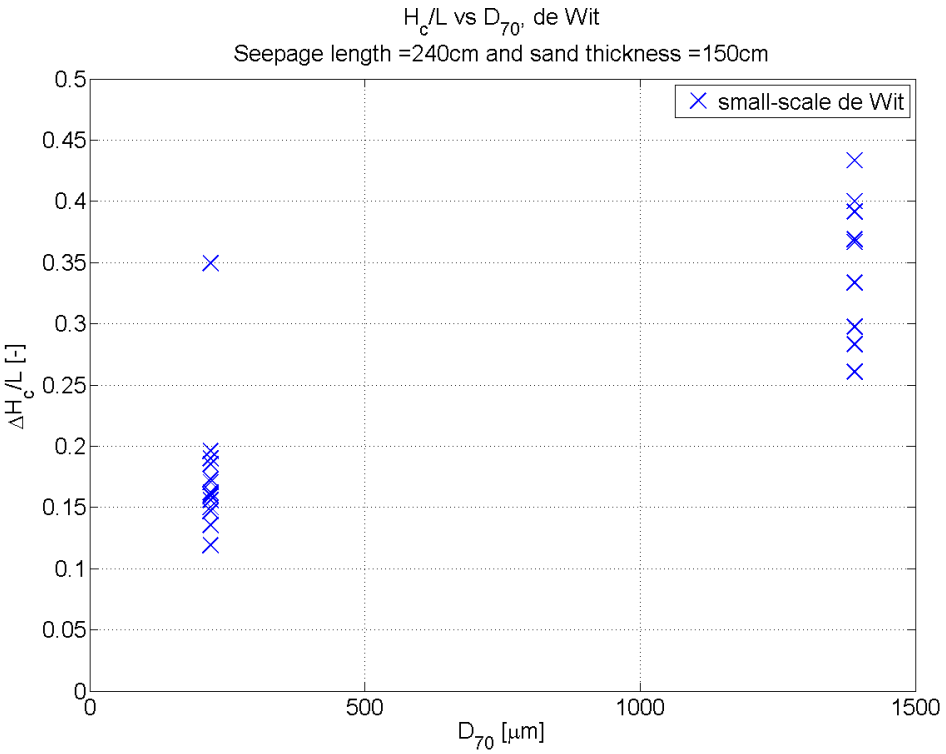

Figure M-9 the plot of the critical gradient against D_{70} for medium-scale de Wit measurements

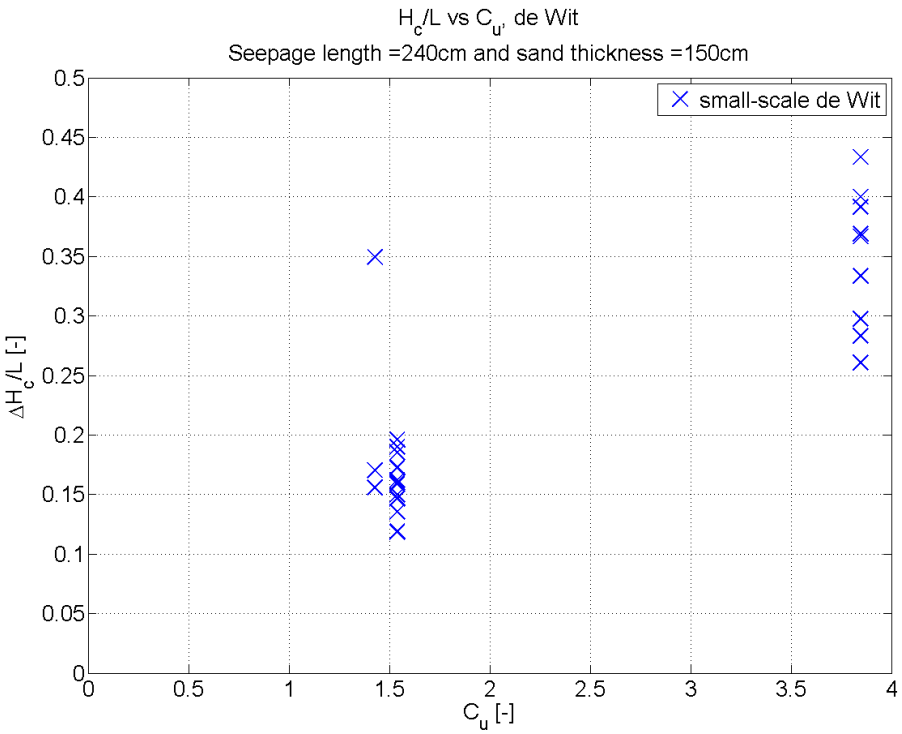

Figure M-10 the plot of the critical gradient against C_u for medium-scale de Wit measurements

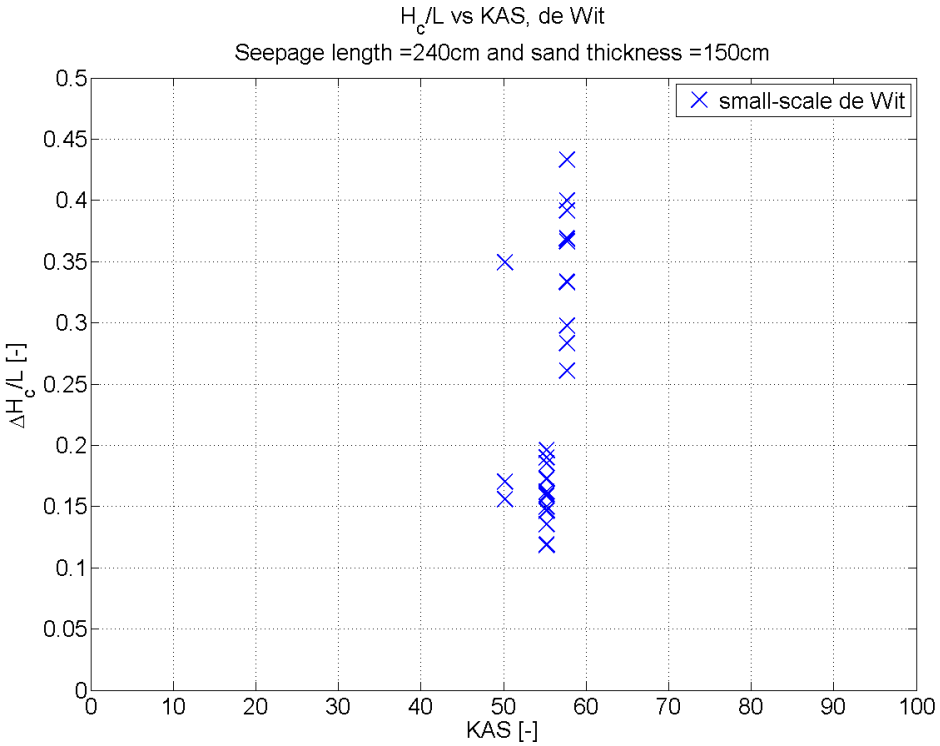

Figure M-11 the plot of the critical gradient against KAS for medium-scale de Wit measurements

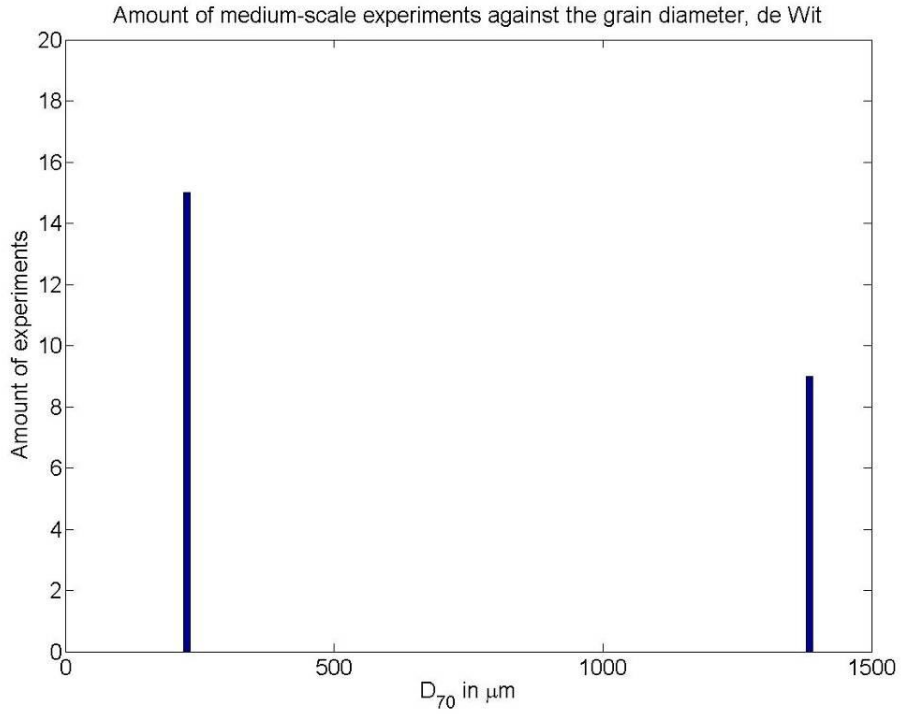

Figure M-12 a histogram of the D_{70} of the sand samples used for the medium-scale de Wit experiments

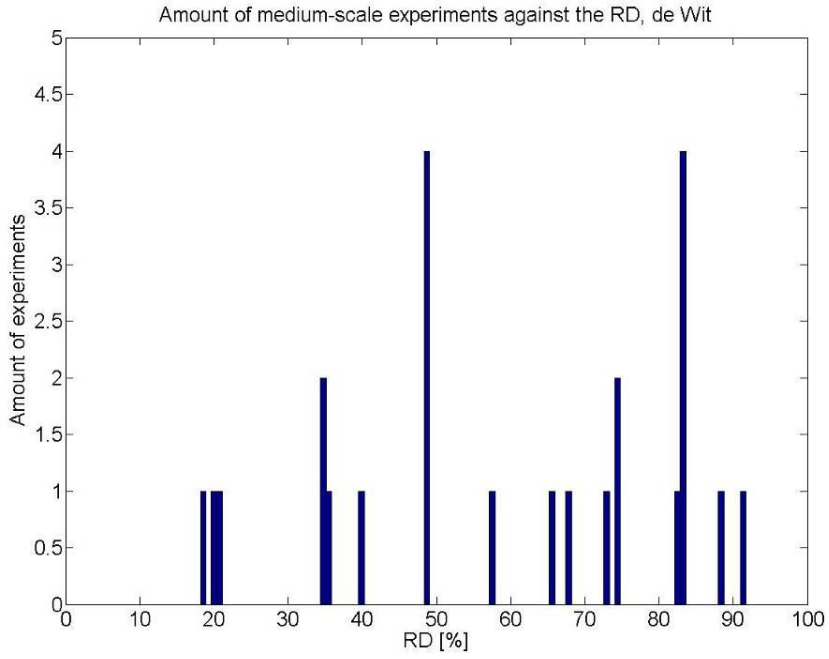

Figure M-13 a histogram of the RD of the sand samples used for the medium-scale de Wit experiments

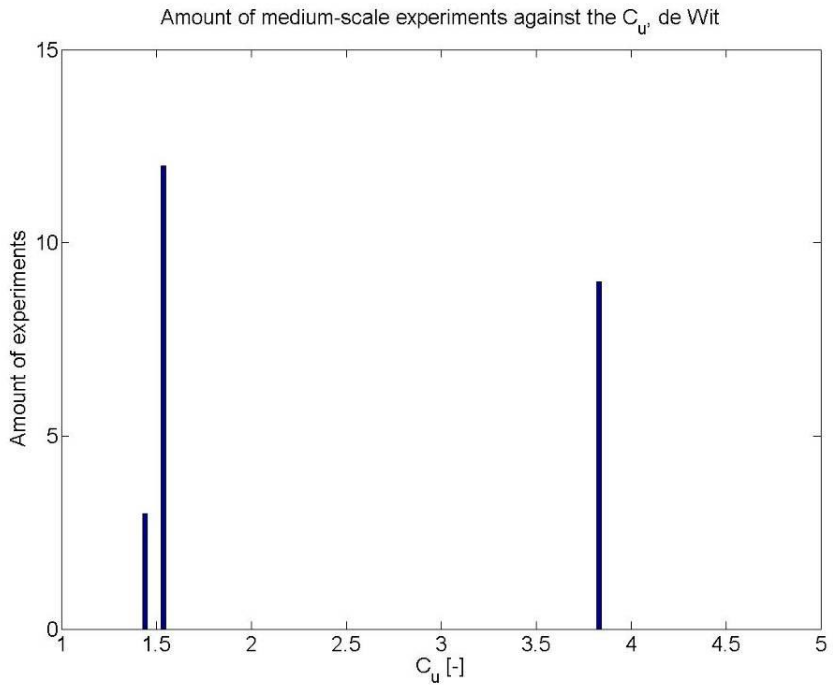

Figure M-14 a histogram of the C_u of the sand samples used for the medium-scale de Wit experiments

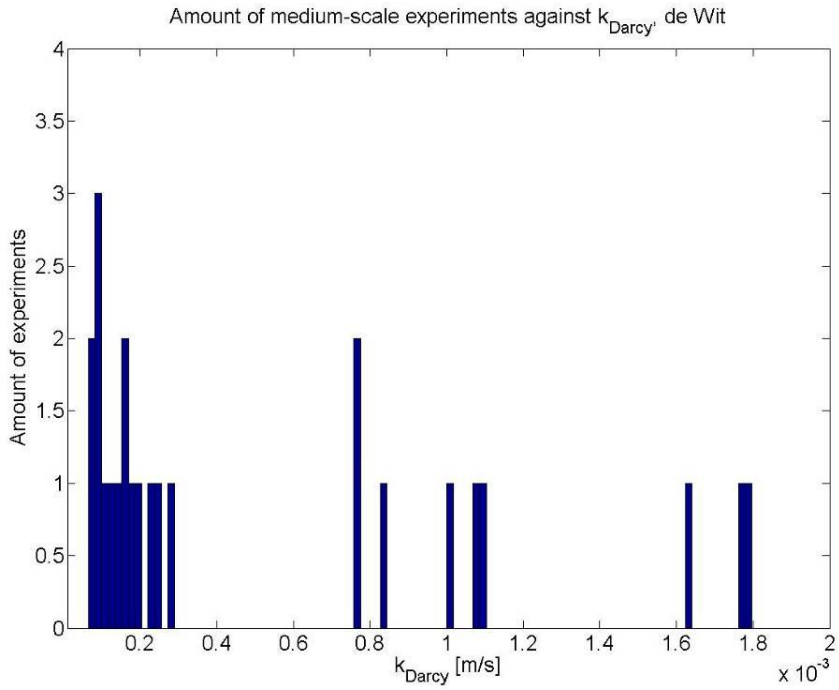

Figure M-15 a histogram of K_{Darcy} of the sand samples used for the medium-scale de Wit experiments

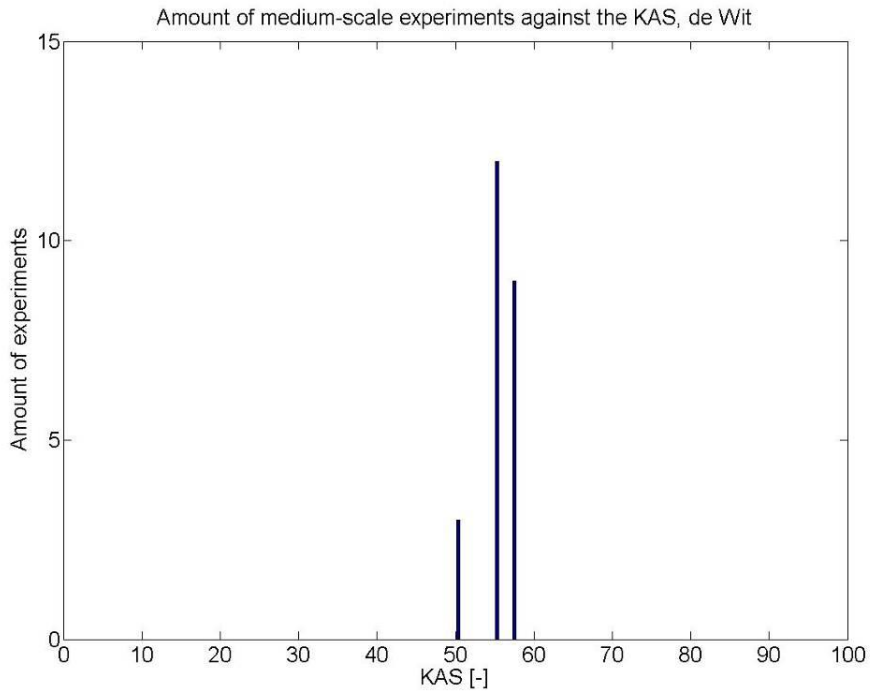

Figure M-16 a histogram of the KAS of the sand samples used for the medium-scale de Wit experiments

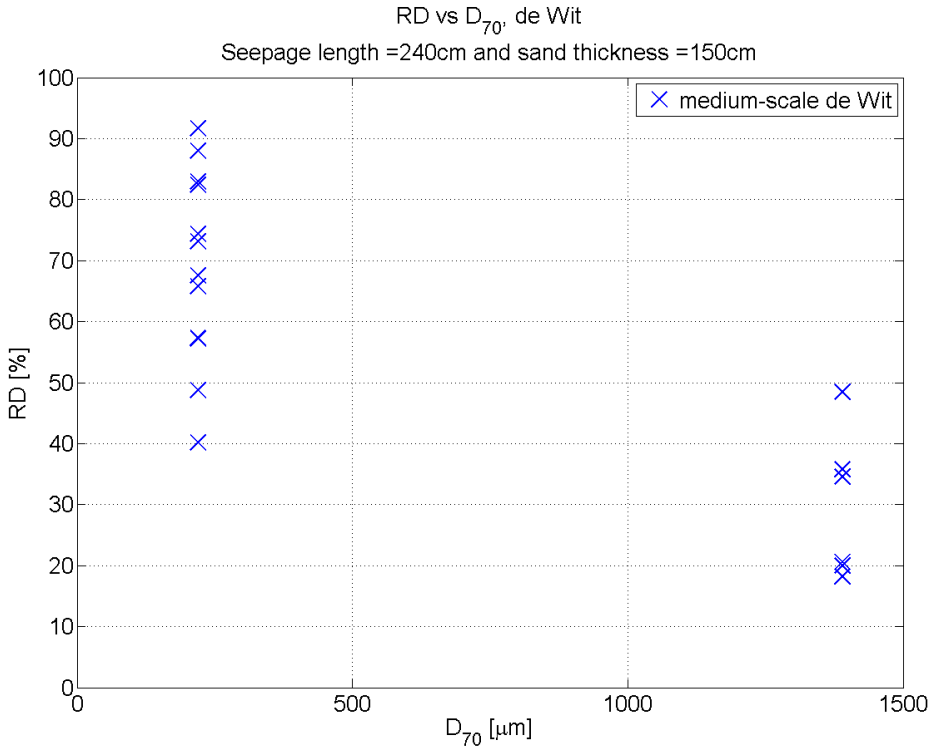

Figure M-17 RD plotted against the D_{70} for the medium-scale de Wit experiments

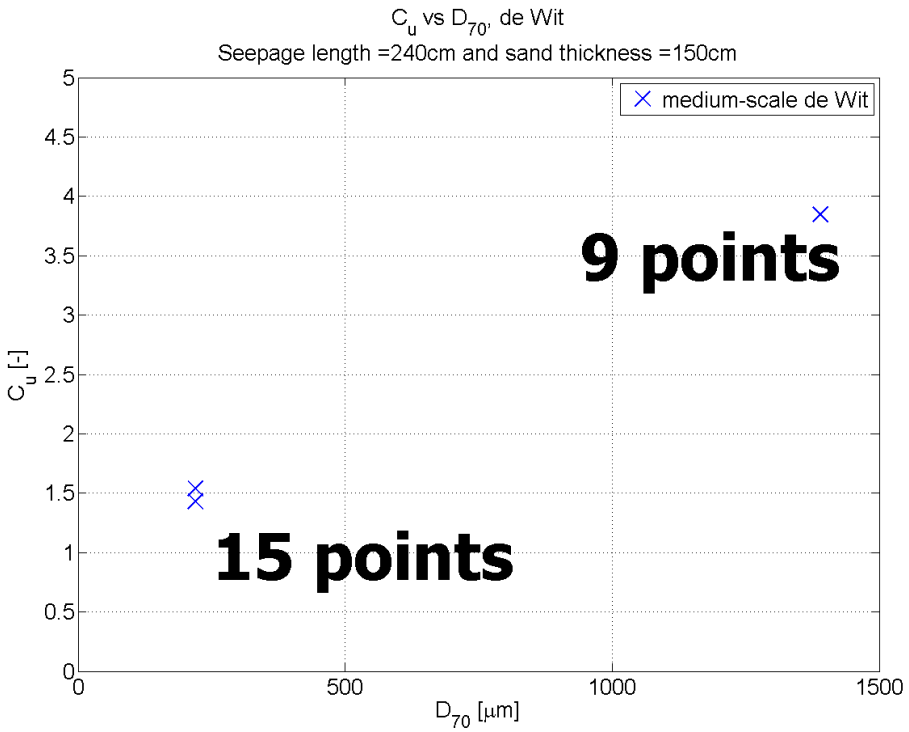

Figure M-18 C_u plotted against the D_{70} for the medium-scale de Wit experiments

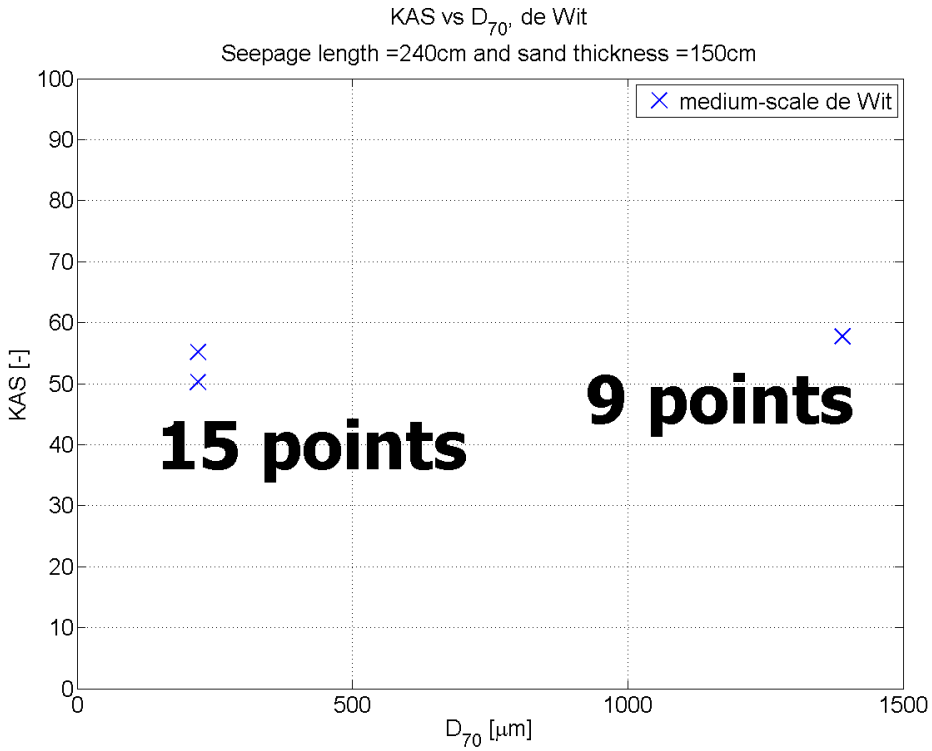

Figure M-19 KAS plotted against the D_{70} for the medium-scale de Wit experiments

N) Appendix N – Figures of Bligh data

In this appendix, several figures are shown. These figures were made by (Kanning, 2010) based on data from Bligh and Lane. The data came from a paper written by Lane (Lane, 1935). The figures of the Bligh formula on the data of Bligh for fine sand and coarse sand are shown in Figure N-1 and Figure N-2. As can be seen, there is a very high scatter in the data points. In Figure N-3 the estimated critical gradient as a function of grain size according to Bligh data is shown.

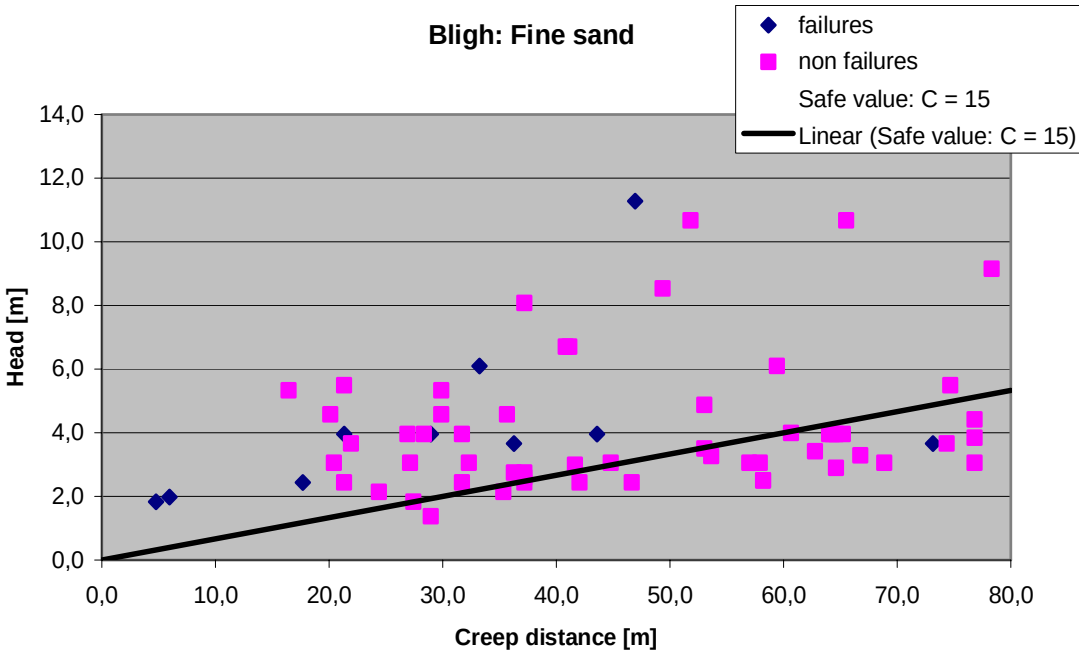

Figure N-1 the head as a function of the creep distance, for failures and non failures for fine sand, when the Bligh formula is applied on Bligh data (Kanning, 2010)

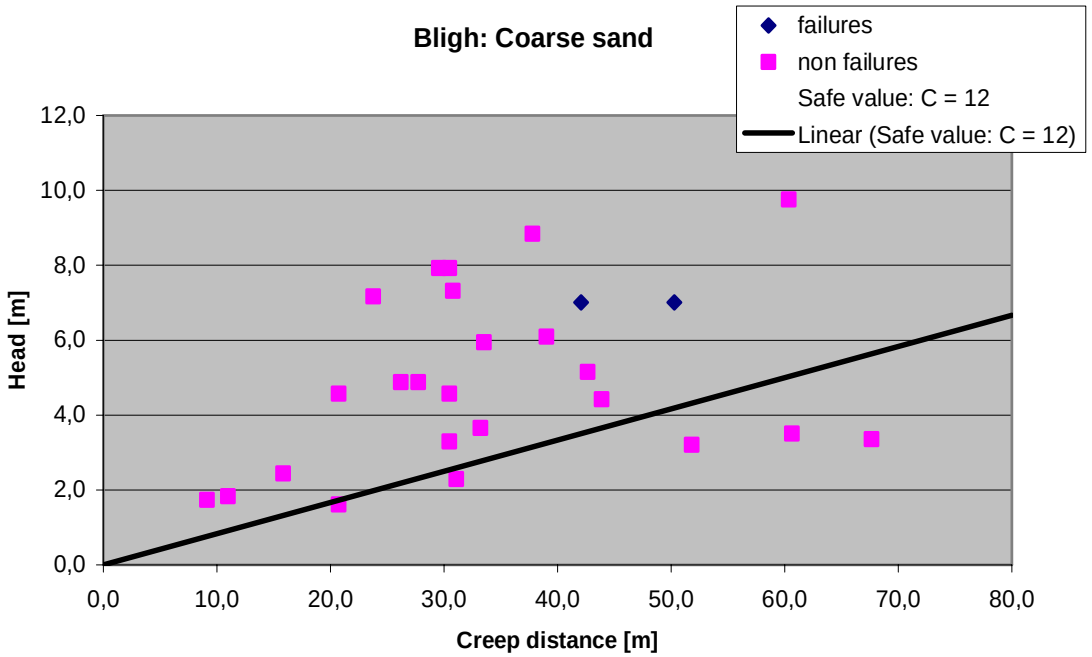

Figure N-2 the head as a function of the creep distance, for failures and non failures for coarse sand when the Bligh formula is applied on Bligh data (Kanning, 2010)

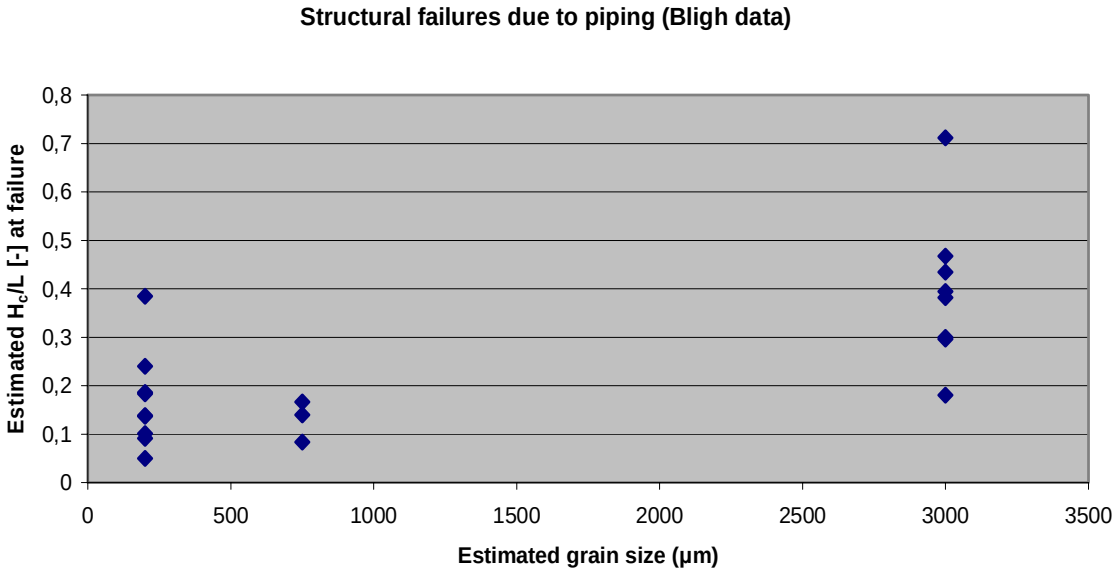

Figure N-3 the estimated critical gradient of failures as a function of grain size according to Bligh data (Kanning, 2010, adapted)

In Figure N-4 and Figure N-5 the estimated critical gradient of failures and non-failures of the Bligh data as a function of grain size is shown.

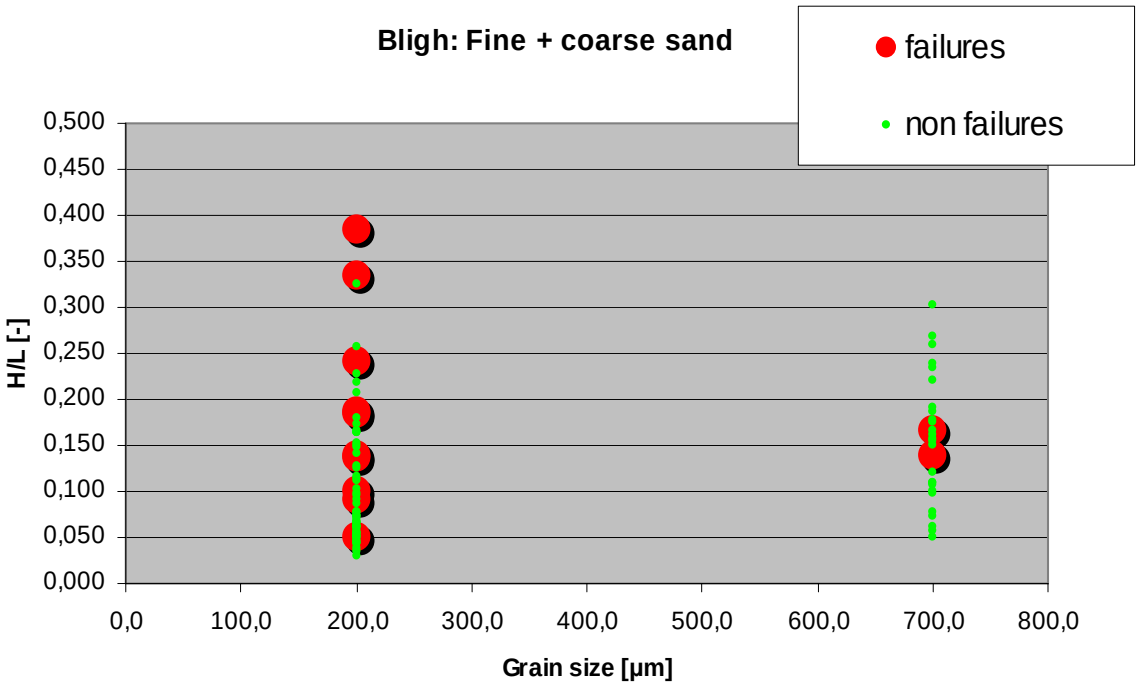

Figure N-4 the estimated gradient of failures and non failures as a function of grain size (only coarse and fine sand) according to Bligh data (Kanning, 2010, adapted)

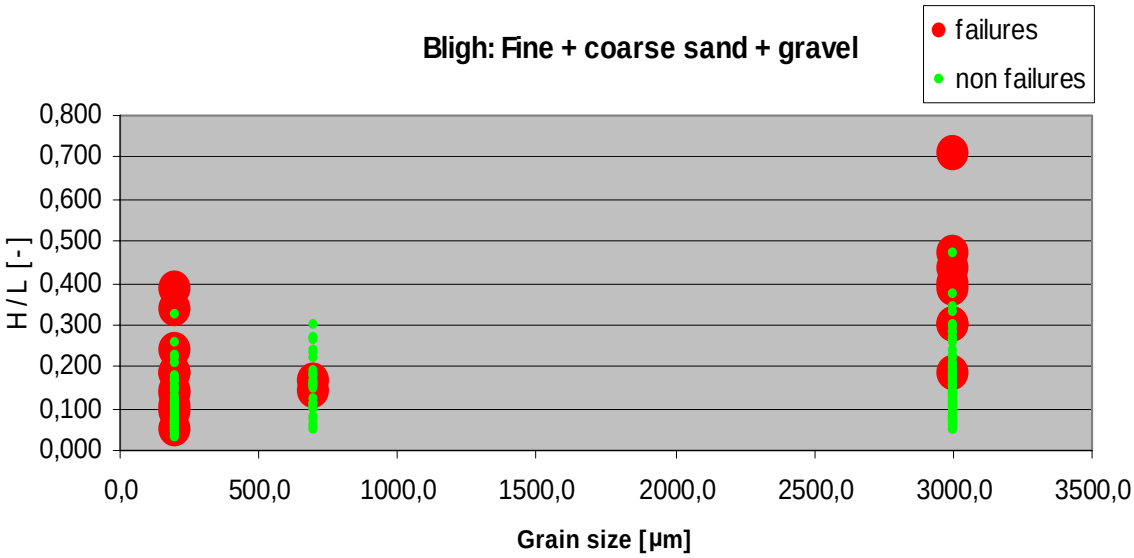

Figure N-5 the estimated gradient of failures and non-failures as a function of grain size (coarse and fine sand and gravel) according to Bligh data (Kanning, 2010, adapted)

O) Appendix O – Additional figures of slurry flow

In this appendix, some additional waves of sand (slurry flow) are showed. The results are much more clear on the video's. The blue arrow displays the front of the sand wave.

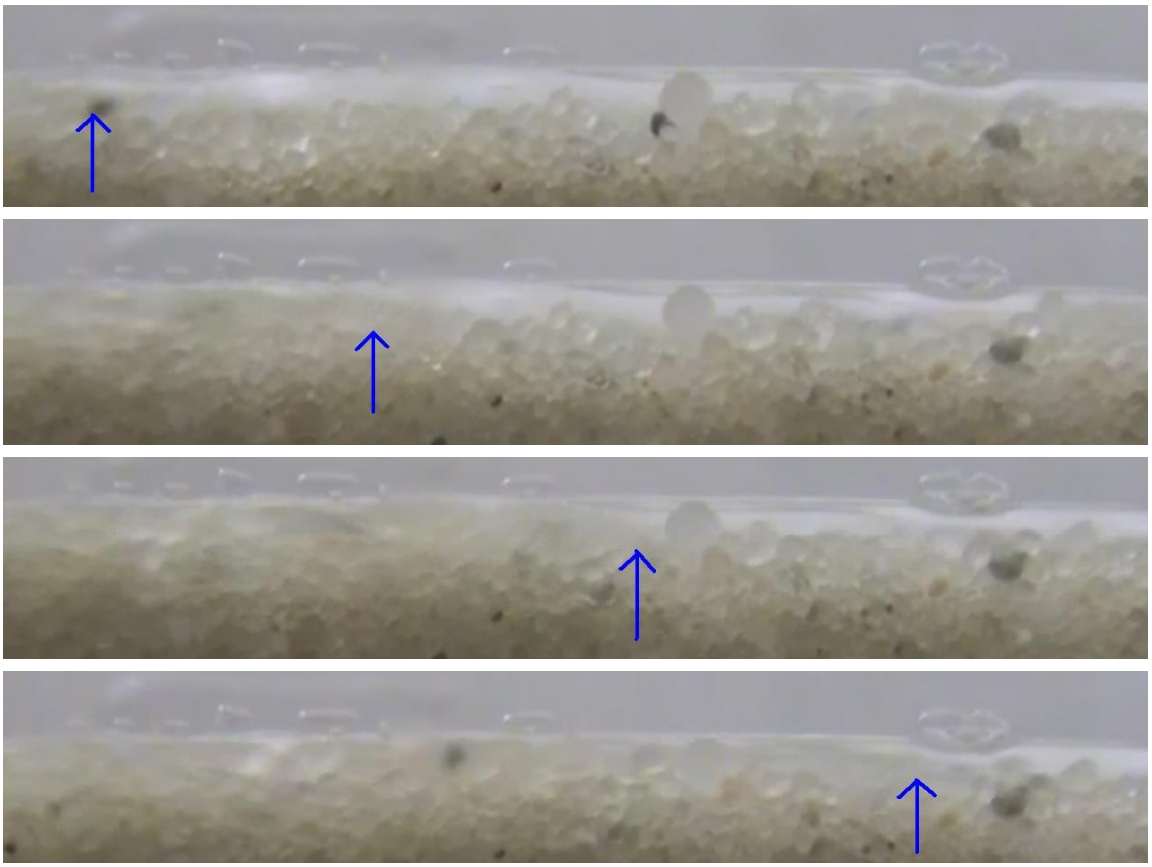

Figure O-1 the movement of a wave of grains in experiment Q14 5:08

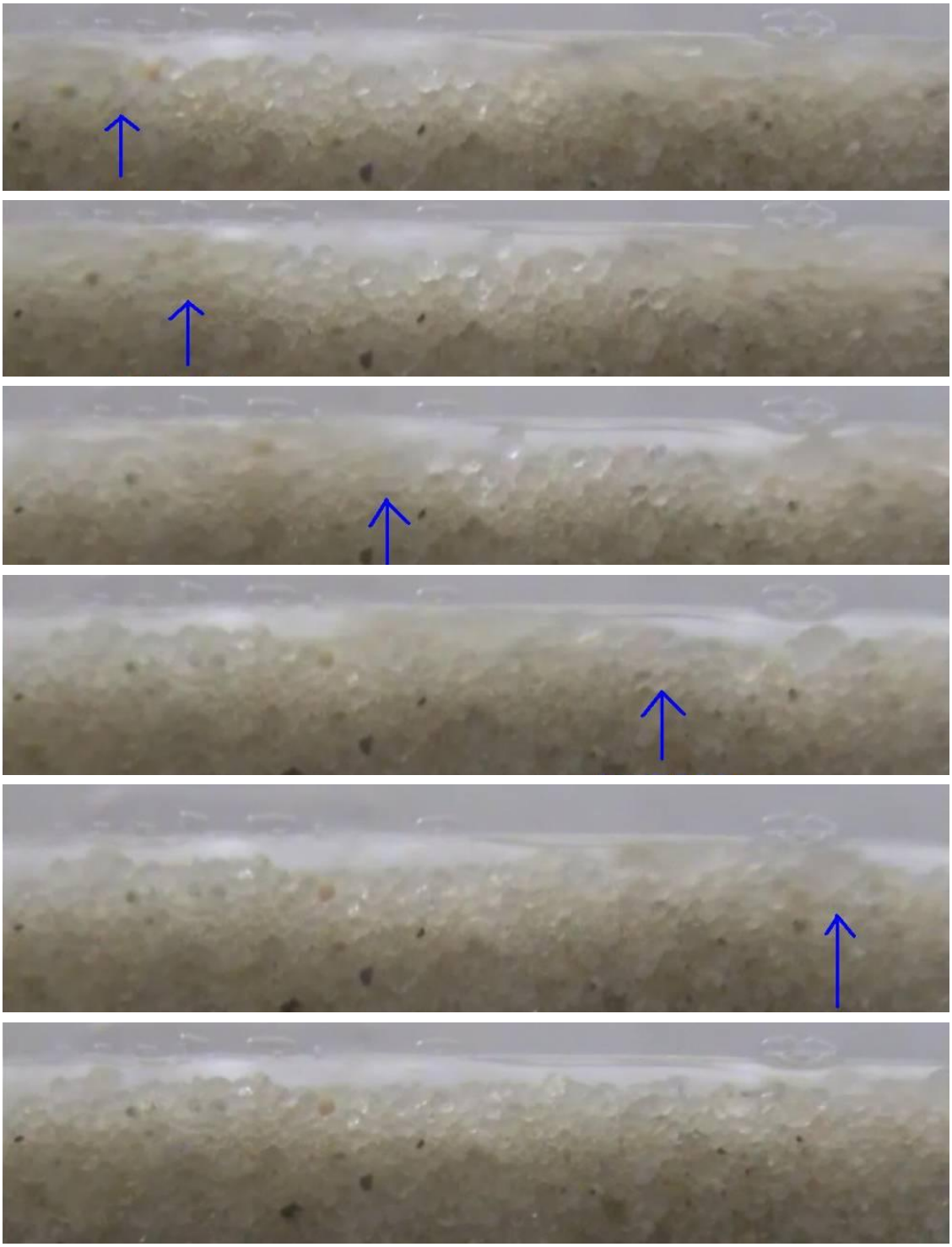

Figure O-2 the movement of a wave of grains in experiment Q14 05:10

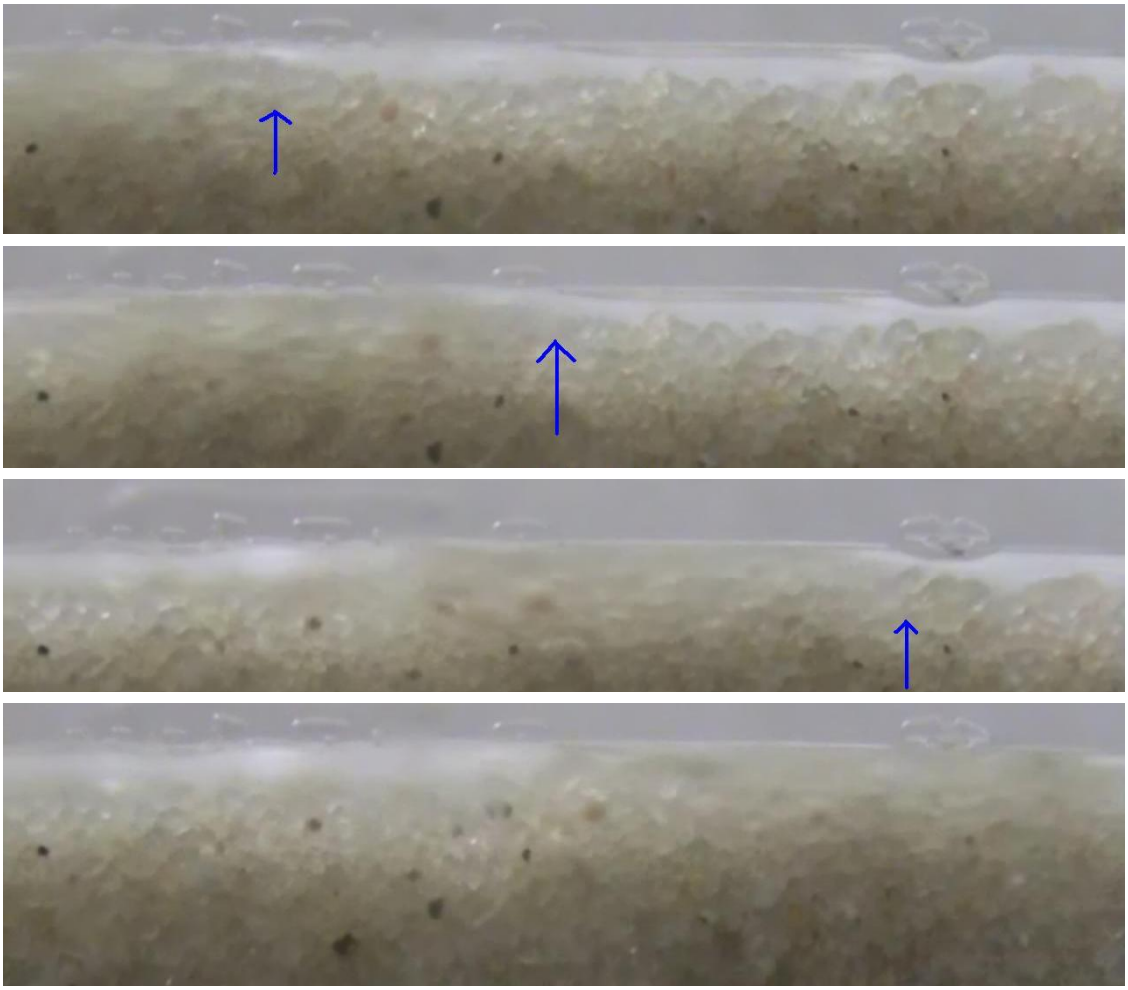

Figure O-3 the movement of a wave of grains in experiment Q14 5:10

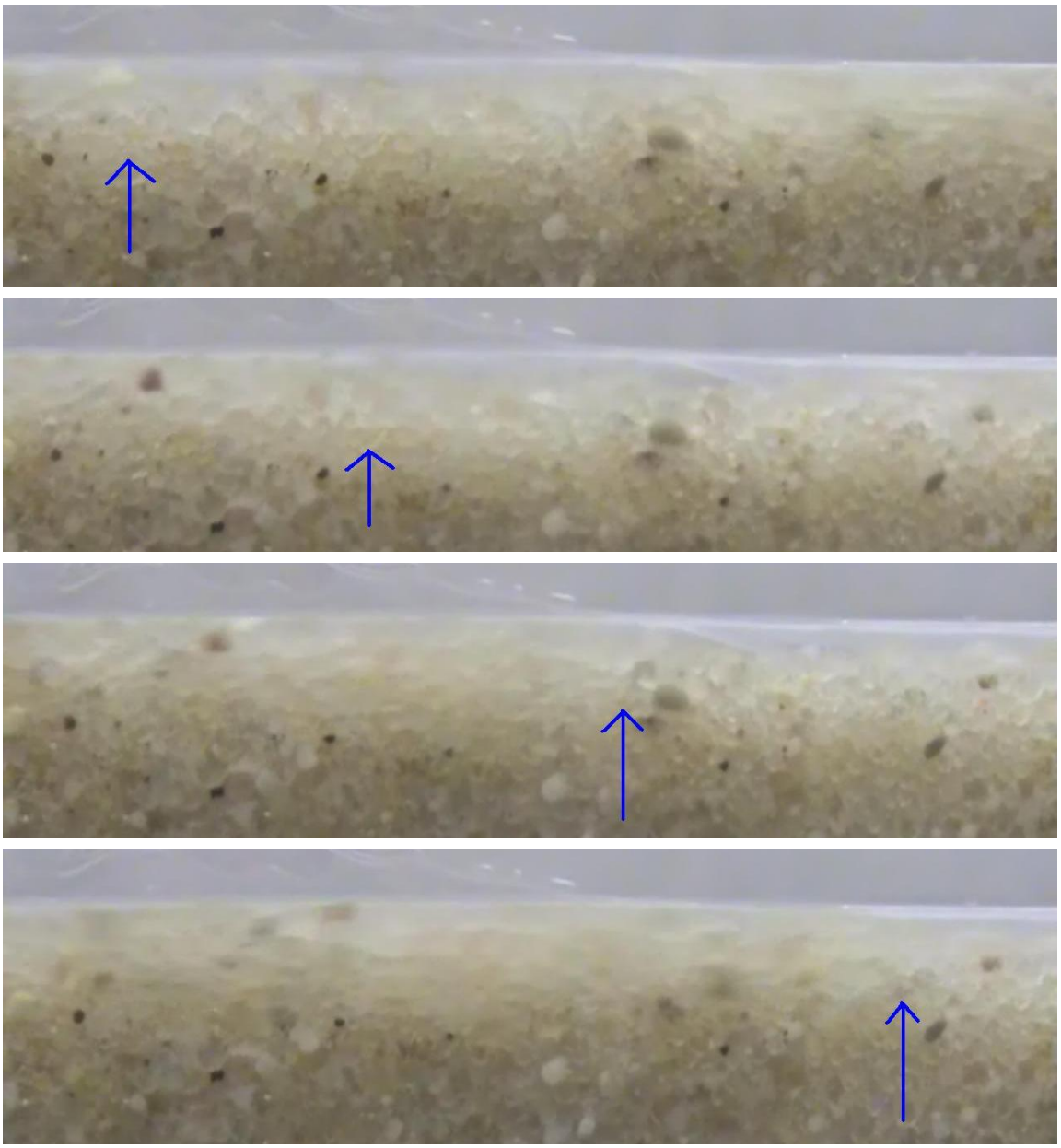

Figure O-4 the movement of a wave of grains in experiment Q06 07:19

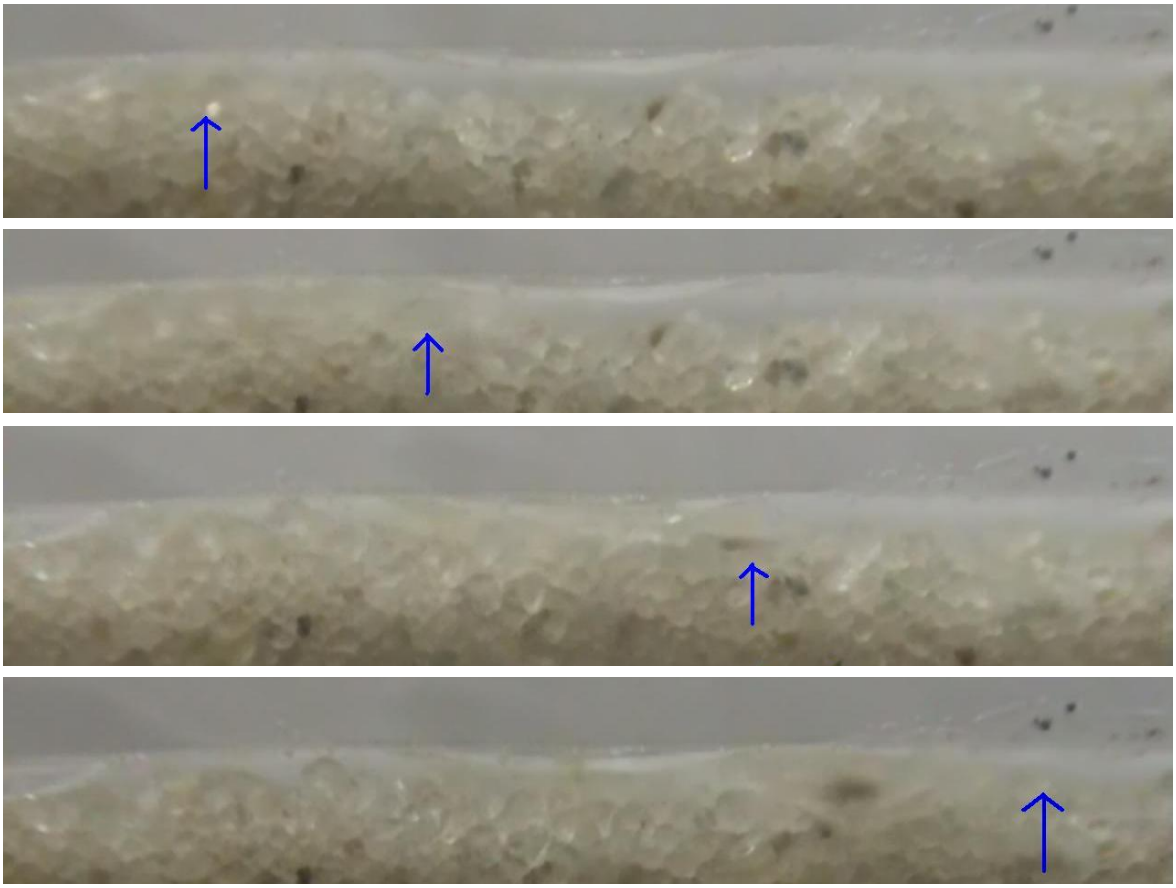

Figure O-5 the movement of a wave of grains in experiment Q15 8:22

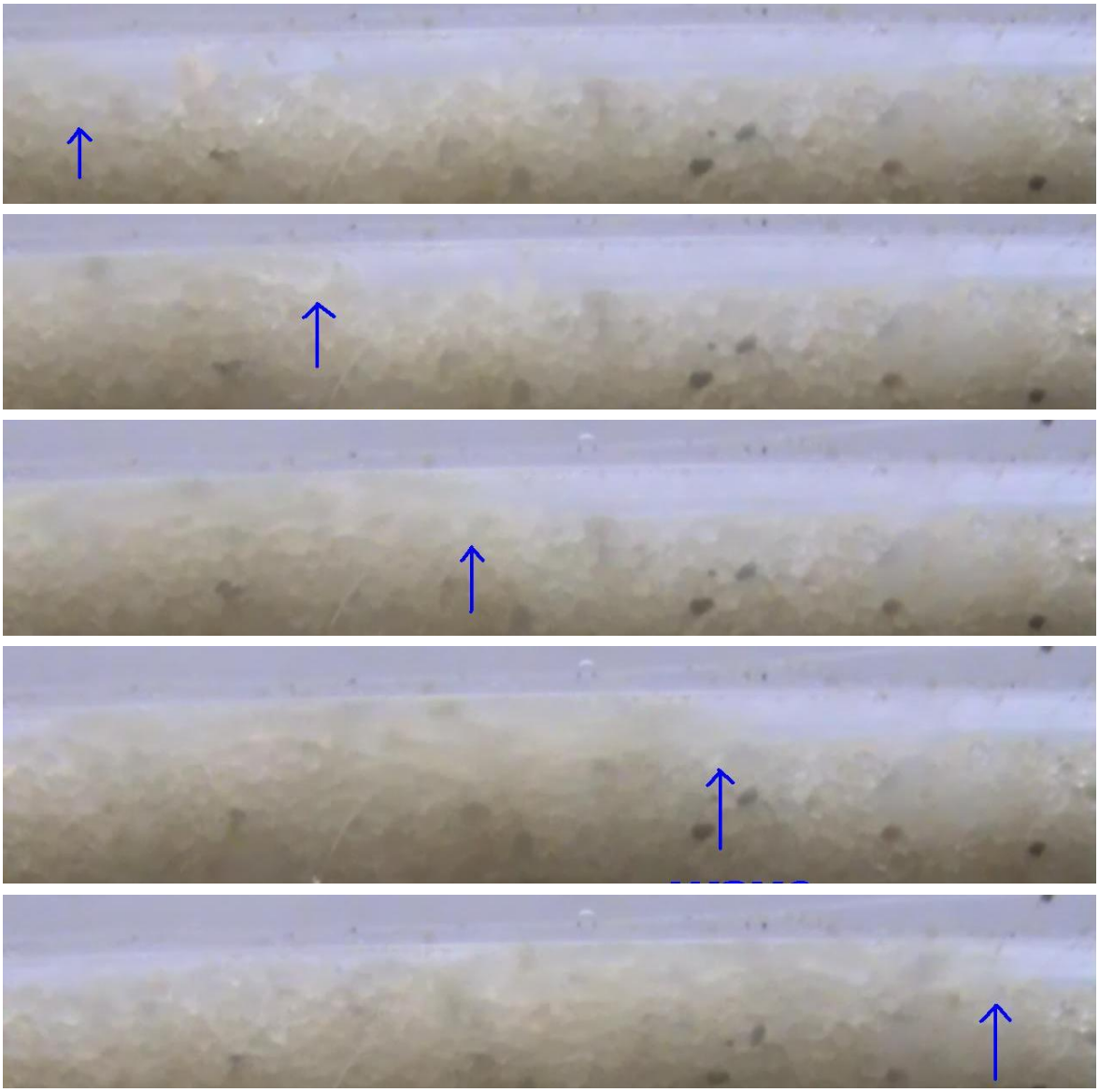

Figure O-6 the movement of a wave of grains in experiment Q18 1:41

P) Appendix P – The factual reports of the one-dimensional test facility

In this appendix, the factual reports of the experiments done with the one-dimensional test facility is treated.

Experiments Q01 to Q05 have been performed with the a test facility with putty on the inside. Experiments Q06 to Q18 have been performed with a test facility without putty on the inside.

Since it is very difficult to measure the relative density accurate, the relative density is estimated.

For experiments Q08 to Q18 (except Q12), the relative density is estimated to be 40-50%. For every experiment, the relative density is a bit lower than the previous one, because the sand was compacted a little less. The relative density is more around 50% for the experiments of Q08 and the 5 following and more around 40% for experiments Q18 and the 5 previous.

Factual report Q01
Date: September 29th
Time: 13:21

Sand type: Baskarp

Table P-1 the properties of the sand and the test facility for experiment Q01

thickness [cm]	1.0015
height [cm]	9.96
wanted length [cm]	38.4
wanted volume [cm^3]	383.0
surface [cm^2]	9.97
n_{max} Baskarp [-]	0.469
n_{min} Baskarp [-]	0.34
wanted relative density [%]	80
n [-]	0.3658
volume void [cm^3]	140.1
volume particles [cm^3]	242.9
mass particles [gr]	643.7
seepage length [cm]	37.0
measured length [cm]	38.4
temperature [°C]	21.0
real volume [cm^3]	383.0
real porosity [-]	0.3658
real relative density [%]	80

Table P-2 the head, discharge and permeability as a function of time for experiment Q01

minutes	stopwatch time	real time	head [cm]	time discharge measurement [s]	volume [cm^3]	discharge 10^{-9} [m^3/s]	k_{Darcy} 10^{-3} [m/s]	remarks
0	0:00:00	13:21:00	1	120	0.38	3.17	0.117	
5	0:05:00	13:26:00	2	180	0.83	4.61	0.086	
10	0:10:00	13:31:00	3	180	1.15	6.39	0.079	
15	0:15:00	13:36:00	4	180	1.61	8.94	0.083	
20	0:20:00	13:41:00	5	180	2.11	11.7	0.087	
25	0:25:00	13:46:00	6	120	1.26	10.5	0.065	
30	0:30:00	13:51:00	7	180	2.27	12.6	0.067	
35	0:35:00	13:56:00	8	180	2.63	14.6	0.068	
40	0:40:00	14:01:00	9	180	3.00	16.7	0.069	
45	0:45:00	14:06:00	10	180	3.09	17.2	0.064	
50	0:50:00	14:11:00	11	180	3.59	19.9	0.067	
55	0:55:00	14:16:00	12	180	4.03	22.4	0.069	
60	1:00:00	14:21:00	13	120	2.63	21.9	0.063	
65	1:05:00	14:26:00	14	180	4.46	24.8	0.066	
70	1:10:00	14:31:00	15	180	4.90	27.2	0.067	
75	1:15:00	14:36:00	16	180	5.20	28.9	0.067	
80	1:20:00	14:41:00	17	180	5.38	29.9	0.065	
85	1:25:00	14:46:00	18	180	5.90	32.8	0.068	
90	1:30:00	14:51:00	19	180	6.24	34.7	0.068	
95	1:35:00	14:56:00	20	180	6.57	36.5	0.068	
100	1:40:00	15:01:00	21	185	7.14	38.6	0.068	
105	1:45:00	15:06:00	22	180	7.02	39.0	0.066	
110	1:50:00	15:11:00	23	180	7.22	40.1	0.065	
115	1:55:00	15:16:00	24	180	7.63	42.4	0.066	
120	2:00:00	15:21:00	25	180	8.03	44.6	0.066	
125	2:05:00	15:26:00	26	180	8.32	46.2	0.066	
130	2:10:00	15:31:00	27	180	8.52	47.3	0.065	
135	2:15:00	15:36:00	28	120	5.88	49.0	0.065	
139	2:19:00	15:40:00	29	120	6.06	50.5	0.065	
143	2:23:00	15:44:00	30	120	6.42	53.5	0.066	
147	2:27:00	15:48:00	31	120	6.47	53.9	0.065	
151	2:31:00	15:52:00	32	120	6.76	56.3	0.065	
155	2:35:00	15:56:00	33	120	7.14	59.5	0.067	
159	2:39:00	16:00:00	34	120	7.24	60.3	0.066	
163	2:43:00	16:04:00	35	120	7.38	61.5	0.065	
167	2:47:00	16:08:00	36	120	7.40	61.7	0.064	
171	2:51:00	16:12:00	37	120	7.64	63.7	0.064	
175	2:55:00	16:16:00	38	120	8.11	67.6	0.066	
179	2:59:00	16:20:00	39	120	8.15	67.9	0.065	
								discharge measurement
183	3:03:00	16:24:00	40	120	9.29	77.4	0.072	invalid
187	3:07:00	16:28:00	41	120	8.64	72	0.065	
								full break
191	3:11:00	16:32:00	42					through

k_{Darcy} average = $6.903*10^{-5}$ m/s

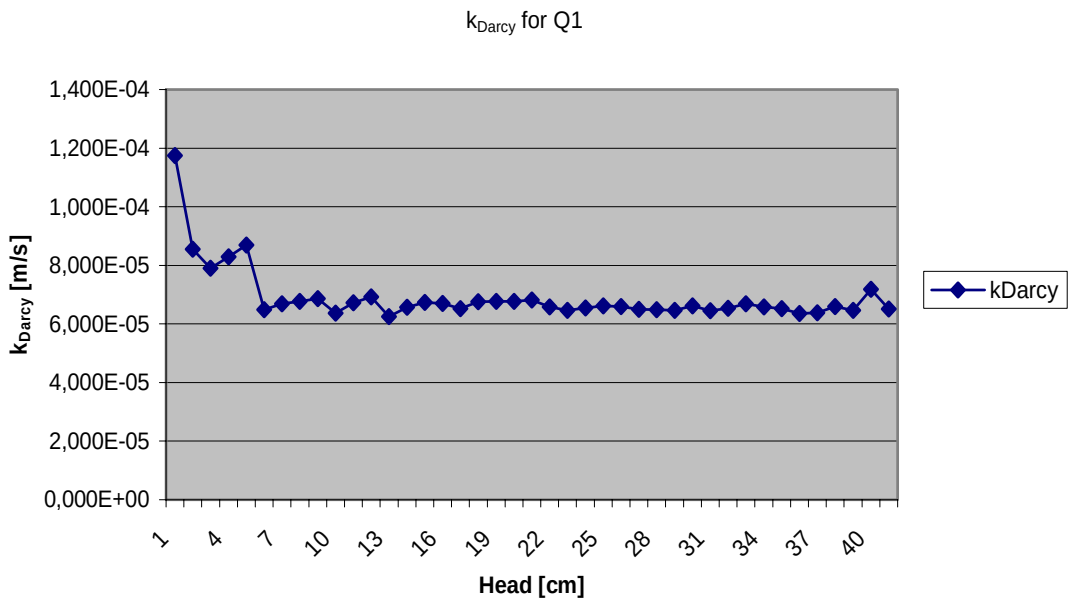

Figure P-1 k_{Darcy} as a function of the head for experiment Q01

Factual report Q2
Date: October 4th
Time: 13:40

Sand type: Baskarp

Table P-3 the properties of the sand and the test facility for experiment Q02

thickness [cm]	1.0015
height [cm]	9.96
wanted length [cm]	38.4
wanted volume [cm^3]	383.0
surface [cm^2]	9.97
n_{max} Baskarp [-]	0.469
n_{min} Baskarp [-]	0.34
wanted relative density [%]	80
n [-]	0.3658
volume void [cm^3]	140.1
volume particles [cm^3]	242.9
mass particles [gr]	643.7
seepage length [cm]	36.5
measured length [cm]	39.2
real volume [cm^3]	391.0
real porosity [-]	0.3787
real relative density [%]	70

Table P-4 the head, discharge and permeability as a function of time for experiment Q02

minutes	stopwatch time	real time	head [cm]	time discharge measurement [s]	volume [cm^3]	discharge 10^{-9} [m^3/s]	k_{Darcy} 10^{-3} [m/s]	remarks
0	0:00:00	13:40:00	1					
3	0:03:00	13:43:00	2					
6	0:06:00	13:46:00	3					
9	0:09:00	13:49:00	4					
12	0:12:00	13:52:00	5					
15	0:15:00	13:55:00	6					
18	0:18:00	13:58:00	7					
21	0:21:00	14:01:00	8					
24	0:24:00	14:04:00	9	2.81	2.81	46.8	0.190	
27	0:27:00	14:07:00	10					
30	0:30:00	14:10:00	11					
33	0:33:00	14:13:00	12					
36	0:36:00	14:16:00	13					
39	0:39:00	14:19:00	14					
42	0:42:00	14:22:00	15	4.63	4.63	77.2	0.188	
45	0:45:00	14:25:00	16					
48	0:48:00	14:28:00	17					
51	0:51:00	14:31:00	18					piping. channel cleared
59	0:59:00	14:39:00	19					
68	1:08:00	14:48:00	20					
71	1:11:00	14:51:00	21					
75.7	1:15:40	14:55:40	22					
81	1:21:00	15:01:00	23					
92	1:32:00	15:12:00	24					
101	1:41:00	15:21:00	25					
105	1:45:00	15:25:00	26					
110	1:50:00	15:30:00	30					
111.7	1:51:40	15:31:40	35					
113	1:53:00	15:33:00	40					

k_{Darcy} average = $1.893*10^{-4}$ m/s

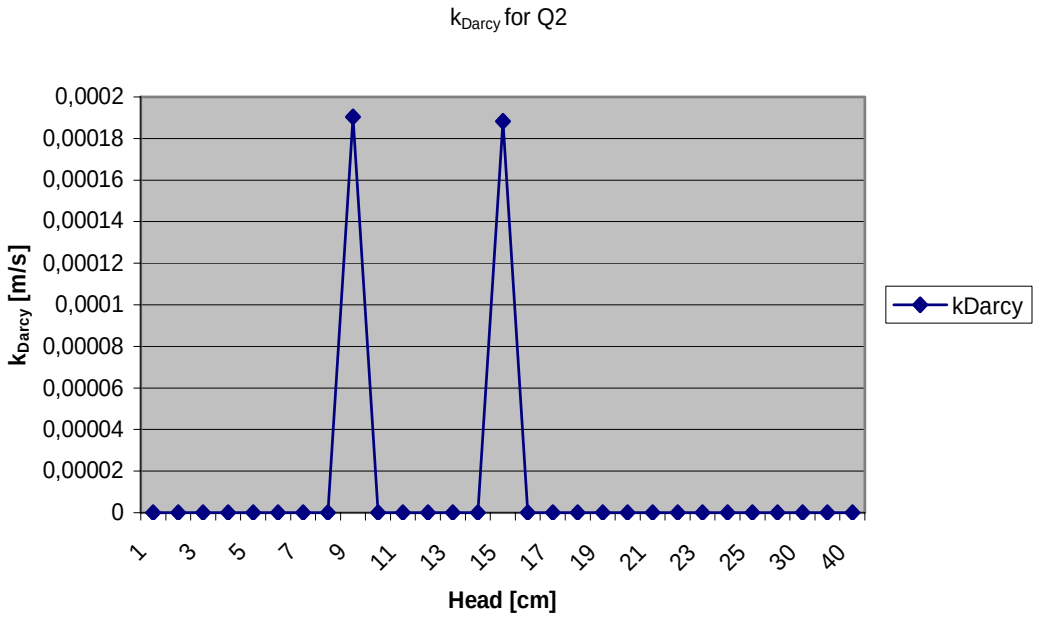

Figure P-2 k_{Darcy} as a function of the head for experiment Q02

Factual report Q03
Date: November 18th
Time: 13:30

Sand type: Baskarp

Table P-5 the properties of the sand and the test facility for experiment Q03

thickness [cm]	1.0015
height [cm]	9.96
wanted length [cm]	38.4
wanted volume [cm^3]	383.0
surface [cm^2]	9.97
n_{max} Baskarp [-]	0.469
n_{min} Baskarp [-]	0.34
wanted relative density [%]	80
n [-]	0.3658
volume void [cm^3]	140.1
volume particles [cm^3]	242.9
mass particles [gr]	643.7
seepage length [cm]	37.2
measured length [cm]	39.2
real volume [cm^3]	391.0
real porosity [-]	0.3787
real relative density [%]	70

Table P-6 the head, discharge and permeability as a function of time for experiment Q03

minutes	stopwatch time	real time	head [cm]	time discharge measurement [s]	volume [cm^3]	discharge 10^{-9} [m^3/s]	k_{Darcy} 10^{-3} [m/s]	remarks
0	0:00:00	13:30:00	1					
2	0:02:00	13:32:00	2					
4	0:04:00	13:34:00	3					
6	0:06:00	13:36:00	4					
8	0:08:00	13:38:00	5					
10	0:10:00	13:40:00	6					
12	0:12:00	13:42:00	7					
14	0:14:00	13:44:00	8					
16	0:16:00	13:46:00	9					
18	0:18:00	13:48:00	10	120	2.3	19.2	0.0715	
20	0:20:00	13:50:00	11					
23	0:23:00	13:53:00	12					
26	0:26:00	13:56:00	13					
29	0:29:00	13:59:00	14					
32	0:32:00	14:02:00	15					
35	0:35:00	14:05:00	16					
38	0:38:00	14:08:00	17					
41	0:41:00	14:11:00	18					
44	0:44:00	14:14:00	19					
47	0:47:00	14:17:00	20					
50	0:50:00	14:20:00	21					
53	0:53:00	14:23:00	22					
56	0:56:00	14:26:00	23					
59	0:59:00	14:29:00	24	120	4.3	35.8	0.0557	
62	1:02:00	14:32:00	25					
65	1:05:00	14:35:00	26					
68	1:08:00	14:38:00	27					
71	1:11:00	14:41:00	25					
73	1:13:00	14:43:00	27					
75	1:15:00	14:45:00	28					
78	1:18:00	14:48:00	29					
81	1:21:00	14:51:00	30					
84	1:24:00	14:54:00	31					
87	1:27:00	14:57:00	32					
90	1:30:00	15:00:00	33					
93	1:33:00	15:03:00	34					
96	1:36:00	15:06:00	35					
99	1:39:00	15:09:00	36					
102	1:42:00	15:12:00	37					
105	1:45:00	15:15:00	38					
108	1:48:00	15:18:00	39					pipin
122	2:02:00	15:32:00	44					

k_{Darcy} average = $6.36*10^{-5}$ m/s

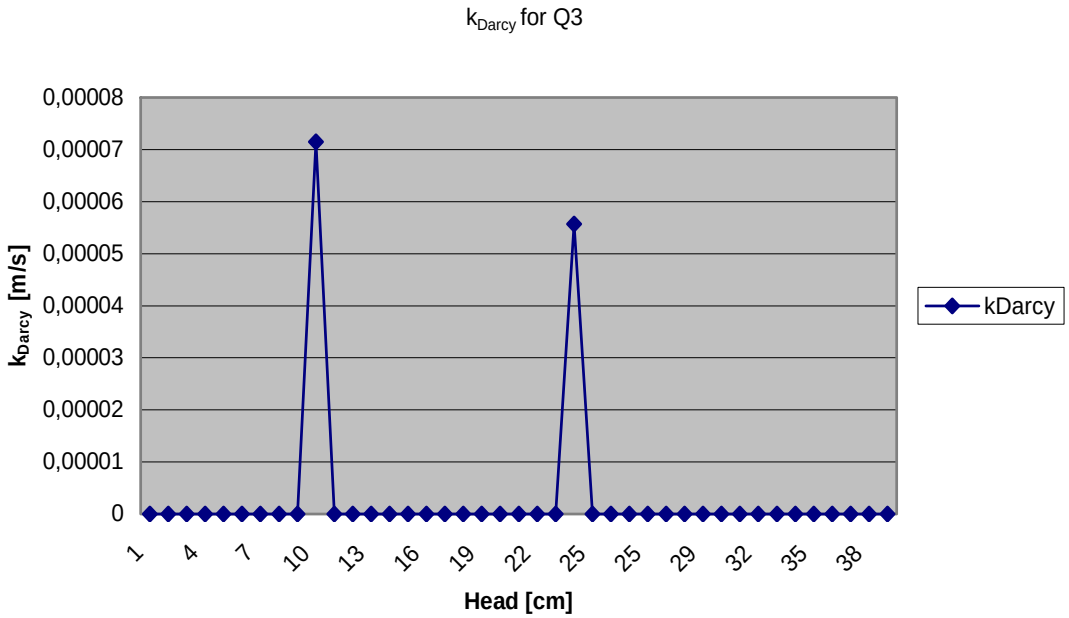

Figure P-3 k_{Darcy} as a function of the head for experiment Q03

Factual report Q04
Date: November 22th
Time: 13:10

Sand type: Ringstrasse Itterbeck Enschede

Table P-7 the properties of the sand and the test facility for experiment Q04

thickness [cm]	1.0015
height [cm]	9.96
wanted length [cm]	38.4
wanted volume [cm^3]	383.0
surface [cm^2]	9.97
n_{max} Ringstrasse Itterbeck Enschede [-]	0.4106
n_{min} Ringstrasse Itterbeck Enschede [-]	0.3201
wanted relative density [%]	80
n [-]	0.3382
volume void [cm^3]	129.5
volume particles [cm^3]	253.5
mass particles [gr]	671.7
seepage length [cm]	37.2
measured length [cm]	38.5
real volume [cm^3]	384.0
real porosity [-]	0.3399
real relative density [%]	78

Table P-8 the head, discharge and permeability as a function of time for experiment Q04

minutes	stopwatch time	real time	head [cm]	time discharge measurement [s]	volume [cm^3]	discharge 10^{-9} [m^3/s]	k_{Darcy} 10^{-3} [m/s]	remarks
0	0:00:00	13:10:00	1					
2	0:02:00	13:12:00	2					
4	0:04:00	13:14:00	3					
6	0:06:00	13:16:00	4					
8	0:08:00	13:18:00	5					
10	0:10:00	13:20:00	6					
12	0:12:00	13:22:00	7					
14	0:14:00	13:24:00	8					
16	0:16:00	13:26:00	9					
18	0:18:00	13:28:00	10	120	10.1	84.2	0.314	
20	0:20:00	13:30:00	11					
23	0:23:00	13:33:00	12					
26	0:26:00	13:36:00	13					
29	0:29:00	13:39:00	14					
32	0:32:00	13:42:00	15					
35	0:35:00	13:45:00	16					
38	0:38:00	13:48:00	17	120	17.8	148.3	0.325	
41	0:41:00	13:51:00	18					
44	0:44:00	13:54:00	19					
47	0:47:00	13:57:00	20					
50	0:50:00	14:00:00	21					
53	0:53:00	14:03:00	22					
56	0:56:00	14:06:00	23					
59	0:59:00	14:09:00	24					
62	1:02:00	14:12:00	25					
65	1:05:00	14:15:00	26					
68	1:08:00	14:18:00	27					
71	1:11:00	14:21:00	28					
74	1:14:00	14:24:00	29					
77	1:17:00	14:27:00	30					
80	1:20:00	14:30:00	31					
83	1:23:00	14:33:00	32					
86	1:26:00	14:36:00	33	120	34	283.3	0.320	
89	1:29:00	14:39:00	34					
92	1:32:00	14:42:00	35					
95	1:35:00	14:45:00	36					
98	1:38:00	14:48:00	37					
101	1:41:00	14:51:00	38					
104	1:44:00	14:54:00	39					
107	1:47:00	14:57:00	40					
110	1:50:00	15:00:00	41					
113	1:53:00	15:03:00	42					
116	1:56:00	15:06:00	43					
119	1:59:00	15:09:00	44					
121	2:01:00	15:11:00	45					

minutes	stopwatch time	real time	head [cm]	time discharge measurement [s]	volume [cm^3]	discharge 10^{-9} [m^3/s]	k_{Darcy} 10^{-3} [m/s]	remarks
124	2:04:00	15:14:00	46					
127	2:07:00	15:17:00	47					
130	2:10:00	15:20:00	48	120	52.5	437.5	0.340	
133	2:13:00	15:23:00	49					
136	2:16:00	15:26:00	50					
139	2:19:00	15:29:00	51					
142	2:22:00	15:32:00	52					
145	2:25:00	15:35:00	53					piping

k_{Darcy} average = $0.325*10^{-3}$ m/s

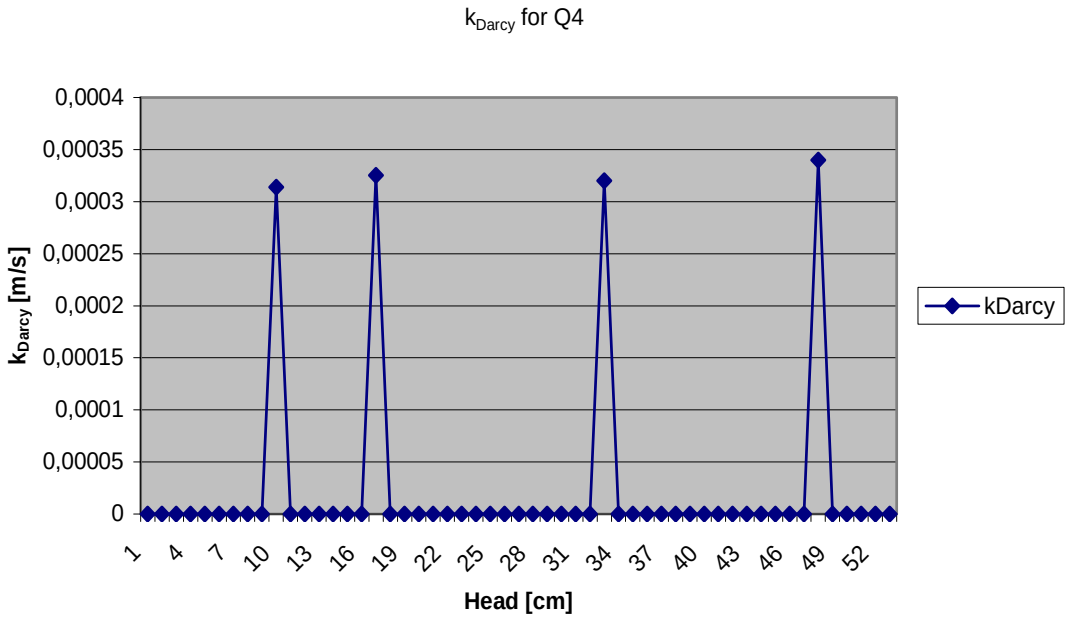

Figure P-4 k_{Darcy} as a function of the head for experiment Q04

Factual report Q05
Date: November 23th
Time: 14:55

Sand type: Ringstrasse Itterbeck Enschede

Table P-9 the properties of the sand and the test facility for experiment Q05

thickness [cm]	1.0015
height [cm]	9.96
wanted length [cm]	38.4
wanted volume [cm^3]	383.0
surface [cm^2]	9.97
n_{max} Ringstrasse Itterbeck Enschede [-]	0.4106
n_{min} Ringstrasse Itterbeck Enschede [-]	0.3201
wanted relative density [%]	50
n [-]	0.365
volume void [cm^3]	139.9
volume particles [cm^3]	243.1
mass particles [gr]	644.2
seepage length [cm]	35.4
measured length [cm]	38.8
real volume [cm^3]	384.0
real porosity [-]	0.372
real relative density [%]	43

Table P-10 the head, discharge and permeability as a function of time for experiment Q05

minutes	stopwatch time	real time	head [cm]	time discharge measurement [s]	volume [cm^3]	discharge 10^{-9} [m^3/s]	k_{Darcy} 10^{-3} [m/s]	remarks
0	0:00:00	14:55:00	1					
1	0:01:00	14:56:00	2					
2	0:02:00	14:57:00	3					
3	0:03:00	14:58:00	4					
4	0:04:00	14:59:00	5					
5	0:05:00	15:00:00	6					
6	0:06:00	15:01:00	7					
7	0:07:00	15:02:00	8					
8	0:08:00	15:03:00	9					
9	0:09:00	15:04:00	10					
10	0:10:00	15:05:00	11					
12	0:12:00	15:07:00	12					
14	0:14:00	15:09:00	13	120	21.1	176	0.480	
16	0:16:00	15:11:00	14					
18	0:18:00	15:13:00	15					
20	0:20:00	15:15:00	16					
22	0:22:00	15:17:00	17					
24	0:24:00	15:19:00	18					Several grains move
26	0:26:00	15:21:00	19					Several grains move
28	0:28:00	15:23:00	20					Several grains move
30	0:30:00	15:25:00	21					Several grains move
32	0:32:00	15:27:00	22					Several grains move
34	0:34:00	15:29:00	23					Several grains move
36	0:36:00	15:31:00	24					Several grains move
38	0:38:00	15:33:00	25					Several grains move
40	0:40:00	15:35:00	26					Several grains move
43	0:43:00	15:38:00	27					piping
49	0:49:00	15:44:00	40					
50	0:50:00	15:45:00	52					

k_{Darcy} average = $0.480*10^{-3}$ m/s

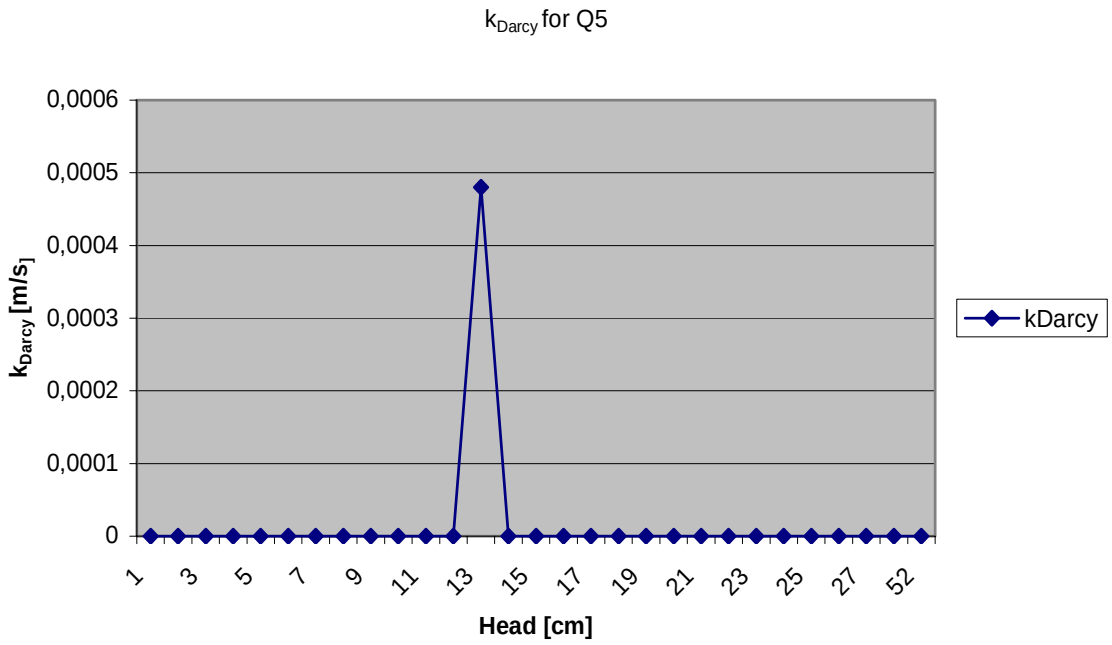

Figure P-5 k_{Darcy} as a function of the head for experiment Q05

Factual report Q06
Date: December 23th
Time: 15:00

Sand type: Ringstrasse Itterbeck Enschede

Table P-11 the properties of the sand and the test facility for experiment Q06

thickness [cm]	0.99
height [cm]	9.97
wanted length [cm]	38.4
wanted volume [cm^3]	379.0
surface [cm^2]	9.87
n_{max} Ringstrasse Itterbeck Enschede [-]	0.4106
n_{min} Ringstrasse Itterbeck Enschede [-]	0.3201
wanted relative density [%]	50
n [-]	0.365
volume void [cm^3]	138.5
volume particles [cm^3]	240.5
mass particles [gr]	692.5
seepage length[*1] [cm]	36.5
measured length [cm]	38.5
estimated relative density [%]	60

[*1] the real seepage length is 4.5cm less, because the sand does not make contact with the cover over the full length

Table P-12 the head, discharge and permeability as a function of time for experiment Q06

minutes	stopwatch time	real time	head [cm]	time discharge measurement [s]	volume [cm^3]	discharge 10^{-9} [m^3/s]	k_{Darcy} 10^{-3} [m/s]	remarks
0	0:00:00	15:00:00	1					
2	0:02:00	15:02:00	2					
3	0:03:00	15:03:00	3					
5	0:05:00	15:05:00	4					
6	0:06:00	15:06:00	5					
8	0:08:00	15:08:00	6					
9	0:09:00	15:09:00	7					
11	0:11:00	15:11:00	8					
12	0:12:00	15:12:00	9					
14	0:14:00	15:14:00	10					
16	0:16:00	15:16:00	11					
18	0:18:00	15:18:00	12					
20	0:20:00	15:20:00	13					
22	0:22:00	15:22:00	14					
24	0:24:00	15:24:00	15	120	21.40	178	0.440	
26	0:26:00	15:26:00	16					
28	0:28:00	15:28:00	17					
30	0:30:00	15:30:00	18					
32	0:32:00	15:32:00	19					
34	0:34:00	15:34:00	20					
36	0:36:00	15:36:00	21					
38	0:38:00	15:38:00	22	120	32.30	269	0.452	
41	0:41:00	15:41:00	23					
43	0:43:00	15:43:00	24					
45	0:45:00	15:45:00	25					
47	0:47:00	15:47:00	26					
49	0:49:00	15:49:00	27					
51	0:51:00	15:51:00	28					
53	0:53:00	15:53:00	29					
55	0:55:00	15:55:00	30					
57	0:57:00	15:57:00	31					small sinus shaped channel of 4cm piping
59	0:59:00	15:59:00	32					
66	1:06:00	16:06:00	33					

k_{Darcy} average = $0.446*10^{-3}$ m/s

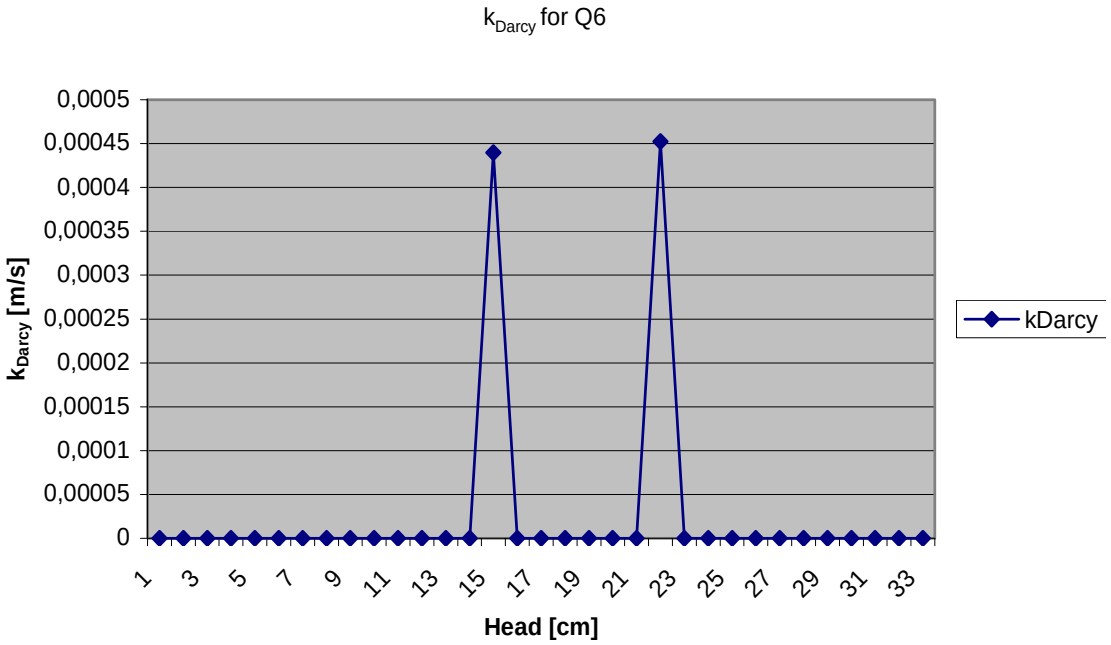

Figure P-6 k_{Darcy} as a function of the head for experiment Q06

Factual report Q07
Date: December 24th
Time: 13:00

Sand type: Ringstrasse Itterbeck Enschede

Table P-13 the properties of the sand and the test facility for experiment Q07

thickness [cm]	0.99
height [cm]	9.97
wanted length [cm]	38.4
wanted volume [cm^3]	379.0
surface [cm^2]	9.87
n_{max} Ringstrasse Itterbeck Enschede [-]	0.4106
n_{min} Ringstrasse Itterbeck Enschede [-]	0.3201
wanted relative density [%]	50
n [-]	0.365
volume void [cm^3]	138.5
volume particles [cm^3]	240.5
mass particles [gr]	692.5
seepage length [cm]	36.5
measured length [cm]	39.5
estimated relative density [%]	60

Table P-14 the head, discharge and permeability as a function of time for experiment Q07

minutes	stopwatch time	real time	head [cm]	time discharge measurement [s]	volume [cm^3]	discharge 10^{-9} [m^3/s]	k_{Darcy} 10^{-3} [m/s]	remarks
0	0:00:00	13:00:00	1					
2	0:02:00	13:02:00	2					
3	0:03:00	13:03:00	3					
4	0:04:00	13:04:00	4					
5	0:05:00	13:05:00	5					
6	0:06:00	13:06:00	6					
7	0:07:00	13:07:00	7					
8	0:08:00	13:08:00	8					
9	0:09:00	13:09:00	9					
10	0:10:00	13:10:00	10					
12	0:12:00	13:12:00	11					
14	0:14:00	13:14:00	12					
15	0:15:00	13:15:00	13					
18	0:18:00	13:18:00	14					
20	0:20:00	13:20:00	15	120	27	225	0.539	
23	0:23:00	13:23:00	16					
25	0:25:00	13:25:00	17					
27	0:27:00	13:27:00	18					
29	0:29:00	13:29:00	19					
31	0:31:00	13:31:00	20					
33	0:33:00	13:33:00	21					
35	0:35:00	13:35:00	22	120	38	317	0.518	
38	0:38:00	13:38:00	23					cloud
43	0:43:00	13:43:00	24					
47	0:47:00	13:47:00	25					
50	0:50:00	13:50:00	26					
54	0:54:00	13:54:00	27					
57	0:57:00	13:57:00	28					
60	1:00:00	14:00:00	29					
64	1:04:00	14:04:00	30					
68	1:08:00	14:08:00	31					
72	1:12:00	14:12:00	32					piping

k_{Darcy} average = $0.529*10^{-3}$ m/s

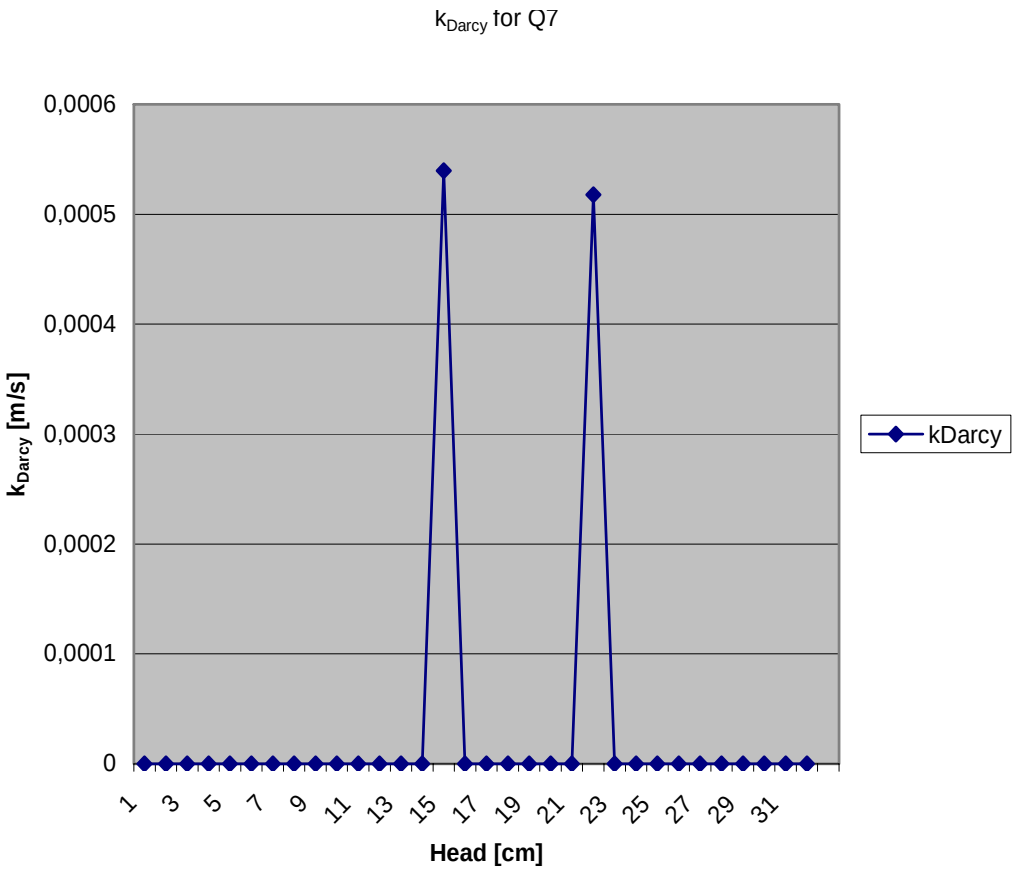

Figure P-7 k_{Darcy} as a function of the head for experiment Q07

Factual report Q08
Date: December 27th
Time: 13:00

Sand type: Ringstrasse Itterbeck Enschede

Table P-15 the properties of the sand and the test facility for experiment Q08

thickness [cm]	0.99
height [cm]	9.97
wanted length [cm]	38.4
wanted volume [cm^3]	379.0
surface [cm^2]	9.87
n_{max} Ringstrasse Itterbeck Enschede [-]	0.4106
n_{min} Ringstrasse Itterbeck Enschede [-]	0.3201
wanted relative density [%]	50
n [-]	0.365
volume void [cm^3]	138.5
volume particles [cm^3]	240.5
mass particles [gr]	717.2
seepage length[*1] [cm]	35.2
measured length [cm]	39.2
estimated relative density [%]	40-50

[*1] the real seepage length is 2cm less, because the sand does not make contact with the cover over the full length

Table P-16 the head, discharge and permeability as a function of time for experiment Q08

minutes	stopwatch time	real time	head [cm]	time discharge measurement [s]	volume [cm^3]	discharge 10^{-9} [m^3/s]	k_{Darcy} 10^{-3} [m/s]	remarks
0	0:00:00	13:00:00	1					
1	0:01:00	13:01:00	2					
2	0:02:00	13:02:00	3					
3	0:03:00	13:03:00	4					
4	0:04:00	13:04:00	5					
5	0:05:00	13:05:00	6					
6	0:06:00	13:06:00	7					
7	0:07:00	13:07:00	8					
8	0:08:00	13:08:00	9					
9	0:09:00	13:09:00	10					
11	0:11:00	13:11:00	11					
13	0:13:00	13:13:00	12					
15	0:15:00	13:15:00	13					
17	0:17:00	13:17:00	14					
19	0:19:00	13:19:00	15	120	21.7	181	0.430	
22	0:22:00	13:22:00	16					
24	0:24:00	13:24:00	17					
30	0:30:00	13:30:00	18					
32	0:32:00	13:32:00	19					
34	0:34:00	13:34:00	20					
36	0:36:00	13:36:00	21					
38	0:38:00	13:38:00	22	120	28.9	241	0.390	
41	0:41:00	13:41:00	23					
43	0:43:00	13:43:00	24					
								sinus shaped
45	0:45:00	13:45:00	25					channel
50	0:50:00	13:50:00	26					
54	0:54:00	13:54:00	27					
57	0:57:00	13:57:00	28					
72	1:12:00	14:12:00	29					
76	1:16:00	14:16:00	30					
82	1:22:00	14:22:00	31					
88	1:28:00	14:28:00	32					
90	1:30:00	14:30:00	33					piping

k_{Darcy} average = $0.410*10^{-3}$ m/s

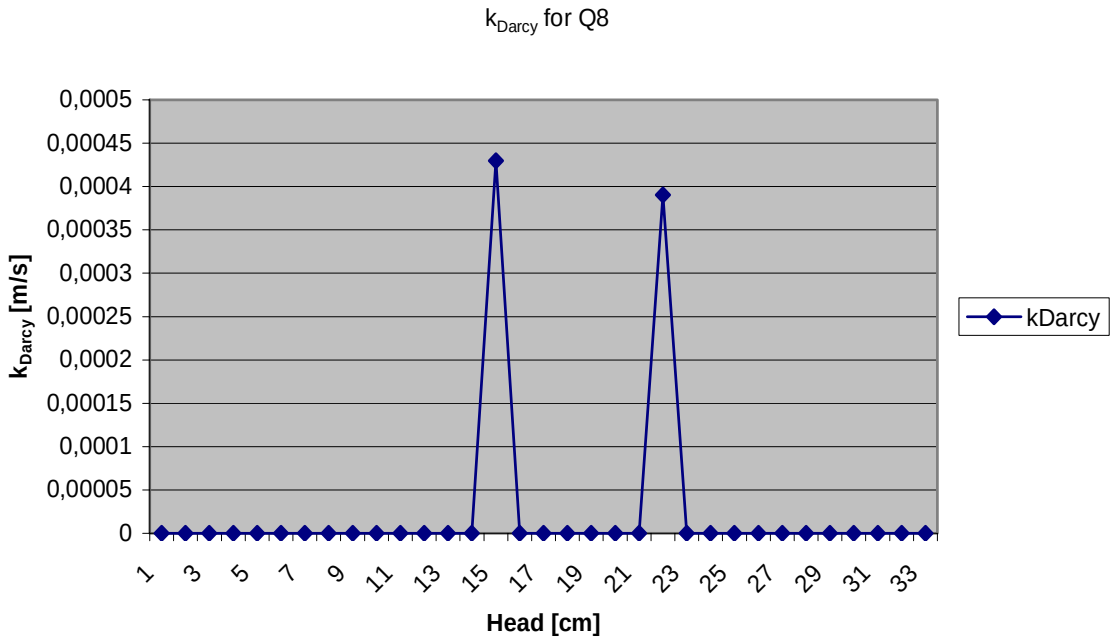

Figure P-8 k_{Darcy} as a function of the head for experiment Q08

Factual report Q09
Date: December 27th
Time: 16:55

Sand type: Ringstrasse Itterbeck Enschede

Table P-17 the properties of the sand and the test facility for experiment Q09

thickness [cm]	0.99
height [cm]	9.97
wanted length [cm]	38.4
wanted volume [cm^3]	379.0
surface [cm^2]	9.87
n_{max} Ringstrasse Itterbeck Enschede [-]	0.4106
n_{min} Ringstrasse Itterbeck Enschede [-]	0.3201
wanted relative density [%]	50
n [-]	0.365
volume void [cm^3]	138.5
volume particles [cm^3]	240.5
mass particles [gr]	764.0
seepage length [cm]	35.2
measured length [cm]	39.2
estimated relative density [%]	40-50

Table P-18 the head, discharge and permeability as a function of time for experiment Q09

minutes	stopwatch time	real time	head [cm]	time discharge measurement [s]	volume [cm^3]	discharge 10^{-9} [m^3/s]	k_{Darcy} 10^{-3} [m/s]	remarks
0	0:00:00	16:55:00	1					
1	0:01:00	16:56:00	2					
2	0:02:00	16:57:00	3					
3	0:03:00	16:58:00	4					
4	0:04:00	16:59:00	5					
5	0:05:00	17:00:00	6					
6	0:06:00	17:01:00	7					
7	0:07:00	17:02:00	8					
8	0:08:00	17:03:00	9					
9	0:09:00	17:04:00	10					
10	0:10:00	17:05:00	11					
11	0:11:00	17:06:00	12					
12	0:12:00	17:07:00	13					
13	0:13:00	17:08:00	14					
14	0:14:00	17:09:00	15	120	27.10	226	0.587	
16	0:16:00	17:11:00	16					
17	0:17:00	17:12:00	17					
18	0:18:00	17:13:00	18					
19	0:19:00	17:14:00	19					
20	0:20:00	17:15:00	20					
								first grains are
22	0:22:00	17:17:00	21					transported
24	0:24:00	17:19:00	22					
26	0:26:00	17:21:00	23					
28	0:28:00	17:23:00	24					
30	0:30:00	17:25:00	25					
32	0:32:00	17:27:00	26					piping

k_{Darcy} average = $0.587*10^{-3}$ m/s

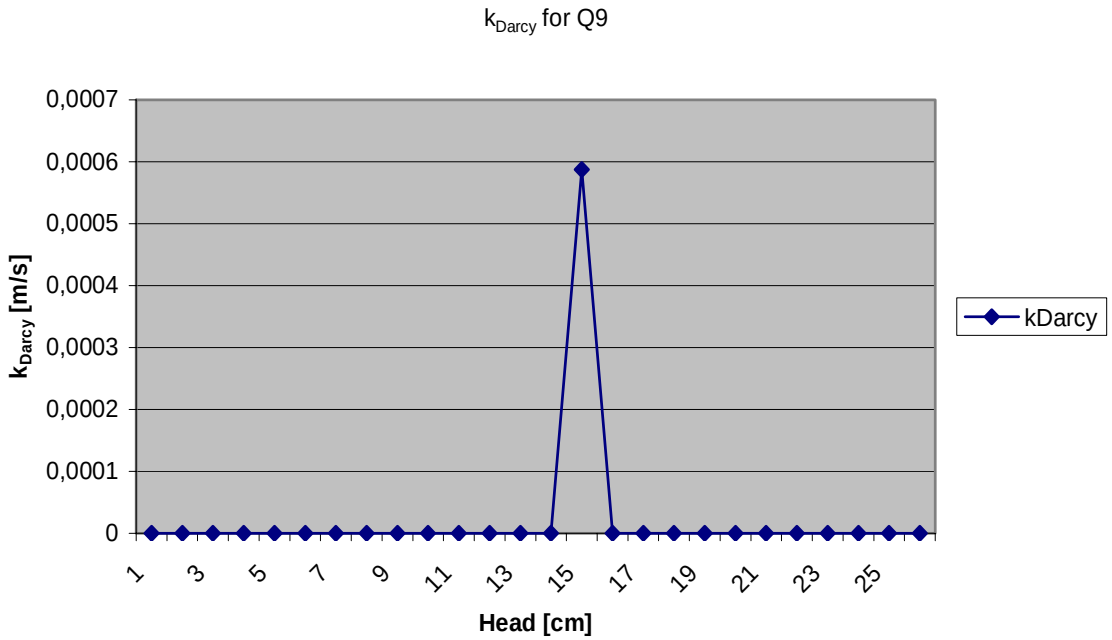

Figure P-9 k_{Darcy} as a function of the head for experiment Q09

Factual report Q10
Date: December 28th
Time: 13:00

Sand type: Ringstrasse Itterbeck Enschede

Table P-19 the properties of the sand and the test facility for experiment Q10

thickness [cm]	0.99
height [cm]	9.97
wanted length [cm]	38.4
wanted volume [cm^3]	379.0
surface [cm^2]	9.87
n_{max} Ringstrasse Itterbeck Enschede [-]	0.4106
n_{min} Ringstrasse Itterbeck Enschede [-]	0.3201
wanted relative density [%]	50
n [-]	0.365
volume void [cm^3]	138.5
volume particles [cm^3]	240.5
mass particles [gr]	656.4
seepage length [cm]	34.5
measured length [cm]	38.0
estimated relative density [%]	40-50

Table P-20 the head, discharge and permeability as a function of time for experiment Q10

minutes	stopwatch time	real time	head [cm]	time discharge measurement [s]	volume [cm^3]	discharge 10^{-9} [m^3/s]	k_{Darcy} 10^{-3} [m/s]	remarks
0	0:00:00	13:00:00	1					
1	0:01:00	13:01:00	2					
2	0:02:00	13:02:00	3					
3	0:03:00	13:03:00	4					
4	0:04:00	13:04:00	5					
5	0:05:00	13:05:00	6					
6	0:06:00	13:06:00	7					
7	0:07:00	13:07:00	8					
8	0:08:00	13:08:00	9					
9	0:09:00	13:09:00	10					
10	0:10:00	13:10:00	11					
11	0:11:00	13:11:00	12					
12	0:12:00	13:12:00	13					
13	0:13:00	13:13:00	14					
14	0:14:00	13:14:00	15	120	33.90	283	0.658	
17	0:17:00	13:17:00	16					
18	0:18:00	13:18:00	17					
								sinus shaped
19	0:19:00	13:19:00	18					channel
25	0:25:00	13:25:00	19					
29	0:29:00	13:29:00	20					piping

k_{Darcy} average = $0.658*10^{-3}$ m/s

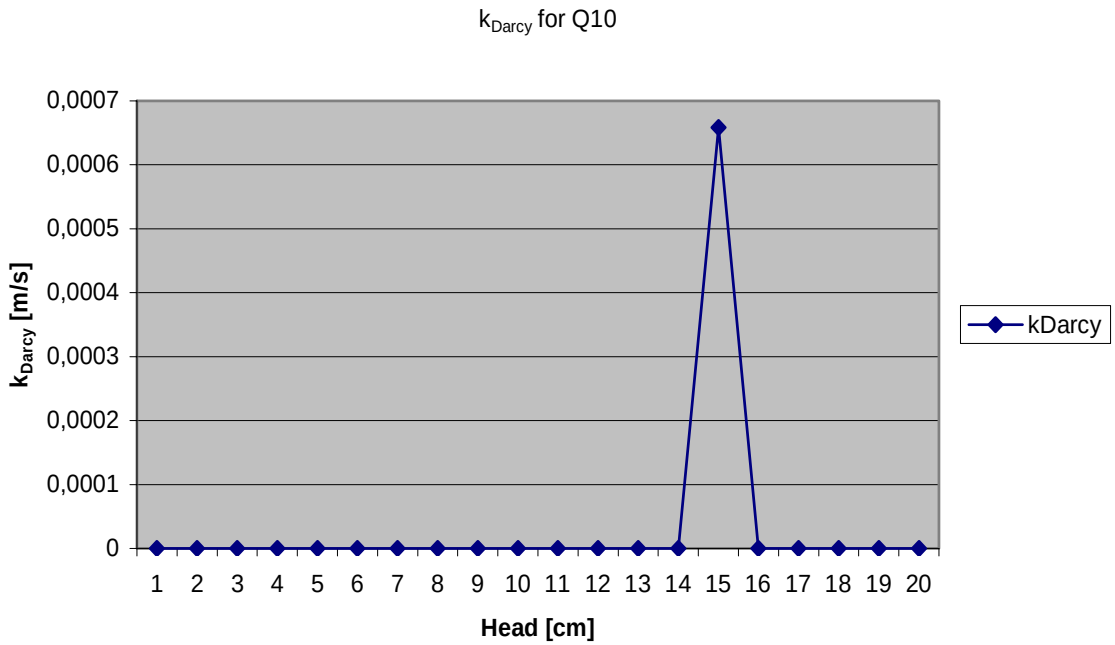

Figure P-10 k_{Darcy} as a function of the head for experiment Q10

Factual report Q11
Date: December 28th
Time: 15:10

Sand type: Ringstrasse Itterbeck Enschede

Table P-21 the properties of the sand and the test facility for experiment Q11

thickness [cm]	0.99
height [cm]	9.97
wanted length [cm]	38.4
wanted volume [cm^3]	379.0
surface [cm^2]	9.87
n_{max} Ringstrasse Itterbeck Enschede [-]	0.4106
n_{min} Ringstrasse Itterbeck Enschede [-]	0.3201
wanted relative density [%]	50
n [-]	0.365
volume void [cm^3]	138.5
volume particles [cm^3]	240.5
mass particles [gr]	667.0
seepage length [cm]	34.0
measured length [cm]	38.5
estimated relative density [%]	40-50

Table P-22 the head, discharge and permeability as a function of time for experiment Q11

minutes	stopwatch time	real time	head [cm]	time discharge measurement [s]	volume [cm^3]	discharge 10^{-9} [m^3/s]	k_{Darcy} 10^{-3} [m/s]	remarks
0	0:00:00	15:10:00	1					
1	0:01:00	15:11:00	2					
2	0:02:00	15:12:00	3					
3	0:03:00	15:13:00	4					
4	0:04:00	15:14:00	5					
5	0:05:00	15:15:00	6					
6	0:06:00	15:16:00	7					
7	0:07:00	15:17:00	8					
8	0:08:00	15:18:00	9					
9	0:09:00	15:19:00	10					
10	0:10:00	15:20:00	11					
11	0:11:00	15:21:00	12					
12	0:12:00	15:22:00	13					
13	0:13:00	15:23:00	14					
14	0:14:00	15:24:00	15	120	34.40	287	0.658	
17	0:17:00	15:27:00	16					
19	0:19:00	15:29:00	17					
21	0:21:00	15:31:00	18					
								sinus shaped
23	0:23:00	15:33:00	19					channel
26	0:26:00	15:36:00	20					
28	0:28:00	15:38:00	21					piping

k_{Darcy} average = $0.658*10^{-3}$ m/s

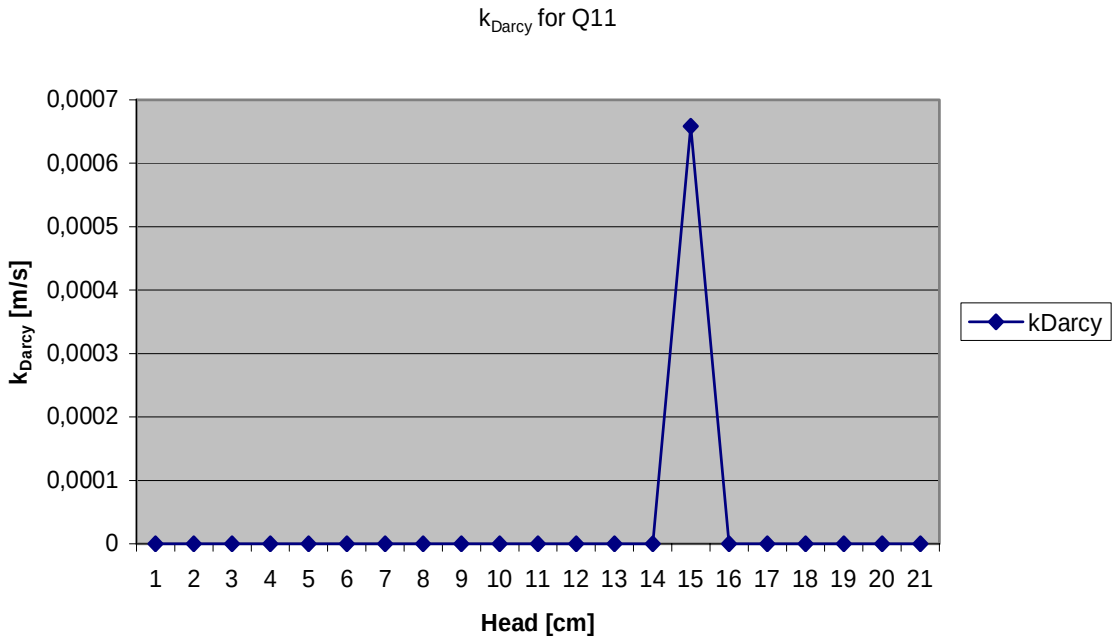

Figure P-11 k_{Darcy} as a function of the head for experiment Q11

Factual report Q12
Date: December 28th
Time: 16:45

Sand type: Baskarp

Table P-23 the properties of the sand and the test facility for experiment Q12

thickness [cm]	0.99
height [cm]	9.97
wanted length [cm]	38.4
wanted volume [cm^3]	379.0
surface [cm^2]	9.87
n_{max} Baskarp [-]	0.458
n_{min} Baskarp [-]	0.346
wanted relative density [%]	50
n [-]	0.402
volume void [cm^3]	152.0
volume particles [cm^3]	266.7
mass particles [gr]	651.6
seepage length[*1] [cm]	34.5
measured length [cm]	38.5
estimated relative density [%]	25

[*1] the real seepage length is 1cm less, because the sand does not make contact with the cover over the full length

Table P-24 the head, discharge and permeability as a function of time for experiment Q12

minutes	stopwatch time	real time	head [cm]	time discharge measurement [s]	volume [cm^3]	discharge 10^{-9} [m^3/s]	k_{Darcy} 10^{-3} [m/s]	remarks
0	0:00:00	16:45:00	1					
1	0:01:00	16:46:00	2					
2	0:02:00	16:47:00	3					
3	0:03:00	16:48:00	4					
4	0:04:00	16:49:00	5					
6	0:06:00	16:51:00	6					
8	0:08:00	16:53:00	7					
10	0:10:00	16:55:00	8					
12	0:12:00	16:57:00	9					
14	0:14:00	16:59:00	10	120	4.70	39.2	0.137	
17	0:17:00	17:02:00	11					
								forward erosion
19	0:19:00	17:04:00	12					occurs
21	0:21:00	17:06:00	13					
29	0:29:00	17:14:00	14					
32	0:32:00	17:17:00	15					
								break
36	0:36:00	17:21:00	16					through

k_{Darcy} average = $0.137*10^{-3}$ m/s

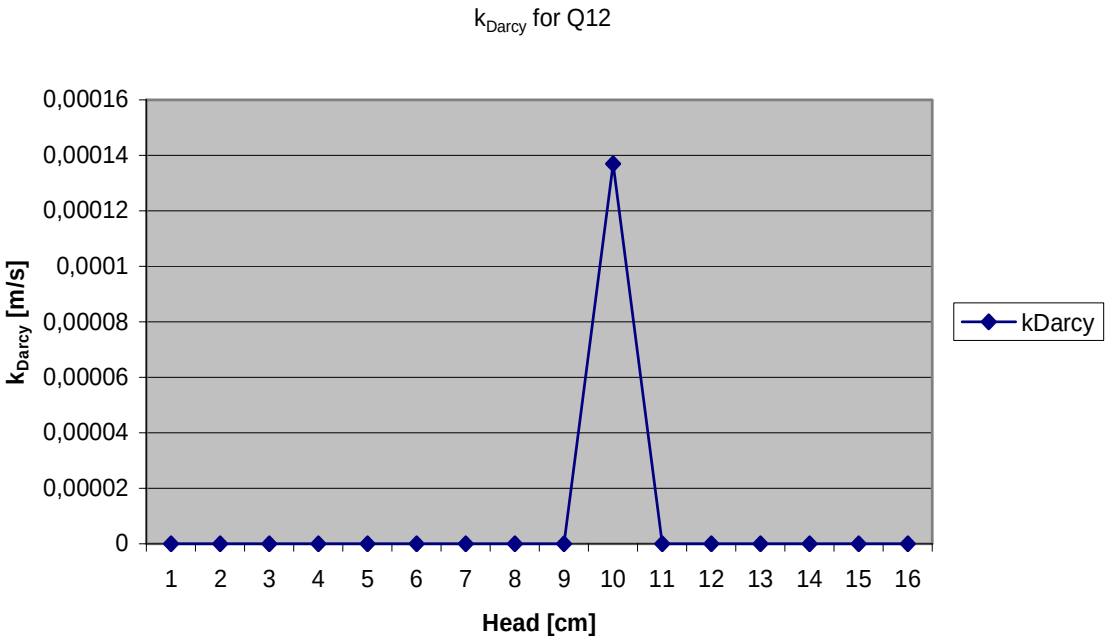

Figure P-12 k_{Darcy} as a function of the head for experiment Q12

Factual report Q13
Date: December 29th
Time: 14:06

Sand type: Ringstrasse Itterbeck Enschede

Table P-25 the properties of the sand and the test facility for experiment Q13

thickness [cm]	0.99
height [cm]	9.97
wanted length [cm]	38.4
wanted volume [cm^3]	379.0
surface [cm^2]	9.87
n_{max} Ringstrasse Itterbeck Enschede [-]	0.4106
n_{min} Ringstrasse Itterbeck Enschede [-]	0.3201
wanted relative density [%]	50
n [-]	0.365
volume void [cm^3]	138.5
volume particles [cm^3]	240.5
mass particles [gr]	666.6
seepage length [cm]	34.0
measured length [cm]	38.5
estimated relative density [%]	40-50

Table P-26 the head, discharge and permeability as a function of time for experiment Q13

minutes	stopwatch time	real time	head [cm]	time discharge measurement [s]	volume [cm^3]	discharge 10^{-9} [m^3/s]	k_{Darcy} 10^{-3} [m/s]	remarks
0	0:00:00	14:06:00	1					
1	0:01:00	14:07:00	2					
2	0:02:00	14:08:00	3					
3	0:03:00	14:09:00	4					
4	0:04:00	14:10:00	5					
5	0:05:00	14:11:00	6					
6	0:06:00	14:12:00	7					
7	0:07:00	14:13:00	8					
8	0:08:00	14:14:00	9					
9	0:09:00	14:15:00	10					
10	0:10:00	14:16:00	11					
11	0:11:00	14:17:00	12					
12	0:12:00	14:18:00	13					
13	0:13:00	14:19:00	14					
14	0:14:00	14:20:00	15	120	34.60	288	0.682	
17	0:17:00	14:23:00	16					
19	0:19:00	14:25:00	17					
								sinus shaped channel
21	0:21:00	14:27:00	18					piping
25	0:25:00	14:31:00	19					

k_{Darcy} average = $0.682*10^{-3}$ m/s

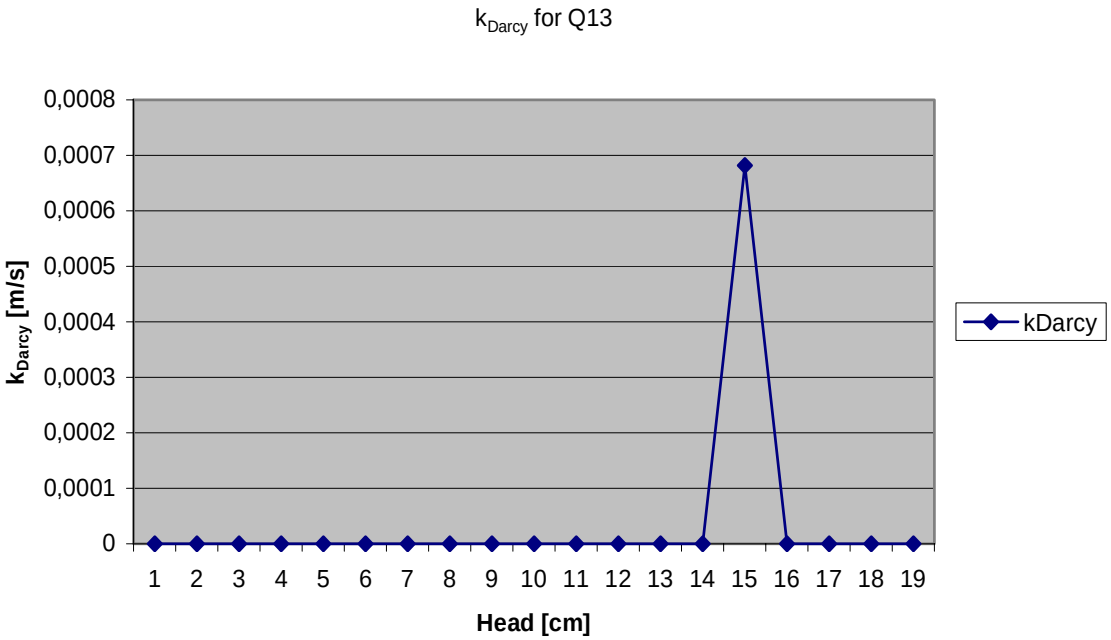

Figure P-13 k_{Darcy} as a function of the head for experiment Q13

Factual report Q14
Date: December 29th
Time: 16:15

Sand type: Ringstrasse Itterbeck Enschede

Table P-27 the properties of the sand and the test facility for experiment Q14

thickness [cm]	0.99
height [cm]	9.97
wanted length [cm]	38.4
wanted volume [cm^3]	379.0
surface [cm^2]	9.87
n_{max} Ringstrasse Itterbeck Enschede [-]	0.4106
n_{min} Ringstrasse Itterbeck Enschede [-]	0.3201
wanted relative density [%]	50
n [-]	0.365
volume void [cm^3]	138.5
volume particles [cm^3]	240.5
mass particles [gr]	666.7
seepage length [cm]	34.0
measured length [cm]	38.5
estimated relative density [%]	40-50

Table P-28 the head, discharge and permeability as a function of time for experiment Q14

minutes	stopwatch time	real time	head [cm]	time discharge measurement [s]	volume [cm^3]	discharge 10^{-9} [m^3/s]	k_{Darcy} 10^{-3} [m/s]	remarks
0	0:00:00	16:15:00	1					
1	0:01:00	16:16:00	2					
2	0:02:00	16:17:00	3					
3	0:03:00	16:18:00	4					
4	0:04:00	16:19:00	5					
5	0:05:00	16:20:00	6					
6	0:06:00	16:21:00	7					
7	0:07:00	16:22:00	8					
8	0:08:00	16:23:00	9					
9	0:09:00	16:24:00	10					
10	0:10:00	16:25:00	11					
11	0:11:00	16:26:00	12					
12	0:12:00	16:27:00	13					
13	0:13:00	16:28:00	14					
14	0:14:00	16:29:00	15	120	34.50	288	0.689	
17	0:17:00	16:32:00	16					
19	0:19:00	16:34:00	17					
21	0:21:00	16:36:00	18					sinus shaped channel piping
24	0:24:00	16:39:00	19					

k_{Darcy} average = $0.689*10^{-3}$ m/s

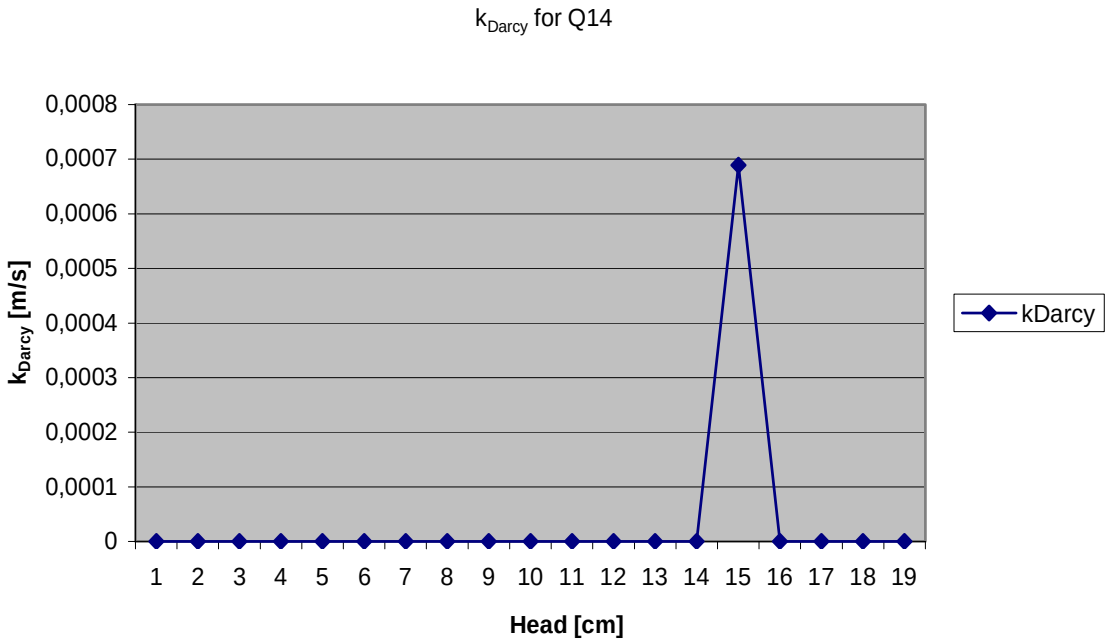

Figure P-14 k_{Darcy} as a function of the head for experiment Q14

Factual report Q15
Date: December 30th
Time: 14:20

Sand type: Ringstrasse Itterbeck Enschede

Table P-29 the properties of the sand and the test facility for experiment Q15

thickness [cm]	0.99
height [cm]	9.97
wanted length [cm]	38.4
wanted volume [cm^3]	379.0
surface [cm^2]	9.87
n_{max} Ringstrasse Itterbeck Enschede [-]	0.4106
n_{min} Ringstrasse Itterbeck Enschede [-]	0.3201
wanted relative density [%]	50
n [-]	0.365
volume void [cm^3]	138.5
volume particles [cm^3]	240.5
mass particles [gr]	665.7
seepage length [cm]	35.5
measured length [cm]	39.0
estimated relative density [%]	40-50

Table P-30 the head, discharge and permeability as a function of time for experiment Q15

minutes	stopwatch time	real time	head [cm]	time discharge measurement [s]	volume [cm^3]	discharge 10^{-9} [m^3/s]	k_{Darcy} 10^{-3} [m/s]	remarks
0	0:00:00	14:20:00	1					
1	0:01:00	14:21:00	2					
2	0:02:00	14:22:00	3					
3	0:03:00	14:23:00	4					
4	0:04:00	14:24:00	5					
5	0:05:00	14:25:00	6					
6	0:06:00	14:26:00	7					
7	0:07:00	14:27:00	8					
8	0:08:00	14:28:00	9					
9	0:09:00	14:29:00	10					
10	0:10:00	14:30:00	11					
11	0:11:00	14:31:00	12					
12	0:12:00	14:32:00	13	120	30.40	253	0.701	
16	0:16:00	14:36:00	14					
17	0:17:00	14:37:00	15					
19	0:19:00	14:39:00	17					piping

Accidentally, the head was increased from 15cm to 17cm.

k_{Darcy} average = $0.701*10^{-3}$ m/s

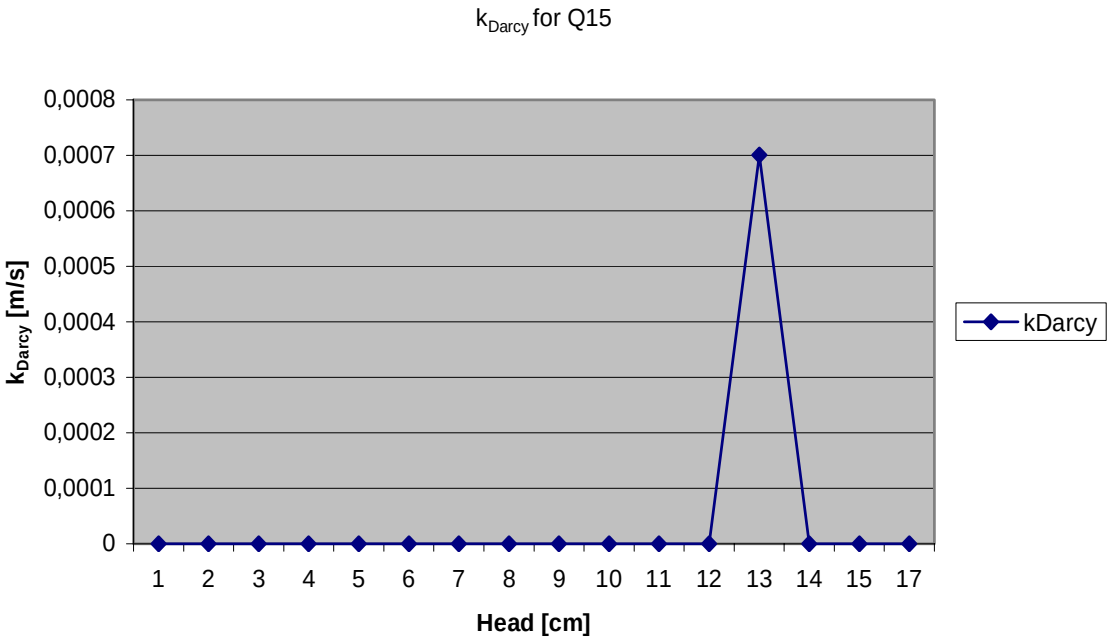

Figure P-15 k_{Darcy} as a function of the head for experiment Q15

Factual report Q16
Date: December 30th
Time: 16:40

Sand type: Ringstrasse Itterbeck Enschede

Table P-31 the properties of the sand and the test facility for experiment Q16

thickness [cm]	0.99
height [cm]	9.97
wanted length [cm]	38.4
wanted volume [cm^3]	379.0
surface [cm^2]	9.87
n_{max} Ringstrasse Itterbeck Enschede [-]	0.4106
n_{min} Ringstrasse Itterbeck Enschede [-]	0.3201
wanted relative density [%]	50
n [-]	0.365
volume void [cm^3]	138.5
volume particles [cm^3]	240.5
mass particles [gr]	666.2
seepage length[*1] [cm]	33.0
measured length [cm]	38.0
estimated relative density [%]	40-50

[*1] the real seepage length is 1.5cm less, because the sand does not make contact with the cover over the full length

Table P-32 the head, discharge and permeability as a function of time for experiment Q16

minutes	stopwatch time	real time	head [cm]	time discharge measurement [s]	volume [cm^3]	discharge 10^{-9} [m^3/s]	k_{Darcy} 10^{-3} [m/s]	remarks
0	0:00:00	16:40:00	1					
1	0:01:00	16:41:00	2					
2	0:02:00	16:42:00	3					
3	0:03:00	16:43:00	4					
4	0:04:00	16:44:00	5					
5	0:05:00	16:45:00	6					
6	0:06:00	16:46:00	7					
7	0:07:00	16:47:00	8					
8	0:08:00	16:48:00	9					
9	0:09:00	16:49:00	10					
10	0:10:00	16:50:00	11					
11	0:11:00	16:51:00	12	120	34.40	287	0.799	first transport of grains
14	0:14:00	16:54:00	13					
16	0:16:00	16:56:00	14					piping

k_{Darcy} average = $0.799*10^{-3}$ m/s

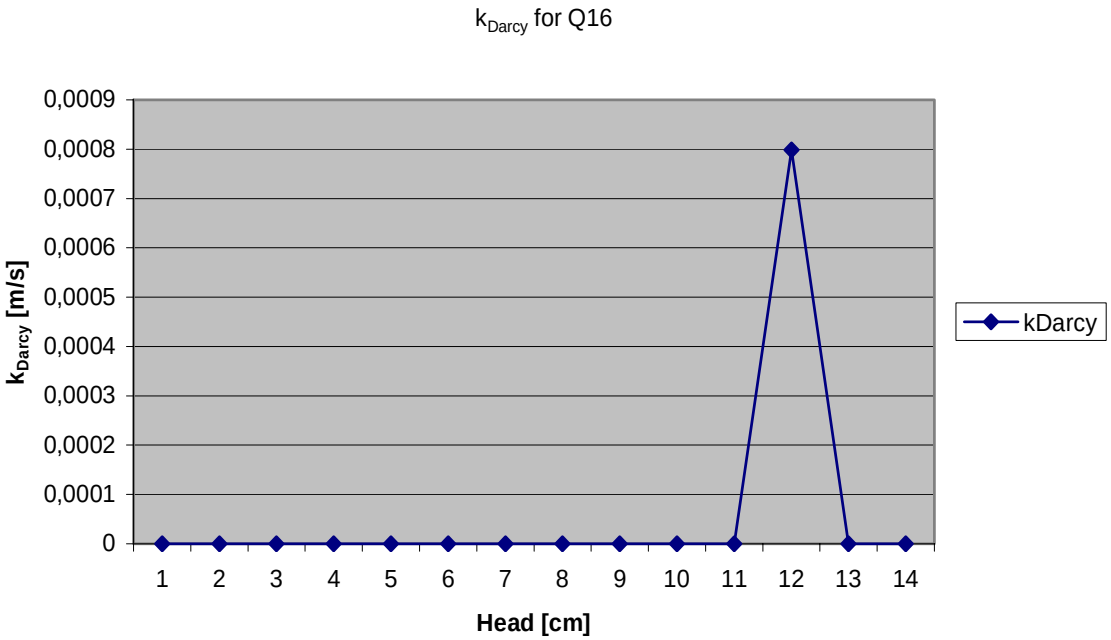

Figure P-16 k_{Darcy} as a function of the head for experiment Q16

Factual report Q17
Date: December 31th
Time: 13:45

Sand type: Ringstrasse Itterbeck Enschede

Table P-33 the properties of the sand and the test facility for experiment Q17

thickness [cm]	0.99
height [cm]	9.97
wanted length [cm]	38.4
wanted volume [cm^3]	379.0
surface [cm^2]	9.87
n_{max} Ringstrasse Itterbeck Enschede [-]	0.4106
n_{min} Ringstrasse Itterbeck Enschede [-]	0.3201
wanted relative density [%]	50
n [-]	0.365
volume void [cm^3]	138.5
volume particles [cm^3]	240.5
mass particles [gr]	667.1
seepage length [cm]	35.5
measured length [cm]	39.5
estimated relative density [%]	40-50

Table P-34 the head, discharge and permeability as a function of time for experiment Q17

minutes	stopwatch time	real time	head [cm]	time discharge measurement [s]	volume [cm^3]	discharge 10^{-9} [m^3/s]	k_{Darcy} 10^{-3} [m/s]	remarks
0	0:00:00	13:45:00	1					
1	0:01:00	13:46:00	2					
2	0:02:00	13:47:00	3					
3	0:03:00	13:48:00	4					
4	0:04:00	13:49:00	5					
5	0:05:00	13:50:00	6					
6	0:06:00	13:51:00	7					
7	0:07:00	13:52:00	8					
8	0:08:00	13:53:00	9					
9	0:09:00	13:54:00	10					
10	0:10:00	13:55:00	11	120	31.30	261	0.853	
11	0:11:00	13:56:00	12					sinus shaped channel
14	0:14:00	13:59:00	13					
18	0:18:00	14:03:00	14					
20	0:20:00	14:05:00	15					piping

k_{Darcy} average = $0.853*10^{-3}$ m/s

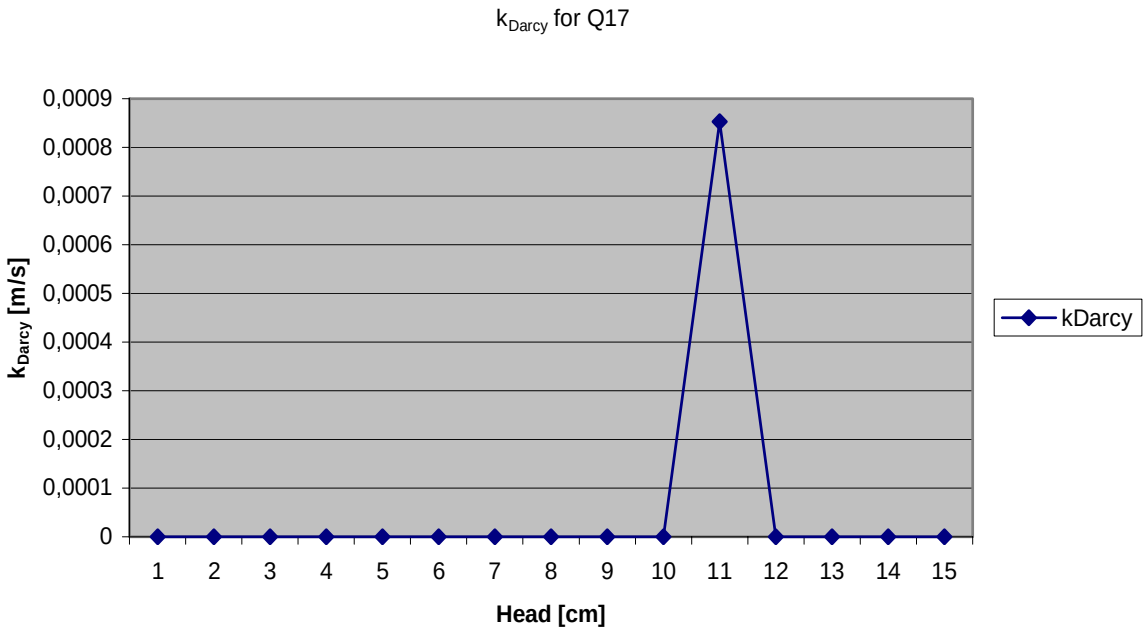

Figure P-17 k_{Darcy} as a function of the head for experiment Q17

Factual report Q18
Date: December 31th
Time: 15:30

Sand type: Ringstrasse Itterbeck Enschede

Table P-35 the properties of the sand and the test facility for experiment Q18

thickness [cm]	0.99
height [cm]	9.97
wanted length [cm]	38.4
wanted volume [cm^3]	379.0
surface [cm^2]	9.87
n_{max} Ringstrasse Itterbeck Enschede [-]	0.4106
n_{min} Ringstrasse Itterbeck Enschede [-]	0.3201
wanted relative density [%]	50
n [-]	0.365
volume void [cm^3]	138.5
volume particles [cm^3]	240.5
mass particles [gr]	666.1
seepage length [cm]	36.5
measured length [cm]	39.0
estimated relative density [%]	40-50

Table P-36 the head, discharge and permeability as a function of time for experiment Q18

minutes	stopwatch time	real time	head [cm]	time discharge measurement [s]	volume [cm^3]	discharge 10^{-9} [m^3/s]	k_{Darcy} 10^{-3} [m/s]	remarks
0	0:00:00	15:30:00	1					
1	0:01:00	15:31:00	2					
2	0:02:00	15:32:00	3					
3	0:03:00	15:33:00	4					
4	0:04:00	15:34:00	5					
5	0:05:00	15:35:00	6					
6	0:06:00	15:36:00	7					
7	0:07:00	15:37:00	8					
8	0:08:00	15:38:00	9					
9	0:09:00	15:39:00	10	120	43.90	366	1.353	cloud visible
13	0:13:00	15:43:00	11					
15	0:15:00	15:45:00	12					sinus shaped channel
18	0:18:00	15:48:00	13					piping increased head to
20	0:20:00	15:50:00	50					50cm

k_{Darcy} average = $1.353*10^{-3}$ m/s

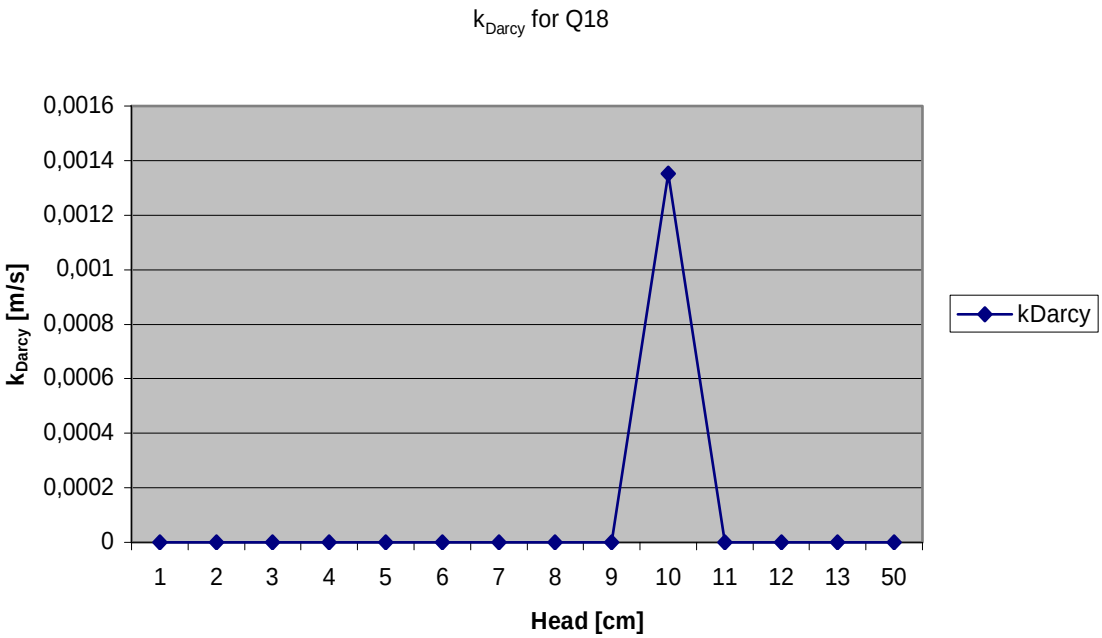

Figure P-18 k_{Darcy} as a function of the head for experiment Q18